THE USE OF AN ENERGY ANALYSER FOR THE MEASUREMENT OF THE TOTAL ENERGY DISTRIBUTION OF FIELD-EMITTED ELECTRONS FROM TUNGSTEN

A THESIS SUBMITTED FOR THE DEGREE OF
MASTER OF SCIENCE
IN THE UNIVERSITY OF ASTON IN BIRMINGHAM

ROGER ALAN CHAPMAN, B.Sc.

Physics Department,
September, 1971.

ABSTRACT

A retarding potential analyser designed by Hartwig and Ulmer has been used to determine the variation of the width of the energy distribution of thermionically emitted electrons with beam current.

An electron gun was developed which was used with the Hartwig and Ulmer analyser to determine the half-width and shape of the total energy distribution of the electrons field emitted from tungsten at a vacuum of about 10^{-9}Torr.

Fowler-Nordheim plots and collector current measurements were obtained for different values of gun parameters and general observations on the nature of field-emission were made including the effect of adsorption on emission current. F-N plot results for particular emitters were combined with the half-widths of relevant energy distributions to give a mean value for the work function of tungsten. A technique was developed for making field-emitters having a radius of about 250Å as confirmed by scaning electron microscope measurements.

Other techniques included a method of computing equipotential values in a system of electrodes with cylindrical symmetry, the measurement of very small currents of about 10^{-14} A, and the use of a.c. field desorption for the emitter cleaning. Effects seen during emitter cleaning were described.

The analyser had three faults (a) the collector current was too small, (b) the lens effect at the entrance of the collector cage limited resolution and (c) it was very difficult to align the emitted beam with the analyser axis. (a) and (c) were remedied by the construction of a

simple analyser with fewer electrodes which were coated with phosphor. Although it was not attempted to improve the resolution, this might have been done by the use of a grid at the cage entrance. A criticism of the analyser was given.

Contents

CHAPTER 1. Introduction

Field-emission is the process whereby when a sufficiently high electric field is applied to a surface, electrons are able to tunnel through the potential barrier at the surface.

Although field-emission was discovered in 1897 by R. W. Wood, it was not studied in detail until the 1920's. Schottky showed that the potential barrier at the metal surface can be modified by the application of a strong electric field so that it becomes narrowed and its height lowered. It was thought the explanation of field-emission ought to be that very strong electric fields lowered the barrier sufficiently for electrons to be emitted without any input of energy, e.g. by heating; however the field strength would need to be as large as 10^8 V/cm. Field-emission occurred at lower field strengths, and so another explanation needed to be found. Fowler and Nordheim developed a wave mechanical theory whereby electrons were able to tunnel through the potential barrier and this was successful in explaining field-emission.

If a diverging beam of electrons from a field emitter hits a phosphor screen a magnified picture (about 10^6) of the emitter surface will be produced. This is called a field-emission microscope and enables observations to be made at nearly atomic level.

Field-emission provides a method of investigating the band structure of various materials including semi-conductors, and since it is very sensitive to the condition

of the emitting surface, it can be used to gain information on the adsorption of various substances on the emitting surface.

The purpose of this project was to construct an analyser suitable for the measurement of the total energy distribution of field emitted electrons. The most notable early field-emission analyser was built by Young and Muller.[1] It had a spherical collector and both this one and the improved version of Arthur[2] suffered from a loss of electrons by secondary emission, an empirical correction to the energy distribution being required. Later analysers e.g. by Van Oostrom[3] and Plummer and Young[4] overcame the problem of secondary emission and had improved sensitivity and resolution. However, when this project began, far more information was available on thermionic emission analysers and it was from this group that an analyser was chosen. This was one used by Hartwig and Ulmer[5] for thermionic emission.

After initial experiments an electron gun for field emission was developed and was used in conjunction with the analyser to determine the total energy distribution of field emitted electrons from tungsten.

Stable field-emission requires ultrahigh vacuum conditions. UHV technology offers two basic pumping systems based on either a diffusion pump (oil or mercury) or an ion pump. With either system it is necessary to bake part to remove adsorbed gases and water from the walls of the experimental chamber. A two-stage mercury pump was available and so this was used, backed with a rotary pump and separated from the chamber by two liquid nitrogen traps. A vacuum of 6×10^{-10} Torr could be obtained.

Since even after baking, a field emitter will be covered in adsorbed gases it is necessary, both for stable emission and for accurate studies of the emitting material, to clean the surface. This can be done either by heating it up (thermal desorption) or applying a high positive potential to the tip which causes adsorbed matter to be desorbed. If a biased a.c. potential is applied, the tip can be examined in a field-emission microscope whilst it is being cleaned. Field desorption requires fields as high as 500 MV/cm at which value, tungsten will evaporate from its lattice.

The measurement of current in an energy analyser requires the use of a sensitive electrometer, preferably with feedback to reduce the long time constant which handicaps measurements in experiments in which the clean surface of an emitter rapidly becomes contaminated. In addition precautions have to be taken to reduce spurious currents e.g. by "guarding".

In Chapter 2 the basic theory of field and thermionic emission is given.

In Chapter 3 the different types of energy analyser are discussed, and in Chapter 4 the different parts of the apparatus are described, total energy distributions are given in Chapter 5 and a value for the mean work function of tungsten is derived.

The discussion chapter (Chapter 6) describes what has been achieved in the project and suggests ways of improving the system.

CHAPTER 2. Théory

2.1. The theory of field-emission from metals

2.1.1.1. Introduction

We assume that the free electron model applies within the metal, that the temperature is $0^{o}K$ and that the surface is plane. The potential energy of an electron remote from the metal surface is defined as being zero. As an electron approaches the surface, it induces an equal and opposite charge at the metal and the electron becomes attracted to the surface by coulomb attraction which results from the charge induced in the metal. The resulting potential of the electron is:

$$V_{image} = -\frac{e^2}{4x}$$

for an electron of charge e, at a distance x from the surface. The electrons in the metal have a constant potential energy:

$$V(x) = -W_a \quad x<0$$

Now if a strong electric field is applied to the surface, the potential barrier will become lower and narrower and electrons will be able to tunnel through it. This process is field-emission. The electric field will give a contribution to the potential energy of:

$$V_{field} = -eFx$$

Therefore the potential energy of an electron outside the metal will be given by:

$$V(x) = -eFx - \frac{e^2}{4x} \quad x>0$$

where F is the electric field strength.

If we identify the electrons in the metal by their momentum components p_x, p_y and p_z, then the number of electrons per unit volume with momentum in the range p_x to $p_x + dp_x$, p_y to $p_y + dp_y$ and p_z to $p_z + dp_z$ is $n(p_x, p_y, p_z)\, dp_x dp_y dp_z$.

Fig.2.1

The potential energy of an electron as a function of its distance from the metal surface

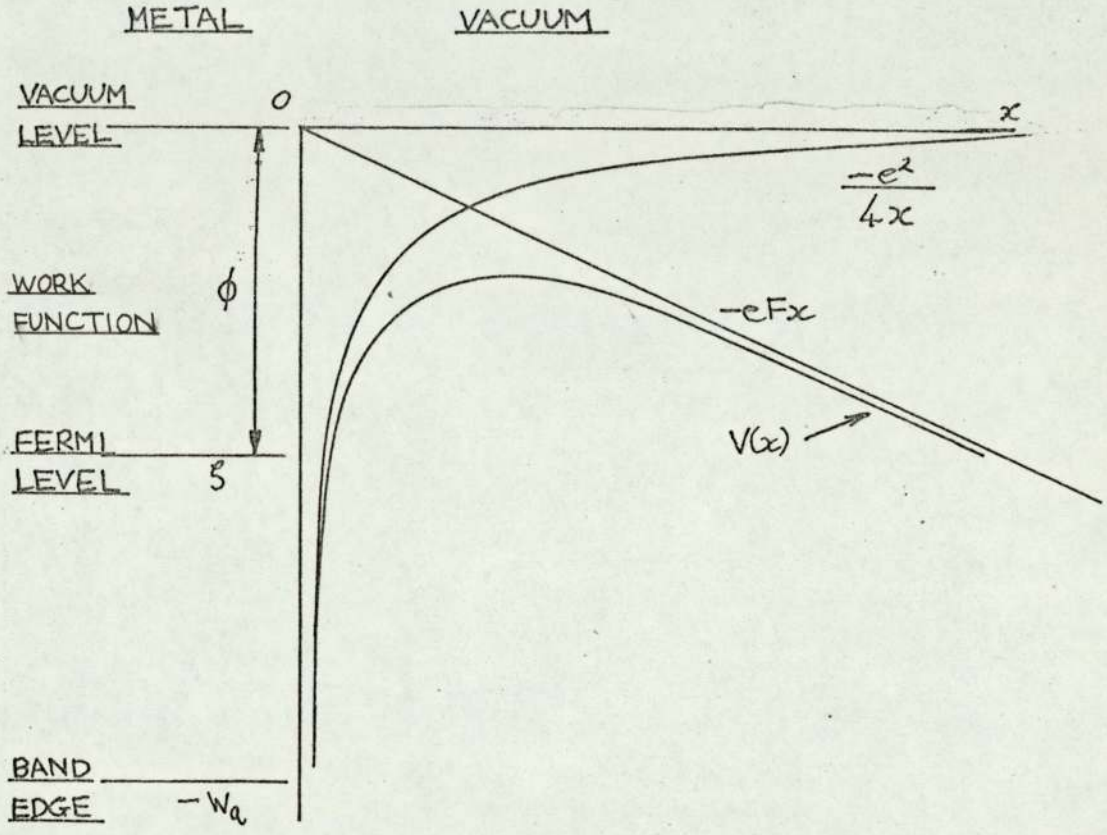

The number of allowed energy states corresponding to an element of momentum space dpx dpy dpz is

$$\frac{2\,dp_x\,dp_y\,dp_z}{h^3}$$ (h is Planck's constant)

because for each volume of phase space there are two states for a free particle of spin $\frac{1}{2}$. The number of electrons occupying states in the given momentum range is the product of the number of allowed states and the electron distribution function:

$$n(p_x,p_y,p_z)\,dp_x\,dp_y\,dp_z = \frac{2}{h^3}\,dp_x\,dp_y\,dp_z\,f(E)$$

where f(E) is the electron distribution function, and E is the total electron energy. The number of electrons with energies in the required range arriving perpendicular to the surface per second per unit area is:

$$v_x\,n(p_x,p_y,p_z)\,dp_x\,dp_y\,dp_z = 2\frac{v_x}{h^3}\,dp_x\,dp_y\,dp_z\,f(E)$$

The x part of the electron energy is:

$$W = E - \frac{p_y^2}{2m} - \frac{p_z^2}{2m} = \frac{p_x^2}{2m} + V(x)$$

where E is the total electron energy, m is the mass of the electron and v_x its velocity perpendicular to the barrier.

There are two energy distributions for the emitted electrons which need to be considered.

2.1.1.2. The normal energy distribution

The number of electrons with the x part of their energy between W and W+dW incident on unit area of the surface per unit time is the supply function, N(W)dW. If this is multiplied by the probability of penetration of the barrier D(W), we obtain the number of electrons within the range W to W+dW which leave unit area of the surface per unit time; this is the normal energy distribution.

2.1.1.3. The total energy distribution

The same probability for barrier penetration is

used as for the normal energy distribution D(W). However, the supply function is now the number of electrons within the range E to E+dE whose x part of their total energy lies in the range W to W+dW incident on the surface per unit area per unit time, N(W,E)dWdE.

Therefore, P(W,E)dWdE = N(W,E)D(W)dWdE is the number of electrons in the given energy ranges penetrating the barrier. Then the total energy distribution is:

$$P(E)\,dE = \int_W P(W,E)\,dW dE$$

2.1.1.4. Transmission coefficient

The transmission coefficient is the probability that an electron with a given energy will penetrate the potential barrier. It is found by solving the quantum mechanical problem of electrons incident on the barrier.

$$W = \frac{p_x^2}{2m} + V(x)$$ (V(x); electron potential energy)

The Schrodinger time-independent equation for the motion of electrons in the x-direction is:

$$\frac{d^2u}{dx^2} + \frac{2m}{\hbar^2}[W - V(x)]\,u = 0$$

where u(x) is the wave function and $\hbar = h/2\pi$

A WKB approximation is made:

$$D(W) = \exp\left[-\int_{x_1}^{x_2}\sqrt{\frac{8m}{\hbar^2}[V(x)-W]}\,dx\right]$$
$$= \exp\left[\frac{-2\sqrt{m}\sqrt{2}}{\hbar}\int_{x_1}^{x_2}[V(x)-W]^{1/2}\,dx\right]$$

where $x_1 \rightarrow x_2$ is the width of the potential barrier at the Fermi level. The approximation is only valid when $W \ll V_{max.}$ which corresponds to field-emission. $V_{max.}$ can be found by setting the derivative of $V(x) = -Fex - e^2/4x$ to zero; hence $V_{max.} = -3.8F^{\frac{1}{2}}$ where x is in Å and F in V/Å. Using:

$$V(x) = -W_a \quad x < 0$$

$$= -eFx - e^2/4x \qquad x>0$$

$$-\log D(W) = -\frac{2\sqrt{2m}}{\hbar}\int_{x_1}^{x_2}[V(x)-W]^{\frac{1}{2}}\,dx$$

where $\left.\begin{matrix}x_1\\x_2\end{matrix}\right\} = \frac{|W|}{2eF}\left(1 \pm \sqrt{1-\frac{e^3F}{W^2}}\right)$

are the zeros of the radicand.

This integral has been evaluated so that the transmission coefficient:

$$D(W) = \exp\left[\frac{-4\sqrt{2m|W|^3}}{3\hbar eF}\,v\left(\frac{\sqrt{e^3F}}{|W|}\right)\right] \text{ where if } y^* = \frac{(e^3F)^{\frac{1}{2}}}{|W|}$$

$$v(y^*) = \frac{1}{2^{\frac{1}{2}}}\left[1+(1-y^{*2})^{\frac{1}{2}}\left[E(k)-(1-(1-y^{*2})^{\frac{1}{2}})\,K(k)\right]\right.$$

$$k^2 = \frac{2(1-y^{*2})^{\frac{1}{2}}}{1+(1-y^{*2})^{1/2}}$$

K(k) and E(k) are elliptical integrals which have been evaluated. The electrons emitted by field-emission all come from the neighbourhood of the Fermi level. Therefore it is possible to write:

$$\left[\frac{-4(2m|W|^3)^{\frac{1}{2}}}{3\hbar eF}\,v(y^*)\right]$$

as a power series expansion at $W = \zeta$. Using only the first two terms, we get:

$$D(W) = \exp[-c + (W-\zeta)/d]$$

where $c = \frac{4(2m|\zeta|^3)^{1/2}}{3\hbar eF}v(y)$; $d = \frac{\hbar eF}{2(2m|\zeta|)^{\frac{1}{2}}t(y)}$

$$t(y) = v(y) - \tfrac{2}{3}\,y\left(\frac{dv(y)}{dy}\right) ; \quad y = \frac{(e^3F)^{1/2}}{\phi}$$

If numerical values are inserted for the constants it is found that $c = \frac{6.83 \times 10^{7} |S|^{3/2}}{F} \nu \left(3.79 \times 10^{-4} \frac{F^{\frac{1}{2}}}{S}\right)$

$$d = \frac{9.76 \times 10^{-9} F}{|S|^{1/2} t(3.79 \times 10^{-4} F^{1/2}/S)} \quad eV$$

2.1.1.5 Calculation of the supply function

We calculate the number of electrons of energy E hitting a surface dS in unit time. If the total velocity vector is v, A is the angle between the normal to the surface and the velocity vector, and B the azimuthal angle in the surface plane, the volume contributing electrons of velocity v from solid angle C(at A and B), is $|v|\,dS\cos A$. The number of electrons in this solid angle with energies between E and E+dE is $n(E)dE\,|v|\,dS\cos A$. Of all these electrons, only those having velocity vectors pointing at dS, will hit area dS. This fraction is $1/4\pi$ times the element of solid angle subtended in velocity space by vectors of magnitude $|v|$ pointing at area dS. In real space this is $dC = \sin A\, dA\, dB$. Thus the flux of electrons from the solid angle dC incident on area dS is:

$$\frac{1}{4\pi} n(E)\, dE\, |v| \cos A \sin A\, dA\, dB$$

Now the component of kinetic energy perpendicular to the surface is: $W = \frac{1}{2} m v^2 \cos^2 A$

$$dW = -m v^2 \cos A \sin A\, dA$$

$$|v| \cos A \sin A\, dA = \frac{-dW}{[2m(E-V)^{1/2}]}$$

The number of electrons with energy within the range E to E+dE whose x part of the energy lies in the range W to W+dW, incident upon the surface x=0 per area per unit time

$$N(W,E)\,dW\,dE = \text{(number arriving at A per solid angle)} \times \text{differential solid angle.}$$

$$= \frac{n(E)\,dE\,|v|\cos A \sin A\,dA\,dB}{4\pi}$$

$$= \frac{-n(E)\,dW\,dE}{2[2m(E-V)]^{1/2}} \quad \text{(integrating on B)}$$

n (E)dE is the Fermi-Dirac function with energy measured relative to an electron at rest at infinity.

$$n(E)\,dE = \frac{4\pi(2m)^{3/2}(E-V)^{1/2}\,dE}{h^3 \exp[(E-\zeta)/kT]+1}$$ k: Boltzmann's constant

$$N(W,E)\,dW\,dE = \frac{-4\pi m\,dW\,dE}{h^3\left(\exp\left[\frac{(E-\zeta)}{kT}\right]+1\right)}$$ (The supply function)

2.1.1.6 The total energy distribution.

The total energy distribution is the integral over W of

$$N(W,E)\,D(W)\,dW\,dE$$

$$P(E)\,dE = \int_{W=E}^{-W_a} N(W,E)\,D(W)\,dW\,dE$$

When $W=-W_a$ the integrand is nearly zero and as integration is made easier by making the upper limit $-\infty$, $-W_a$ is replaced by $-\infty$. Therefore integrating:

$$P(E)dE = \frac{4\pi md}{h^3} \exp\left(-c - \frac{\zeta}{d}\right) \frac{e^{E/d}}{\exp\left[\frac{(E-\zeta)}{kT}\right]+1} dE$$

2.1.1.7. The Fowler-Nordheim equation

The Fowler-Nordheim equation gives the electric current per unit area. It is obtained by either integrating the total or normal energy distribution and multiplying by the charge on the electron:

$$J = 1{\cdot}54 \times 10^{-6} \frac{F^2}{\phi t^2(y)} \exp\left(-6{\cdot}83 \times 10^7 \frac{\phi^{3/2}}{E} v(y)\right)$$

2.1.1.8. The normal energy distribution

The normal energy distribution is the number of electrons in the range W to W+dW tunnelling through the barrier. It is given by $P(W)dW = N(W)\,D(W)dW$ where N(W) is the supply function and equals the number of electrons whose x-component of their energy lies within the range W to W+dW, incident on the surface per unit area and time. D(W) is the probability of penetration of the barrier. In terms of velocities, the number of electrons in unit volume in the momentum range $dp_x dp_y dp_z$ is:

$$N(v_x, v_y, v_z)\, dv_x dv_y dv_z = 2\left(\frac{m}{h}\right)^3 \left(1 + \exp\frac{(E-\zeta)}{kT}\right)^{-1} dv_x dv_y dv_z$$

$$E = m/2\,(v_x^2 + v_y^2 + v_z^2)$$

The number of electrons with velocities along the emission direction x in the range between v_x and v_x+dv_x is found by integrating over dv_y and dv_z, after changing to polar

coordinates in the v_{yz} plane.

$$N(v_x)\,dv_x = \frac{4\pi m^2 kT}{h^3} \log_e\left(1 + e^{\frac{-\zeta - W}{kT}}\right) dv_x$$

The normal energy distribution is found from the product of the flux $v_x N(v_x)dv_x$ and the barrier penetration (or transmission) coefficient. Changing to energy using $dW = mv_x dv_x$, and $\phi = -\zeta$

$$P(W)\,dW = \frac{4\pi m(\phi - W)}{h^3} \exp\left[-c + \frac{W + \phi}{d}\right] dW$$

Integrating over all values of W yields:

$$J = \frac{e^3 F^2}{8\pi h \phi t^2(y)} \exp\left[\frac{-4(2m)^{1/2}\phi^{3/2}}{3\hbar e F} v(y)\right]$$

where J is in the current density. If J is in A/cm^2, the field strength F is in V/cm and the work function in eV

$$J = 1.54 \times 10^{-6} \frac{F^2}{\phi t^2(y)} \exp\left[-6.83 \times 10^7 \frac{\phi^{3/2}}{F} v(y)\right]$$

2.1.1.9. The Fowler-Nordheim plot

The Fowler-Nordheim equation gives the relationship between field-emission current density, work function and electric field strength. The current density can be replaced by the measurable quantity I, the emission current, since I=JA. A typical emitter shape is a hemisphere on the end of a cylindrical shank. Although the electric field at the surface of a sphere of radius r at a potential V is F=V/r, the field at the surface of the emitter is V=/kr where k is a factor arising from the effect of the emitter shank: k=5 typically. The geometrical factor β = 1/kr,

substituting in the Fowler-Nordheim equation: since $F=\beta V$

$$I = 1.5\times10^{-6}\frac{\beta^2 V^2 A}{\phi t^2(y)}\exp\left[-6.83\times10^{7}\frac{\phi^{3/2}}{\beta V}v(y)\right]$$

t(y) is a slowly varying function in the normal range of work functions of metals and approximately equals unity. At constant voltage the emission current depends on both the work function and the geometrical factor. Greater emission comes from planes of low work function and areas where the local electric field is greater because of the geometry of tip. Protrusions on the surface can cause compression of the equipoential lines and a local increase in field strength and emission current. If $\log_{10} I/V^2$ is plotted against $1/V$ a straight line results, the slope of which is given by:

$$m = -2.97\times10^{7}\frac{\phi^{3/2}}{\beta}s(y)$$

where $$s(y) = v(y) - \frac{y}{2}\left[\frac{dv(y)}{dy}\right]$$

s(y) is also a slowly varying function and approximately equals 0.95. At very high current densities (above about $10^7 A/cm^2$) the line departs from linearity because of space charge effects, i.e. mutual repulsion of electrons.

Obtaining a constant emission current at a particular value of V does not ensure that either β, ϕ or A has remained constant, since either of the parameters could have changed in such a way as to give a constant current. Similarly obtaining a constant slope for the Fowler-Nordheim plot does not ensure that ϕ has been constant, since β can vary, e.g. by ion bombardment.

Charbonnier and Martin[1] introduced a useful parameter, K=m/V.

$$K = m/V = -2.97 \times 10^{7} \frac{\phi^{3/2}}{F} s(y)$$

Thus K is a function of the work function and the field strength. The variation of s(y) with ϕ is shown in figure 2.2 where it can be seen that s(y) is practically constant over the normal range of work functions. They showed that if the current density J was plotted against K, then a family of straight lines was formed, each corresponding to a different work function. It was noted that for work functions in the range 4 to 10eV, the lines were so close together as to be virtually identical. The variation of K with ϕ is shown in figure 2.3 for a current density of $J = 10^{3} A/cm^{2}$, where the approximately constant value of K for the work function range 3.0 to 7.0eV can be seen. Since practically all metals and contaminated metal surfaces have work functions in this range, this means that for a given point on a Fowler-Nordheim plot, since V and I are known, the emitting area of the surface and current density can be determined without knowing the work function accurately.

2.1.2. Field emission at temperatures above 0°K

Young[2] derived an expression for the emitted current density when kT < d:

$$J = \frac{e^{3}F^{2}}{8\pi h \phi t^{2}(y)} \exp\left[\frac{-4(2m)^{1/2}\phi^{3/2}}{3\hbar eF} v(y)\right] \frac{\pi kT/d}{\sin(\pi kT/d)}$$

Variation of s(y) with work function

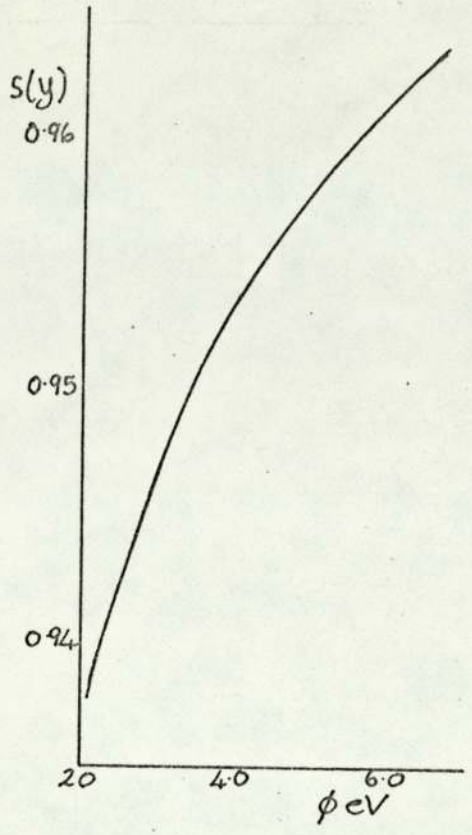

Fig. 2.2

Variation of $K = \frac{m}{V}$ with current density

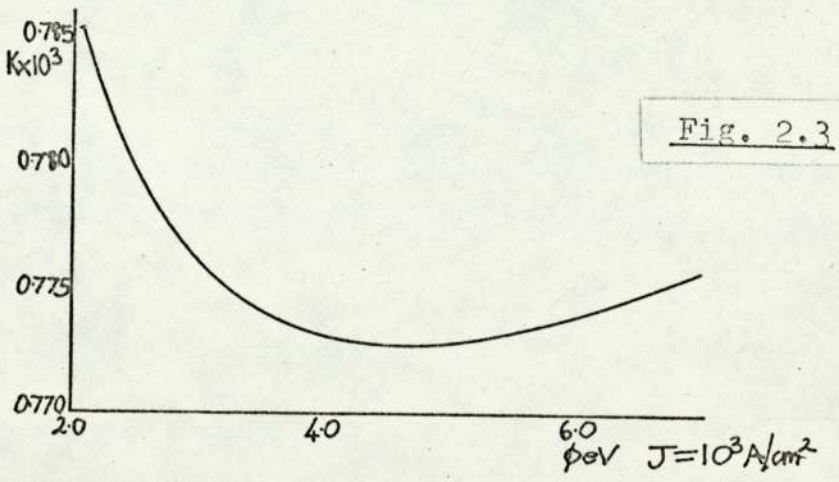

Fig. 2.3

which can be re-written as:

$$J_T = J_0 \frac{\pi kT/d}{\sin(\pi kT/d)}$$

where J_0 is the current density at 0^oK.

Figure 2.4 shows the total energy distributions, for different temperatures, for a particular value of electric field and work function. At 0^oK it can be seen that there is no emission from above the Fermi level and that below it the distribution drops off exponentially as the barrier penetration probability decreases.

As the temperature is raised from 0^oK, some electrons are given energies above the Fermi level. Those moving towards the barrier will have a large probability of being able to escape since under an applied electric field, the barrier is thinner at higher electron energies. Thus the energy distribution becomes wider. Table 2.I shows values of the energy distribution halfwidth, for different temperatures, σ_T and current densities for a work function of 4.4eV. It can be seen that at 0^oK there is more than 100 per cent increase in σ_T with increasing current density ($1\text{-}10^7 A/cm^2$) whereas at higher temperatures, the change is less. In the range of current densities most often encountered ($J=10^2\text{-}10^5 A/cm^2$) the difference $\sigma_T - \sigma_0$ is approximately 95meV.

At 0^oK the full width of the distribution is given by:

$$\sigma_0 = 6.76 \times 10^9 \frac{F}{\phi^{1/2}(eV)}$$

$$= 0.693\, d$$

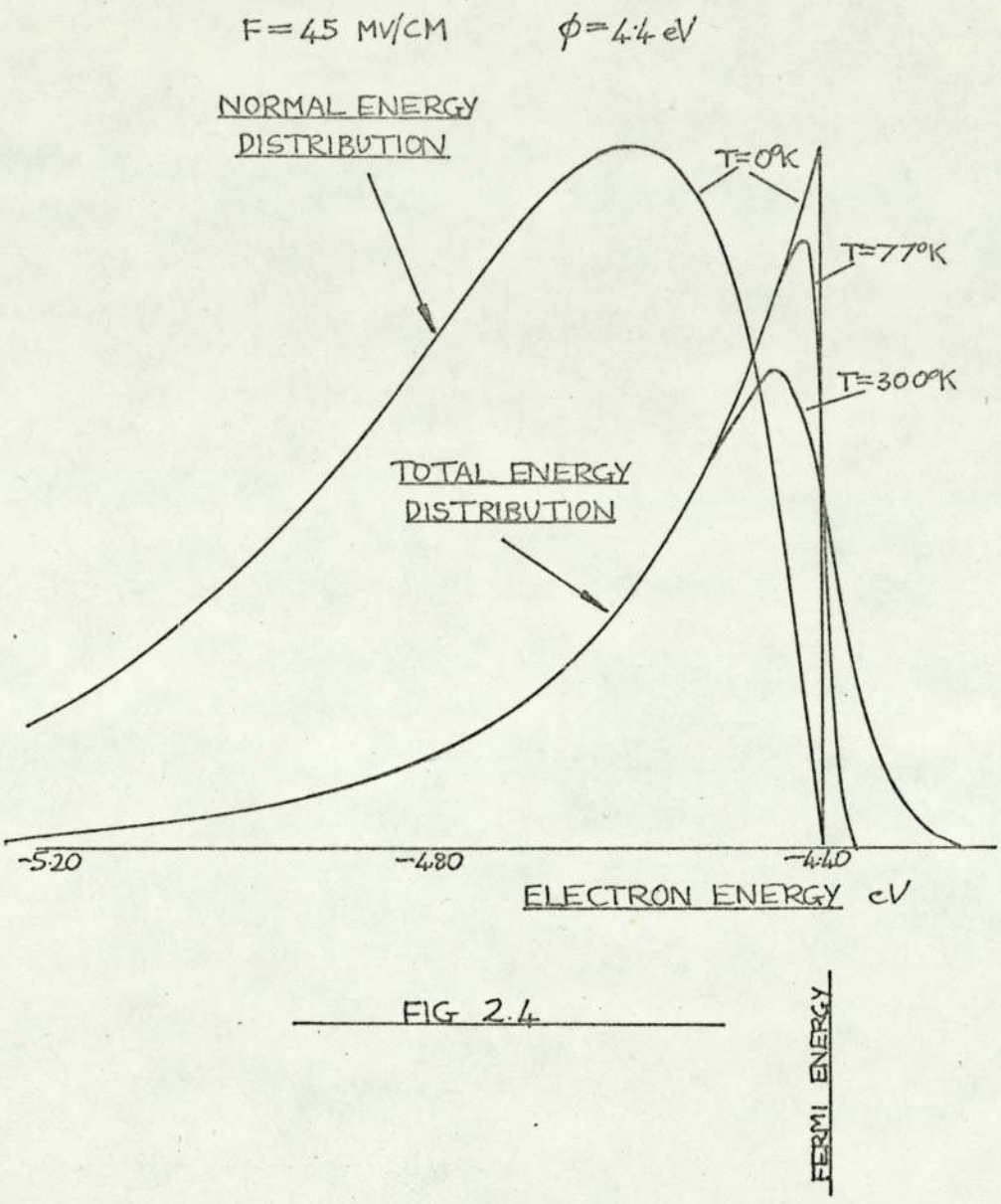
F=45 MV/CM
ϕ=4·4 eV
NORMAL ENERGY DISTRIBUTION
T=0°K
T=77°K
T=300°K
TOTAL ENERGY DISTRIBUTION
-5·20
-4·80
-4·40
ELECTRON ENERGY eV
FERMI ENERGY

FIG 2.4

Table of halfwidths σ_T in meV for ϕ = 4.4eV and log J = 0 to 7 for the temperatures 0 and 300°K

TABLE 2.I

Log J	Temperature °K	
	0	300
0	78	171
1	85	179
2	94	188
3	105	200
4	118	214
5	135	232
6	158	256
7	189	290

Young[3] and Van Oostrom[4] said that the expression for the width of the distribution at temperatures above 0°K was complex and they do not quote it.

It can be shown that the maximum of the energy distribution occurs at:

$$E_{max} = \zeta - kT \log_e\left(\frac{d}{kT} - 1\right)$$

Thus as the temperature increases, the maximum in the distribution curve corresponds to emission from deeper in the conduction band. If the above equation is substituted in the total energy distribution equation, we get:

$$P_{max}(E) = \frac{4\pi m (d - kT)}{h^3} \exp\left[-c - \frac{kT}{d} \log_e\left(\frac{d}{kT} - 1\right)\right]$$

As the temperature increases, the height of the distribution becomes less.

2.1.3. Discussion of the total energy distribution and comparison with the normal energy distribution.

Figure 2.4 shows the total energy distributions for different temperatures for F = 45MV/cm and ϕ = 4.4eV. The steep rising edge represents the beginning of the Fermi 'sea' of electrons at the Fermi energy. The exponential decline of each curve is due to the decrease of the barrier penetration probability. As the temperature is increased, the maximum of each curve decreases. At 0°K the half-width of the distribution is 0.14eV.

For comparison, the normal energy distribution is shown in which the maximum remains the same over a wide range of temperatures. The normal energy distribution is about three times wider than the total energy distribution. The total energy distribution reveals details of the supply

function but not of the nature of the barrier whilst the opposite applies to the normal energy distribution.

2.1.4. Factors affecting emission.

2.1.4.1. The geometrical factor β

β is a factor determined by the radius and shape of a tip and the separation between it and other electrodes. It relates the local electric field strength to the potential difference between the tip and the anode. $F = \beta V$
It is usually determined by examination of the tip in an electron microscope. If the tip is smooth and the radius constant, the β will remain constant: however, if for example the surface was bombarded with ions, then β would be expected to change.

It decreases monotonically with increasing angle from the emitter apex. This corresponds to a decrease in local field strength with increasing angle, which is about 0.15% per degree; thus even at very large angles the field strength is sufficient for emission to occur when a very high field is present at the apex. The emission current decreases more rapidly than the field strength as would be expected from the Fowler-Nordheim equation. If the tip is heated to a high temperature in order to thermally desorb surface contaminants, facets will develop on the emitter because of the different surface energies of different regions. The surface of the emitter can then be smoothed by field evaporation.

β can be rewritten as $\beta = 1/kr$ where r is the emitter radius and $k \approx 5$.

2.1.4.2. Approximate determination of emitter radius r

Gomer[5] describes a method of obtaining an approximate value for the radius from the slope of the Fowler-

Nordheim plot.

$$m = -2.97 \times 10^{7} \frac{\phi^{3/2}}{\beta} s(y) \quad , \quad 2.1. \qquad F = \beta V \quad 2.2$$

Since s(y) approximately equals unity, this can be rewritten as: $m = -2.97 \times 10^{7} \phi^{3/2} kr \qquad k \approx 5$

$$m = -2.97 \times 10^{7} \phi^{3/2} \times 5 \times r$$

$$= -14.85 \times 10^{7} \phi^{3/2} r$$

$$r = \frac{m \times 10^{-7}}{14.85 \times \phi^{3/2}} \quad cm$$

Thus r can be found if ϕ is known. Gomer describes an iterative procedure in which s(y) is initially assumed to be unity. Since $s(y) \approx 1$, substitution in equn. 2.1 gives a minimum value for kr (ϕ must be known). This value of kr is then substituted in equn.2.2 to give a mean value for the electric field strength corresponding to the range of voltages used in the experiment. From the value of F, y can be calculated and a new value of s(y) found from tables. This represents a minimum value for kr. By iteration, a more accurate value for r can be found.

2.1.4.3. Emitting area A

The current density can be determined at any point on the Fowler-Nordheim plot from the corresponding value of K, without knowing the work function accurately. The emitting area can also be found since the current I is known and this should be constant for the particular plot.

The total emission current depends on β , ϕ and A; however the influence of ϕ and β is greater than that of A since they appear in the exponential term of the current equation. Since emission comes preferentially from the low

work function planes of the emitter, the area determined will be composed of these. In the case of normal drawn tungsten wire, the axis corresponds to the[110]direction, however although this plane is very large, a substantial part of the emission current from such drawn wires comes from many planes of much smaller area, because of their relative low work functions ($\phi_{110} \approx 6eV$). If either varies because of ion bombardment, or ϕ varies because of adsorption, then A will change.

2.1.4.4. Work function

The work function is the only parameter in the Fowler-Nordheim equation which is peculiar to the material of the emitter. It is the difference between the Fermi level and the potential energy in vacuo and comprises (a) the chemical potential of the electrons, and (b) the electrostatic potential difference difference between the inside and outside of the metal. It determines which planes will contribute most to the total emission current and is sensitive to the presence of gases which can become adsorbed.

The work function can be determined by four methods:

(a) from the slope of the Fowler-Nordheim plot

$$m = -2.97 \times 10^7 \frac{\phi^{3/2}}{\beta} s(y)$$

since β is known from the tip shape, ϕ can be determined absolutely.

(b) in adsorption studies, a mean value of ϕ might be assumed for the clean surface, and thus the work function for the surface with adsorbed material present can be determined from the change in slope of the F-N plot.

(c) the probe hole technique in which only the emission current from one plane is measured, gives a plot for the particular plane. If its geometrical factor is known, then the work function for the particular plane can be determined. Usually β is not known, therefore sometimes a Fowler-Nordheim plot is obtained for the total emission, a mean value of ϕ assumed, and a mean value of β calculated. This is then used to give the work function for the particular plane; the assumption being more acceptable for smooth surfaces than for those with facets.

A correction can be applied to allow for the fall off in electric field strength with increasing angle. The relationship between β and the angle from the apex Θ can be found for two identified planes of known angular separation and similar work functions, from the respective slopes of the Fowler-Nordheim plots.

(d) It is possible to determine the work function and β simultaneously from the Fowler-Nordheim plot and the half-width of the total energy distribution.

The equation relating the halfwidth and the work function is:

$$m\sigma_0 = 2{\cdot}01\times10^{-5}\,\phi V\,\frac{s(y)}{t(y)}$$

Since $K = \frac{m}{V}$; $K\sigma_0 = 2{\cdot}01\times10^{-5}\,\phi\,\frac{s(y)}{t(y)}$

where σ_0 is the halfwidth at $0^{\circ}K$.

K can be obtained from the Fowler-Nordheim plot and log J from the graph of log J against K (assuming ϕ lies between about 4 and 7 eV). If J is known and ϕ is known approximately, then the corresponding value of the electric field strength, s(y) and t(y) can be found from tables. Ref. Chapter 3 11.

Values of the halfwidth at 0°K and 300°K have been calculated for ϕ = 4.4eV and various values of log J. The correction to the halfwidth over the typical range of J (10^2 - 10^5 A/cm^2) only varies from 94 to 97 meV. Thus it is possible to calculate the work function.

2.1.5. The (110) plane of tungsten and patch fields

The (110) plane of tungsten is of interest because it is the central plane of field-emission of normally drawn wire, and appears to have an unusually high work function, the exact value of which has been the subject of several papers. It is much larger than neighbouring planes, being about thirty times bigger than the (100) face, for example.

There is a relatively sharp step at the junction of the (110) plane and adjacent areas of the tip. Atoms in this boundary region are less tightly bound and therefore more easily field evaporated. This results in a larger radius of curvature for the (110) plane than other planes.

Values of work function by macroscopic methods give $\phi \approx$ 5.1 - 5.3eV. However, the work function determined from field emission measurements is much higher being about 6eV. Swanson and Crouser[6] thought that anomalously high values of work function could be due to the effect of patch fields.

The field emitted current depends on the electric field strength; besides the applied electric field, dipole layers on the surface have dipole moments which vary from one facet to another. Thus the presence of different facets of different work functions gives rise to electrostatic fields at the surface. When two or more facets are considered, the resulting field is called a "patch field". Such fields are highly localised and have very short range. Young and Clark[7] considered a particular plane as a disc at a potential equal to the negative of the average work function of tungsten. For example, if the (110) plane has a work function of 6eV and a radius of 50Å and is surrounded

by a region of work function 4.5eV, the resulting electric field would be 6-3MV/cm (Young and Clark). Young pointed out that if the effect of the patch field was taken into account, then the work function of the (110) plane would be greater than 6eV. Since the macroscopic work function is only about 5.2eV, Swanson and Crouser could not accept that ϕ_{110} might be greater than 6eV, as given by the measurement of the slope of Fowler-Nordheim plot. They thought that either the effect of patch fields was more subtle than previously thought, or that perhaps the Sommerfeld free electron model does not apply for the (110) electrons.

Young and Clark suggested that the broad range of work functions obtained for the (110) plane might have partly been caused by surface imperfections, grain boundaries or single or multiple atom steps at the plane edges.

Plummer and Rhodin[8] investigated the effect of the surface perfection of the (110) tungsten plane on emission current, by depositing tungsten atoms on a clean surface from a heated tungsten wire. The emission current was measured and the surface of the tip examined in a field ion microscope. They concluded that the field emitted current depends significantly on the atomic perfection of the surface and that this is primarily due to a change in work function caused by a change in the distribution of charge on surfaces of different atomic perfection.

Plummer and Young[9] investigated the electron energy levels of adsorbed atoms. The atomic potential of the adsorbate is represented as a square well as shown in figure 5.34. Thus the adsorbate changes the potential barrier as seen by electrons tunnelling from the metal, and

enhances the emission. The effect is one of resonance since the transmission of electrons through the compound barrier will be most pronounced when the incident electrons from the metal have the same energy as the virtual level of the adsorbed atom. In experiments on the effect of the adsorption of barium on tungsten, they found that the (110) region of tungsten had a work function of 5.7eV, as calculated by using both the total energy distribution and Fowler-Nordheim plot results.

2.2. Resolution of the field emission microscope

The resolution of the field-emission microscope is the minimum distance between two points on the emitter which produce two separate images on the screen. Two factors determine the resolution. Firstly, electrons leaving a specific region on the emitter will hit the screen at different positions according to their transverse velocity. The value of the transverse displacement between an electron with transverse velocity v_t and one with no transverse velocity is:

$$D/2 = 2 v_t t$$

where t is the time it takes for an electron to travel from the tip to the screen. Thus the width of the region on the tip will appear to have been increased by $\delta = \frac{D/2}{M}$ where M is the magnification factor. This increase is the resolution determined by this effect. $M = \frac{x}{\beta r}$ where x is the tip-to-screen distance, r is the tip radius and β is a geometrical factor arising from the effect of the emitter shank on the field at the tip.

Gomer[11] shows that:

$$\delta = 4 v_t r_t \beta \left(m/2eV_0\right)^{1/2}$$

But $E_t = \frac{1}{2} m v_t^2$ therefore $\delta = 4 r_t \beta \left(\frac{E_t}{eV_0}\right)^{1/2}$ in terms of energy. (r_t tip radius, eV_0 electron total energy.)

Gomer derived an expression for the average value of the energy of electrons in the transverse direction in terms of $\Delta = E_F - E_x$ and combined this with an expression for the maximum value of Δ. Substitution in the above equation gave the resolution due to the statistical distribution of momenta in the plane transverse to the emission direction (E_F Fermi energy and E_x energy in the x-direction)

$$\delta = 2.62\times10^{-4}\beta\left(\frac{r_t}{k\alpha\phi^{1/2}}\right)^{1/2} \text{ cm} \; ; k=\frac{1}{\beta r},$$

$$\alpha = (1-y)^{1/2} \text{ and } y = 3.8\times10^{-4}\frac{F^{1/2}}{\phi}$$

The second factor is the diffraction limit resulting from the wave nature of the electron. Electrons leaving a region on the tip of width δ_o will, by Heisenberg's uncertainty principle, have a momentum in the transverse direction of: $p_t = mv_t = \hbar/2\delta_o$ therefore $v_t = \hbar/2m\delta_o$

As shown before, the resolution of electrons of velocity v_t is $\delta = 4v_t r_t \beta \left(m/2eV_o\right)^{1/2}$ therefore $\delta = r_t\beta/\pi\delta_o\left(\frac{h^2}{2meV_o}\right)^{1/2}$

The de Broglie wavelength of an electron is $\lambda = h/p$

$= \left(h^2/2meV_o\right)^{1/2}$ for an electron of energy eV_o

therefore $\delta = r_t\beta\lambda/\pi\delta_o$

Thus two areas on the emitter each of width δ_o, can just be resolved when their distance apart is δ. The mean resolution is: $(\delta\delta_o)^{1/2} = \left(\frac{r_t\beta\lambda}{\pi}\right)^{1/2}$

Gomer has combined the factors contributing to the resolution of the microscope to give an overall resolution of

$$\delta = 2.62\times10^{-4}\beta r_t^{1/2}\left(\frac{1.16}{\beta V^{1/2}} + \frac{1}{k\alpha\phi^{1/2}}\right)^{1/2} \text{ cm}$$

For an emitter of 10^{-5}cm radius, with a work function of 4.5eV, operating at 2500V, the overall resolution would be 43Å.

2.3. Field desorption

Field desorption is a method of cleaning surfaces by the application of a high electric field which strips off ions of the adsorbed layers. Because of the high local field strength needed for field desorption, the technique is particularly suitable to field emitters. If a sufficiently high field is applied, ions from the emitter itself may be removed, in this case the process is called field evaporation. At room temperature oxygen can be desorbed from tungsten with a field of 400 MV/cm, and at 500 MV/cm tungsten begins to be evaporated.

After desorption at a suitable field strength, the polarity is usually reversed and the field emission pattern examined. Cooper and Muller[10] used a positively biased a.c.; thus in the positive part of the cycle, field desorption takes place and in the negative part of the cycle the field-emission pattern can be examined. The peak to peak voltage is gradually increased and the bias voltage adjusted to limit the emission current to a level sufficient for examination to the pattern throughout desorption.

As the desorption voltage is increased, the emitter surface becomes progressively cleaner, the apparently random distribution of bright and less bright spots giving way to a symmetrical pattern characteristic of emission from certain planes of the field emitter.

2.3.1. Theory

The mechanism of field desorption is explained by first considering the potential energy of various systems of atoms and ions in the vicinity of a metal surface, both with an electric field absent and present.

The potential energy diagram for a non-adsorbed atom A in the vicinity of a metal M surface when there is negligible interaction, is shown in figure 2.5. If the atom is ionized, the curve for the system $M^- + A^+$ has the form of an image potential.

2.3.2. Strong covalent binding

In the case of strong covalent chemisorption, the ionization energy is very much bigger than the work function of the metal and the potential energy curve for $M^- + A^+$ will lie above that for M + A, the difference between them being $(I - \phi)$. This is the case for the desorption of oxygen. (Figure 2.6).

When an electric field is applied, the curve for M + A drops slightly because of the polarization energy of the atom in the field. The curve for $M^- + A^+$ turns downward to intersect M + A at x_c. For an atom to leave the metal surface it must have enough energy to pass over the barrier. In the presence of a moderately strong electric field, the barrier is lowered slightly having a height $Q = H_a - \frac{1}{2} \alpha F^2$, where H_a is the heat of adsorption of the atom, F the applied electric field strength, and α the polarizibility. The atom is thus vibrationally desorbed and at x_c it is ionized. (There is also a small correction to the height of the barrier which is the field-bond interaction energy.) (Figure 2.7)

At higher electric fields, the height of the barrier Q (the activation energy of desorption) is even less, and the distance x_c, at which the curves $M^- + A^+$ and M + A intersect, is less than that which corresponded to the attractive part of the potential energy curve in the absence of the field. (Figure 2.8).

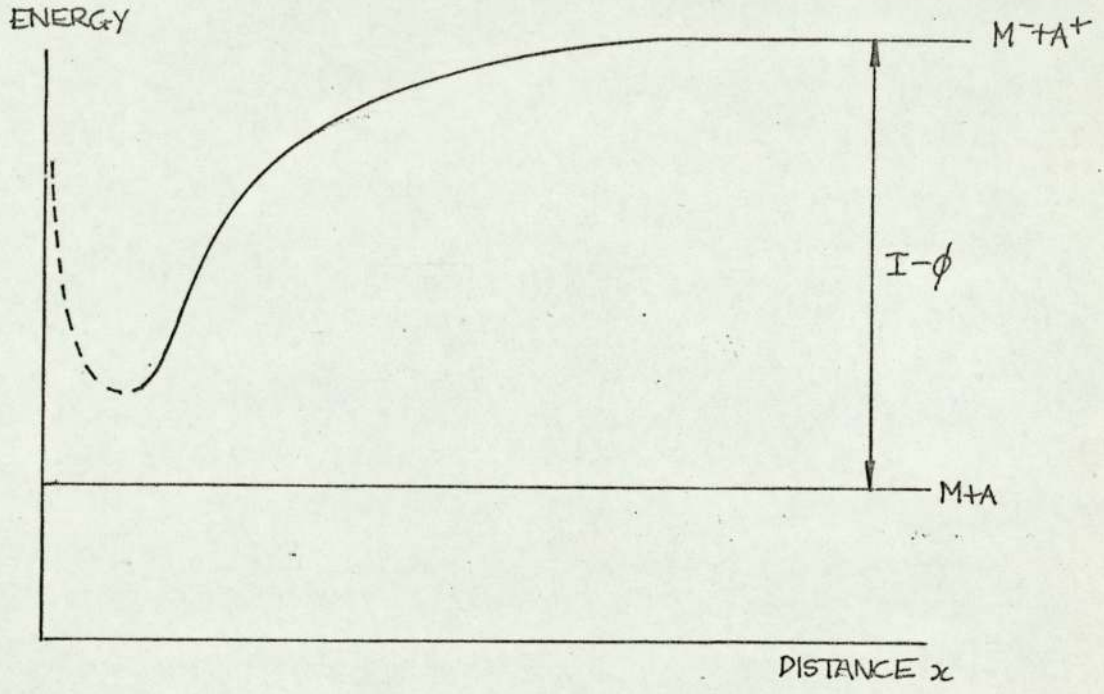

FIG. 2.5

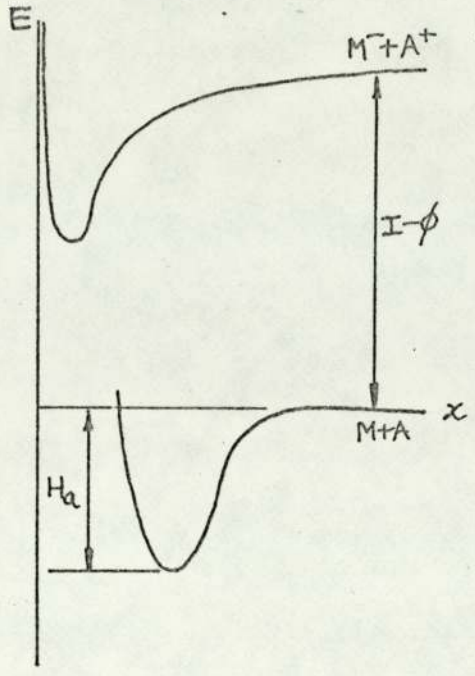

FIG. 2.6

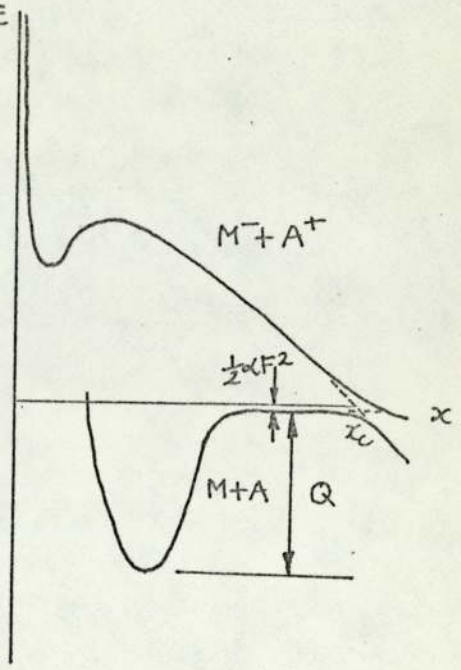

FIG. 2.7

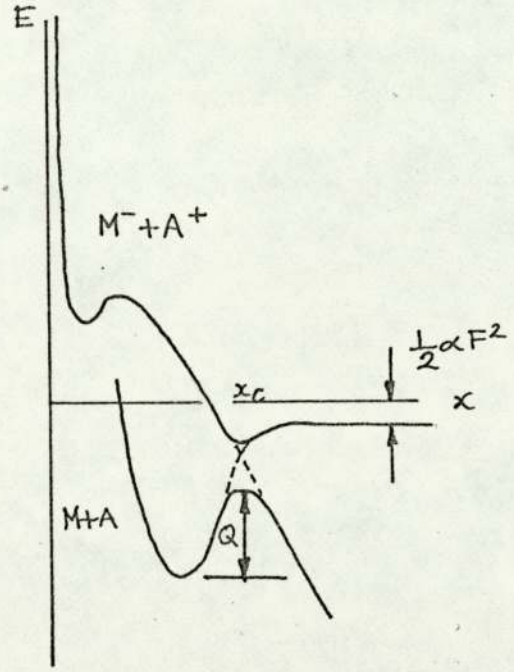

FIG. 2.8

2.3.3. Weak covalent or ionic binding

If $I - \phi$ is small, then the two curves will intersect, even in the absence of a field. At small separations the ionic curve $M^- + A^+$ will lie below the neutral curve M + A. In this case vibrational desorption can occur. (Figure 2.9). At moderate fields, the two curves intersect twice making it possible for either vibrational desorption followed by ionization to occur, or for ionic evaporation to occur directly. (Figure 2.10).

At higher field strengths the ionic curve is lowered so much that the two curves do not intersect. (Figure 2.11). The maximum in the ionic curve lies $(n^3 e^3 F)^{\frac{1}{2}}$ below the zero of the field-free curve, where ne is the charge on the positive ions and F the field strength. The height of the barrier, Q, is the binding energy of the ion Q_o, reduced by this term $(n^3 e^3 F)^{\frac{1}{2}}$. Desorption of electro-positive adsorbates and field evaporation occurs only by vibrational excitation over the barrier, without field ionization occuring. The desorption energy Q_o is given by:

$$Q_o = H_a + I - \phi$$

i.e. it is the sum of the energy required to evaporate a neutral atom plus the energy needed to ionize it minus the energy gained when the electron is returned to the metal.

The time constant for the desorption process is given by: $\tau = \tau_o \exp(Q/kT)$

where $\tau_o = 1/\nu$, ν is the vibrational frequency of the bound particle.

The desorption field strength is given by:

$$F = n^{-3} e^{-3} \left(H_a + I - \phi - kT \log_e \tau/\tau_o \right)^2$$

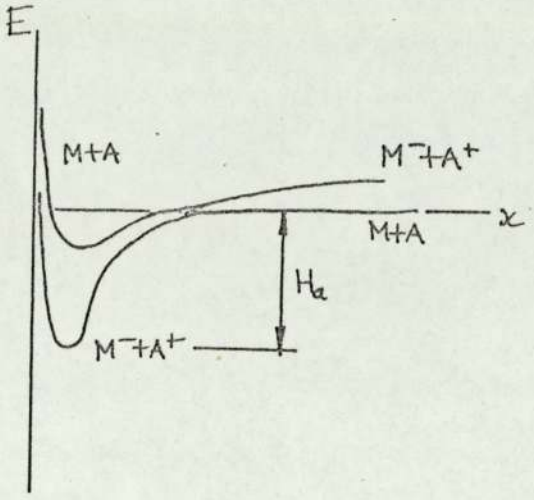

FIG. 2.9

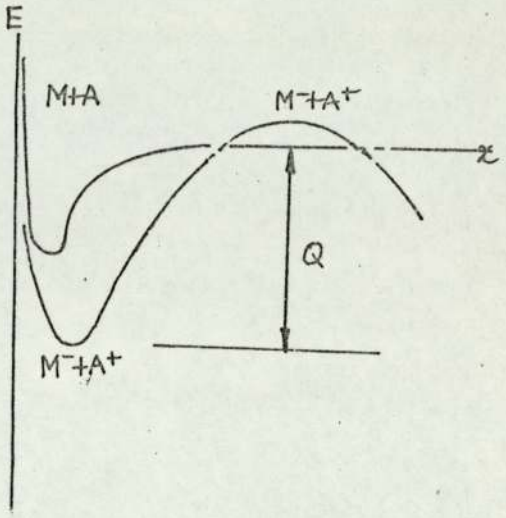

FIG. 2.10

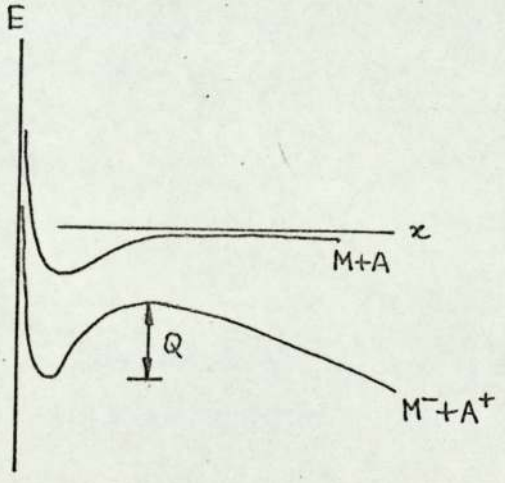

FIG. 2.11

Thus the field required to desorb a particular adsorbate depends on the work function of the surface and the temperature, As the coverage of the adsorbate increases, the field needed to desorb it increases. This is because the ions near the desorption site being considered, produce a field which opposes the applied one.

2.4. Thermionic emission

2.4.1. Introduction

Thermionic emission is the release of electrons by a heated body by reason of the temperature of the body. The emission current density depends on the work function of the surface and the temperature. If a metal is heated in vacuo to a temperature of about 2000°C, and an electrode at a positive potential with respect to the metal surface is placed near it, the current density passing through the second electrode (the anode) can be of the order of several A/cm^2.

2.4.2. The Dushman-Richardson equation

The potential energy of an electron in a solid will vary because of the varying field caused by nuclei and other electrons. In the Sommerfeld free-electron model, the electrons are assumed to be valence electrons of the atoms. The potential of a conduction electron in a metal will be constant. Such an electron will be in a potential well, the bottom of which will correspond to the energy of an electron at rest. At 0°K all energy levels up to the Fermi level will be full. The Fermi energy ranges from 2.1eV for potassium to 11.7eV for aluminium. The energy of an electron at rest outside the metal is called the vacuum level.

For an electron to escape from the metal, it must have momentum in the direction perpendicular to the surface of p_{x_0} where

$$\frac{p_{x_0}^2}{2m} = E_S$$

E_S being the height of the potential barrier. However, even if $p_x \geqslant p_{x_0}$ the electron will not necessarily leave the metal since there is a chance it will be reflected by

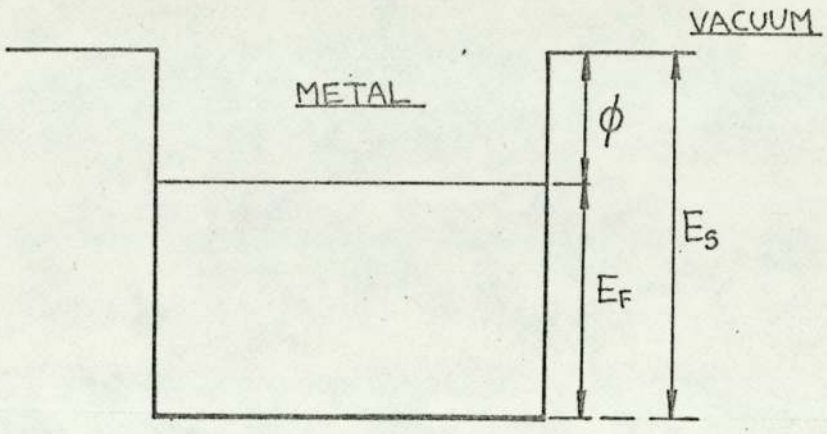

E_F FERMI ENERGY ϕ WORK FUNCTION
x DIRECTION PERPENDICULAR TO THE BARRIER.

FIG. 2.12 THE SOMMERFELD MODEL

the potential barrier. The probability of an electron escaping is therefore given by $1-r(p_x)$ where the reflection coefficient depends on the momentum in the x-direction and also on the barrier shape. The number of electrons having momentum in the x-direction between p_x and $p_x+\delta p_x$ is given by $n(p_x)\,dp_x$. The number of electrons arriving at the barrier per second per unit area is $v_x\, n(p_x)\,dp_x$ where v_x is the velocity in the x-direction.

Therefore the current density is:

$$j=\int_{p_{x_0}}^{\infty} e v_x n(p_x)[1-r(p_x)]\,dp_x = \frac{e}{m}\int_{p_{x_0}}^{\infty} p_x\, n(p_x)[1-r(p_x)]dp_x$$

An average value of the coefficient r is usually used. The number of possible energy states for an electron, corresponding to a momentum element $\delta p_x \delta p_y \delta p_z$, is

$$\frac{2\,\delta p_x\,\delta p_y\,\delta p_z}{h^3}$$

where h is Planck's constant. The number of energy states occupied is given by the Fermi function

$$F(E)=\frac{1}{\exp(E-E_F)/kT+1}$$

Therefore the number of electrons in states with momenta between p_x and $p_x+\delta p_x$, p_y and $p_y+\delta p_y$ and p_z and $p_z+\delta p_z$ is

$$\frac{2\,\delta p_x\,\delta p_y\,\delta p_z}{h^3} \times \frac{1}{\exp(E-E_F)/kT+1}$$

$$n(p_x)dp_x=\frac{2}{h^3}\,dp_x\int_{-\infty}^{+\infty}\int_{-\infty}^{+\infty}\frac{dp_y\,dp_z}{\exp(E-E_F)/kT+1}$$

For thermionically emitted electrons $E>E_F$ and $\exp\frac{(E-E_F)}{kT}\gg 1$

Integrating

$$n(p_x)dp_x=\frac{4\pi mkT}{h^3}\exp\frac{E_F}{kT}\exp\left(\frac{-p_x^2}{2mkT}\right)dp_x \qquad 2.3$$

Therefore the emission current density

$$j = A(1-r)T^2 e^{-\phi/kT}$$

where $\phi = E_S - E_F$, $A = \frac{4\pi emk^2}{h^3} = 120$ amp/cm^2/deg^2

It should be noted in applying this equation that the work function

(a) varies from one crystallographic plane to another:

(b) is different if gases are adsorbed on the emitter surface:

(c) changes slightly with temperature and electric field strength.

If the applied potential is not large enough, space charge will build up in front of the emitter.

2.4.3. Three-halves power law (Child's law)

If we consider a thermionic emitter and an anode which are both parallel planes, the three halves power law describes the relationship between the emission current density and the potential difference between the electrodes when space charge is present.

If the cathode is at $x = 0$ and the anode $x = d$ and the potentials of the cathode and anode are 0 and V_a respectively, then the potential at any point between the electrodes is given by Poisson's equation

$$\frac{d^2V}{dx^2} = -\frac{\rho}{\varepsilon_0} = \frac{ne}{\varepsilon_0}$$

where ε_0 is the absolute permittivity of the medium and n is the number of electrons per cubic metre. At a point distance x from the cathode where the potential is V, an electron of mass m and velocity v will have a kinetic

energy $\frac{1}{2}mv^2 = eV$. The current density for all such electrons will be $j = nev$

Therefore $\frac{d^2V}{dx^2} = \frac{ne}{\varepsilon_0} = \frac{j}{v\varepsilon_0} = \frac{j}{\varepsilon_0}\sqrt{\frac{m}{2eV}} = \frac{a}{V^{1/2}}$

where $a = \frac{j}{\varepsilon_0}\sqrt{\frac{m}{2e}}$. Multiplying by $2\frac{dV}{dx}$ and integrating,

$$\left(\frac{dV}{dx}\right)^2 - \left(\frac{dV}{dx}\right)_0^2 = 4aV^{1/2}$$

where $\left(\frac{dV}{dx}\right)_0$ is the electric field at the cathode. The maximum current density will occur if $\left(\frac{dV}{dx}\right)_0 = 0$

In this case

$$\frac{dV}{dx} = 2a^{1/2}V^{1/4}$$

$$V^{3/4} = \frac{3}{2}a^{1/2}x$$

The integration constant is zero because $V = 0$ at $x = 0$

At the anode $V_a^{3/2} = \frac{9ad^2}{4} = \frac{9}{4\varepsilon_0}\sqrt{\frac{m}{2e}}\,d^2j$

Thus the current density is proportional to the three halves power of the anode potential. Since $j = nev$ and the current density is independent of x, the density of electrons is greatest near the cathode where the velocity is smallest. This concentration of electrons reduces the electric field at the cathode, their electric field being directed oppositely to the applied field.

The current density is given by

$$j = 2.34 \times 10^{-6}\frac{V_a^{3/2}}{d^2}$$

where j is in A/cm^2, V_a in volts and d in cm. As the anode voltage is increased, the density of the space charge will no longer be large enough to nullify the electric field at the cathode. The current density will depart

from the three-halves power under these conditions. The limiting current density will be determined by the cathode temperature for an emitter of a given metal.

2.4.4. The velocity distribution of thermionically emitted electrons.

The velocity distribution can be derived from the Dushman equation, which gives the number of electrons emitted per cm^2 per second and the equation for the number of electrons arriving at the barrier per cm^2 per second which have velocities in the range δv_x and momentum $p_x > p_{x_0}$

The Dushman equation, assuming r=0 is;

$$N = (4\pi mk^2/h^3)T^2 e^{-\phi/kT} \qquad 2.4$$

Since $p_x = m v_x$ equn. 2.3 page 31 becomes:

$$n(v_x)v_x dv_x = \left(\frac{4\pi m^2 kT}{h^3}\right) e^{E_F/kT} e^{-mv_x^2/2kT} v_x dv_x \qquad 2.5$$

If v_{ex} represents the velocity of an emitted electron perpendicular to the surface, then

$$\frac{1}{2} m v_{ex}^2 = \frac{1}{2} m v_x^2 - E_F - \phi$$

$$v_{ex}\, dv_{ex} = v_x dv_x$$

The velocity distribution of emitted electrons $(f(v_{ex})ev_{ex})$ can therefore be derived by dividing equn. 2.5 by equn. 2.4 Hence

$$\frac{f(v_{ex})\,dv_{ex}}{N} = \left(\frac{mv_{ex}}{kT}\right) \exp\left(-\frac{mv_{ex}^2}{2kT}\right) dv_{ex}$$

which is Maxwellian.

2.4.5. Discussion of the thermionic energy distribution

Most of the experiments on thermionic emission described elsewhere were designed to test the energy analyser which was based on that of Hartwig and Ulmer.[12] Their analyser was used to investigate the Boersch[13,14] effect of thermionic emission, i.e. the broadening of the energy distribution of an electron beam which depends on the beam current. For this reason similar experiments to those carried out by Hartwig and Ulmer were done on the Boersch effect.

2.4.5.1. The energy resolution of an analyser

The thermionic emission distribution is Maxwellian and the total average energy of the emitted electrons is 2kT. Although the measured width of the energy distribution should be the same as the theoretical width, it is usually broader, and experiments have been carried out by many workers to explain this.

The energy resolution of an energy analyser is $e\Delta V$ which is the smallest energy difference which can be resolved by the analyser. It is proportional to the energy of the electron beam eV. The specific energy resolution of the analyser can be defined as $\Delta V_a/V$ where ΔV_a is the halfwidth of a perfectly homogeneous electron beam of energy eV. In practice the thermal distribution of velocities of electrons in the beam and the electron optics of the accelerating field will cause ΔV_a to be broadened to say ΔV_b. The Maxwellian form of the energy distribution can be written as:

$$f(x)\,dx = x\,e^{-x}\,dx$$

where x=eV/kT; k is the Boltzmann constant and T the absolute temperature.

$$f(x) = \frac{n(eV)}{n_e}$$

where n is the number of electrons having energies between eV and eV+edV and n_e is the total number of electrons. The halfwidth of the energy distribution is given by:

$$\Delta V_b \approx 0.21 \times 10^{-3} T$$

where T is in degrees Kelvin. Boersch defined a halfwidth ΔV_{63} which corresponds to the smallest energy interval containing $(1-\frac{1}{e})n_e \approx 63\%$ of the total number of electrons n_e. This can be determined from the normalised integrated energy distribution which is obtained from the graph of the collector current against the retarding potential.(See Chapter 3.)

$$\Delta V_{63} = 2kT/e = 0.172 \times 10^{-3} T$$

therefore for a thermionic emitter at 2500°K, the best resolution obtainable would be 0.43eV. Boersch and others found that if electrons are allowed to form a beam before being analysed, the energy distribution is no longer Maxwellian; it is much wider than would be expected from the above equation, corresponding for example to a cathode temperature of 30 000°K. The bandwidth corresponding to the actual temperature is only obtained at current densities less than 10^{-9}A/mm^2.

Hartwig and Ulmer found that the distribution of electron velocities in the acceleration region is not an equilibrium one, whereas the one in the transverse direction is. They assumed that after the electrons pass through the accelerating region, they interact to bring about an equilibrium distribution in the coordinate system moving

with the mean velocity of the beam, which is Maxwellian. The new distribution as measured by the analyser is broader and more symmetrical. The energy broadening can be represented by

$$\frac{\Delta V_{63} - \Delta V_o}{\Delta V_o} = \text{constant} \times \frac{j^{1/3}}{V^{1/6}}$$

where j is the saturated beam current density, i.e. the current density at the collector when no retarding field is applied and ΔV_o is the bandwidth for very small current densities (corresponding to the temperature of the cathode). Thus the broadening of the energy distribution depends on the current density, the accelerating potential and the filament temperature.

Later workers have criticised Hartwig and Ulmer's explanation of broadening. Simpson and Kuyatt[15] pointed out that the mechanism whereby the electrons reach equilibrium is not explained and that the electron densities used in the experiments are too small to give Coulomb interaction. In addition Hartwig and Ulmer's experiments were performed at 10^{-6}Torr, at which pressure ions might affect results.

CHAPTER 3. Energy Analysers

3.1. General

The measurement of the energy distribution of field-emitted electrons depends on the assumption that the energy of the electrons does not change during the emission process. When an electric field is applied to an emitter, its potential barrier narrows and if the electrostatic field is strong enough, electrons will be able to tunnel through the barrier. In order to obtain a field of the required strength (about 4×10^7 Vcm^{-1}), the emitter is made into the shape of a needle and the anode, which is a short distance away, is usually at a potential of between 1000 and 5000V with respect to the emitter. The field-emitted electrons come from the region around the Fermi level of the cathode. Figure 3.1 is a schematic potential energy diagram for the field emission analyser. After being accelerated towards the anode, the electrons pass through a hole in it and are then retarded in the region between the anode and the collector. If the cathode is at 0 V and the potential of the collector is then varied, at a particular bias corresponding to the work function of the collector, electrons will just be collected. Thus if the current flowing in the circuit is measured as a function of the potential difference between the metal emitter and the collector, at a voltage difference equal to the work function of the collector, the current will sharply increase.

The ideal cut-off integrated energy distribution curve is shown in figure 3.2 , curve 1. However this curve would only occur for monoenergetic electrons at 0°K. In practice the ideal cut-off does not occur because some

Schematic potential energy diagram for a field-emission analyser

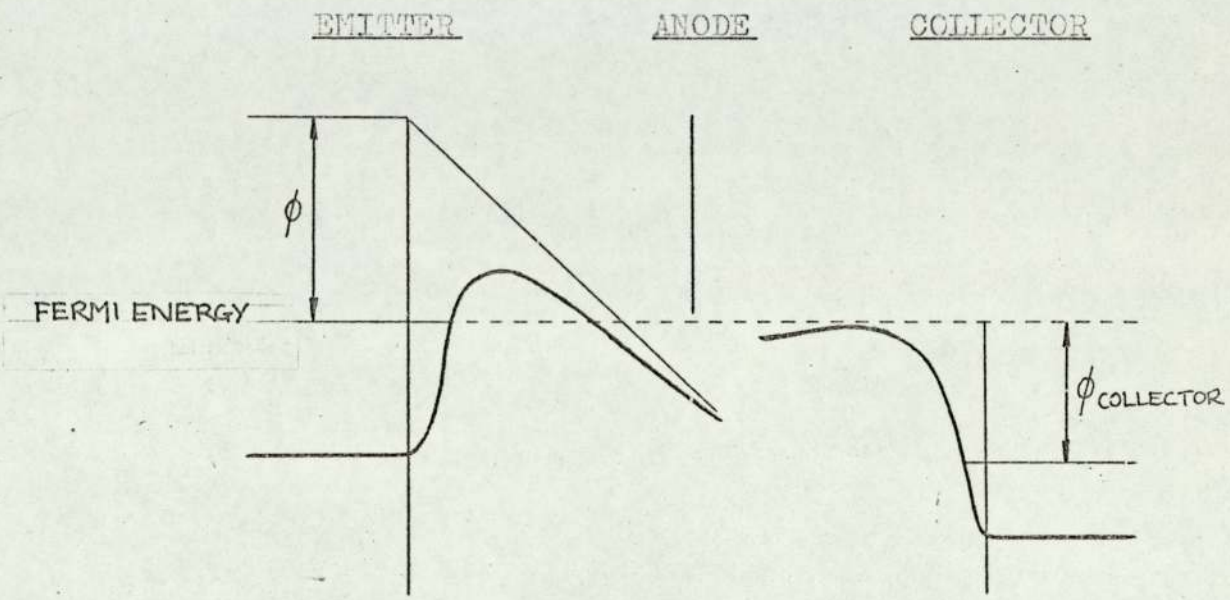

FIG. 3.1

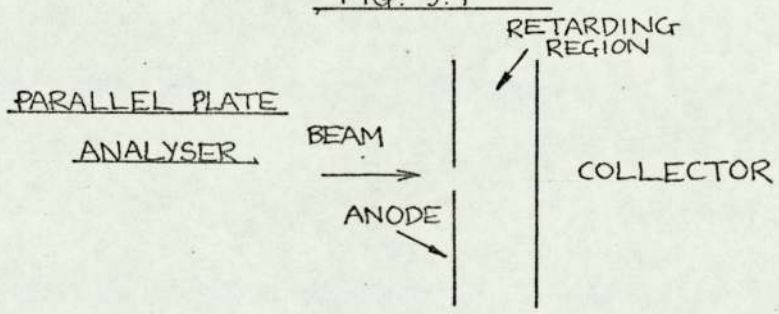

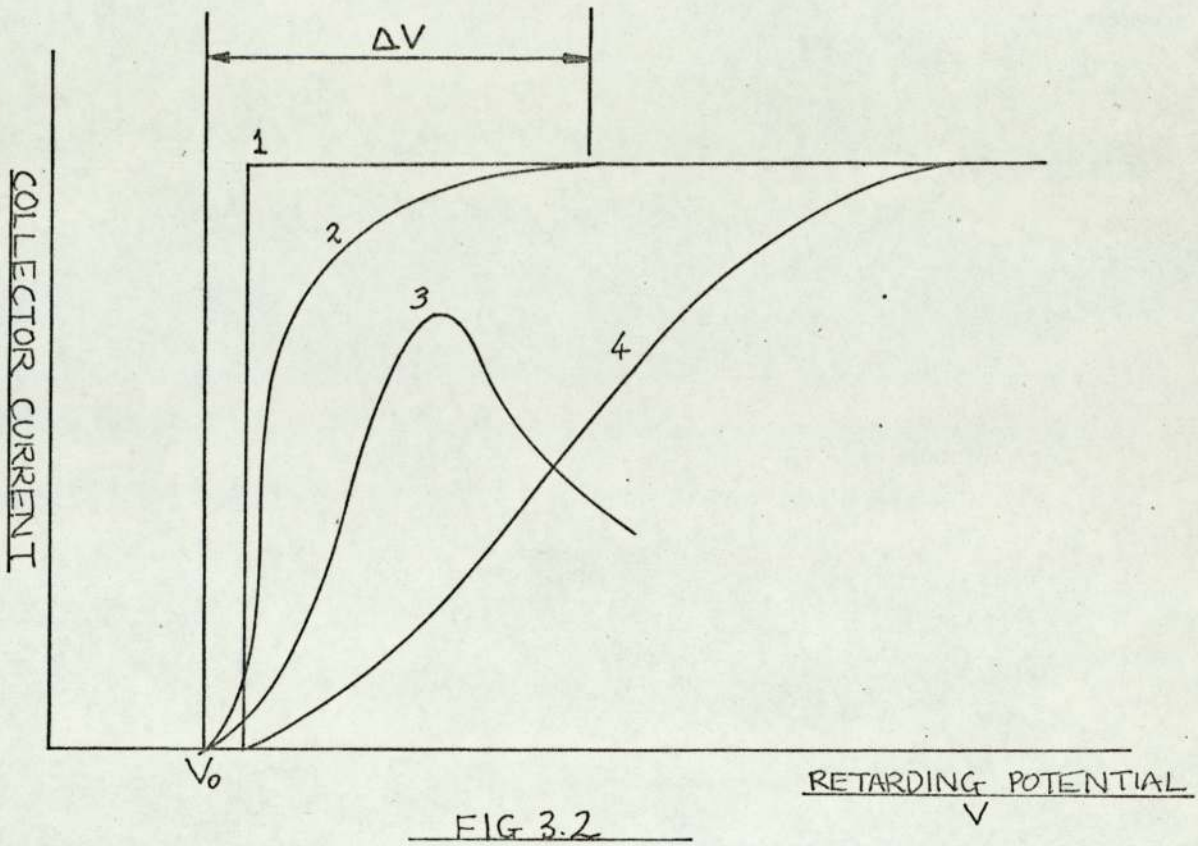

FIG 3.2

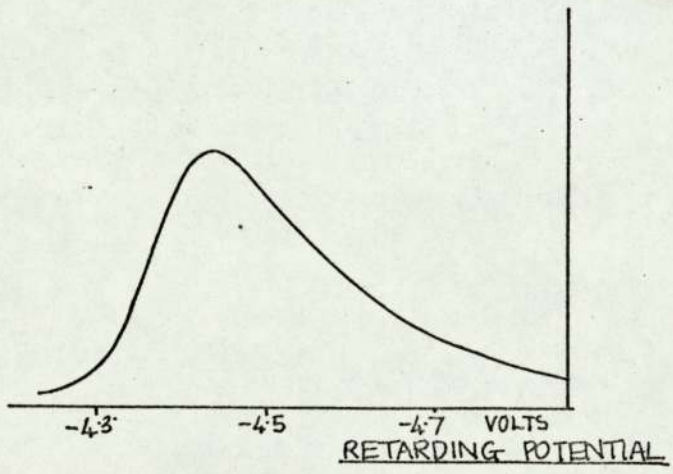

FIG. 3.3

Fig.3.2 Integrated energy distribution

Curve 1 Ideal
2 At a temperature above absolute zero
3 With secondary emission at the collector
4 Tip off-axis

Fig.3.3 Typical total energy distribution

electrons are always emitted from below the Fermi level and some from above it at temperatures above $0^{\circ}K$. Curve 2 illustrates this.

The current density, which is given by the Fowler-Nordheim equation is

$$j = e\int P(E)\,dE$$

Where $P(E)\,dE$ is the total energy distribution, e the electronic charge and j the current density. In terms of the potential difference V between the emitter and collector,

$$i_{COLL.} = \int_{\phi_{COLL.}-\phi_{tip}+V}^{\infty} P(E)\,dE$$

or $$\frac{di_{COLL.}}{dV} \approx P(\phi_{COLL.} - \phi_{tip} + V)$$

where $\phi_{COLL.}$ is the work function of the collector

ϕ_{tip} is the work function of the tip.

Thus if the collector current is plotted as a function of the emitter to collector bias, and the resulting curve is differentiated, the total energy distribution will be obtained. A typical total energy distribution curve is shown in figure 3.3.

In order to measure the total energy of the emitted electrons and not just a component of the energy, it is necessary for them to arrive perpendicularly to the collector. In this case the electrons will exchange their kinetic energy for potential energy. For monoenergetic electrons, the curvature of the equipotentials in front of the collector is only critical in that it determines the path of the electrons as they approach the collector. Thus if we imagine a given electron as ascending a potential

hill as it loses kinetic energy, it does not matter what path the electron takes up the hill, provided that it reaches the top perpendicularly. If the electrons do not arrive perpendicularly to the collector, the energy distribution will be broader than that predicted by theory (Young 1959)[1].

Sometimes the broadening of the total energy distribution is shown in the integrated distribution as a falling off from saturation. In addition the integral curve shows a slope on the rise which is the result of trajectory effects. The width ΔV (see figure 3.2) can be taken as a measure of the resolution of the analyser. One of the factors limiting resolution in a parallel plate analyser is the fact that a beam of electrons will have a finite angular aperture θ which is the deviation from the axis of the most inclined electron trajectory. In order to see how this affects the resolution we consider the electron kinetic energy as being made up of transverse and axial parts. The transverse component will determine the resolution of the analyser. For electrons of energy eV_0

$$\frac{\Delta V_0}{V_0} = \frac{\Delta E}{E} = \frac{\frac{1}{2} m v^2 \sin^2\theta}{\frac{1}{2} m v^2} = \sin^2\theta$$

where :

V_0 is the cut-off potential (see fig.3.2)

E is the electron energy

m is the mass of an electron having velocity v

It would appear that by reducing the angle θ using a small aperture, we could improve the resolution. However this is not the case because in all analysers there is a lens effect which sets a lower limit to ΔE .

The focal length of the lens is given by: $\frac{1}{f} = \frac{(E_2 - E_1)}{4V_0}$ where E_2 and E_1 are the electric field strengths on either side of the aperture and the electrons have energy eV_0. Therefore if $E_1 \approx E_2$, the power of the lens will be very small. This principle is applied in Hartwig and Ulmer's analyser (see section 3.2.1.1.).

3.2. Types of analyser

In seeking a suitable design for a field-emission energy analyser the following points were considered. It should have a good resolution, be simple to construct, be suitable for ultrahigh vacuum and have negligible secondary emission.

There are basically three kinds of electrostatic retarding potential analyser depending on the location of the retarding field with respect to the collector, and the collector potential.

(a) Those for which the retarding field is in front of the collector, in which case the collector potential is gradually raised to the cathode potential and the energy distribution is measured. This group can be subdivided into those with a plane collector and those with a hemispherical collector.

(b) The filter type which has a collector at anode potential and a lens in front which is gradually increased in negative potential, filtering out more and more energetic electrons as the potential is raised.

(c) The third type of analyser is the inverse retarding field analyser. This has a Faraday cage with an entrance and exit aperture. The electrons pass through the cage to a retarding potential electrode which reflects back electrons

of progressively higher and higher energy into the collector cage as the retarding potential is increased.

3.2.1. First type

3.2.1.1. Plane collector

In the design of the electrodes for the retarding region two factors need to be considered:

(a) there is a small immersion lens formed between the aperture stop preceding the collector cage and its entrance. This lens tends to diverge the beam and so the entrance to the cage needs to have a slightly bigger diameter than that of the stop. It is found that beyond a certain critical distance from the axis of the lens, electrons are reflected back which, if they were paraxial, would reach the collector. The power of the lens can be reduced by increasing the diameter of the entrance aperture of the collector cage, in which case the critical diameter will be increased.

(b) If the incident beam is strong, a high percentage of secondary electrons will be emitted from the walls of the collector. These can be prevented from escaping and thereby causing an erroneous current reading, by keeping the entrance aperture of the cage as small as possible.

One possible solution would be to cover the opening of the cage with a fine mesh. However, unless this is kept clean it will cause difficulties. In addition the mesh itself would lead to secondary emission and there would be a lens effect at each opening in the mesh.

The two effects (a) and (b) are contradictory and in practice a compromise has to be found.

Boersch (1954)[2] designed an analyser having a resolution of 0.004 eV for 60 keV electrons. It had an aperture stop of 0.1 mm in diameter and the beam had a diameter smaller than the minimum distance mentioned above. Boersch found that there was an optimum cage aperture diameter which was 2/5 of its distance from the aperture stop. This analyser was thought unsuitable in this work because the beam defining aperture was very small and this would severely reduce the magnitude of the collector current. Also it would need a collimating system since it was designed for a parallel beam. Fig.3.4.

Haberstroh (1956)[3] designed an analyser for 45 keV electrons with a collimating system consisting of a 0.1 mm aperture, a drift space of 1.2 m, followed by two small apertures C and D and a cylinder E. These were all at anode potential. G, H and the cage I were at near cathode potential. The cylinder E was to reduce the possible lens effect at the aperture D. Fig.3.5.

In this design, as the beam leaves E it is slightly divergent. However G has a slightly converging effect and so the beam enters the collector cage normally.

The initial defining aperture is too small to be easily constructed. Also it would severely reduce the beam current which already is small in field-emission. This analyser would need to incorporate a collimation system and the whole device would need to be scaled down, leading to a reduction in resolution, and therefore was not chosen.

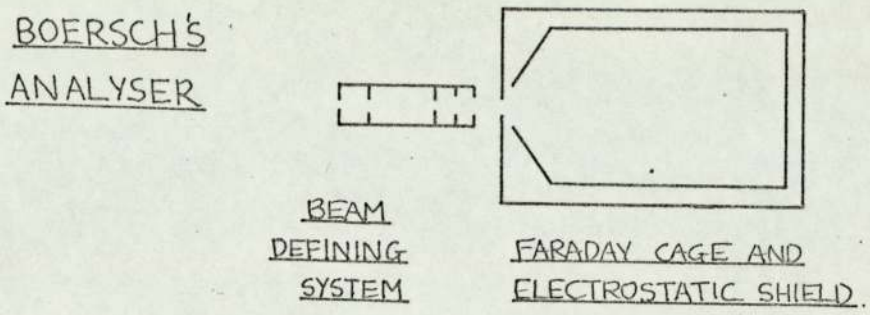
BOERSCH'S
ANALYSER
BEAM
DEFINING
SYSTEM
FARADAY CAGE AND
ELECTROSTATIC SHIELD.

FIG. 3.4.

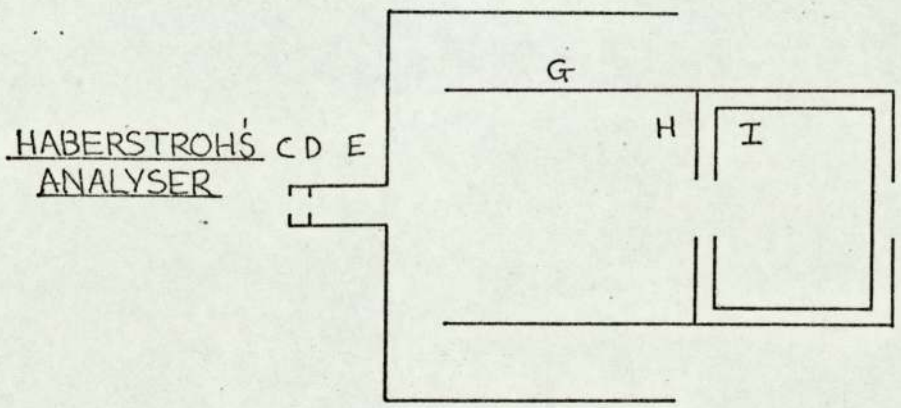
HABERSTROH'S
ANALYSER
C D E
G
H
I

FIG. 3.5

Holscher (1966)[4] designed an analyser for the measurement of collector work function. Electrons from a field emitter at -4.5V passed through an aperture stop 1 mm in diameter at an anode potential of 600 V. The potential of the second aperture was varied in order to make the electrons arrive normal to the collector to give a true measurement of their total energy. The third electrode was at 600 V and the fourth was an aperture stop of 1 mm diameter; this was at a low potential of 7.0 V so that the small potential gradient between this electrode and the collector, minimised errors due to surface roughness of the collector and any non-perpendicularity of the collector to the axis. As for the analyser of Young and Muller[5]*, there was a drop in collector current for very high anode voltages. The resolution was found to be about 0.03 eV. Fig.3.6

Hartwig and Ulmer (1962)[6] designed an analyser for thermionic emission. A beam of electrons was produced by a simple Wehnelt cylinder gun which was then accelerated to the first aperture of the anode cylinder. This aperture and the second one were each 1 mm in diameter and about 5.25 cm apart. Their purpose was to produce a collimated beam. The beam then passed through a small aperture 0.5 mm in diameter, then through a 10 mm tube 4 mm in diameter, and reached the aperture of a Faraday cage. The retarding region was in front of the Faraday cage which was about 1.5 mm behind the last anode aperture. The cage was surrounded by a shield at anode potential. The analyser will only function correctly if the effect of the lens formed at the 0.5 mm diameter aperture in the retarding region is as small as possible.

* See page 46.

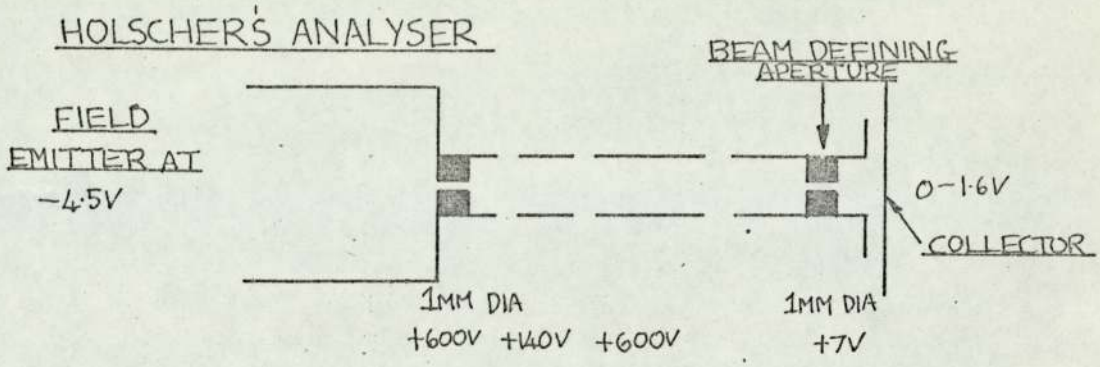

FIG. 3.6

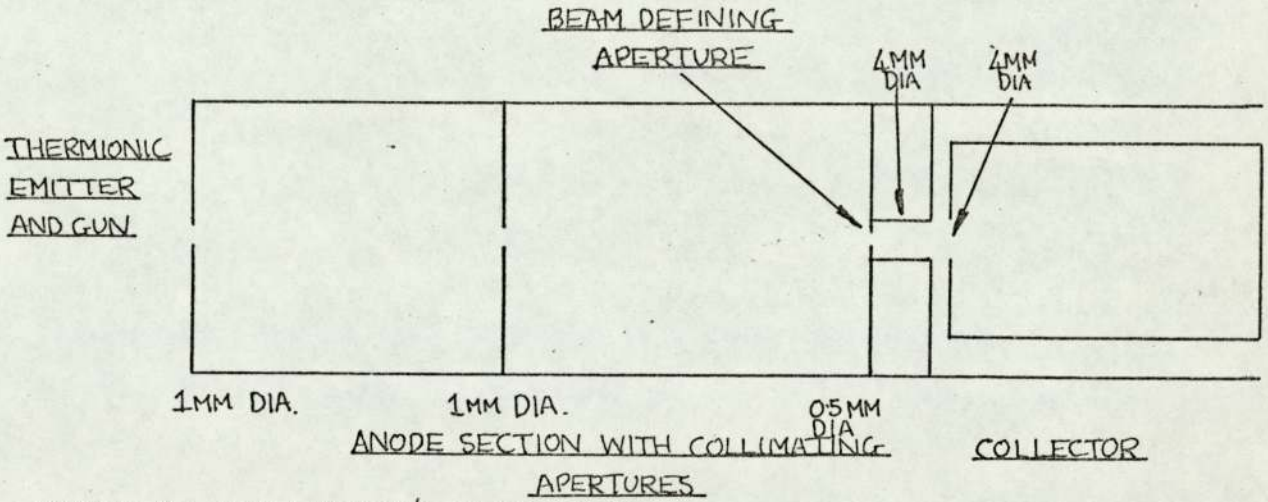

HARTWIG AND ULMER'S ANALYSER

FIG. 3.7.

In order to achieve this, the 0.5 mm diameter aperture was separated from the retarding potential region by a tube 10 mm long, 4 mm wide, which was at anode potential. Fig.3.7.

Plummer and Young [7] constructed an analyser with a collector which incorporated an electron multiplier, figure 3.8. . Emitted electrons were imaged on a phosphor coated electrode with an aperture of 0.08 inches which was at a high potential. Beyond the aperture there was a short field-free cylinder to reduce the lens effect at the aperture. The beam was then focused to form a parallel beam and retarded by a series of cylindrical rings at progressively decreasing potentials and a 1000 line / inch flat mesh. The transmitted electrons were focused on the first dynode of an electron multiplier.

The mesh was flat to within 1/1000 inch and was coated with platinum black to give a unipotential surface. The product of the mesh size and the difference between electric fields above and below it, limited the resolution to about 8 meV. Electron optical effects also limited the resolution. These were minimised by the field free cylinder below the first electrode and also by making the electrode diameters very much greater than that of the beam. The overall resolution was about 10 meV.

The system had an electrostatic deflection lens to deflect emitted electrons from chosen planes to the probe hole.

PLUMMER AND YOUNG'S ANALYSER

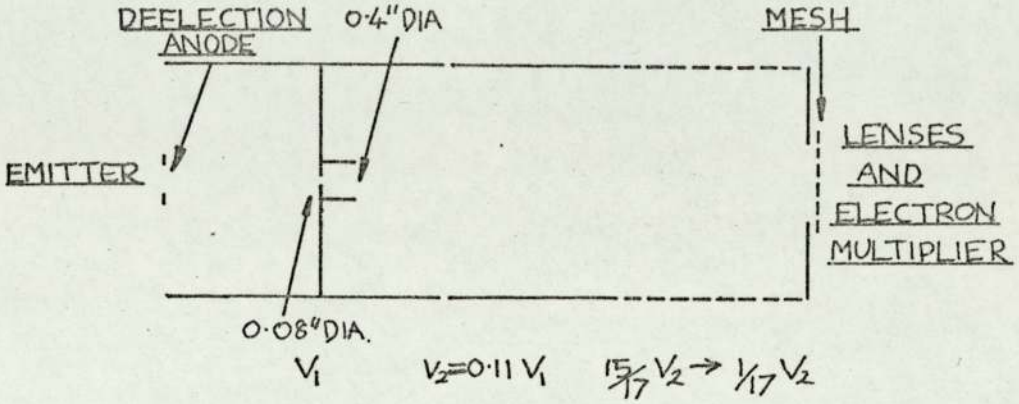

FIG. 3.8

Both the incorporation of an electron multiplier in the analyser and the fact that its design was optimised using a computer led to a high sensitivity. A useable energy distribution could be obtained with a total current through the probe hole of only 10^{-13}A, and the arrival of a single atom on the surface was easily recognised as a sharp increase in current.

3.2.1.2. Spherical collector

If the electron beam is very narrow, e.g. from a point source, but has a finite angular aperture, it can be analysed by a spherical analyser. In this type of analyser the electrons come from a real or virtual point source at the centre of a hemisphere.

Young and Muller[8] used a spherical retarding analyser which had an aperture stop of 1.5 mm diameter, a focusing cylinder, a large anode aperture, and a spherical collector. The anode voltage was adjusted to give zero field at the 1.5 mm aperture, thus reducing the lens effect at this aperture. The electrons pass through the focusing cylinder, the potential of which is adjusted to produce a beam which appears to diverge from the centre of the spherical collector, and thus arrive perpendicular to the collector. Fig. 3.9.

They found that as the retarding potential was decreased, the collector current did not stay constant but dropped off. They attributed this to the secondary emission of electrons at the collector and they corrected their curves to suit the theoretical ones, by introducing an exponential curve. The resolution for tungsten emitters was 0.02 to 0.03 eV. (3 parts in 100 000).

Arthur (1964)[9] built an analyser based on that of Young and Muller[10] having a resolution of 0.05eV. It consisted of an aperture 0.08 inches in diameter followed by a narrow collimating tube, then a spherical anode aperture of relatively large diameter and a spherical collector. The lens effect at the large anode aperture causes the beam to diverge and when the emitter is positioned correctly, the electrons appear to be leaving a point at the centre of the small aperture. The centre of the collector is at this point and so electrons reach it normally. In order to reduce the effect of electrons entering the small aperture with transverse momentum, the collimator was included. As this analyser is like that of Young and Muller it would be thought that there would be secondary emission: however this is not mentioned by Arthur. Fig.3.10.

Van Oostrom (1965)[11] also used an analyser with a hemispherical collector. The analyser consisted of an anode at potential V_A followed by a focusing electrode, and a collector surrounded by a shielding electrode at a near ground potential. The beam is focused in the region of the centre of the collector, as the potential of the middle electrode V_L is varied. All the electrons passing through the centre arrive perpendicular to the collector and have their total energy measured. The collector was kept near earth potential and the potential of the cathode was varied to obtain the energy distribution. The ratio of the potential of the middle lens to that of the anode was found to be an important quantity since it determines whether or not primary electrons are reflected.

Van Oostrom realised that reflection of primary electrons could cause errors so he tried to reduce the

YOUNG AND MULLER'S ANALYSER FIG. 3.9

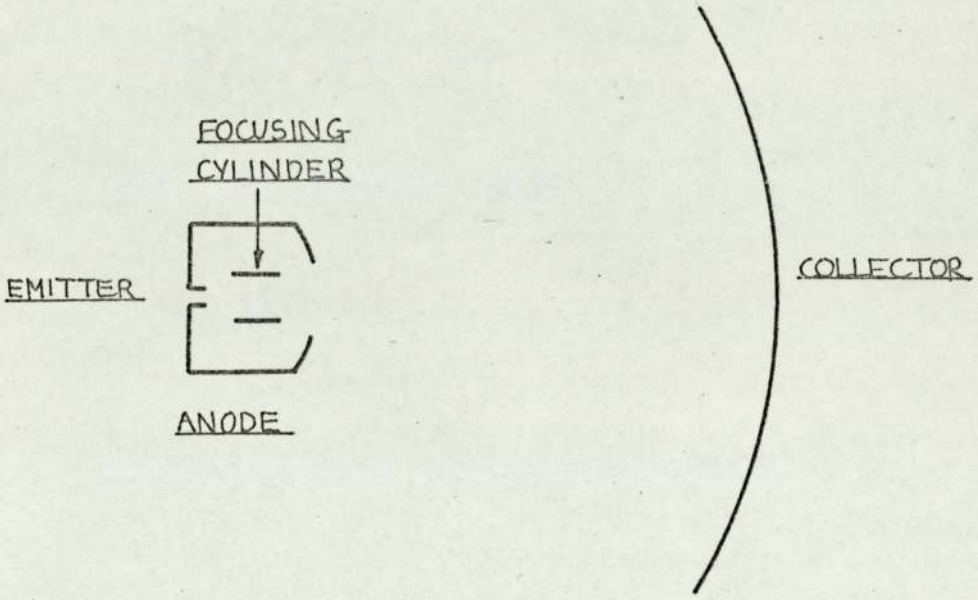

ARTHUR'S ANALYSER FIG. 3.10

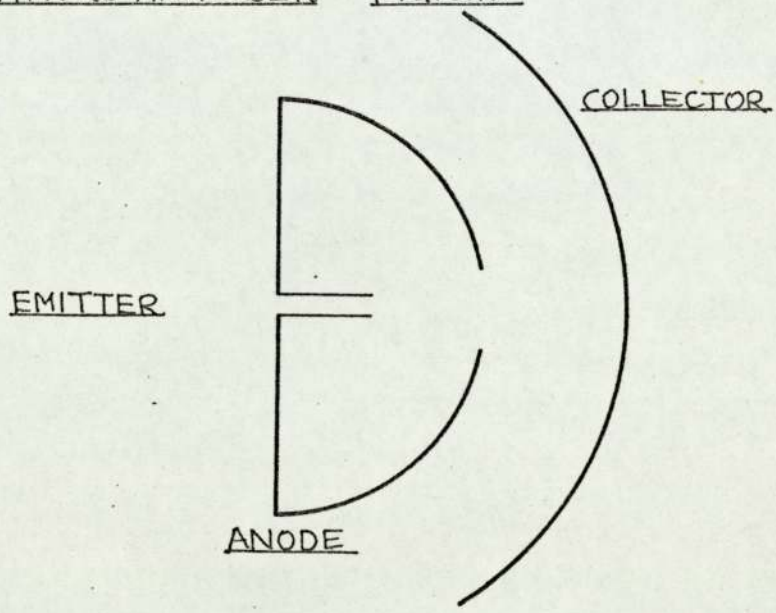

VAN OOSTROM'S ANALYSER

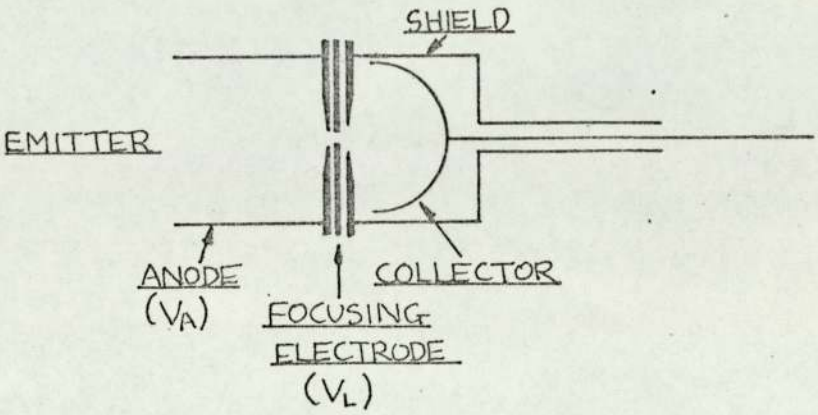

FIG. 3.11

reflection coefficient by reducing the potential at the entrance of the Faraday cage. For values of V_L/V_A greater than 0.25, the graphs of collector current against retarding potential show a drop with decreasing collector voltage. Thus Van Oostrom used a low value of V_L/V_A. The energy resolution of the analyser was 0.01 eV. Fig.3.11

3.2.2. Second type

The second type of energy analyser is the filter type. The negative electrode is in front of the collector which is at anode potential, as the negative potential is reduced, more energetic electrons pass through and are collected.

One of the simplest types of filter analysers consists of a collimating aperture, a gauze covered aperture, a further collimating aperture, and a Faraday cage. The electrons enter the filter as a slightly divergent beam but a tube surrounding the gauze produces slightly curved equipotentials thus the electrons arrive at the gauze perpendicularly. For a fine mesh the potential at the centre of a hole is only slightly less than that of the mesh itself, and so the total energy of the electrons can be measured by varying the potential of the gauze. The collector current is measured as a function of the gauze bias. However, this analyser needs a beam which is already collimated unless a collimating system is to be constructed in front of the filter. Thirlwell [12] (1964) placed an additional collimating aperture in front of this filter and obtained a poor resolution.

Frost [13] (1958) used an Einzel-lens as a velocity filter which does not have a gauze. For a parallel beam,

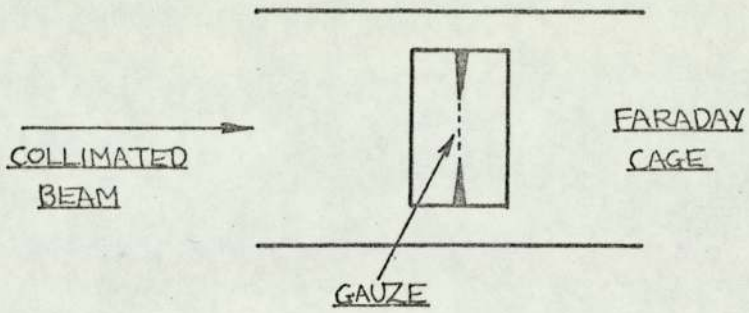

FILTER TYPE FIG. 3.12

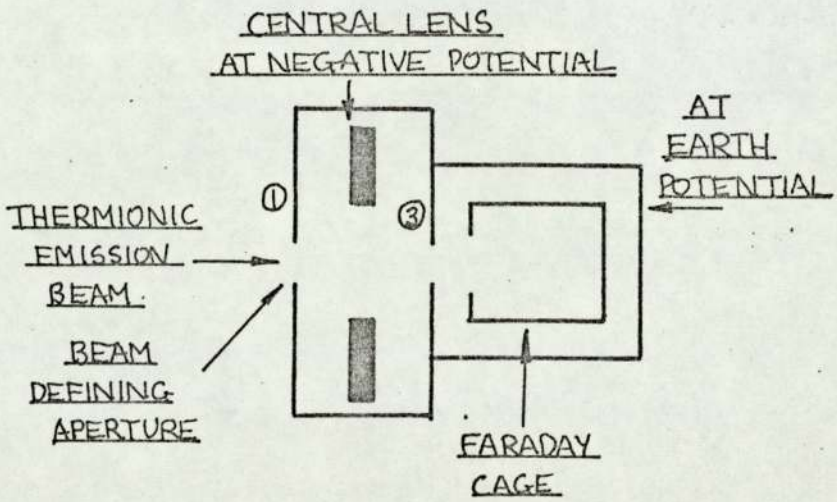

FROST'S ANALYSER FIG. 3.13

① AND ③ ARE AT THE SAME POTENTIAL.

Fig.3.13 This is an einzel lens. The central electrode is at a lower potential than those on either side, giving a saddle field.

the resolution was found to increase as the beam became narrower, e.g. for a front aperture of 0.01 mm diameter, the resolution was 1 in 10^4. For the centre lens, the negative potential gradually increases with distance from the centre, and so electrons near the axis will pass through the filter when those far away will be reflected. The central electrode is quite thick because the saddle field becomes flatter with increasing thickness of this electrode and with increasing diameter of its aperture. As mentioned before, the best resolution of this filter is obtained for small beam diameters which means that the collector current will be small. In Frost's design the resolution increased with decreasing beam diameter, a beam diameter of only 0.5 mm giving a poor resolution. An electron multiplier was needed to measure the current. Thus because of the very small currents produced by having to use such a small beam, this type of analyser was not chosen. Fig.3.13.

Simpson and Marton (1961)[14] designed a filter lens of five electrodes. The first and the last apertures were at earth potential and were wide, the second and fourth were larger, and the central one was small. The middle three were at a high negative potential which could be varied. This system forms two immersion lenses back to back with their focus at the centre of the saddle of the central lens. Thus before reaching the saddle, the beam is decelerated and after leaving the saddle, it is accelerated to the original energy. As the negative potential of the central electrodes is varied, the energy of the beam can be determined. This filter provides a good resolution for a

SIMPSON AND MARTON'S ANALYSER FIG. 3.14

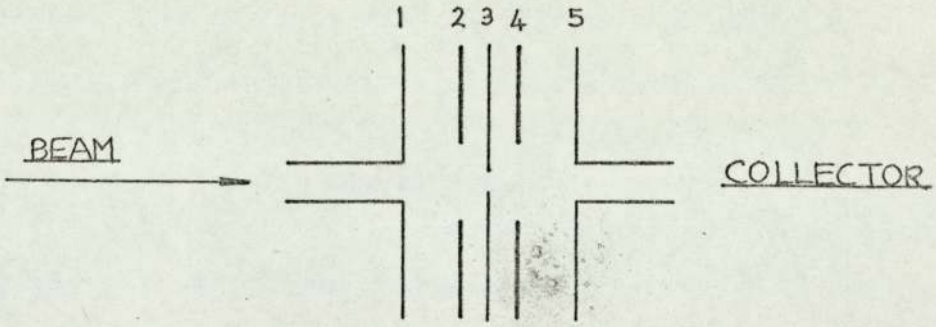

1 AND 5 EARTHED
2, 3 AND 4 AT A VARIABLE HIGH NEGATIVE POTENTIAL

BECK AND MALONEY'S ANALYSER FIG. 3.15

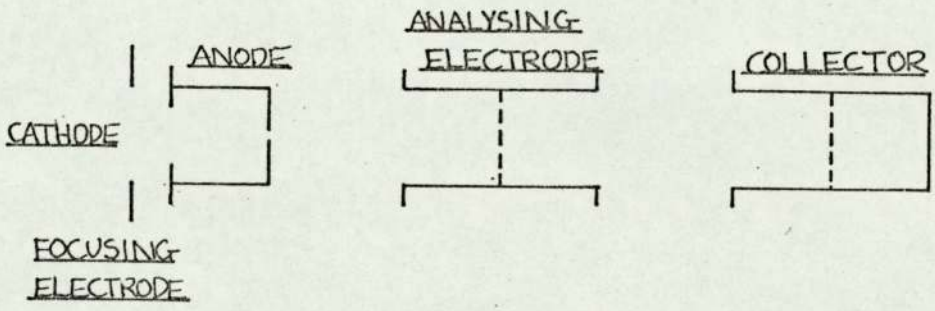

relatively wide beam. Fig.3.14.

In 1967 Beck and Maloney[15] designed an analyser which they claimed was an improved version of the Boersch type. It is similar to Frost's arrangement but the thick central lens, which was introduced to reduce the high negative potential needed to reduce the axis potential to zero, is replaced by a gauze. The anode, which is at earth potential, was designed to reduce the lens effect at the anode aperture, by the inclusion of a cylindrical section between the cathode and the small aperture. The cylindrical analysing electrode is beyond the anode, with the mesh grid at its centre. Following this is the collector cage with a grid mesh to reduce the influence of reflected primary electrons. Fig.3.15.

3.2.3. Third type

The inverse retarding field analyser works on the principle that the beam is allowed to pass through the collector cage before being reflected by the retarding potential back into the cage. A collimated beam first passes through a defining aperture and then the collector, both being at anode potential (earth). The beam then enters a cage which is at high negative potential. Electrons having energy less than the potential applied to this cage are reflected and collected in the collector cage. The collector current is measured as a function of the potential of last cage. (See Boersch and Schweda[16]). Fig.3.16.

The current measured in the collector cage for the high energy side of the spectrum is small, and so a high sensitivity range of the current measuring instrument can be used. Similarly by measuring the current in the last cage, a good measurement of the low energy part of the

BOERSCH AND SCHWEDA'S ANALYSER

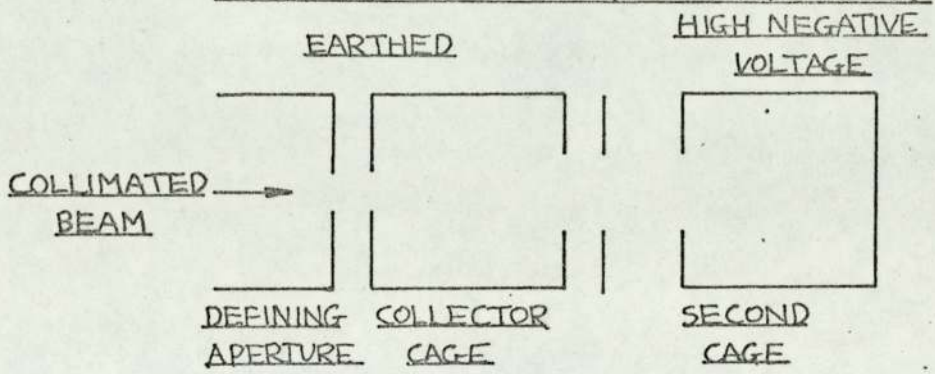

FIG. 3.16

spectrum can be determined. Fluctuations in the beam current can be detected by running the currents from the two cages. This analyser is more useful for high energy beams than for field-emission ones. Unfortunately the first aperture of the system is small, thus limiting the beam currents and also there are eight further apertures, the arrangement of which is complicated.

3.3. Measurement of the total-energy distribution of field emitted electrons.

Before 1958 good agreement had been found between normal energy theory and experimental results for field emitted electrons. However, in 1958 Young and Muller[17] designed an analyser of greater resolution than previous ones. They used tungsten emitters and were able to show that the retarding potential analyser measured the total energy distribution which is about one third as wide as the predicted normal energy distribution.

Their analyser was the spherical type and had a claimed resolution of 0.03eV which was the difference in energy between the peak of the experimental total energy distribution and the theoretical distribution determined by Young. However, they had to introduce an empirical correction to allow for electrons reflected at the collector.

Following the work of Young and Muller, experiments on metals and semiconductors led to distributions which were wider than those predicted by Stratton (1964)[18] at the ambient temperature. Limited resolution, bad alignment, emission from too large a tip area and the hot electron process have all been claimed as causes of wide distributions.

Russell (1963)[19,20] measured the distribution from fractured silicon tips. The resolution of his analyser was claimed to be about 0.09eV. He measured the distribution from a tungsten emitter and found it to be 0.6eV which is three times the half-width measured by Young and Muller at room temperature. The distribution from silicon was also wide, being about 0.4eV for the valence band, and 0.9eV for the conduction band. These discrepancies were too big to be due to the limited resolution of his analyser, and are

probably caused by other experimental errors.

Russell reported that as the field on the tip was increased from zero, field emission came from the valence band. There was a constant internal potential drop V_i and the value of the Fermi level at the surface indicated that it was p-type. The distribution was again too wide. As the field was increased the V_i drop increased; however there was no emission from the conduction band thus there was no field penetration. Russell attributed the rise in V_i to an IR drop in the emitter shank. Since Russell's work, no one has reported emission from the valence band, which puts some doubt on his results.

Shcherbakov and Sokol'skaya (1963)[21,22] investigated the energy distribution of field emitted electrons from cadmium sulphide and showed that the energy broadening resulted from heating of the electron gas and carrier generation which was caused by an increase in the internal field. The creation of strong fields within the emitter was due to the passage of electric current through the high resistance material.

Their energy analyser was like that of Young and Muller. It was tested by using it to obtain the total energy distribution for tungsten. Shcherbakov and Sokol'skaya found that the width of the distribution for tungsten depended on the position of the emitter tip. In order to take account of secondary electrons, a wide range of retarding potentials were used and two different materials were chosen as collectors. Each graph of collector current against retarding potential showed a saturation region. Shcherbakov and Sokol'skaya assumed that the number of slow electrons which were reflected was therefore small and could be

neglected. The half-width of the distribution for tungsten was 0.25 to 0,28eV at room temperature which should be compared with a theoretical width of 0.22eV. The curves show a decrease in collector current as the retarding potential increased; this was due to reflection of higher energy electrons and a correction for reflection would result in a smaller value of the half-width, thus the effect of reflection should not have been neglected.

Shcherbakov and Sokol'skaya measured the emission from cadmium sulphide. As the internal field in the emitter increased, the spectra broadened and the distribution maxima moved towards higher electron energies. The broadening of the energy spectra was associated with the departure from linearity of the current-voltage characteristics. Heating of the tip due to the passage of large currents was not responsible for this non-ohmic behaviour since only low emission currents were used. When the emitter was heated to 700°C, the over-all energy distribution width was 2.3eV; however, in the presence of a strong field, the energy width increased to 4eV; thus wide distributions were primarily caused by high fields, and not by high temperatures. The increase in potential drop at the emitter led to an increase in the energy of the electrons. The probability of barrier penetration depends on energy and so as the potential drop at the emitter increased, so did the emitter current. However, as Stratton (1964)[18] pointed out, even for a very small internal potential drop, unusually wide half-widths were observed. Also further increases in the half-widths occurred before the internal fields were high enough to lead to changes in the conductivity.

Arthur (1964)[23] obtained the energy distribution of field emitted electrons from germanium. The analyser used was based on that of Young and Muller[8] and had a resolution of 0.05eV. The surface of the emitter was atomically clean and the crystals were doped forming various types from degenerate n to degenerate p. For 0.0006 ohm-cm p-type germanium, an energy distribution was obtained which corresponded to the theoretical distribution for emission from a degenerate conduction band. The high energy tail altered slightly with temperature. Partial annealing of the tips at 500°K was found to reduce the width of the distribution. Two curves were given for 0.06 ohm-cm p-type germanium showing:

(a) the distribution after partial annealing and

(b) the distribution after the tips had been subjected to field evaporation.

The first curve was broader than the second and had a secondary peak or "shoulder" about 0.15 V below the main one. The second curve was also broad but field evaporation had removed the secondary peak. Arthur supports the observation that the distribution was consistent with a degenerate conduction band by saying that the emission occurred from just below the Fermi level and did not depend on doping or temperature. This is consistent with Stratton's theory (1964)[18].

The second peak of Arthur's distribution was dependent on the tip position and surface treatment (since field evaporation removed it). Stratton's theory (1962)[24] predicts that the conduction band edge should be about 0.3 V below the Fermi level; however all Arthur's distributions show emission from below this value. He suggested that as the distribution was apparently so sensitive to surface

treatment, then perhaps the broadening on the low energy side of the distribution was due to emission from surface states. Arthur pointed out that arguments against this were:

(a) that there was evidence of surface degeneracy which would place an upper limit of 10^{13} surface states per cm^2:

(b) that adsorption of oxygen did not alter the emission, although it must have altered the surface states.

Arthur's results outlined above were obtained with no internal field in the crystals. Thus no electron heating was possible for these crystals. However, for p-type crystals at higher current densities, large internal fields did develop and the distributions were wider, indicating hot electron emission.

Swanson and Crouser (1967)[25] measured the field emission from several crystallographic planes of tungsten to investigate the effect of band structure on the distribution of emitted electrons. They considered a form of Stratton's equation:

$$J(\epsilon) = \frac{J_0}{d} f(\epsilon) e^{\epsilon/d} \left[1 - \frac{1}{2\pi} \int_0^{2\pi} \exp\left(- \frac{E_m}{d} \right) d\phi_p \right]$$

where $J(\epsilon)$ is the field-emission current density per unit total energy ϵ relative to the Fermi level $\epsilon = E - E_F$

$f(E)$ is the electron distribution function

E_m is the maximum value of E_{yz} perpendicular to the emission direction x for a specified energy surface ϵ and polar angle ϕ_p in the yz plane. When E_m is large $E_m/d \gg 1$ the above equation becomes:

$$J(\epsilon) = \frac{J_0}{d} \left(\frac{e^{\epsilon/d}}{1 + e^{\epsilon/pd}} \right)$$

where J_0 is the current density at 0°K. $p = \frac{RT}{d}$

d depends on the rate of change of the tunnelling probability with ϵ ;

$$d = \frac{\hbar e F}{2(2m\phi)^{1/2} t(y)}$$

ϕ is the work function and the other symbols have their usual meanings.

Band structure effects only contribute to the emission through the integral. When E_m is about the same magnitude as d or smaller, band structure effects will be important. d is typically 0.1 — 0.2eV and so E_m will need to be less than 0.2eV. Thus for band structure effects to be important the Fermi surface of the metal will need to be small and highly curved.

Swanson and Crouser found that for all directions investigated, and a large range of temperatures, they were able to obtain results similar to those of Young and Muller and also Van Oostrom. However, for the [100] direction there was a broad shoulder 0.35eV below the Fermi level. They concluded that the Hartree-Sommerfeld free-electron model was successful for most of the planes of tungsten which gave distributions similar to those derived by Young for the free-electron model. The [100] direction was thought to have small closed energy surfaces near E_F which would lead to a significant band structure term and a modification to the current density.

3.4. Determination of the equipotential distribution for an electrode system

It was decided to determine the equipotential distribution in the Faraday cage in order to find the effect of the lens at the entrance on electron trajectories since electrons should arrive normally to the collector.

Initially carbon resistance paper was used, the electrode shapes being painted in with silver paint. Since most of the cage is at a low potential, the method was not sensitive enough to enable trajectories to be determined near the back of the cage. A computer program was therefore written.

The electric field strength E is given by:

$$E = - \text{grad } V$$

where V is the potential. The potential distribution around a system of electrodes is determined by the geometry and potentials of the electrodes. Neglecting space charges, the potential distribution can be determined from Laplace's equation: $\nabla^2 V = 0$

In practice this equation is very difficult to solve by integration, however, it can be solved by numerical computation. For the two dimensional case, Laplace's equation becomes:

$$\frac{\partial^2 V}{\partial y^2} + \frac{\partial^2 V}{\partial x^2} = 0$$

In numerical methods, the potentials of points within a system of electrodes are extrapolated from the potentials of the electrodes. A grid is usually fitted to the electrode system. In the case of plane electrodes this is

simple; the electrode equipotential surfaces are made to coincide with lines of the grid. The potential V_0 at any grid point is given by the potentials of the neighbouring points V_1, V_2, V_3, V_4, If g is the distance between the lattice lines, then:

$$\frac{V_2-V_0}{g} - \frac{V_0-V_4}{g} \approx \left(\frac{\partial V}{\partial y}\right)_{2,0} - \left(\frac{\partial V}{\partial y}\right)_{0,4} \approx g\left(\frac{\partial^2 V}{\partial y^2}\right)_0$$

and $$\frac{V_1-V_0}{g} - \frac{V_0-V_3}{g} \approx \left(\frac{\partial V}{\partial x}\right)_{1,0} - \left(\frac{\partial V}{\partial x}\right)_{0,3} \approx g\left(\frac{\partial^2 V}{\partial x^2}\right)_0$$

Therefore from Laplace's equation:

$$V_0 \approx \frac{1}{4}(V_1+V_2+V_3+V_4)$$

By assuming an initial potential distribution, e.g. that the electrodes are at certain potentials, and that other points are at zero potential, new potential values can be found for each point. The procedure is repeated until the potential distribution has been found with the required degree of accuracy.

At the junction of two meshes of different size, g is not constant. Using the spacings h_1, h_2, h_3 and h_4 shown in figure 3.17, the slopes at the midpoints are given by:

$$\left(\frac{\partial V}{\partial x}\right)_{0,1} = \frac{V_1-V_0}{h_1}, \quad \left(\frac{\partial V}{\partial x}\right)_{3,0} = \frac{V_0-V_3}{V_3}$$

Therefore $$\left(\frac{\partial^2 V}{\partial x^2}\right)_0 = \frac{\left(\frac{V_1-V_0}{h_1}\right) - \left(\frac{V_0-V_3}{h_3}\right)}{\frac{h_1+h_3}{2}}$$

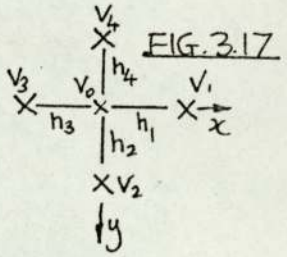

FIG. 3.17

$$\approx \left(V_1 h_3 + V_3 h_1 - V_0(h_1+h_3)\right)\frac{2}{h_1 h_3 (h_1+h_3)}$$

$$\frac{\partial^2 V}{\partial y^2} = \left(V_2 h_4 + V_4 h_2 - V_0(h_2+h_4)\right) \frac{2}{h_2 h_4 (h_2+h_4)}$$

$$\nabla^2 V = \left(\frac{\partial^2 V}{\partial y^2}\right)_0 + \left(\frac{\partial^2 V}{\partial x^2}\right)_0$$

$$= \left(V_1 h_3 + V_3 h_1\right) \frac{2}{h_1 h_3 (h_1+h_3)} +$$

$$\left(V_2 h_4 + V_4 h_2\right) \frac{2}{h_2 h_4 (h_2+h_4)} - 2V_0 \left(\frac{1}{h_1 h_3} + \frac{1}{h_2 h_4}\right)$$

We wish to determine a new value of V_0:

Now $\nabla^2 V = \psi - V_0 \beta$

where $\psi = \left(V_1 h_3 + V_3 h_1\right) \frac{2}{h_1 h_3 (h_1+h_3)} + \left(V_2 h_4 + V_4 h_2\right) \frac{2}{h_2 h_4 (h_2+h_4)}$

and $\beta = 2\left(\frac{1}{h_1 h_3} + \frac{1}{h_2 h_4}\right)$

$$\nabla^2 V = 0$$

$$\therefore \psi - V_0 \beta = 0$$

$$V_0 = \frac{\psi}{\beta}$$

V_o is calculated from initial potential conditions at each mesh point. The procedure is repeated several times, the potential distribution becoming more like the true one each time. If

$$V_{o\,new} - V_{o\,old} = C \quad \text{a constant}$$

then $$V_{o\,final} = V_{o\,initial} + C' \quad \text{where} \quad C' > C$$

$$V_{o\,new} = \frac{\psi_{old}}{\beta_{old}}$$

A correction factor is introduced where $1 < \alpha < 2$ the aim being to obtain the final distribution rapidly by over correcting:

$$V'_{o\,new} = V_{o\,old} + \alpha C$$

$$= V_{o\,old} + \alpha (V_{o\,new} - V_{o\,old})$$

$$= V_{o\,old} (1-\alpha) + \alpha V_{o\,new}$$

$$= V_{o\,old} (1-\alpha) + \frac{\alpha \psi}{\beta}$$

The final potential distribution is arrived at by iteration. Normally 50 iterations are sufficient to get an accuracy of 0.05V, but often 100 were carried out. This technique was used not only to calculate the equipotentials at the cage, but also between the emitter and first anode. The results are discussed in the relevant sections. (Sections 5.2.4 and 5.3.6.)

CHAPTER 4 Experimental systems

4.1. Ultrahigh vacuum system

4.1.1. Introduction

Pressures in the ultrahigh vacuum range are required for field-emission work for two reasons. Firstly because adsorbed layers of molecules influence emission, and secondly because the life of an emitter is increased with decreasing pressure. Gas molecules impinge on a surface at a rate which is given by:

$$\frac{dn}{dt} = \frac{P}{(2\pi mkT)^{1/2}} \text{ molecules/cm}^2 \text{ sec.}$$

where P is the pressure

n is the number of molecules impinging during a time t

m is the mass of the molecule

k is Boltzmann's constant

T is the absolute temperature.

Graph 4.1 shows the time for a monolayer of nitrogen to form at certain pressures if the sticking probability is (a) 0.1 and (b) 1.

During the application of an electric field to an emitter, the inhomogeneity of the electric field around the tip causes polarized molecules to be attracted to the emitter surface. Thus the rate of gas impact is higher than would be expected if no field was present.

Gas molecules are either non-polar (do not possess a permanent dipole moment, e.g. hydrogen, nitrogen, oxygen and carbon dioxide), or polar (possess a permanent dipole moment, e.g. carbon monoxide). The application of an electric field causes distortion of the molecule and thus an induced dipole moment. In the case of polar molecules, the permanent dipole moment is also present. The strength

Time taken for a monolayer of nitrogen to form on a surface. Sticking probability α

FIG. 4.1.

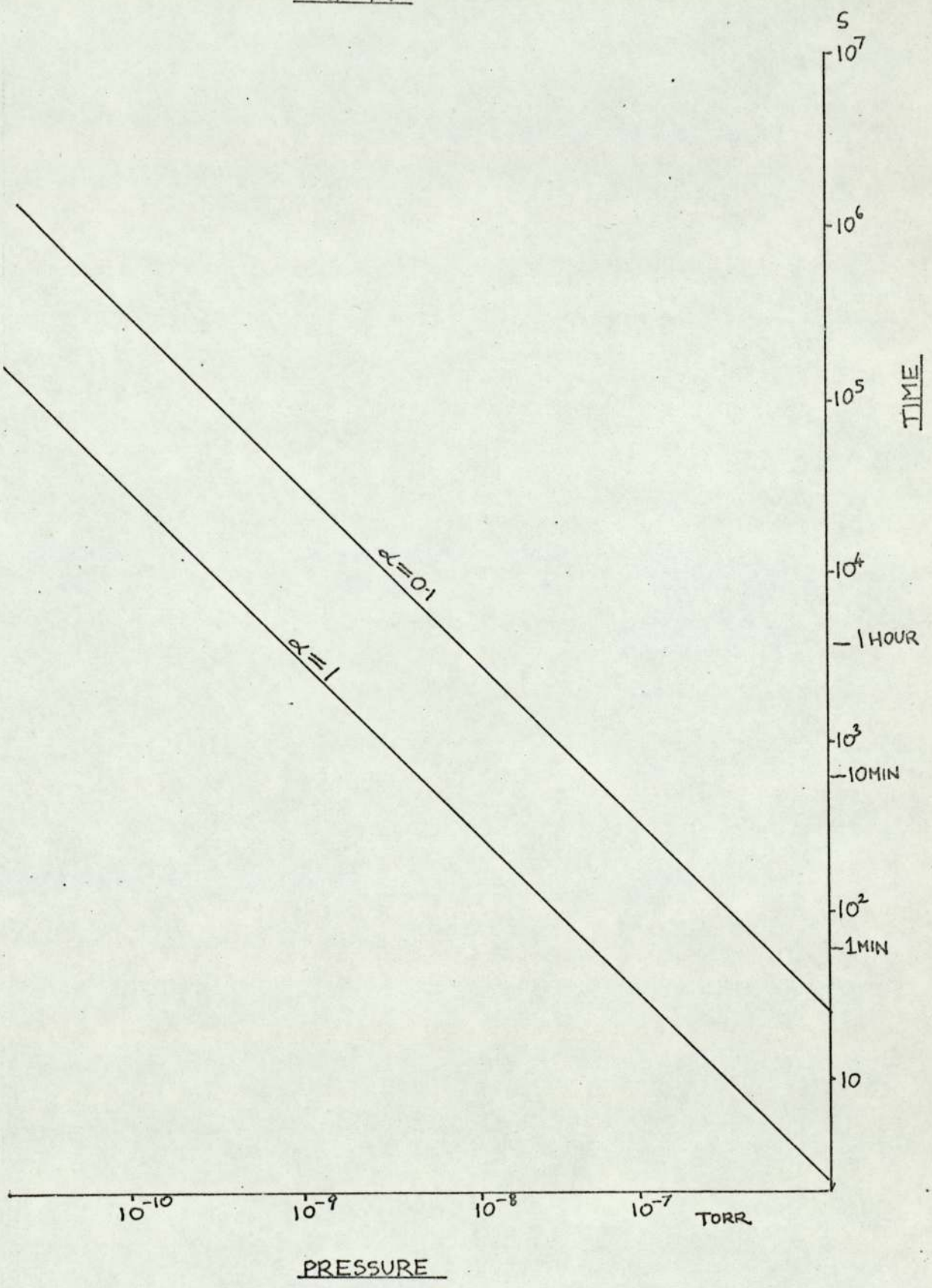

of the electric field affecting any one molecule is determined not only by the applied field, but also by the electric field of neighbouring molecules which have also acquired dipole moments. This local effect is very small in vacuo. Thus in the non-uniform electric field around the emitter, gas molecules will be attracted to the tip. For an emitter at 300°K, in a vacuum of 10^{-9}Torr, a monolayer of nitrogen molecules would form in about thirty minutes if the probability of molecules sticking to the surface was unity. In an electric field the number of molecules arriving at the emitter is increased by a factor

$$\left(1+\frac{\alpha F^2}{2}+\frac{\mu F}{RT}\right)$$

where α is the polarizibility, and μ the permanent dipole moment of the molecule; in the case of a non-polar molecule $\mu = 0$.

If the electron field strength is 50MV/cm then the time taken for a monolayer to form will be decreased by about 0.63. If a sticking probability of 0.5 was assumed, then a monolayer of nitrogen molecules would form in about forty minutes.

If the vacuum is poor, then the emitter tip will be damaged by ion bombardment. This causes pitting of the surface and field enhancement occurs at the corresponding hillocks. Local emission then tends to become excessive, leading to vacuum arcing and the destruction of the tip.

4.1.2. Description

The vacuum system used is based on a two-stage mercury diffusion pump, with two liquid nitrogen traps between the pump and the experimental chamber to prevent back-streaming of mercury vapour to the chamber. The pressure is measured by an ionization gauge and in the early

stages of the work, partial pressures of residual gases were measured with a "Minimass" mass spectrometer. The diffusion pump is backed with a rotary pump. A glass reservoir is on the high pressure side of the diffusion pump which enables the diffusion pump to continue pumping if the rotary pump has to be disconnected for a short while. Between the two pumps is a molecular sieve trap with a valve on the low pressure side to facilitate baking the trap, without the resulting gases and water vapour passing into the low pressure part of the system. On the high pressure side of the sieve trap there is a hand operated valve, a Pirani gauge and a magnetically operated air admittance/isolation valve, which is to prevent oil from the pump entering the rest of the system if the power fails. Fig. 4.2 and 4.3.

The conductance of a cylindrical tube eight feet long, diameter ½ inch is 0.3 cu/ft/min. and for a tube 1 inch in diameter, the conductance is 1.5 cu/ft/min. The effective pumping speed cannot exceed the rate at which gas can pass through the tube connecting the pump and the system. Thus in order to get a good pumping speed it is necessary to use connecting tubes of large diameter. The internal diameter of joining tubes in this system is 1½ inches.

4.1.3. Procedure

In order to obtain pressures below 10^{-8} Torr, it is necessary to bake the system on the high vacuum side of the diffusion pump. Before assembly all the glassware was cleaned by washing in concentrated nitric acid and rinsing with distilled water. Some metal parts were cleaned by heating to about 1000°C in dry hydrogen or cracked ammonia (precise conditions depending on the particular metal), others by degreasing. The degreasing procedure is to clean

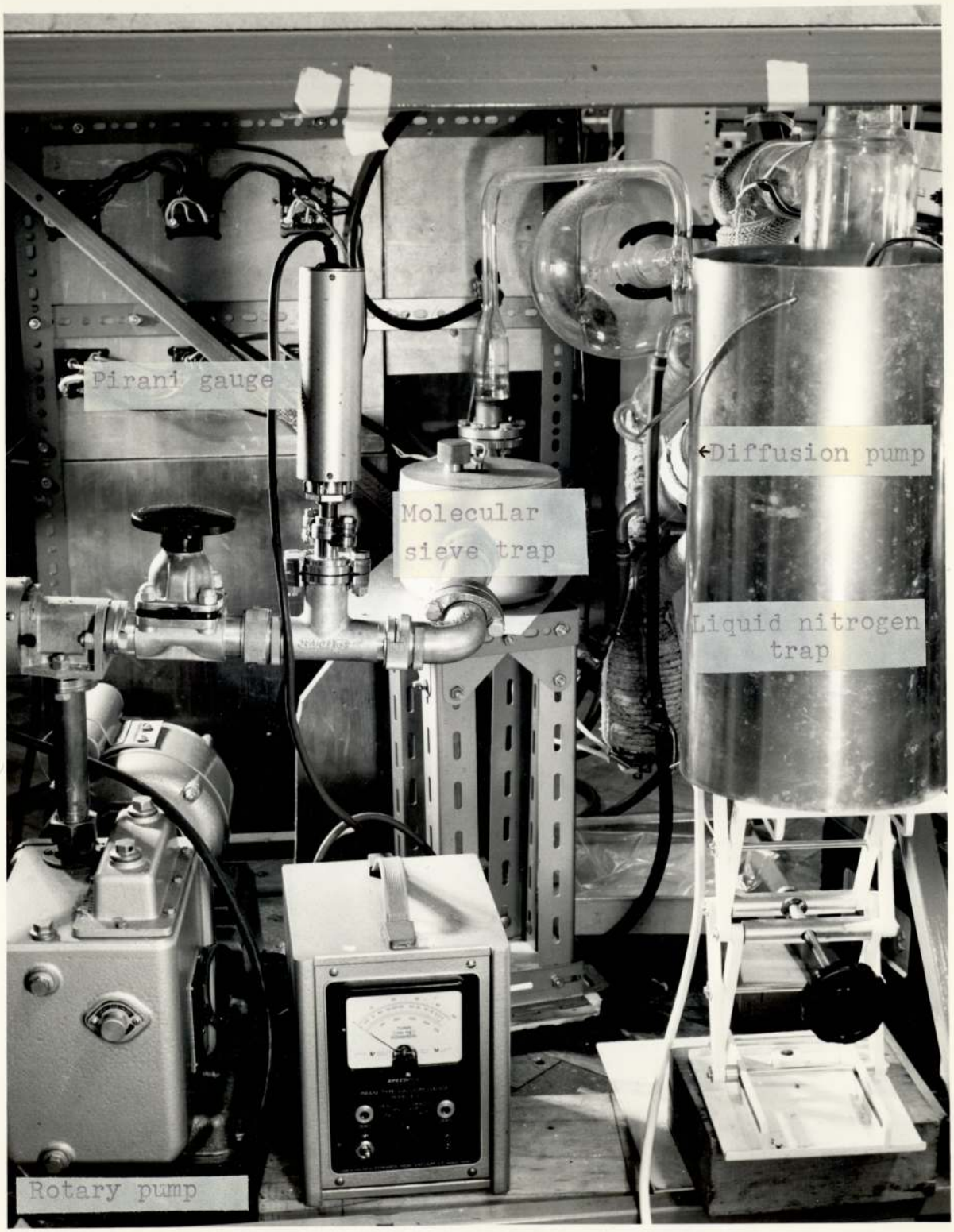
Pirani gauge
Molecular sieve trap
←Diffusion pump
Liquid nitrogen trap
Rotary pump

Fig. 4.2

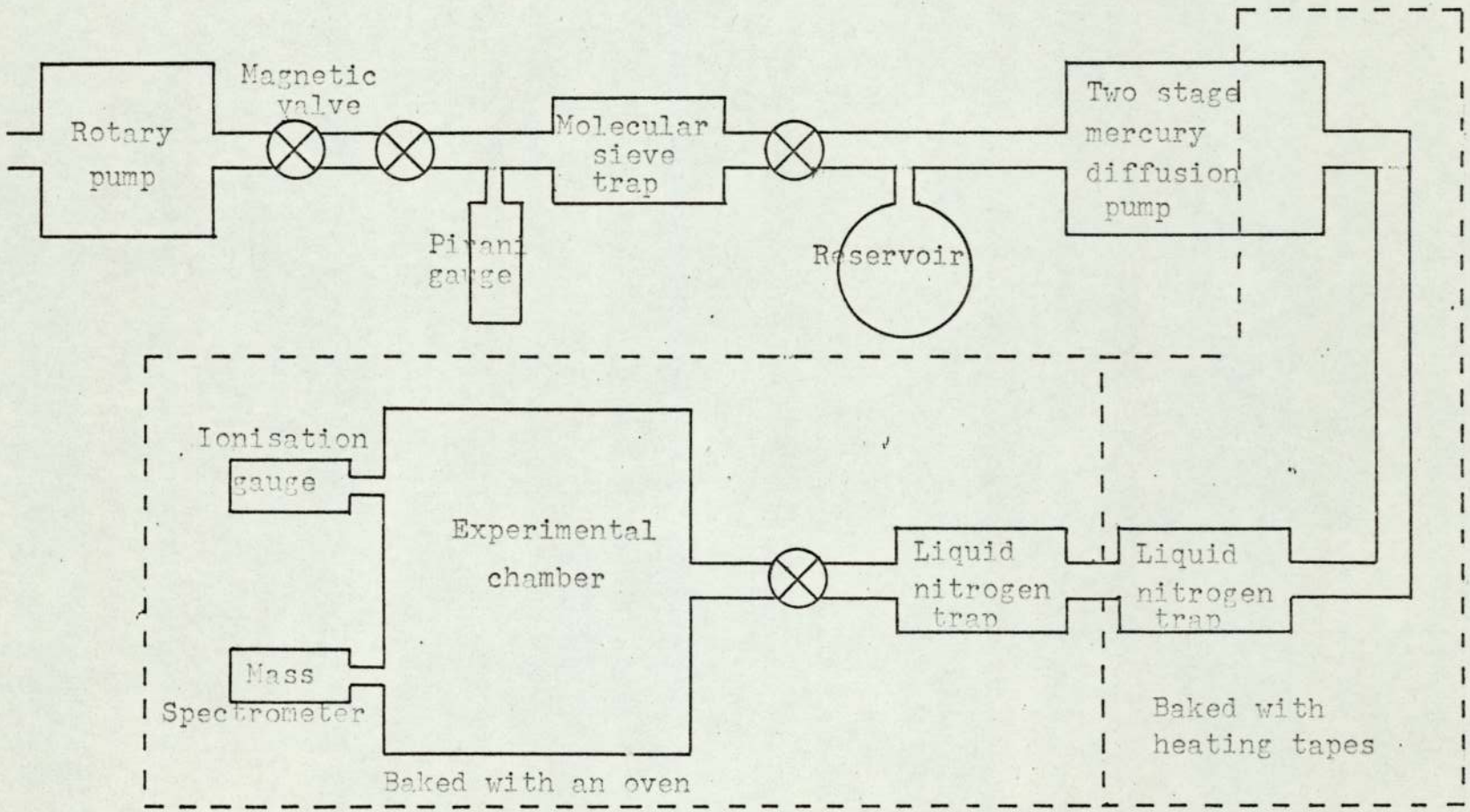

ULTRAHIGH VACUUM SYSTEM

FIG. 4.3.

the parts in detergent, distilled water and iso-propyl alcohol, using an ultrasonic vibrator at various stages. In the final cleaning stage, each item is slowly withdrawn from the vapour of iso-propyl alcohol.

The lower trap and the top jet of the diffusion pump are initially baked using heating tapes wrapped around these parts which heat them up to 100°C. The chamber, ionization gauge, and top cold trap are baked for about three days at a temperature of 350°C, mainly to bake the water vapour off the surface of the glass. After the lower trap cools, it is surrounded by a dewar vessel containing liquid nitrogen. The oven is then removed, and after the upper trap has cooled to room temperature, it is surrounded by liquid nitrogen.

4.1.4. Oven

The bake-out oven consists of a double wall of aluminium held apart by strips of sindanyo. Glass fibre is packed between the walls as thermal insulation. Eight electrical heating elements are spaced around the inside of the oven, each one having a power rating of one kilowatt.

The oven temperature is controlled by a bimetal thermostat which is the sensing device of a vacuum switch. (Sunvic hot-wire vacuum switch type F 103/4M). As a safety device, a Regulator type ERP-X is included in the circuit to limit the current. The oven takes about three hours to reach 350°C which is a typical bake-out temperature. A hoist is used to lift the oven off the sindanyo topped bench above which it is suspended.

4.2. Experimental chamber

4.2.1. Introduction

The experimental chamber needed to incorporate an energy analyser, a field emission microscope, and a mechanism for positioning emitters with respect to the analyser and microscope. Since an emitter has a limited life-time, several were mounted on a demountable rotating wheel. Two glass chambers were built in turn, the first shattering before any useful experiments could be carried out using it. A drawing of the first chamber is shown in figure 4.4.

4.2.2. The first experimental chamber

The glass chamber had two main branches set 14° apart. One held the energy analyser and the other the field emission microscope, field desorption loop, and a shield.

A long glass tube acted as a liquid nitrogen reservoir and on its end was a structure holding several emitters spaced around a wheel. The tube contained a rod for carrying current to the emitter.

By pushing bellows, it was possible to move the emitter structure from the field emission microscope to the energy analyser along an arc. Thus after a chosen emitter was cleaned and examined in the field emission microscope , it could be moved over to the analyser for the total energy distribution to be determined. The tip could be accurately positioned using three adjusting screws. The tip mechanism was designed to consist of a wheel holding several emitters which was capable of being rotated by use of a rotary motion feedthrough to drive a worm~~wheel~~ and worm. wheel.

FIRST EXPERIMENTAL CHAMBER

FIG. 4.4.

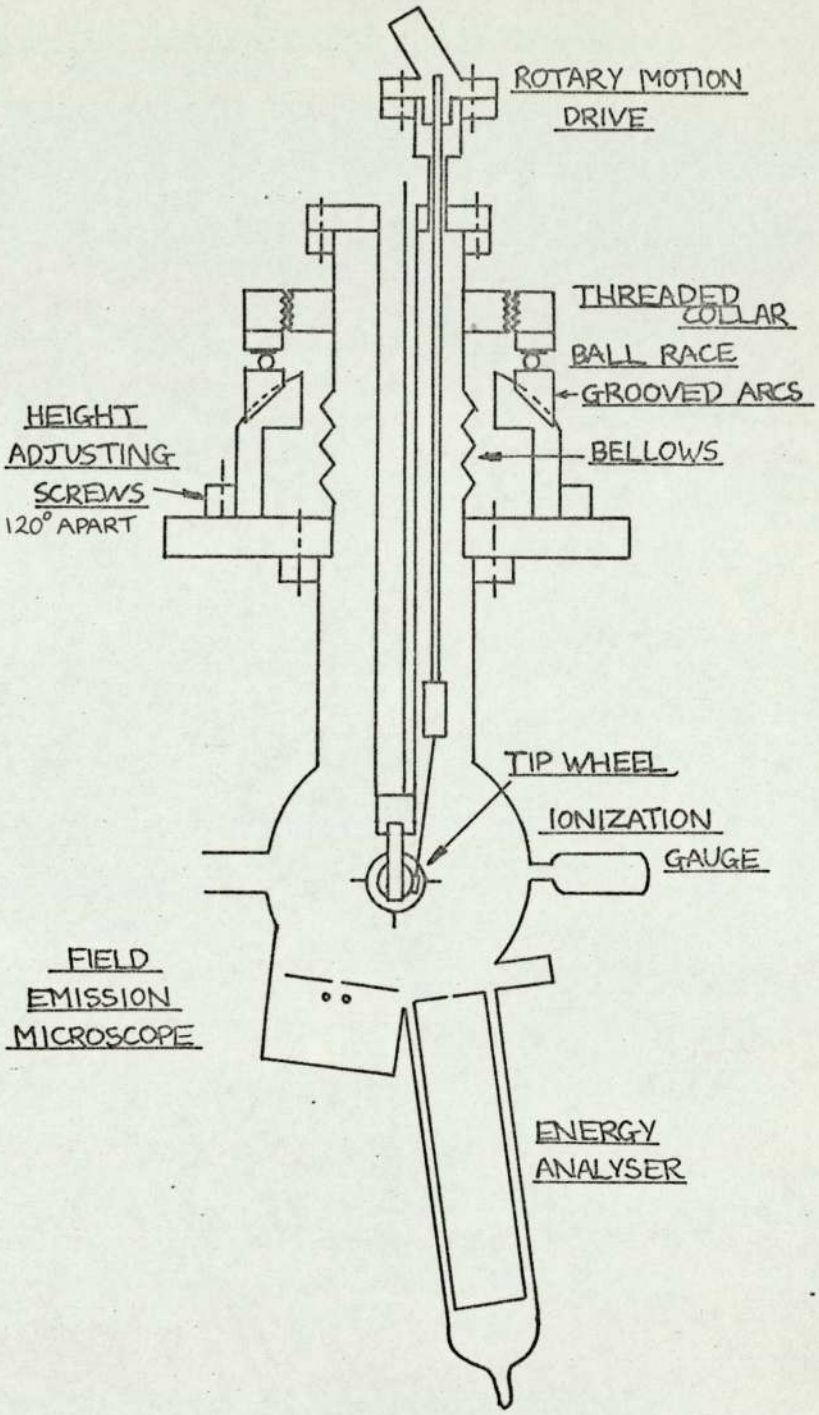

4.2.3. Adjusting mechanism

The adjusting mechanism was common to both glass chambers used. When designed, it was required to move an emitter through 14°, to take it from an axial position in the field-emission microscope to a position on the axis of the energy analyser. The emitter could be moved along the axis of each in turn by turning the large threaded collar shown. The three screws set 120° apart were for fine adjustment. When the second glass chamber was built, all the adjustments required could be made with the latter three screws, Figs. 4.4 and 4.5.

4.2.3.1. Description

The base of the mechanism is a large plate which bolts onto the flange of the lower glass chamber. A bellows, tube, and flange are welded onto the baseplate. The unit which bolts onto the upper flange of the glass chamber, consists of a copper tube on which is sealed a long glass nitrogen reservoir tip assembly, and a tube and flange holding the rotary motion feedthrough. The nitrogen reservoir is made of glass, both so that the nitrogen can be seen, and to insulate the tip assembly from the rest of the mechanism.

When the adjusting mechanism was used with the first chamber, the flexibility of the bellows made it possible to move the tip mechanism both up and down and in an arc. A collar rested on the baseplate, the height of which was made adjustable by three screws which located in dimples on the baseplate. The collar supported two columns, the tops of which were grooved parts of a circle. A flat ring with two mating pieces located on the curves. On top of this was a ball race and threaded collar which screwed onto

the ring, the tip mechanism could be moved along an arc and moved from the field emission microscope to the analyser. By turning the collar on the ball race, the tip mechanism could be moved up and down.

When used with the second experimental chamber, nearly all the tip adjustments were made using only the three screws set 120° apart.

FIG. 4.5
Adjusting mechanism

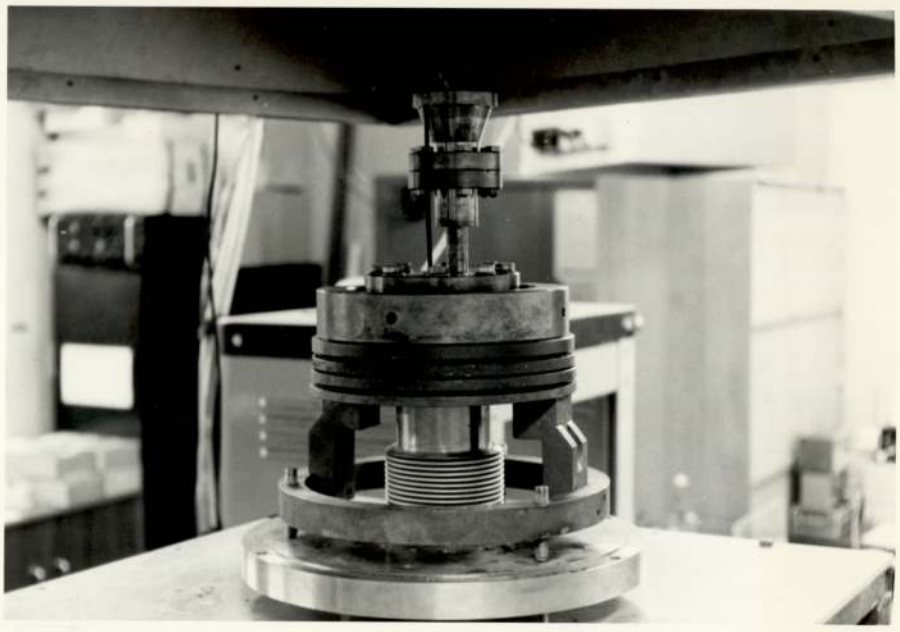

4.2.4. Second experimental chamber

The first experimental chamber had two practical faults which were as follows:

(a) the electrometer lead was inadequately "guarded" from leakage currents from the anode. For example, the resistance of the path between the electrometer and anode leads passing through the wall of the chamber was approximately 10^{14} ohms. Thus, if the anode potential was 1000V, the leakage current was 10^{-11}A;

(b) any bake-out grease or dust which entered the chamber when it was opened, fell onto the screen which was almost impossible to clean without being damaged.

The second experimental chamber was designed to incorporate both a field-emission microscope with a large screen and an energy analyser. A chosen emitter could be moved from the field-emission microscope to the analyser simply by rotating the tip wheel. Fig.4.6.

4.2.4.1. Description

Figure 4.7 shows the analyser mounted vertically in the glass chamber, along the main axis of the system. The field-emission microscope is at right angles to the axis, and a chosen emitter can easily be rotated from the microscope to the axis of the analyser. Final adjustment of the emitter to align it on the analyser axis is provided by the three screws of the adjusting mechanism used for the first chamber. There is also a mass spectrometer head, ionization gauge, optical window, desorption loop, and shield.

The field-emission microscope has a coating of tin oxide which covers the whole of the glass surface of the microscope except for a band of uncoated glass at the junction

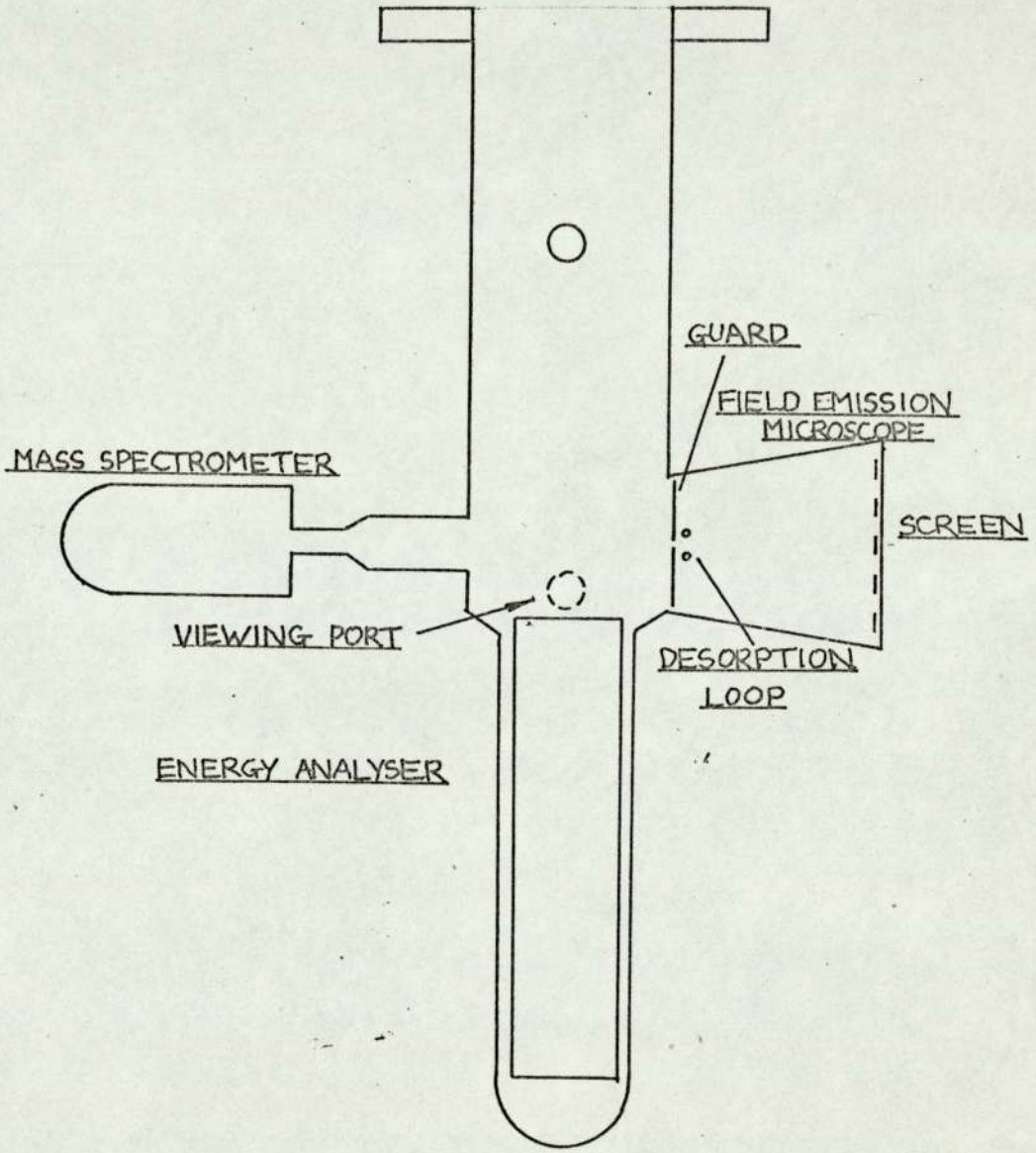

SECOND EXPERIMENTAL CHAMBER

FIG. 4.6

Second experimental chamber and adjusting mechanism.

FIG. 4.7

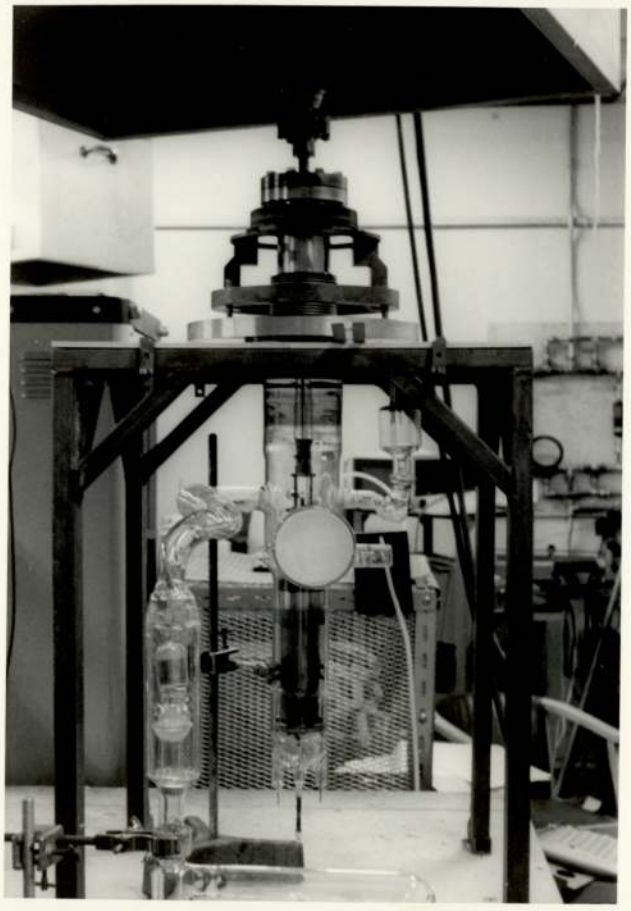

with the main part of the chamber. The phosphor screen was deposited from a suspension in acetone. A shield at earth potential at the entrance to the microscope shields emitters adjacent to the one being observed from the high field present in the microscope.

The tip adjusting mechanism is the same one as used with the first chamber.

4.3. Energy Analyser

The design of the energy analyser was based on that of Hartwig and Ulmer (1963)[1], with a claimed resolution of $\frac{\Delta E}{E} \approx 5 \times 10^{-6}$, described elsewhere.

4.3.1. Material

Several metals can be used in the construction of electrodes. The usual ones are nickel, copper, aluminium, molybdenum, tungsten, tantalum, monel and stainless steel.

The properties required for electrode construction can be summarised as follows:

the material must have -

(a) strength and ductility so that the electrode shapes can be easily formed:

(b) moderate conductivity, and a small coefficient of secondary emission:

(c) chemical freedom from oxidation:

(d) resistance to corrosion, absorption of only a small amount of gas:

(e) a low vapour pressure at the outgassing temperature:

(f) a melting point well above the highest degassing temperature.

All of the metals listed have most of the properties described, and could be used. However, it was decided not to use a magnetic material since this would cause the electron beam to be deflected, For this reason, nickel, monel, and some types of stainless steel were excluded. Copper oxidises easily, thus producing a very big surface area for adsorption of gases, and aluminium absorbs too much gas. Tungsten is very hard to form, and tantalum is very expensive. This leaves stainless steel and molybdenum.

It was thought that stainless steel would tarnish more easily than molybdenum, and rust has been seen to develop around welded joints in stainless steel. Since both tarnishing and rust might act as traps for gas, molybdenum was chosen as the material for the analyser.

4.3.2. Construction (Figures 4.8 and 4.9)

The analyser consists of a tube 195mm long, containing a system of apertures and an insulated Faraday cage with a guard ring. Following the direction of the beam, there are apertures of the following diameter: 1mm, 0.8mm, 0.5mm, and 4mm. The collector cage is beyond these and has a 4mm diameter opening. The fourth aperture is rivetted in position, but the first three can each be aligned by adjusting three screws passing through the wall of the tube spaced 120° apart. The cage is held in position by a ceramic insulator which is screwed onto a collar on the end of the tube. When the analyser is used for thermionic emission, a ceramic insulator is fitted over the initial aperture and holds a molybdenum electrode which acts as a grid. By adjustment of a screw, the spacing between the grid and first aperture can be varied. When the analyser is to be

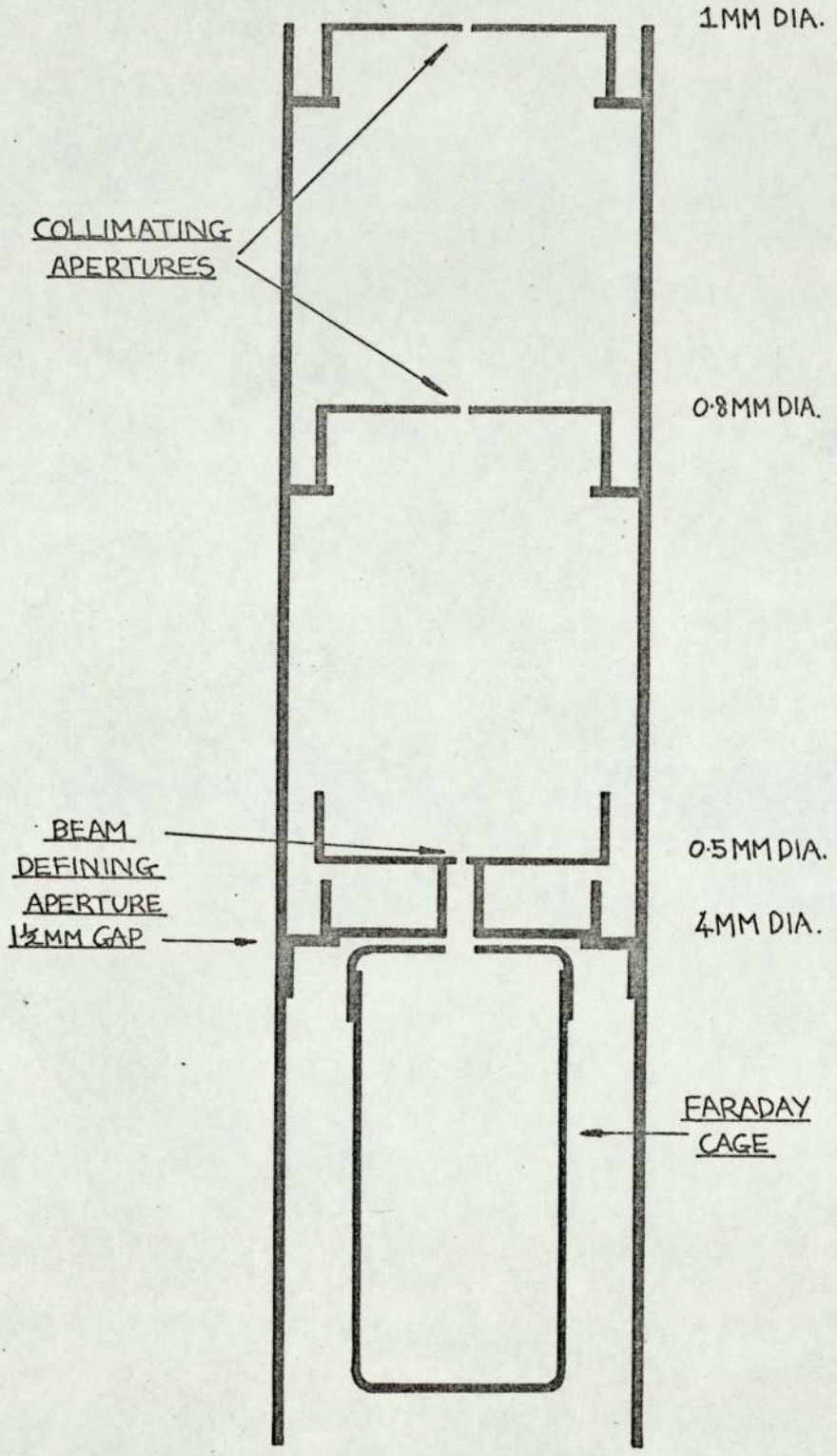

Electrode arrangement in the energy analyser.

FIG. 4.8

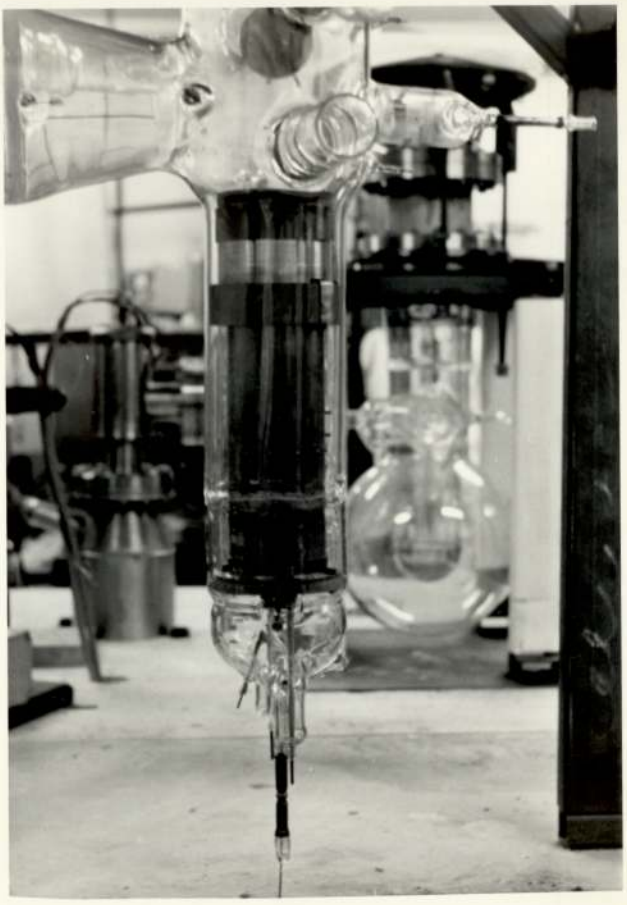

FIG. 4.9.

used for field-emission, the grid plate is removed and the gun q.v. sits on the top plate of the analyser.

Small holes were drilled in the body of the analyser and grooves were cut in the screws holding the apertures in place. These facilitate the outgassing of the analyser.

4.3.3. Faraday cage holder (Figure 4.10)

A holder was needed to support the Faraday cage within the cylindrical body of the analyser. There were three main considerations to be satisfied in its design:

(a) The cage needed to be accurately located on the axis of the analyser, and with its aperture at an exact distance of 1.5mm from the adjacent 4mm aperture.

(b) The cage holder needed to have such a high resistance that any leakage current would be as small as possible and much smaller than the currents to be measured.

(c) It needed to be able to expand during the bake-out without cracking.

The ceramic, pyrophyllite ($3\text{-}4SiO_2.Al_2O_3.H_2O$), was chosen for the body of the holder since this material was readily available. However, its resistivity was only about 10^{11} ohm-cm. Thus if the analyser was at an anode potential of 1000V and the cage near earth potential, the reading on the electrometer connected to the cage would be of the order of 10^{-14}A which is of the same order of magnitude as the currents to be measured. To avoid this an earthed guard ring was incorporated in the holder. The effect of the guard ring is to put the 1000V potential drop across the analyser cylinder and the guard ring. The only current shown on the electrometer is that resulting from the voltage across the electrometer input being across the resistance of the

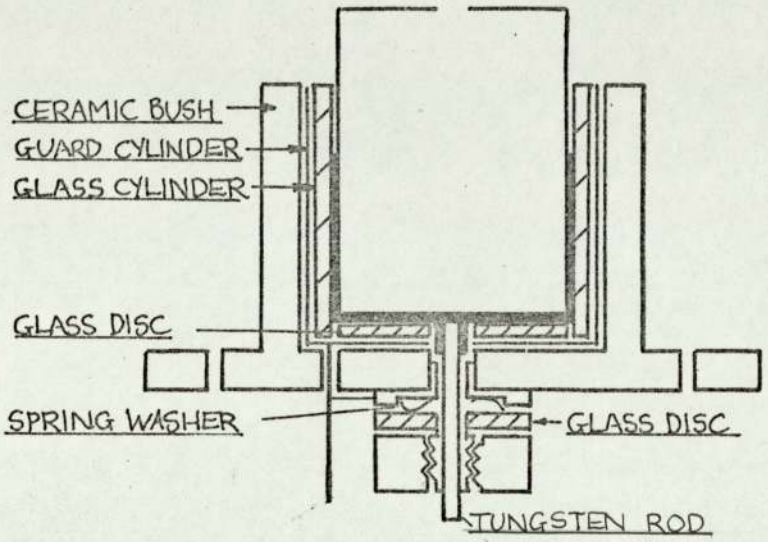

FARADAY CAGE HOLDER

FIG. 4.10

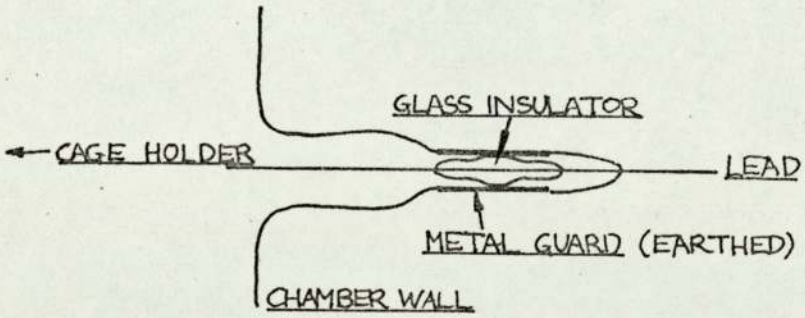

material between the guard and the electrometer lead.

In construction the cage was supported rigidly by a stainless steel cup, into whose base was pushed a tungsten rod.

Surrounding the cup was a glass cylinder, which was a loose fit, and a glass disc, both of which provided the insulation between the guard cup and the cage. The guard was made of molybdenum sheet. All these components rested in a ceramic cup which was a sliding fit in the molybdenum cylinder of the analyser.

The tungsten rod protruded through a hole in the ceramic bush. A threaded tube was screwed onto it and a nut screwed on the tube to hold the cage in position. However, since the expansion of the tungsten rod was considerably more than that of pyrophyllite, the rod would expand more than the pyrophyllite bush during bake-out and the cage would become loose. This was avoided by inserting a spring washer between the nut and the bush so that the latter would be tightened onto the spring washer which would then take up the additional expansion of the rod. The insulation between the rod and the bush was increased by the glass disc and the washer was connected to the cage guard lead so that the nut was also guarded. A lead goes from the tungsten rod to a tungsten leadthrough in the wall of the chamber. Clearly there would be a leakage path between the cage leadthrough at the point it passes through the chamber wall and the anode leadthrough. The cage lead was, therefore, also guarded with a metal tube as shown which could be earthed.

4.4. Lubrication in ultrahigh vacuum

Normal liquid and semi-solid grease lubricants are unsuitable for ultrahigh vacuum because they have high vapour pressures and cannot be baked. The absence of oxygen in vacuum reduces natural lubrication between moving parts which normally occurs when the oxide layers act as thin film lubricants. Most metals weld together under these conditions, however certain pairs do not. A. B. Osborn[2] tested various non-welding pairs to see if they could be used as bearing materials. Each pair constituted a shaft running in a bush. These were baked to 400°C and operated in a vacuum 10^{-10} Torr. He concluded that pure iron and silver were a very good pair. Unfortunately iron is not a good vacuum material, because it easily rusts. The only satisfactory pair was molybdenum and silver. Molybdenum and silver are both good conductors of heat and electricity and so were chosen as components of the tip assembly.

Molybdenum and silver were used successfully in this system. After baking very slight force was sometimes needed to free the tip mechanism and a slight temporary increase in pressure was noted as the mechanism was freed.

4.5. Tip assembly

The lifetime of a field emitting tip is short and it was realised that if a system of several interchangeable tips could be used, then the time spent in evacuating the system would be greatly reduced. The tip assembly was designed to enable each of six tips mounted round the circumference of a wheel, to be moved into position by the rotation of the wheel. This motion was in principle achieved by using a rotary motion feedthrough to turn a

worm which rotated a gearwheel mounted on the same axis as the tipwheel.

4.5.1. Construction

Figure 4.11 shows the tip mechanism. Two molybdenum columns are screwed onto a copper block which is welded onto a copper collar. The two columns have silver bushes inset near their ends and these bear a molybdenum axle pointed at each end. A molybdenum gear wheel and a coaxial silver tipwheel are mounted on the axle. The tipwheel has six holes 60° apart to take tip holders or tips which can be held in position by screws. Also mounted on one of the columns is a molybdenum yoke to hold the silver worm which is driven by a rod connected to a rotary motion feedthrough. The worm was designed so that thirty turns of the worm would give one turn of the wheel. Because of restrictions imposed by the size and position of the flange supporting the rotary motion feedthrough, it was necessary to bring the shaft from the feedthrough to the worm via a universal coupling and in order to simplify this coupling, the yoke holding the worm is adjustable so that the worm shaft can be easily connected to the coupling. Once the correct position for the yoke is found, it is locked in position.

Since it was intended to cool the tips to liquid nitrogen temperature, the copper block holding the tip mechanism was welded into a copper collar on which was a glass seal. This was joined onto a glass tube which could be used to hold liquid nitrogen for cooling the tip mechanism and tips. A copper rod was screwed into the block to carry current to the tipwheel.

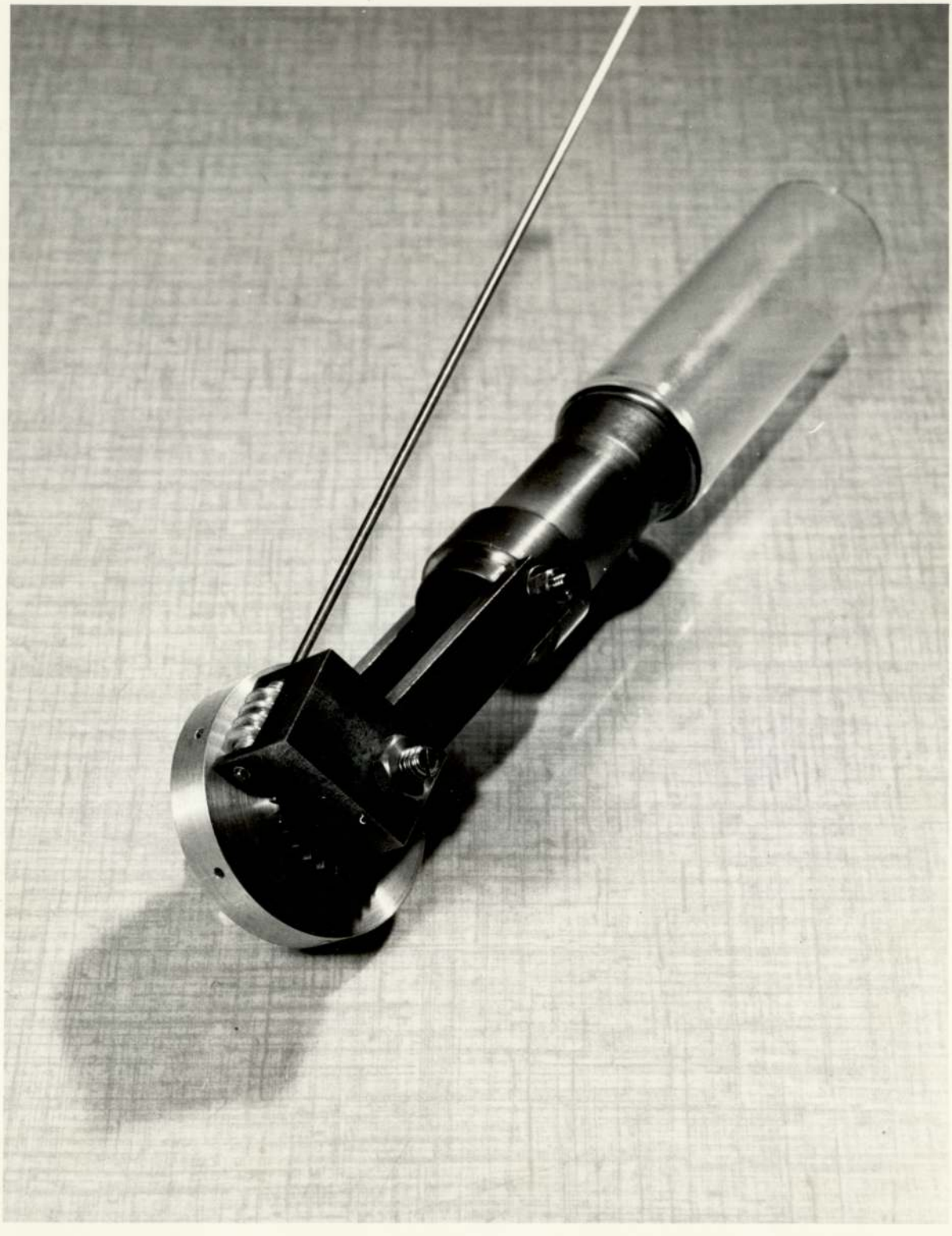

TIP WHEEL FIG.4.11

Tipwheel in the chamber.
FIG. 4.12.

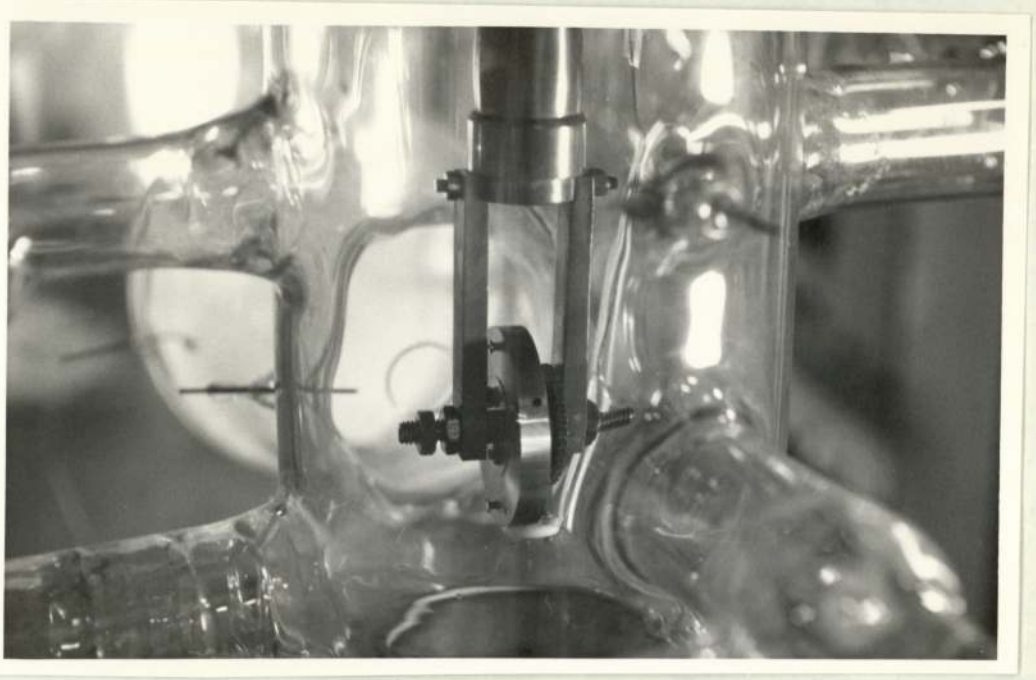

MODIFIED FOR THERMIONIC EMISSION

4.6 Liquid nitrogen replenishing device

It was usual to keep the system under vacuum overnight, and so in order to prevent diffusion of mercury from the pump into the chamber, one liquid nitrogen trap had to be full. A device was constructed which kept the nitrogen in the lower trap at a constant level for about twenty-four hours. This was based on a design of A.Wright of A.E.I. Limited, with the electrical circuit modified to incorporate available components.

4.6.1. General description

The sensing device is a thermistor placed in the dewar containing the liquid nitrogen at about the level at which the liquid is usually maintained. When the thermistor is surrounded by nitrogen, the circuit is in the "off" condition. As the liquid nitrogen evaporates, the thermistor warms up and at a certain temperature it causes a switching circuit to come into action which operates a relay. Two things happen: (a) a pressure release valve connected to the reservoir closes, since one end of the delivery tube is immersed in the nitrogen in the reservoir, the pressure begins to build up, and (b) a small heater in the reservoir heats up thereby increasing the boiling rate of the nitrogen. The pressure in the reservoir continues to increase until it is sufficient to force liquid nitrogen from the reservoir, through the tube into the trap. When the trap has filled to the sensing thermistor, it causes the switching circuit to switch off, the heater goes off, and the valve opens allowing excess nitrogen to escape.

4.6.2. Liquid nitrogen reservoir

The reservoir used was a Union Carbide liquid

nitrogen vessel. A steel delivery tube, contacts for the reservoir heater and a tube to the valve passes through a rubber bung which is held in the neck of the vessel by two hooks on springs.

4.6.3. Pressure release valve

The valve consists of a ball bearing resting on a piston in a small cylindrical tube which is vertically mounted. When the switching circuit closes the relay, it pushes the piston up into the tube and the ball bearing closes a hole in the top of the tube. When the relay opens, the ball bearing drops down with the piston, nitrogen enters from the top hole and escapes from two holes in the side wall of the tube. Thus excess pressure is released from the reservoir.

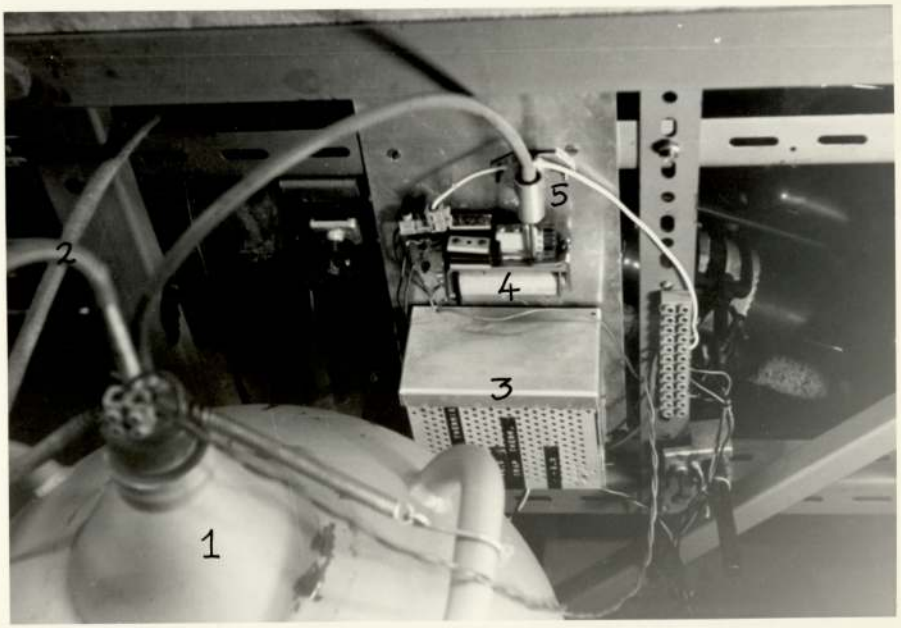

Fig.4.13.

1. Reservoir
2. Delivery tube
3. Switching circuit
4. Relay controlling valve
5. Pressure release valve

4.7. Field emission microscope (Figs.4.6 and 4.14)

4.7.1. Principle

One of the principle applications of field emission is in the field emission microscope in which a highly magnified image of a field emitter is produced on a phosphor screen which is at a positive potential with respect to the emitter. Since very high electric fields are required for field emission ($3\text{-}7 \times 10^7$ Vcm^{-1}), the emitter is made into the shape of a needle. Its end is hemispherical, having a radius which is typically 1000 Å. If the potential of a sphere is V and its radius is r, then the electric field strength $F = \frac{V}{r}$. However, for a field emitter, the shank modifies the local field strength so that $F = \frac{V}{kr}$ where k is about 5 at the apex and increases with polar angle. For an emitter of 1000 Å suitable fields can be obtained with 2-5kV.

In the field emission microscope, electrons leave the emitter with very little kinetic energy and move perpendicularly to the equipotentials surrounding it. As the end of an emitter is approximately hemispherical, the electrons move radially to a phosphor screen at anode potential which is usually a hemisphere concentric with the tip hemisphere, but can be flat. The image consists of a pattern of light and dark areas. For a metal, the emitting area of the tip is much smaller than the grain size and so emission occurs from different work function areas of a single crystal. The dark areas correspond to crystal faces where the atoms are closely packed and the work function is high. The magnification is given by $x/\beta r$ where β is typically 1.5, r is the tip radius and x the distance between the

FIG. 4.14
Field-emission microscope

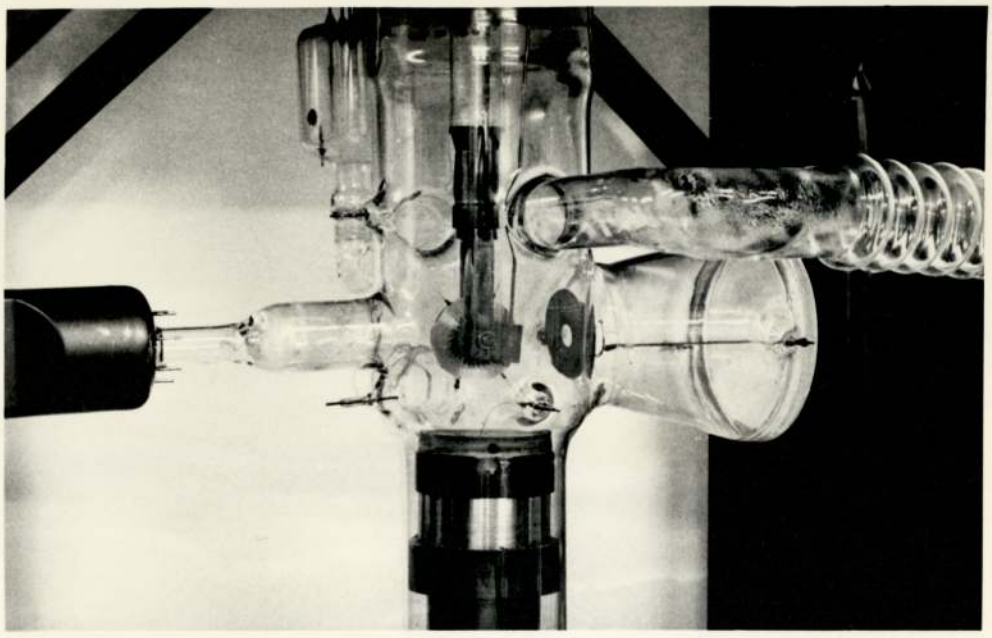

screen and tip; it is of the order of 10^5 - 10^6.

4.7.2. Construction of the field emission microscope

A flat screen was used in this apparatus and was covered with a conductive coating and a phosphor. It was intended to use the microscope in the cleaning of emitters by field desorption. The screen would then be negative with respect to the emitter and there would be the likelihood of field emission from the conductive coating. In order to reduce this effect a loop of wire 6mm in diameter was put at the entrance of the microscope. The emitter was positioned near this loop and on its axis, and its purpose was to reduce the field at the conductive coating and thus reduce the possibility of field emission from the coating. Field desorption cleaning is described in section 4.9.1.

The screen consists of a layer of a suitable phosphor, a conducting layer and an external electric lead. For anode voltages above 5000V, the conducting layer can be an aluminium backing on the vacuum side of the phosphor. The brightness of the image exceeds that for unbacked phosphors because of reflected light. However, for lower voltages, such as 1000V-3000V as used in this apparatus, an aluminium backing is too thick and so the conducting layer is a thin coating of tin oxide which is put on the glass before the phosphor is deposited.

4.7.3. Conductive coating

In order to prepare a conductive coating of tin oxide, the glass is heated to about 450°C. Stannous chloride crystals are first heated up gently, until all the water of crystallisation has been driven out, and then melted. A whitish-yellow vapour is formed which can be

blown onto the surface of the glass. The resulting surface resistivity is between 10^{-2} and 2 ohm-cm depending on the thickness of the film.

4.7.4. Manufacture of the phosphor screen

The phosphor is first ground to break up any lumps and then suspended in acetone, allowed to stand for a short time for the coarser grains to settle and then the suspension of lighter particles is poured into the flask, to a height of 5-10 cm over the glass screen-backing or into a dish on the bottom of which the backing lies. The suspension is allowed to stand 3-8 hours without movement or vibration under a 150W lamp which speeds up the evaporation of the acetone. During this time suspended particles settle out gradually under gravity and form an even layer on the glass. No sticking agent is necessary.

4.7.5. External screen connection

The contact to the screen was a tungsten wire spotwelded perpendicularly onto the end of a 1mm tungsten lead. The latter was pulled through a hole in the wall of the glass until the wire touched the surface and then the lead was sealed into the glass. The tin oxide coating was then put on and covered the wire at the point of contact. To ensure a good contact, the contact point was covered with conducting silver paint.

4.7.6. Preparation of tungsten emitters (Fig.4.15)

Tungsten field emitters are prepared by electrochemical etching which produces a sharp pointed needle terminating in a shape which is approximately hemispherical and has a radius of less than 1000 Å. Tungsten wire is usually drawn so that the [110] orientation is in the axis.

0.2mm diameter wire is usually used and tips are made by etching in a freshly prepared 1N solution of sodium hydroxide. A nickel ring of 10mm diameter is used as one electrode, the tungsten wire being the other. Two methods of etching are used. The first is a drop-off technique. If a current of about 1.8A and a voltage of 10V a.c. is used, etching takes place rapidly and occurs preferentially at the air-electrolyte interface. A neck is formed at the interface which becomes narrower until the weight of the wire below the electrolyte surface causes it to drop off. Before drop-off occurs, the current is seen to drop slowly and just before drop-off, it decreases rapidly. This is taken as a signal to switch off the current, since if etching is allowed to continue, the tip becomes blunt. The emitter is then removed and gently washed with distilled water to prevent any further etching. If the process is run with a high current, a blue flash is seen as the bottom of the wire drops off.

The second method used can be controlled much more easily. Similar voltage and current conditions to those above are used. The emitter is viewed through a microscope giving a magnification of 100X. After etching has proceeded for a few minutes, the shank of the wire is seen to have narrowed. The current is then reduced and the etching process is observed through the microscope. The shank becomes narrower and a long cone forms at the end of the wire. As etching continues, the end of the wire is progressively etched away, the end of the wire retaining a conical shape. After a time the apex of the cone comes into the field of view of the microscope as the length of the cone shortens. At this stage the angle of

the cone is very small and the radius of curvature of the tip is typically 300 Å and often less. The operator chooses when to stop the etching process when the cone is as short as possible without any apparent increase in bluntness of the tip.

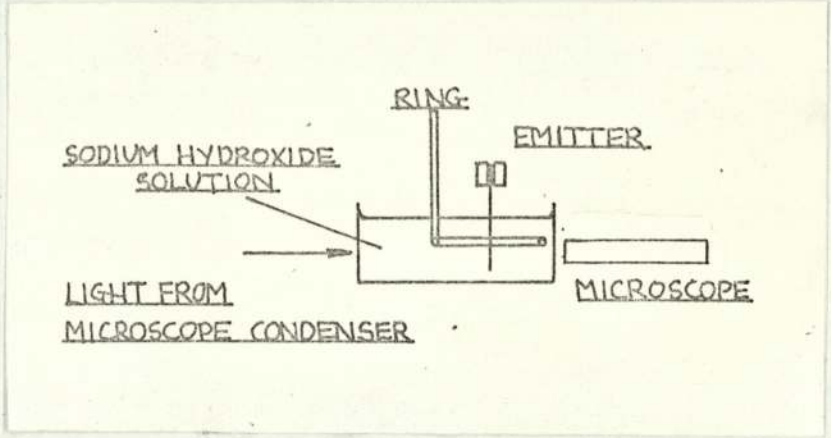

FIG. 4.15 TIP MANUFACTURE

Field emitters

FIG. 4.16

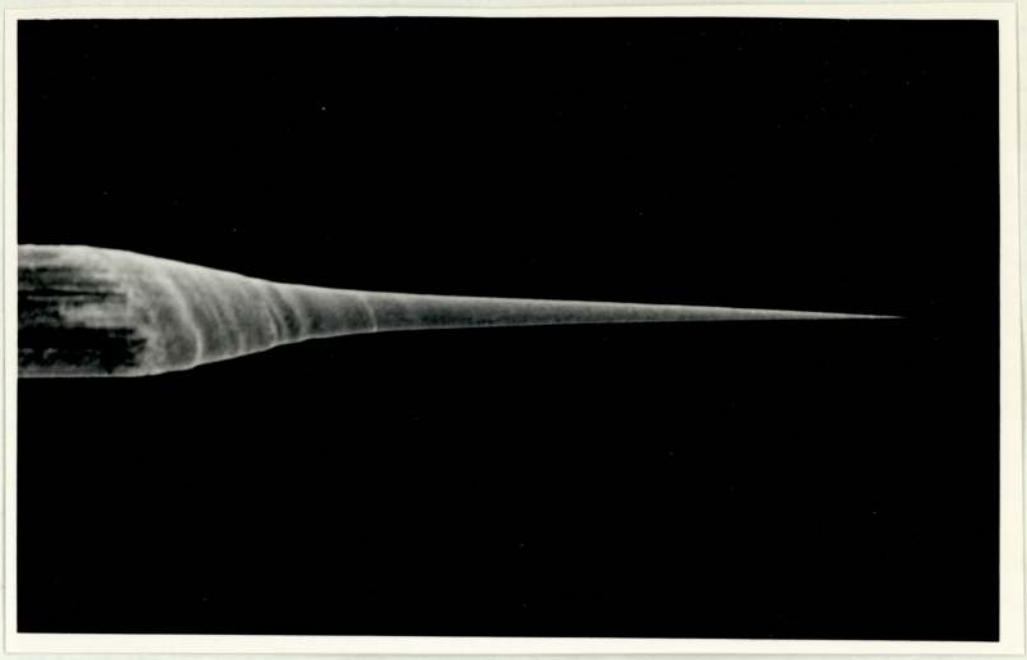

90x

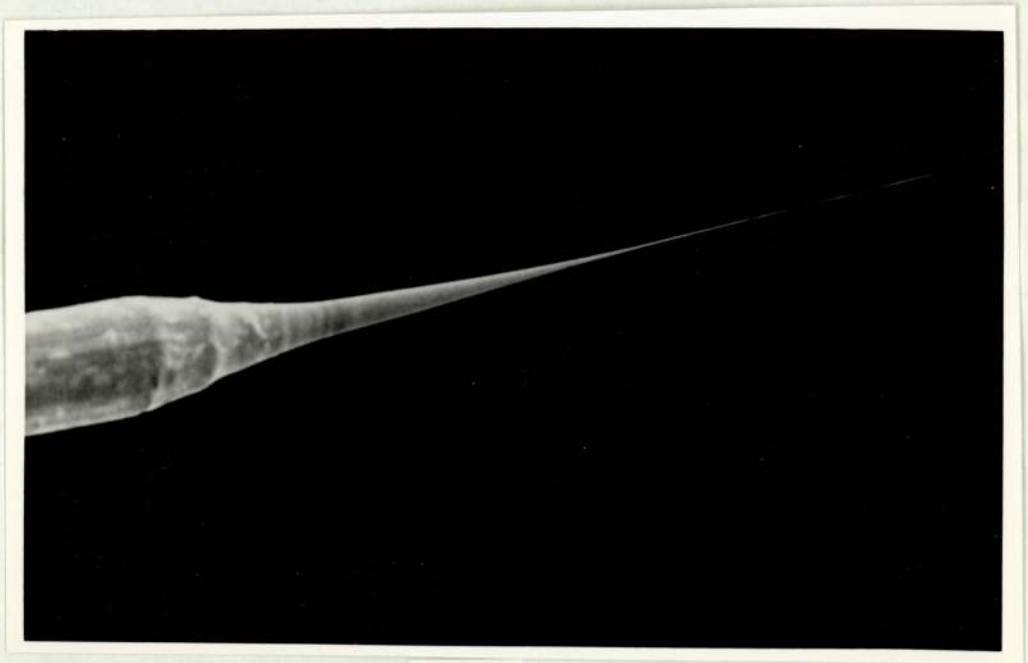

90x

FIG. 4.17

FIG. 4.18

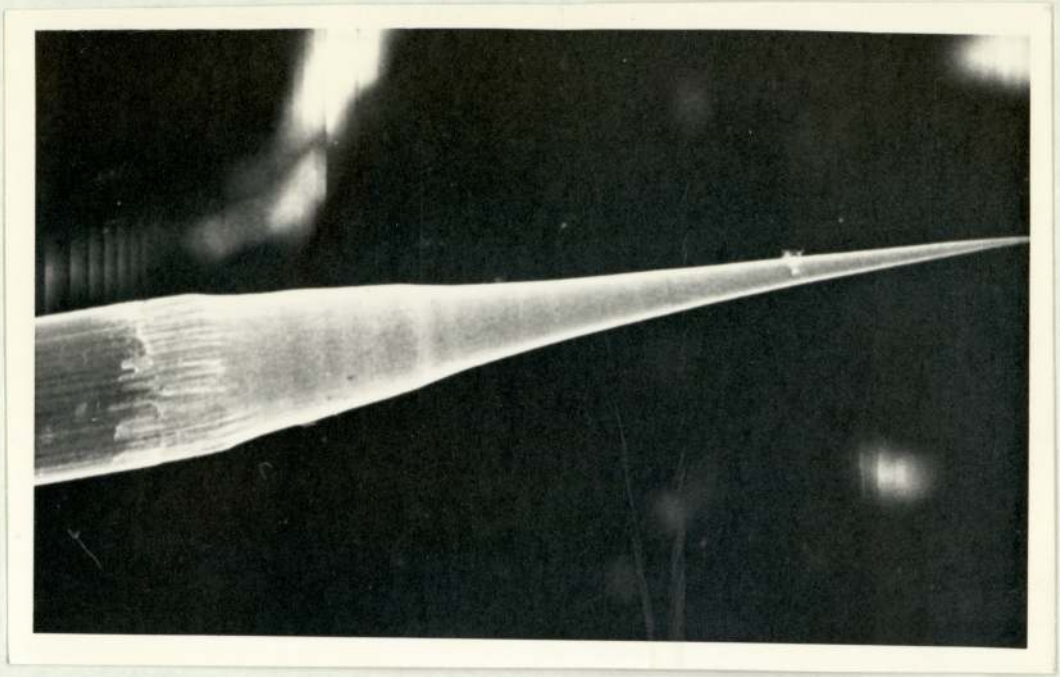

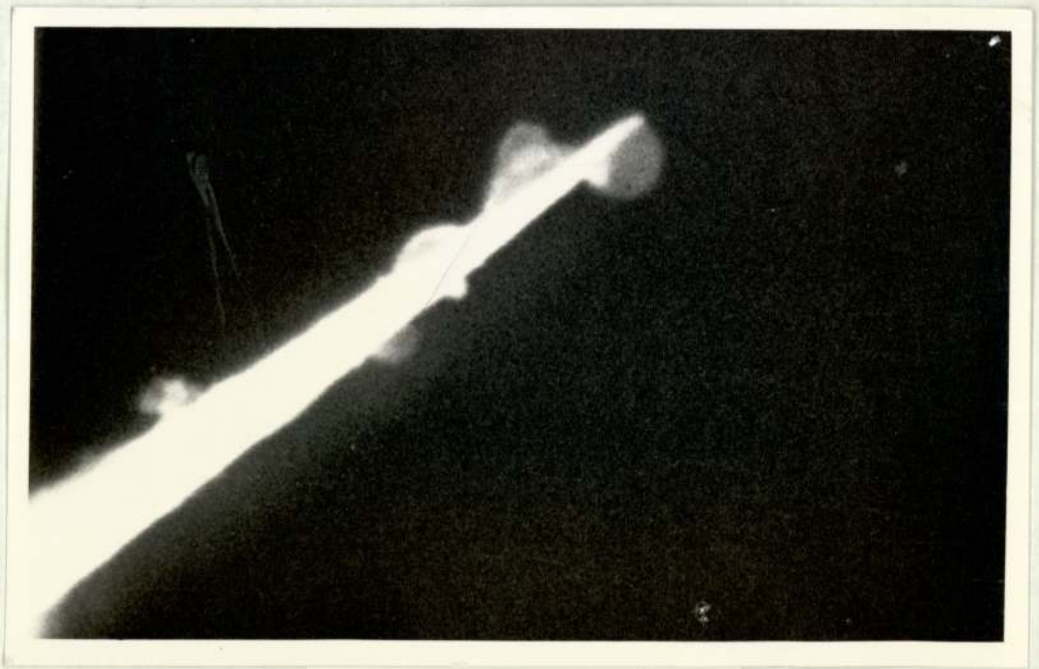

Radius ≈ 300Å

FIG 4.19

FIG. 4.20

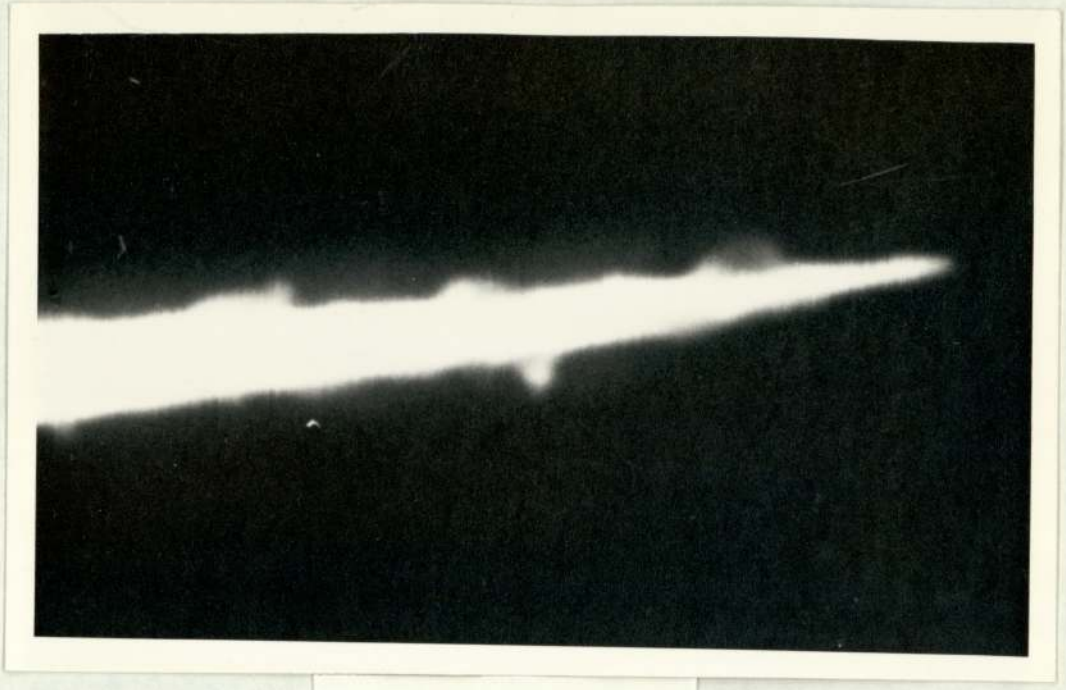

Radius ≈ 250Å
20 000 X

FIG. 4.21

Radius ≈ 250Å
100 000 X
same emitter as above

FIG. 4.22

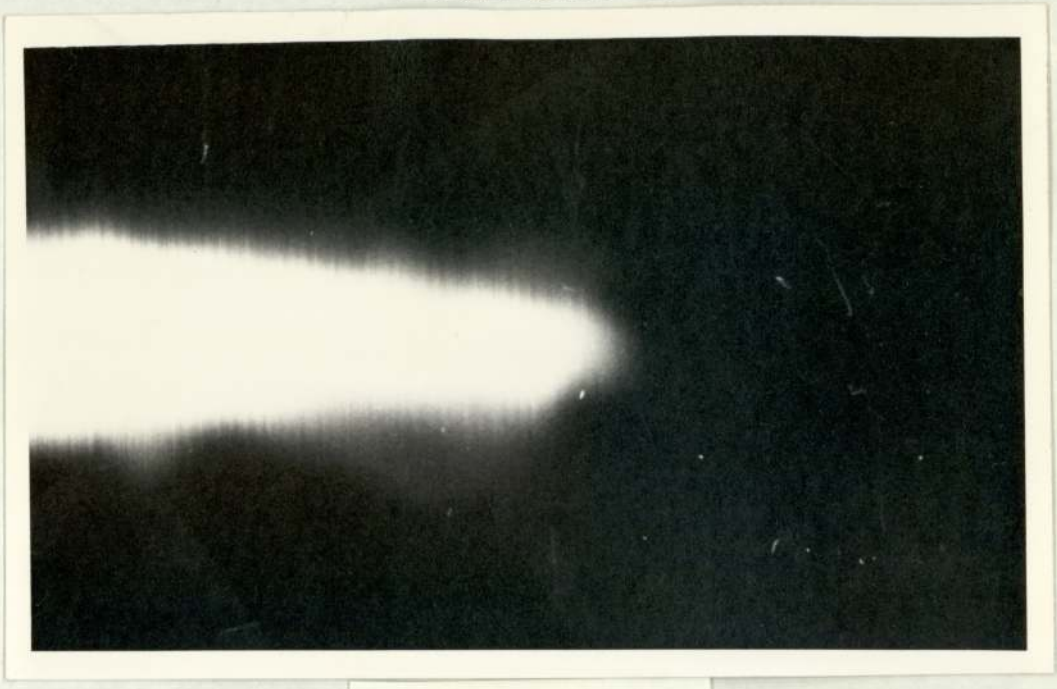

Radius ≈ 650Å
45 000 X

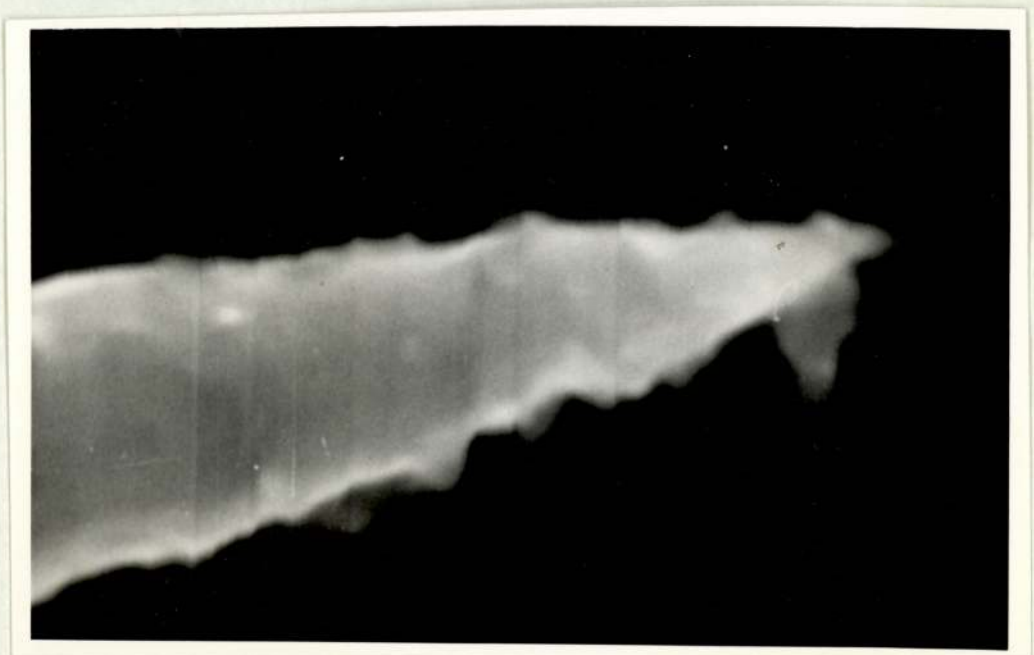

FIG. 4.23

Radius < 250Å
22 000 X

4.8. Mass spectrometry

When the experimental chamber was first assembled, it was necessary to check that:

(a) there were no leaks:

(b) the materials used in the system were not giving rise to excessive long term outgassing:

(c) there was negligible back-streaming from the pump, and

(d) oil from the rotary pump was not getting through the molecular sieve trap into the chamber.

An A.E.I. Minimass spectrometer head was joined onto the glass chamber and used to measure the partial pressures of contaminants in the mass range 12-240. The instrument could also be switched to read the partial pressures of hydrogen (2), and helium (4), the latter being used for leak detection using helium as a probe gas. The Minimass has a different sensitivity to different gases, and the partial pressures read directly on the mater are in terms of nitrogen sensitivity. Correction factors are available to allow the measured partial pressures to be converted to true partial pressures.

4.8.1. Spectrum of an unbaked system

The major peaks expected for an unbaked or lightly baked system would correspond to masses 2(H_2), 17 (OH^+), 18 (H_2O), 28 (CO and N_2), 32 (O_2) and 44(CO_2). Both carbon monoxide and nitrogen contribute to the peak at mass 28; their relative partial pressures can be determined since nitrogen will also have a peak at 14 and carbon monoxide, a peak at 12. Figure 4.2 is a trace obtained for the system before it was baked. The total pressure was about 4×10^{-6} Torr. The principal group of peaks is in the range

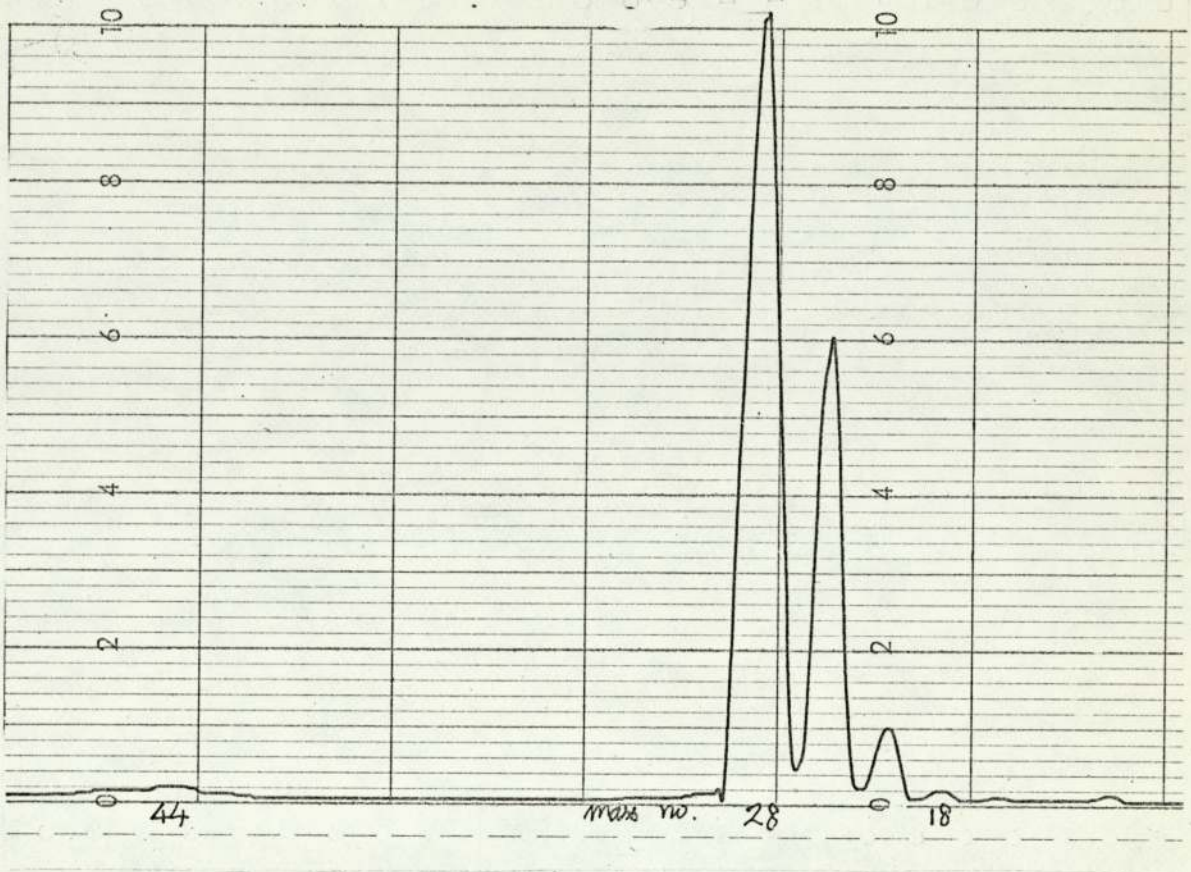

FIG. 4.24

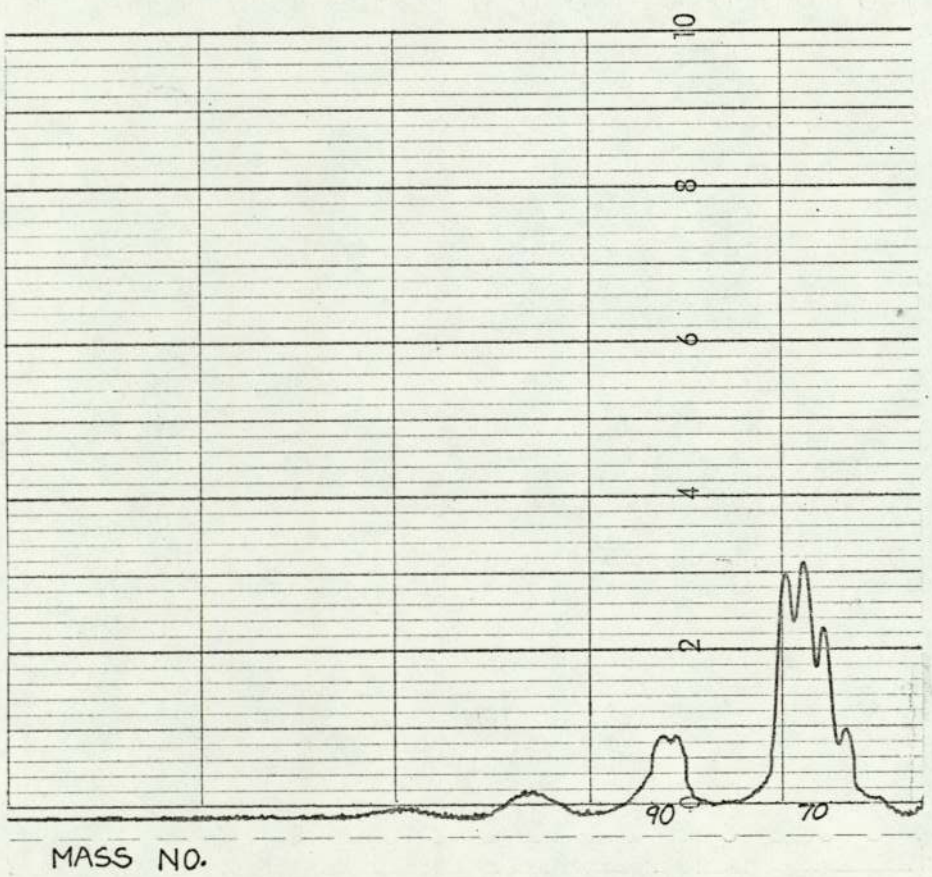

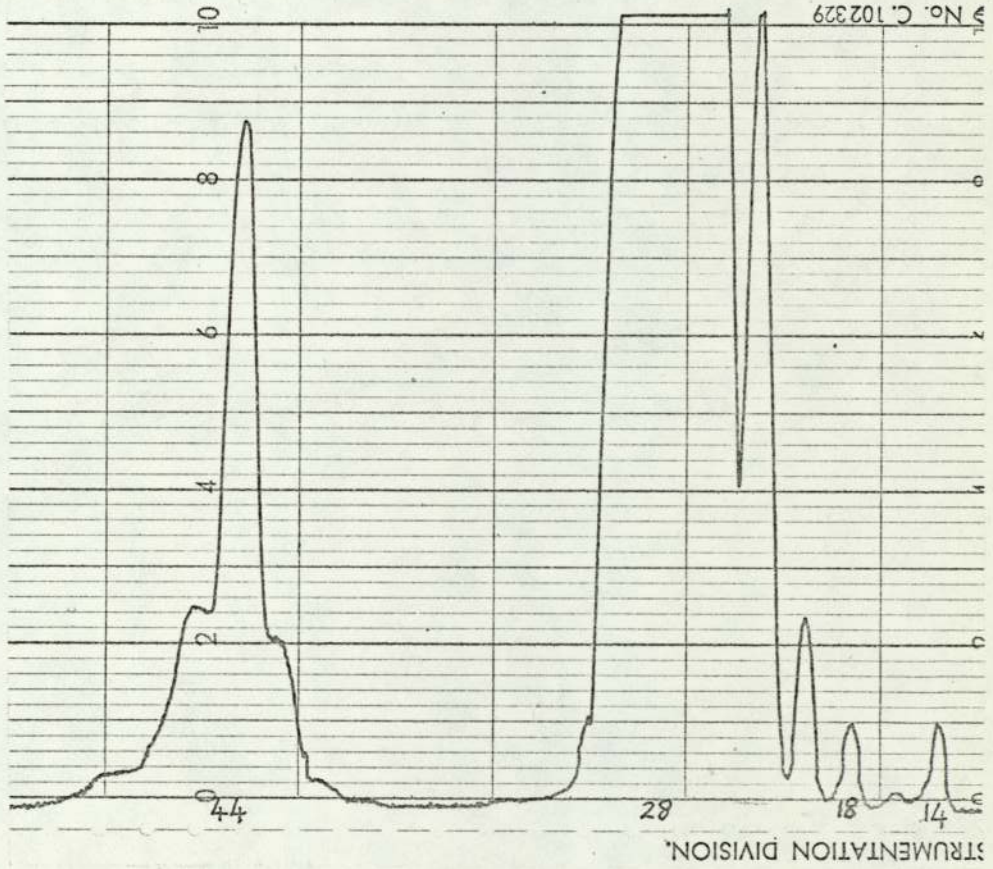

FIG. 4.25
UNBAKED VACUUM SYSTEM

25-32, with smaller peaks at 18 and around 44. When the sensitivity was increased (figure 4.25) peaks 68-72 and 85-100 could be discerned. This spectrum is similar to that obtained for a mercury diffusion pumped chamber, by J.R. Bailey,[3] in respect of the mass numbers above 50. The presence of three major peaks (figure 4.24) around mass number 28 is possibly the result of iso-propyl alcohol being present, since this was used for cleaning the system. The spectrum could be analysed as follows:

Mass number

12 Absent, therefore negligible carbon monoxide present.

14 Nitrogen.

16)
)
18) Water

19, 25-32 Nitrogen, oxygen and iso-propyl alcohol.

44 Carbon dioxide.

42-48 Iso-propyl alcohol, possibly with hydrocarbons, such as finger grease at 43 or oil from the backing pump.

70-100 Probably mercury.

4.8.2. Spectrum of a baked system

The spectrum obtained after the system was baked at 200°C for twenty-four hours is shown in figures 4.26 and 4.27. The principal peaks are 18 (water), 28 (nitrogen), and 44 (carbon dioxide). No peaks could be seen on the higher mass range 48-240. Mercury would give peaks at mass number 100 and in the range 196-204. No peaks were obtained at these mass numbers indicating that mercury was not present. There were secondary peaks at 16 and 17 corresponding to water, and at 14 (nitrogen). It appears that quite high baking temperatures or long baking times are

FIG. 4.26

SYSTEM BAKED AT 200°C FOR 24 HOURS.

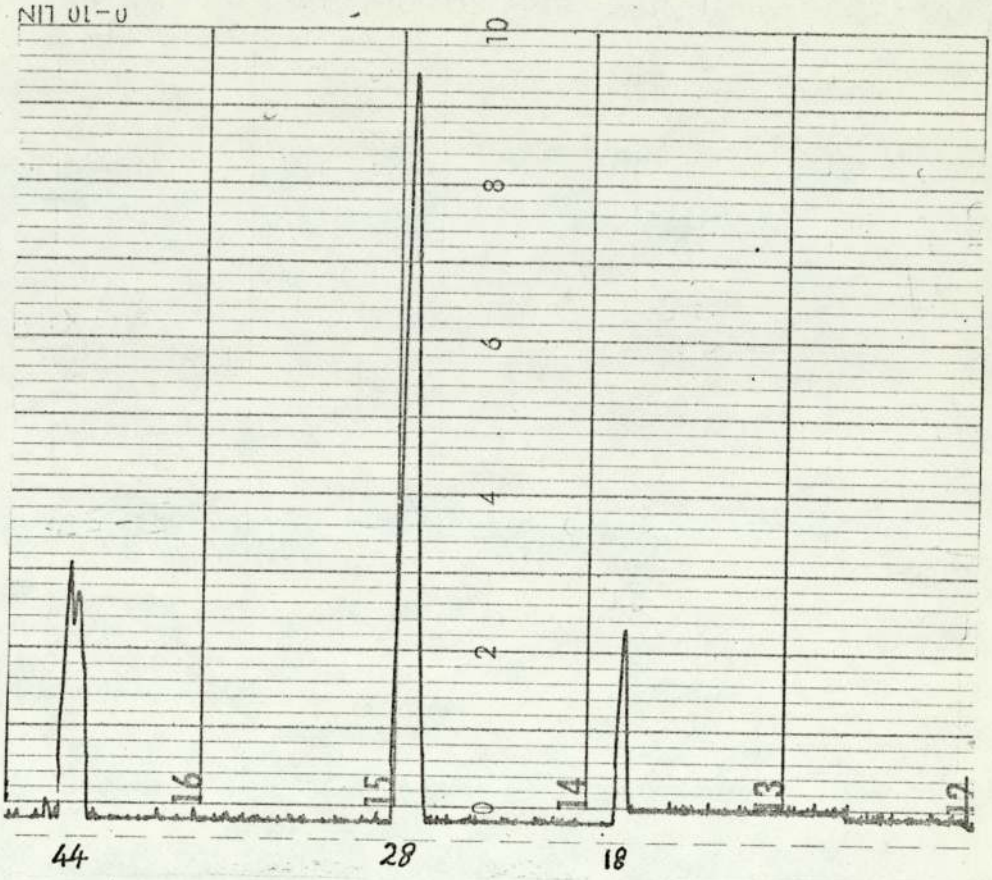

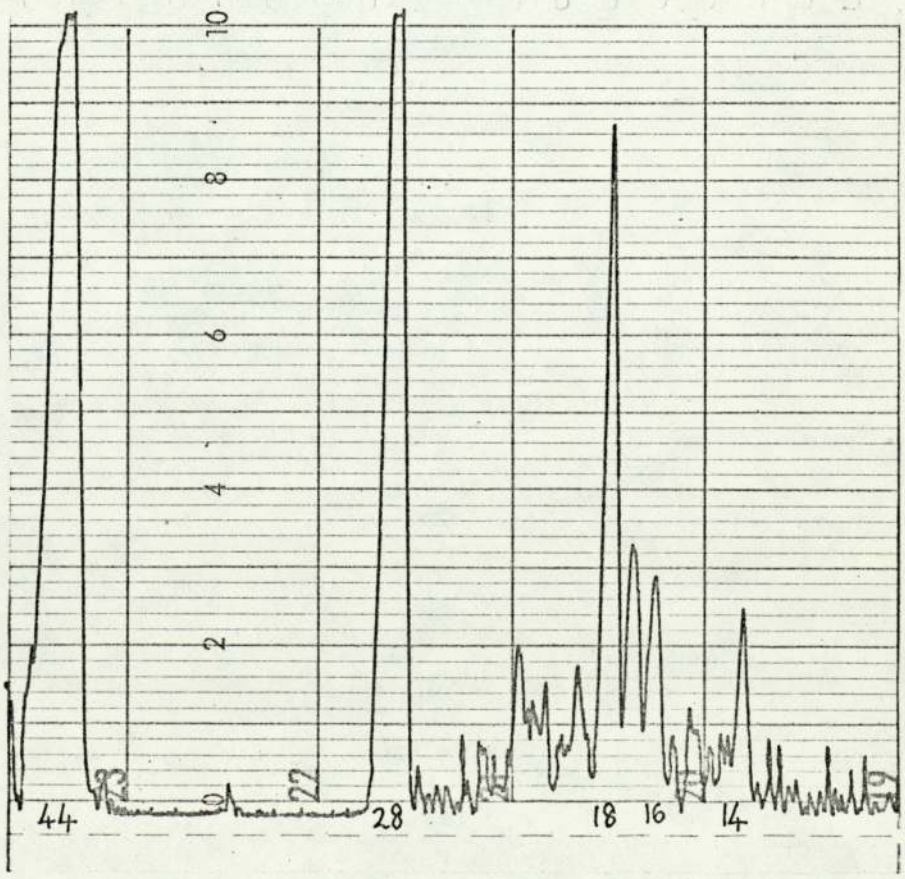

FIG. 4.27

required to remove water from the walls of the chamber, and so the usual procedure was to bake at 250°C - 300°C for three days. This was sometimes repeated and was successful in removing water from the chamber. The final pressure was usually 10^{-9}Torr.

4.9. Experimental system for field desorption

The field-emission microscope is as described elsewhere. It includes an anode ring, about 1 cm in diameter placed near the emitter. This reduces the field between it and the wall of the microscope and other sharp metal points in the system, since these tend to give unwanted emission. An example of this is shown in figure 4.29 where a short bright arc can be seen which resulted from emission from a contact to the phosphor screen.

The alternating potential is produced by a 44kV 20mA oil insulated transformer, the primary of which is supplied by a Variac transformer, model 100R-M. A protective resistance chain of 10^8 ohms is connected to one side of the secondary and a high insulation cable joins this to the field-emission microscope. This cable is kept well away from earthed surfaces so as to reduce the field strength across the insulation of the cable. The other side of the secondary winding is earthed, figure 4.28. . The positive bias is provided by a 0-50kV Brandenberg power supply, model 851 which is connected to the emitter via a protective resistor chain.

4.9.1. Experimental procedure and observations

After a chosen emitter has been positioned in the anode loop of the field-emission microscope, emission current and voltage measurements are made to obtain a Fowler-Nordheim plot for the emitter. The product kr

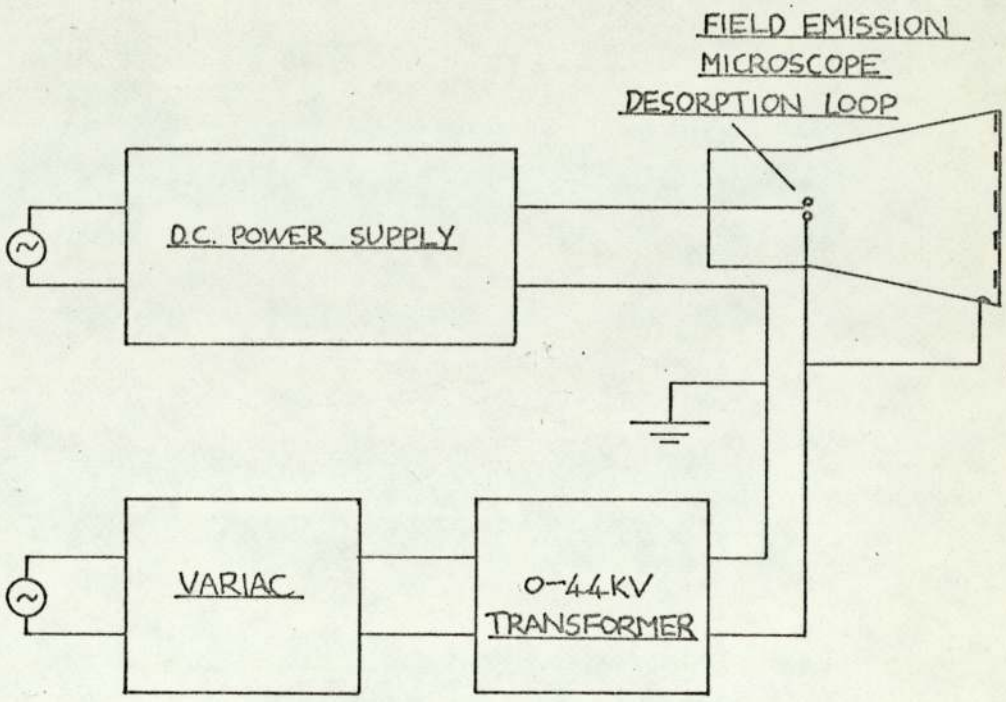

FIG. 4.28

FIELD DESORPTION SYSTEM

where k is the geometrical factor (described elsewhere) and r the tip radius, are then determined. Since the field strength needed for the evaporation of tungsten is about 500 MV/cm, it is possible to calculate the a.c. and d.c. voltages required to clean the emitter tip.

The a.c. voltage is increased slowly, together with the d.c. bias. The field-emission microscope image usually consists of a random array of bright spots distributed against a black background, giving a fine grainy appearance to the image. As the field is increased, the bright spots are seen to scintillate, some to disappear and new ones to appear. They often split into two halves before disappearing. Fig.4.30.

The initial grainy appearance of the image was reported by Good and Muller,[4] and Ashworth.[5] They saw doublets which finally left the surface and concluded that the spots were probably individual molecules. It is possible that the doublets were diatomic oxygen molecules which dissociate into their constituent atoms. Since the resolution of a field-emission microscope is typically 20 - 30 Å, it would be surprising if individual atoms could be detected. Good and Muller explain this by assuming that the doublet is on a protrusion so that the field in front of the molecule is modified to give an increased magnification.

Gomer[6] states that there is no straightforward correlation between molecular shape and image shape but that the doublets are due to very small aggregates, causing local enhancement and divergence of emission. He suggests two possible mechanisms: (a) that the adsorbed molecule is large, having a sufficient number of energy states to prevent field penetration. In this case the adsorbate acts

like a conducting protrusion causing field enhancement. The second mechanism (b) is when field penetration of the adsorbate occurs, an adsorbed molecule constituting a short-range potential well and acting as a window in the barrier for field-emission.

After desorption has proceeded for several minutes, a symmetrical pattern appears (figure 4.29) which is the expected image for [110] orientated tungsten, the bright areas being regions of lower work function.

The dark areas correspond to the relatively high work function planes, (011), (112), ($\bar{1}$12), ($\bar{1}$21) and (121), (figure 4.31). The planes (001) and (010) are not visible, indicating that the surface was not completely clean.

In the early field desorption experiments, occasionally there was breakdown of the insulation and a discharge in the desorption circuit would cause the emitter to be damaged by a short high current pulse. This sometimes resulted in a double headed emitter, (figure 4.32 bottom left-hand corner).

FIG. 4.29

FIG. 4.30

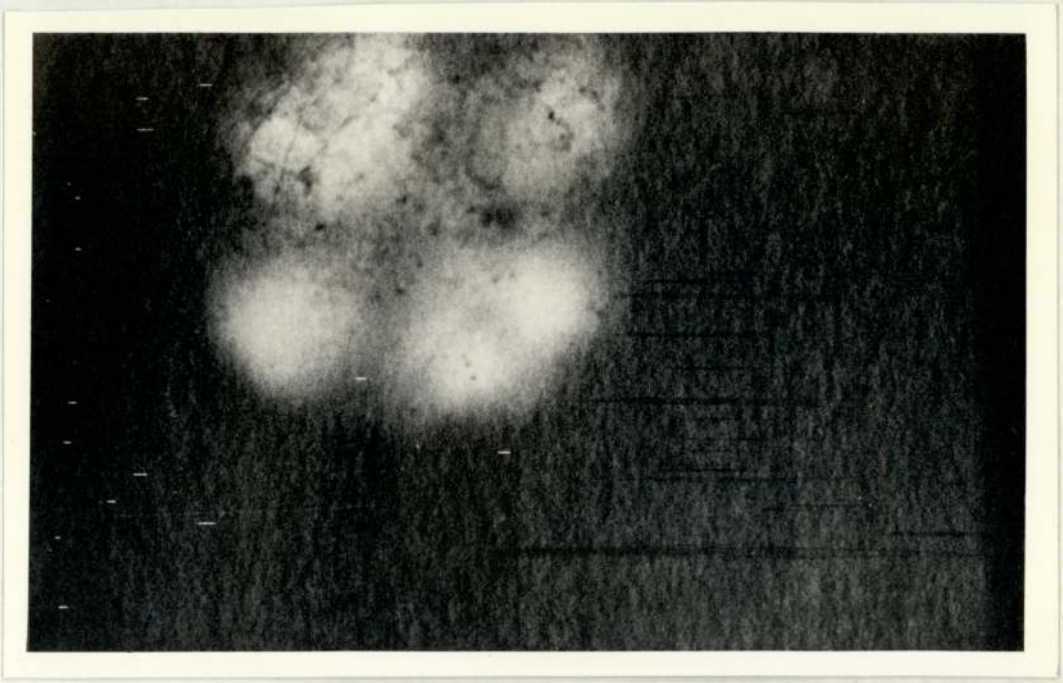

FIG. 4.31

FIG . 4.32

TWO HEADED EMITTER

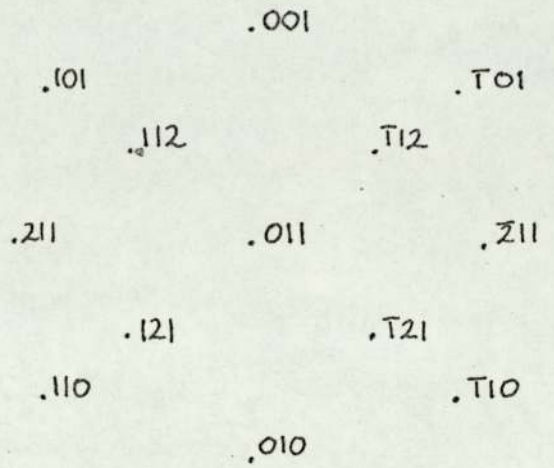

CRYSTALLOGRAPHIC MAP FOR A CUBIC CRYSTAL

4.10. Electrometer measurements

The electrometer used is a Keigthley 610BR which enables currents down to 10^{-14}A to be measured. In principle the instrument is a d.c. vacuum valve voltmeter with an electrometer valve input providing an input resistance greater than 10^{14}ohms. In the normal method of current measurement, the current is determined by measuring the voltage drop across a resistor shunting the amplifier input. The shunting resistor is in the range 10 to 10^{11}ohms. In the "fast" method of use, the shunt resistor is between the amplifier output and input in the feedback loop. This neutralises the effect of input capacitance and increases the response speed. The input voltage drop is reduced to a maximum of one millivolt on any range.

The current being measured is screened from pick-up by enclosing the experimental chamber in shielding made of removable sheets of expanded aluminium and aluminium foil. The retarding potential, which is applied to the collector, is provided by two 9V grid bias batteries and a 10kΩ helipot. The battery and helipot stand on a Perspex platform on PTFE legs within an earthed aluminium box. Connections are made from the electrometer and to the analyser using low noise coaxial cable.

4.10.1. Circuit response time

For the measurement of a current of 10^{-12}A, the electrometer measures a potential drop of 1V across a 10^{12}ohm resistor. The input coaxial cable, the wiring inside the instrument, and the effective capacitance of the input valve grid to the other electrodes result in a capacitance of about 200pF shunting the 10^{12}ohm resistance. The time

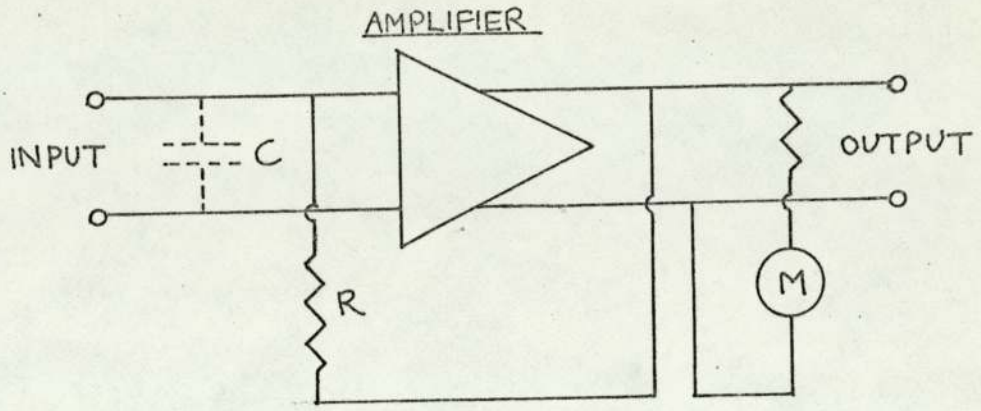

C CAPACITANCE OF INPUT CIRCUITRY

R FEEDBACK RESISTANCE

M METER

FIG. 4.33 .

ELECTROMETER WITH NEGATIVE FEEDBACK.

constant for this system is the product of the capacitance and resistance and is 200s. Accurate readings cannot be made until about four time constants have elapsed thus a measurement cannot be made until approximately twelve minutes have elapsed.

The capacitance can be reduced by shortening the coaxial cable and increasing the distance of the earthed electrostatic screen from the connection to the experimental chamber. The full-scale sensitivity of the instrument is V/R where V is the full-scale voltmeter sensitivity and R is the shunt resistance. The resistance at the electrometer can be reduced, but the voltage sensitivity control needs to be increased so that the current will still give a significant deflection on the scale. If the value of the shunt resistance is decreased and the value of the voltage sensitivity is increased, then the effect of zero drift and the noise generated in the shunt resistor becomes significantly more important.

The Keigthley 610 BR is provided with a negative feedback control to decrease the response time when measuring small currents. The meter and the feedback resistor R are chosen so that full scale deflection occurs when one volt is developed at the output. When a positive current appears, a small positive voltage is developed at the input; however the output voltage becomes negative and reduces the input voltage to one-thousandth of the output voltage. The full-scale output sensitivity is the full-scale output voltage divided by the resistance of the feedback resistor. The capacitance of the input circuitry no longer shorts the high resistance and the time constant is reduced to about a thousandth of what it is without feedback. Fig.4.33.

4.10.2. Effect of grid current

The potential difference developed across the input resistance during current measurement is applied to the grid of an electrometer valve. However, each electrometer valve has itself a current developed in its grid by two sources - (a) electrons from the cathode hitting the grid, and (b) positive ions (caused by thermionically emitted electrons colliding with atoms of residual gas) being attracted to the grid. In practice the grid current in electrometer valves is kept as low as possible and in this instrument is about 5×10^{-14}A. However, this current charges up the external test circuitry when connected and accounts for a reading appearing on the electrometer when no current from an external source is flowing. The grid current appears as a background current during measurements of small current and needs to be taken into account.

4.10.3. Zero drift

The zero drift of the electrometer is due to changes in the cathode of the electrometer valves. These changes appear as a varying grid potential and are of the order of one millivolt per hour, thus if the output of the instrument is not shorted out and the instrument not zeroed before each reading, then an appreciable error can result, e.g. if the instrument is not shorted out or zeroed for an hour and is then used with a voltage sensitivity of 0.01, there will be an erroneous reading of 10% full scale deflection.

4.10.4. Charge generation and charge transfer

Any movement of the connecting cables or external circuitry causes changes to be developed by friction of the

moving parts; these charges appear at the electrometer. For this reason low noise control coaxial cable is used in which the charges generated by the sliding of the braid over the insulating material are conducted away by a layer of graphite; however, the measuring circuit should be mechanically stable.

Charge transfer occurs when a mechanical contact is broken. Thus when the zeroing button is released, a charge will cause a current to appear on the electrometer which will decay in a time depending on the time constant of the internal circuitry of the instrument. For this reason, the input resistance is turned to a low value before releasing the set-zero button and its value is gradually increased to that required for the current measurement.

CHAPTER 5. Results

5.1. Introduction

This chapter is divided into five sections. In the first experiments with the thermionic emission analyser are described leading to a graphical relationship between energy distribution width and beam saturation current. The second is on the development of a suitable field-emission gun and the description of a simple field-emission retarding potential analyser. In the third section a simple field-emission analyser based on experiments with the Hartwig and Ulmer analyser and the electron gun, is described. The fourth section is on experiments based on Fowler-Nordheim plots and the fifth gives results of the measurement of the integrated total energy distribution of tungsten and the determination of the mean work function.

5.2. Thermionic emission experiments

In order to investigate the properties of the energy analyser it was used to determine the effect of beam current density on the width of the energy distribution.

5.2.1. Preliminary experiment

Before the first experimental chamber was available, the energy analyser was tested in a simple chamber using 'O' rings as seals. (See figure 5.1). The unit holding the emitter was obtained from an electron microscope and a brass Wehnelt's cylinder was screwed on the threaded portion . The thermionic emitter and cylinder could be moved across the first aperture of the analyser using the three adjusting screws. The separations of the filament and analyser and also the filament and Wehnelt's cylinder aperture were adjusted before the gun unit was put in position. The position of the Faraday cage was also adjustable. Simple experiments with this system gave information on the magnitudes of the various parameters and experience in using the analyser for thermionic emission. Typical curves of collector current against retarding potential are shown in figure 5.2. The next series of experiments were carried out in the second experimental chamber.

5.2.2. Apparatus for thermionic emission experiments in the second chamber

The analyser was operated in the second chamber using a molybdenum disc as a grid which had an aperture of 2.5 mm. Its separation from the analyser was adjustable and was normally 1-2 mm.

The tip wheel and supporting glass column had been designed for field emission and so minor modifications had

FIG. 5.1

Energy analyser used for thermionic emission

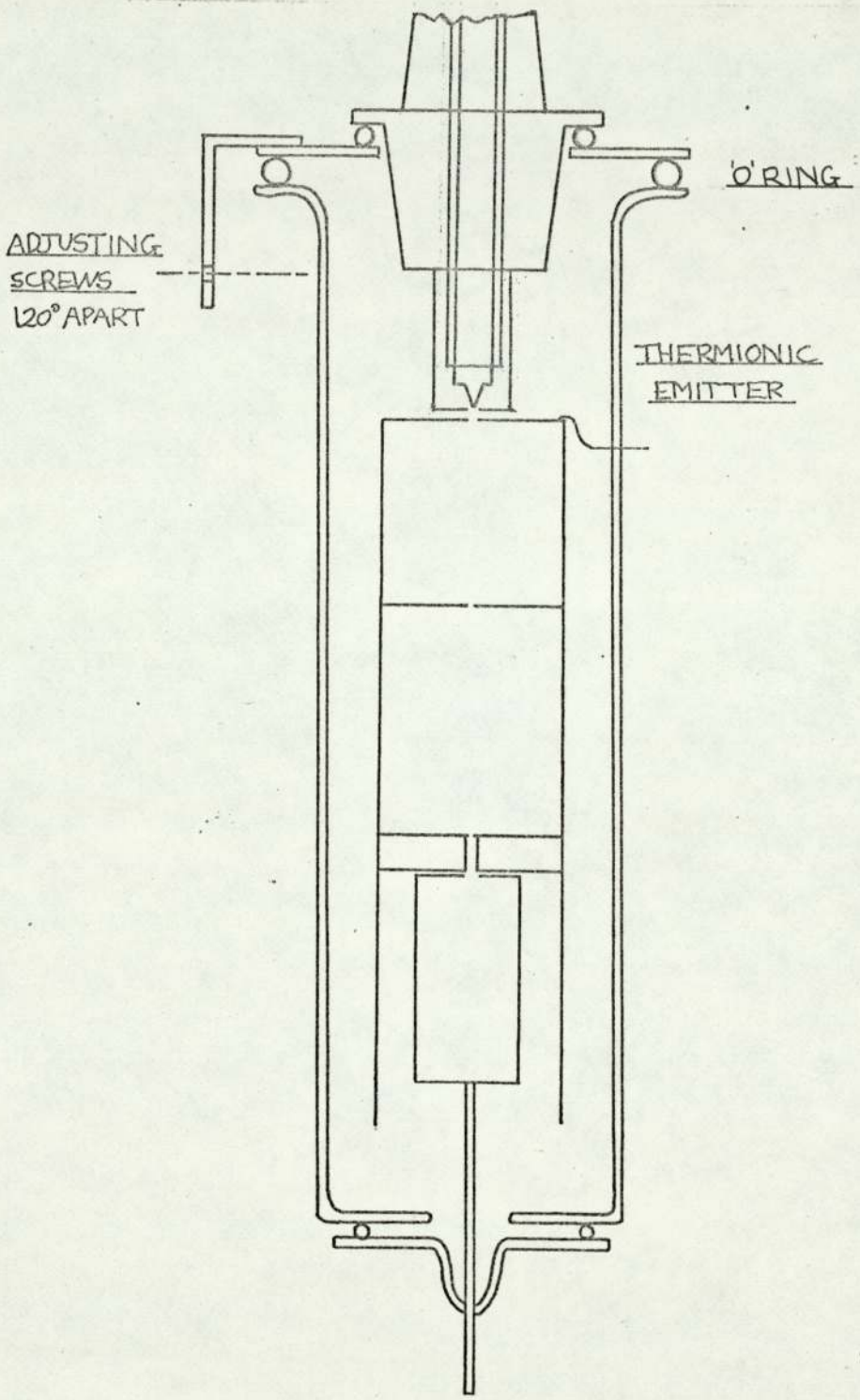

Retarding potential curves

FIG. 5.2.

A ANODE POTENTIAL 1000V GRID BIAS −1·87V MAXIMUM COLLECTOR CURRENT 6.5×10^{-8}A

B " " 1500V " " −2·85V " 1.15×10^{-7}A

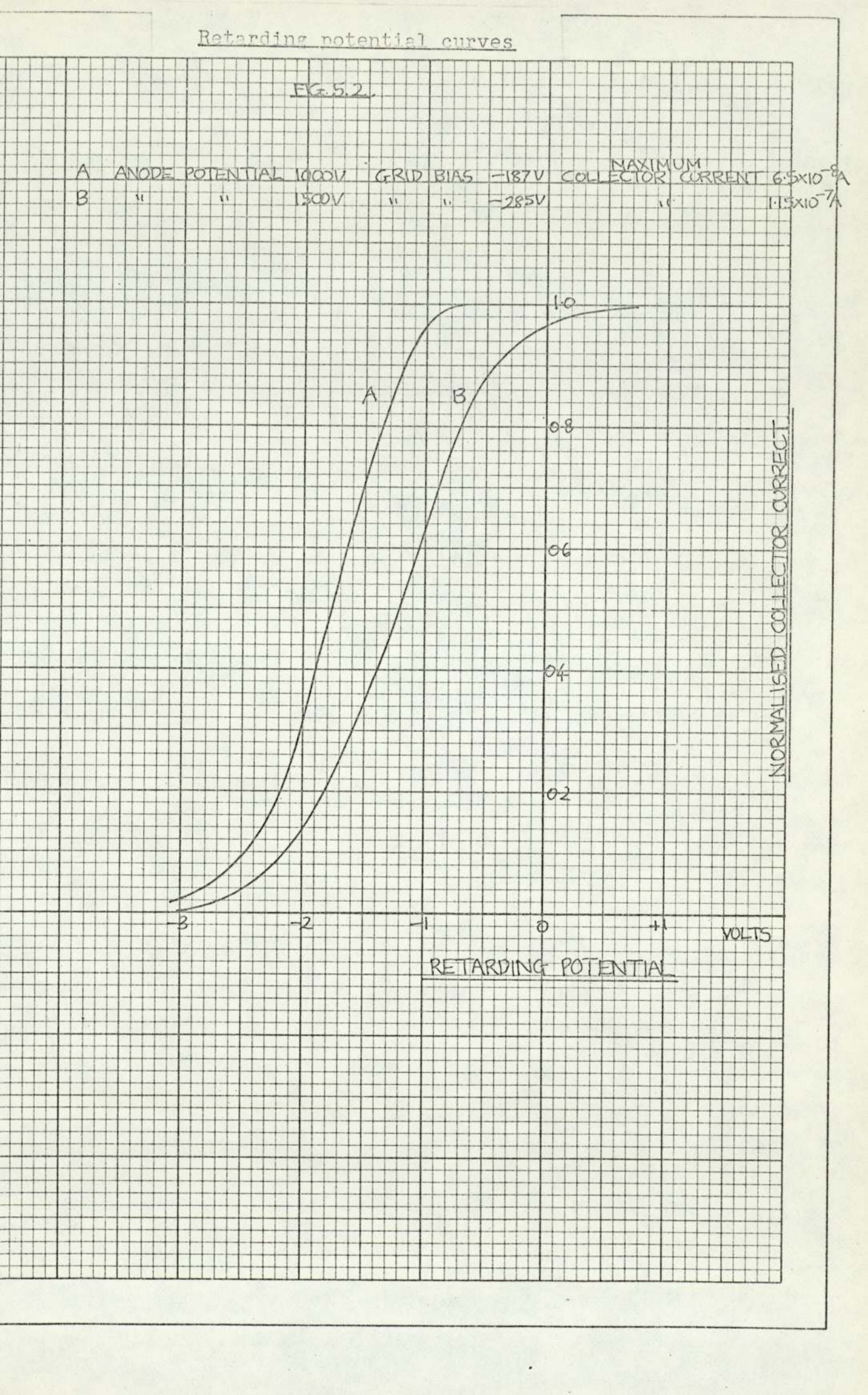

to be made to supply current carrying wires to the filament (see photograph 5.3). A second lead was therefore provided by using an insulated copper wire which ran up on the outside of the glass tube to a tungsten lead passing through the wall of the tube. The analyser was surrounded by some mu-metal shielding to reduce the effect of the magnetic field of the earth on the electron beam.

The system was evacuated to about 10^{-7} Torr and the filament was aligned. The emitter current supply, bias and anode potential were adjusted to give a suitable collector current, (see figure 5.4). At a chosen height of the filament, its position in the plane perpendicular to the axis was adjusted to give maximum collector current. The retarding potential was varied to give the collector current versus retarding potential plot. The temperature of the filament was measured using an optical pyrometer.

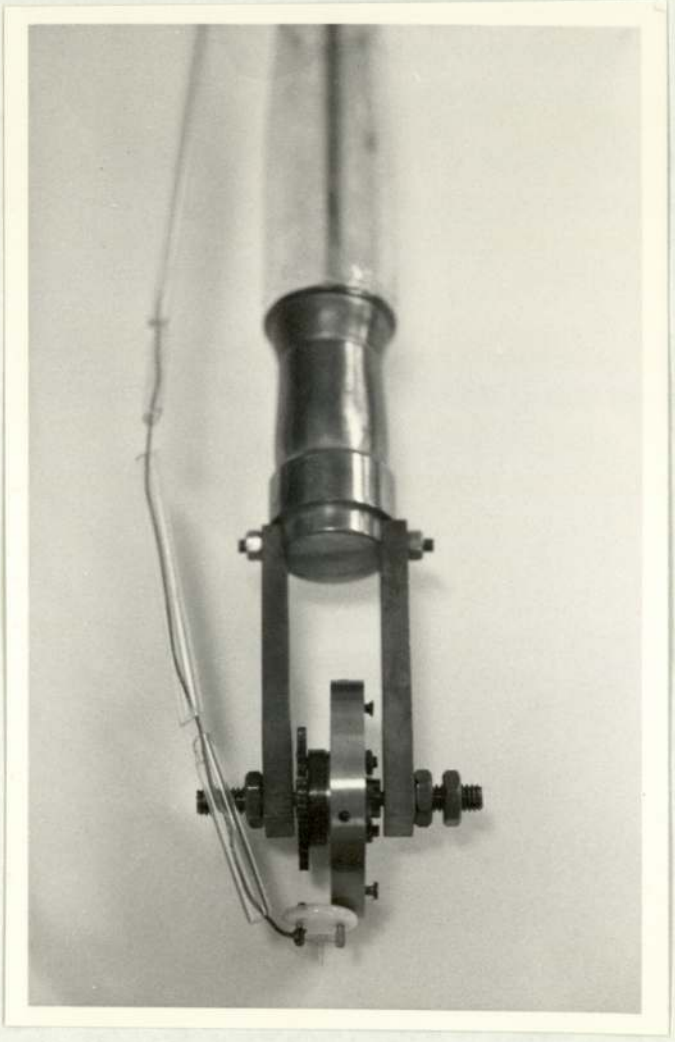

Field-emission tip wheel modified to hold a thermionic emitter. Fig.5.3.

FIG. 5.4

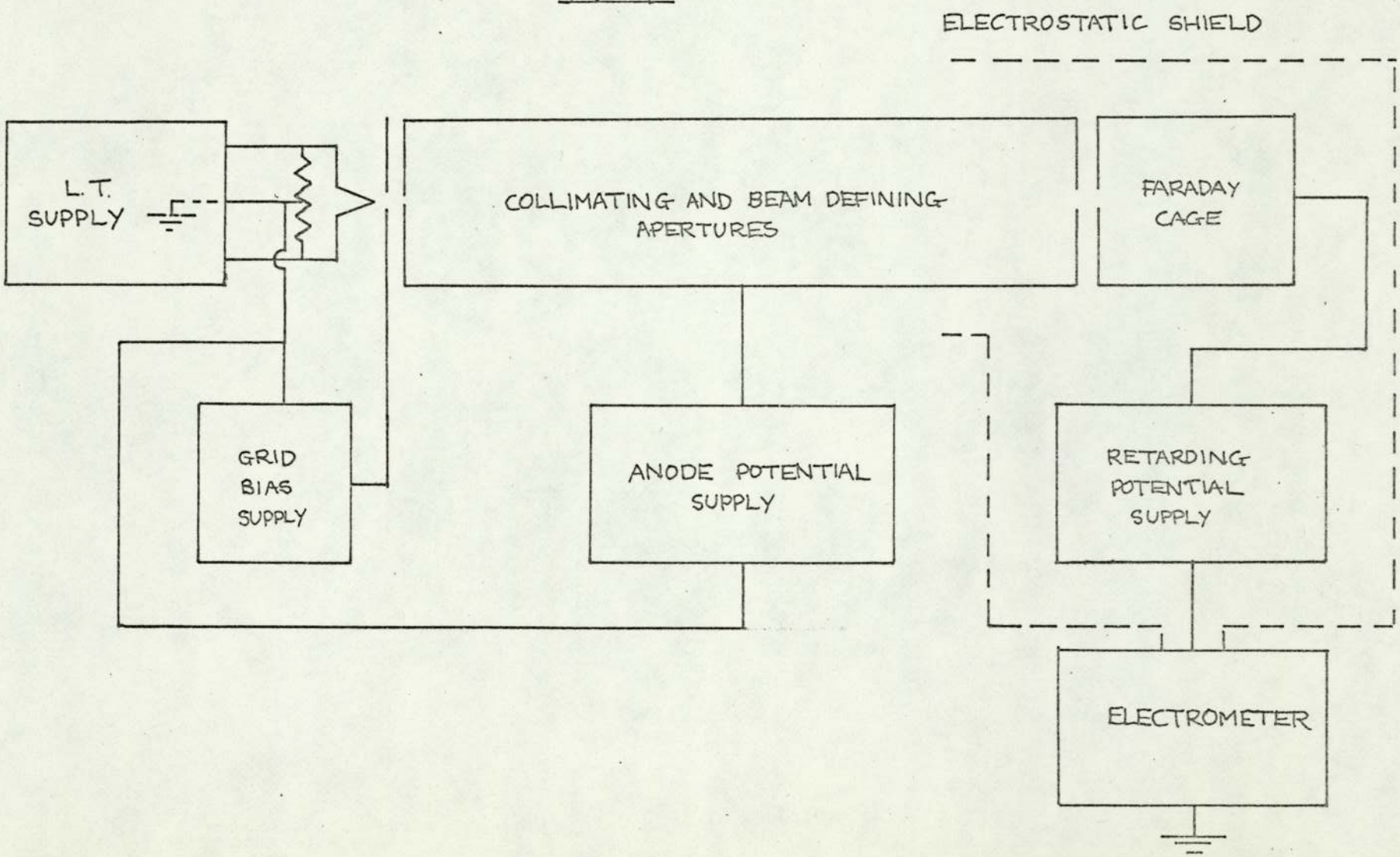

Block diagram of circuit for thermionic emission

5.2.3. Results

5.2.3.1. Variation of anode current with anode voltage

Temperature ~1600°C

Grid bias 0V

Anode-grid separation 3½mm

Filament-grid separation ~1mm

The curve obtained is shown in figure 5.5. It follows approximately the shape that would be expected for a graph of current density against anode voltage for a simple diode system. Even though the current and not the current density has been measured, the curve shows the characteristic increase in gradient, followed by a levelling off as the saturation current is approached.

If the anode current is plotted against $V_a^{3/2}$ where V_a is the anode voltage (Figure 5.6) then the curve is initially a straight line. This presumably is the straight line relationship predicted by Child's law for the space charge limited region of a diode, even though no account has been taken of the varying cross-section of the beam in this triode arrangement.

5.2.3.2. Variation of anode current and collector current with grid bias.

Temperature~1620°C

Collector potential 0V

Anode-grid separation 3½mm

Filament-grid separation ~1mm

Anode voltage 150OV

FIG. 5.5

Variation of anode current with anode voltage

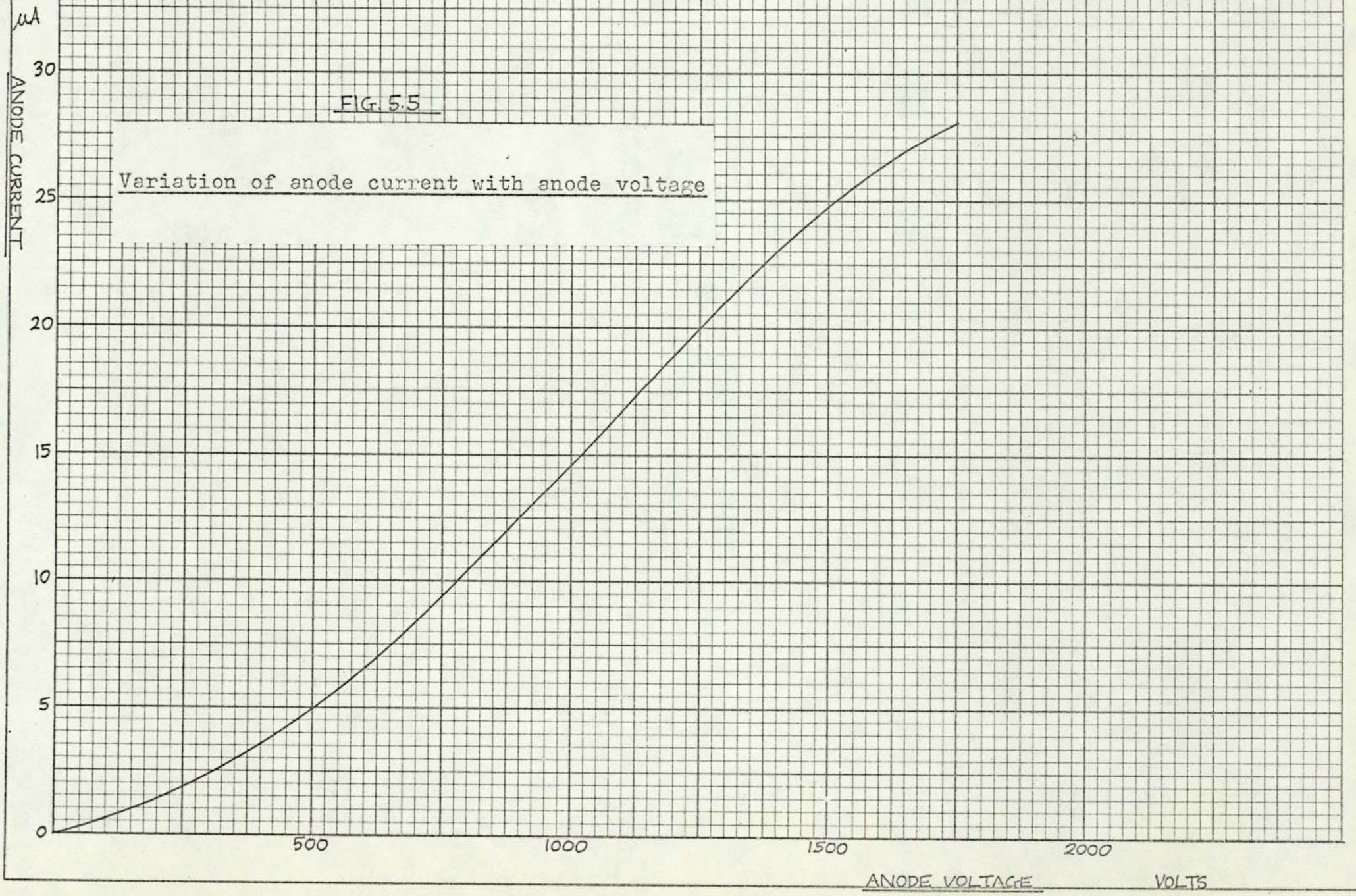

FIG. 5.6

Variation of anode current with anode voltage$^{3/2}$

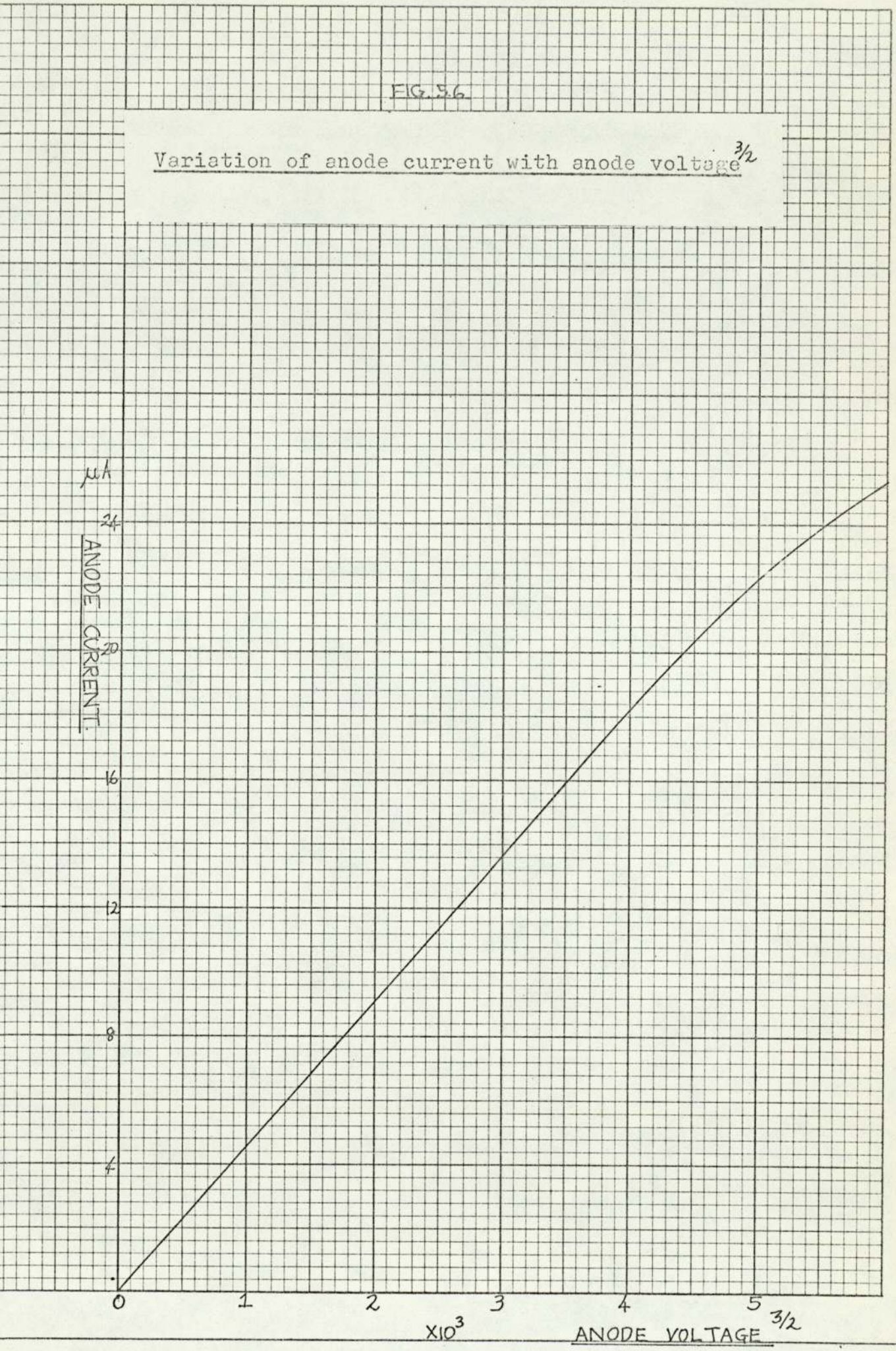

As the grid bias V_G was increased, the anode current I_A appeared to decrease linearly towards a grid bias cut-off value of -560V. An approximately linear relationship between beam current and grid bias would be expected. The collector current I_C increased in an approximately exponential way. The changes in I_A and I_C indicate that as the grid bias is increased, the beam becomes more concentrated. The curve of I_C against V_G would be expected to go through a maximum and decrease as the grid bias is increased to the cut-off point, the latter occurring when the zero equipotential is at the filament tip, or just in front of it, so that emission is suppressed. A broad peak in the curve of collector current against grid bias is shown in figure 5.7.

5.2.3.3. Retarding potential curves

Two sets of retarding potential curves are shown. In each case the curves of collector current against retarding potential were normalised.

Group 1 (Figure 5.8)

Anode voltage 1000V.

Temperature 1600°C.

Anode-grid separation 3½ mm

Filament-grid separation 1 mm

Collector current and anode current against grid bias

FIG. 5.7

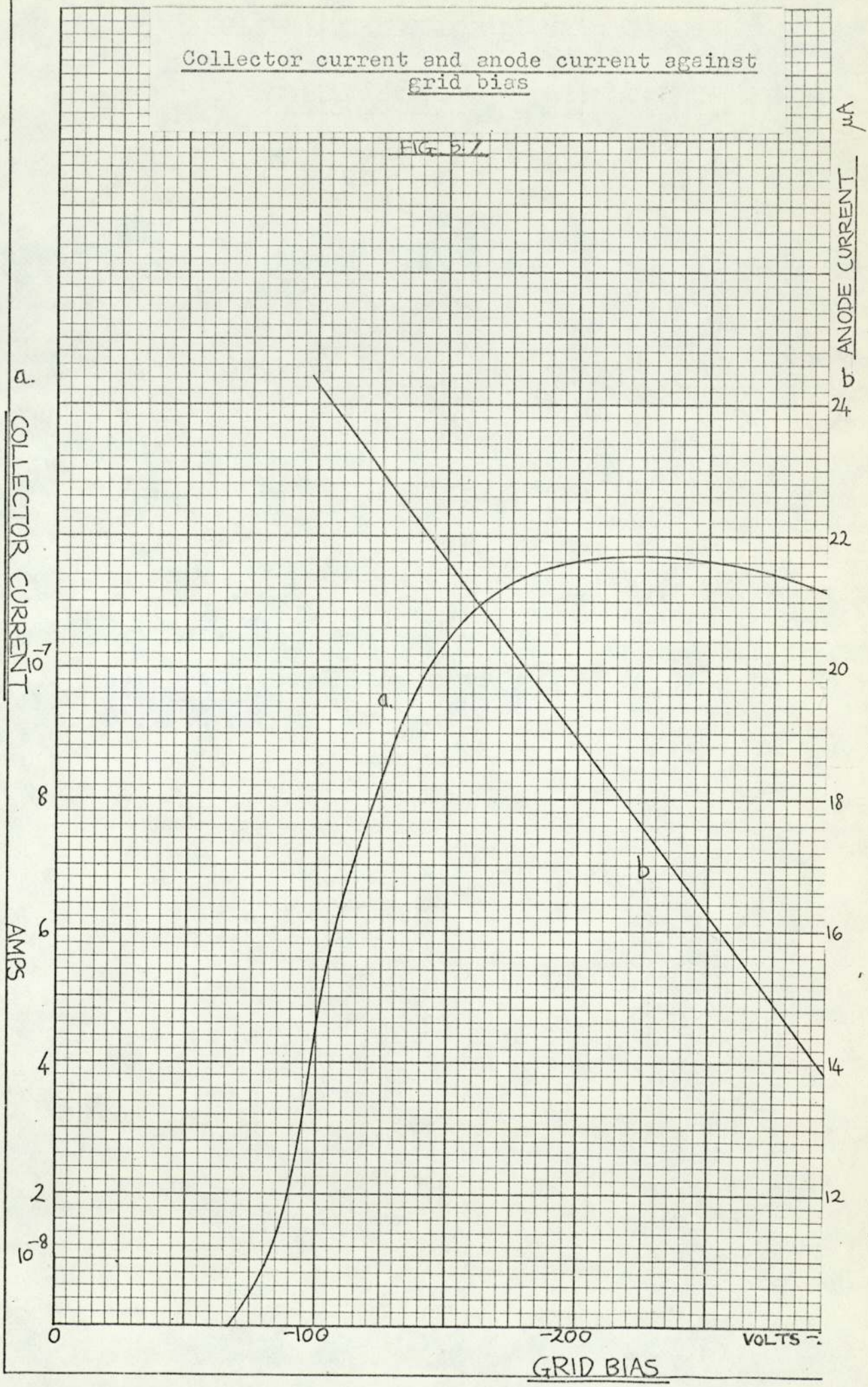

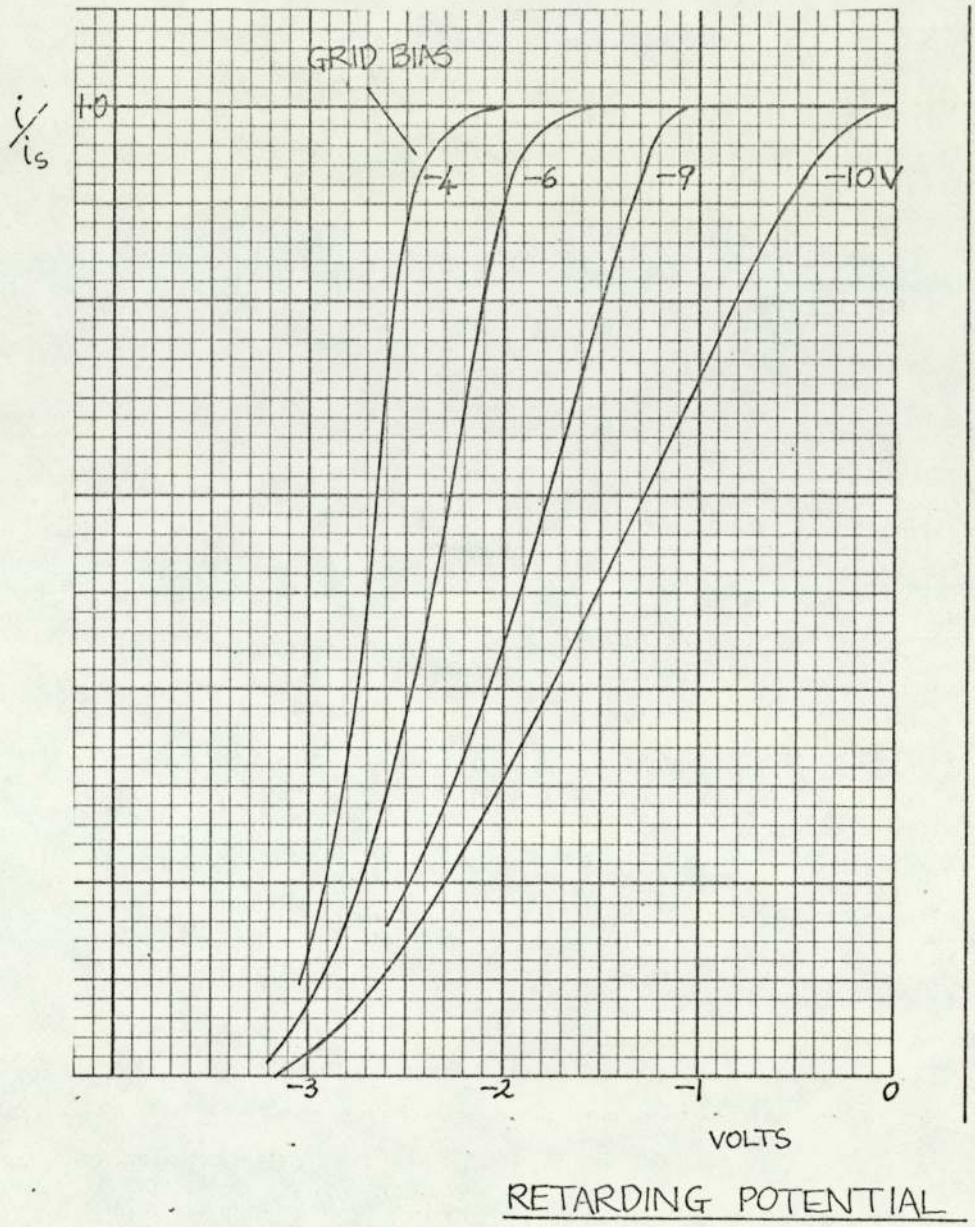

FIG. 5.8

Group 1 retarding potential curves.

Grid bias volts	Emission current μA	Saturation current A_{is}	ΔV_{63}* eV
-10	18.8	1.90×10^{-9}	1.68
- 9	18.9	1.00×10^{-9}	1.05
- 6	19.2	3.75×10^{-10}	0.65
- 5	19.3	1.20×10^{-10}	0.52
- 4	19.4	1.70×10^{-11}	0.42

It can be seen that as the saturation current decreases, the bandwidth ΔV_{63} becomes smaller.

Group 2 (Figure 5.9)

Anode voltage 1000V

Temperature ~ 1600°C

Anode-grid separation 3½mm

Filament-grid separation ~ 1mm

Grid bias volts	Emission current μA	Saturation current A_{is}	ΔV_{63} eV
-6.05	-	0.37×10^{-9}	0.65
-6.60	-	0.63×10^{-9}	0.78
-7.25	19	0.89×10^{-9}	0.98
-8.00	-	1.50×10^{-9}	1.45
-9.00	19	2.12×10^{-9}	1.70

* See section 2.4.5.1.

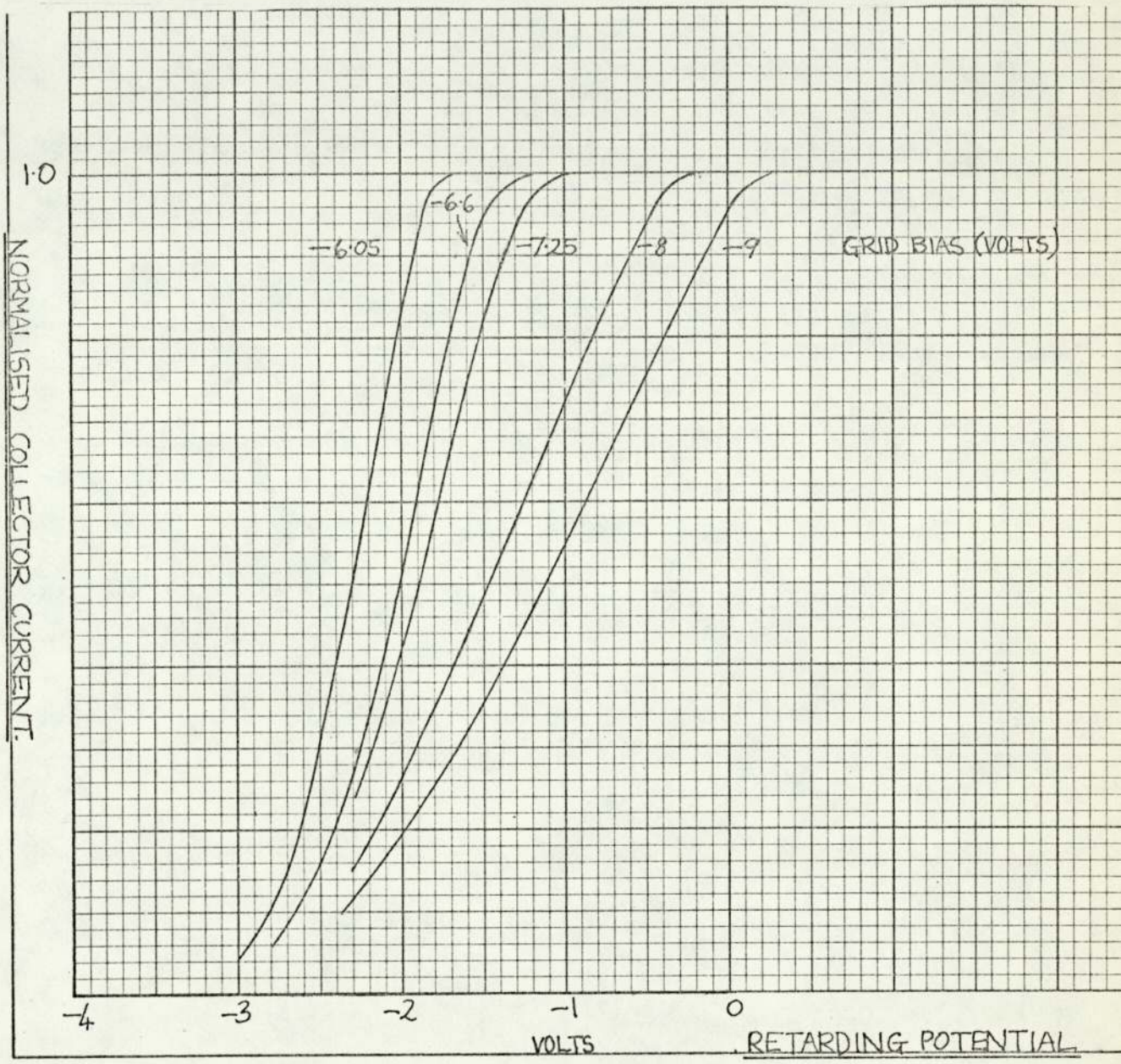

FIG. 5.9
Group 2 retarding potential curves.

5.2.3.4. Variation of energy distribution width ΔV_{63} with saturation current

The two groups of curves show that in the experiments, the width of the integrated energy distribution decreased with decreasing saturation current i_s. In order to see if there was any clear relationship between the two parameters, graphs of ΔV_{63} against the saturation current i_s were plotted (figure 5.10). Strictly the saturation current density should have been plotted, however this would have had to be calculated from the diameter of the aperture before the Faraday cage (0.5 mm). It would then have to be assumed that the beam diameter was never less than 0.5 mm.

It can be seen that the relationships are approximately linear, decreasing to an average value of 0.4eV at $i_s = 0$. The measurements of filament temperature were made with an optical pyrometer, applying corrections for the effect of the glass wall of the chamber on the measured temperature. The corrected temperature was 1600°C. This corresponds to a theoretical distribution width of 0,32eV, which is in fairly good agreement with that predicted from the measurements of ΔV_{63} against i_s.

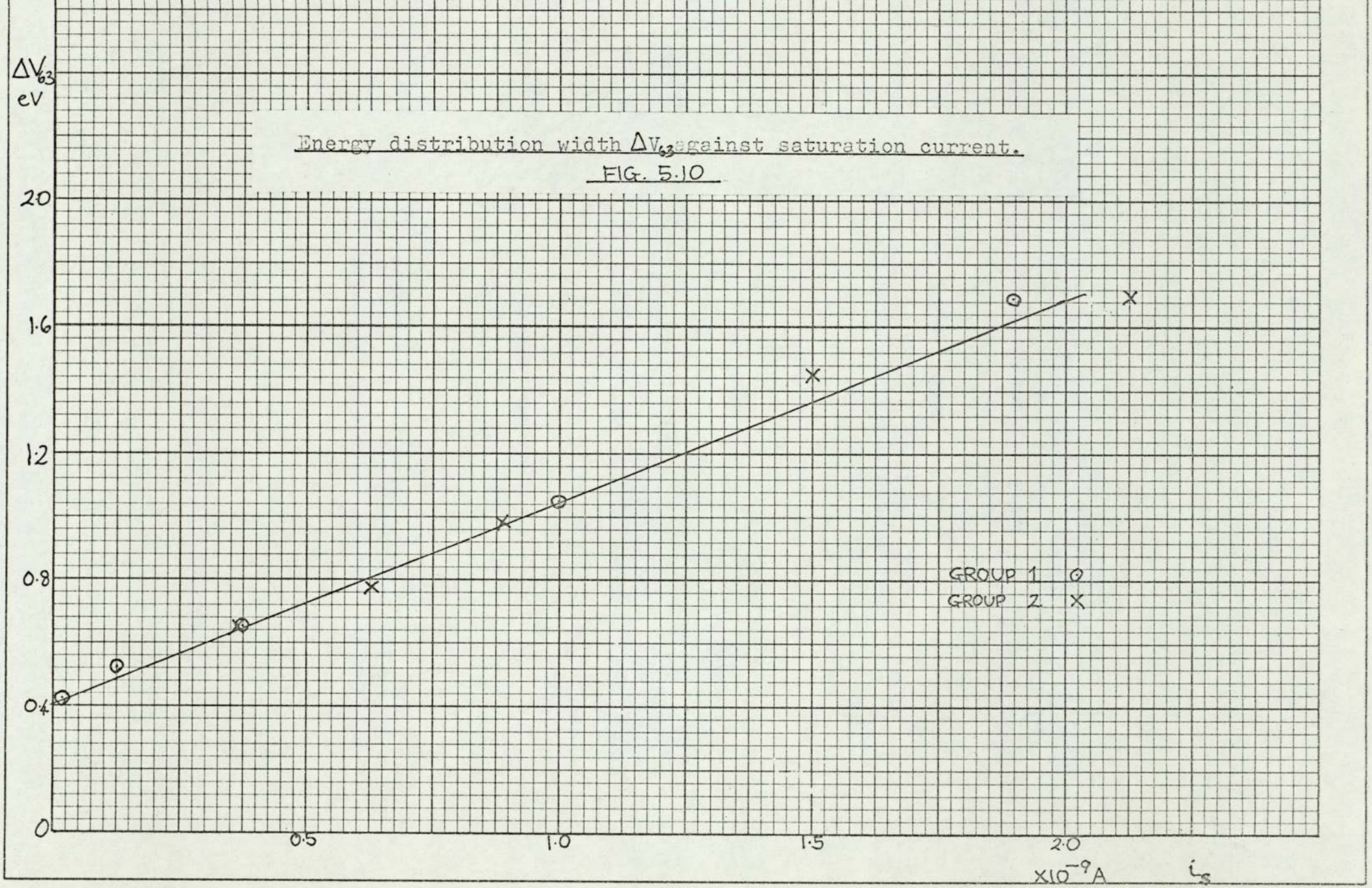

Energy distribution width ΔV_{63} against saturation current.

FIG. 5.10

5.2.4. Equipotential distribution in the Faraday cage

The equipotentials in the region between the 0.5 mm diameter aperture and the bottom of the Faraday cage were computed. The resulting equipotential values are shown in figure 5.11. The most divergent trajectory would be expected to be about 15' to the axis. Because of the difficulty of measuring such a small angle, a trajectory for an electron leaving the 0.5 mm diameter aperture at 3^{o} to the axis is shown. It is clear that the beam is virtually parallel until it enters the cage and at 15% of the anode potential the electron path begins to deviate sharply from the axis as the electric field strength becomes less. Even though this divergence is less for a 15' trajectory, the lens effect at the cage entrance will reduce the resolution of the analyser. Although decreasing the diameter of the beam defining aperture would improve the resolution, it would also decrease the current being measured. An alternative solution would be to place a mesh across the Faraday cage opening.

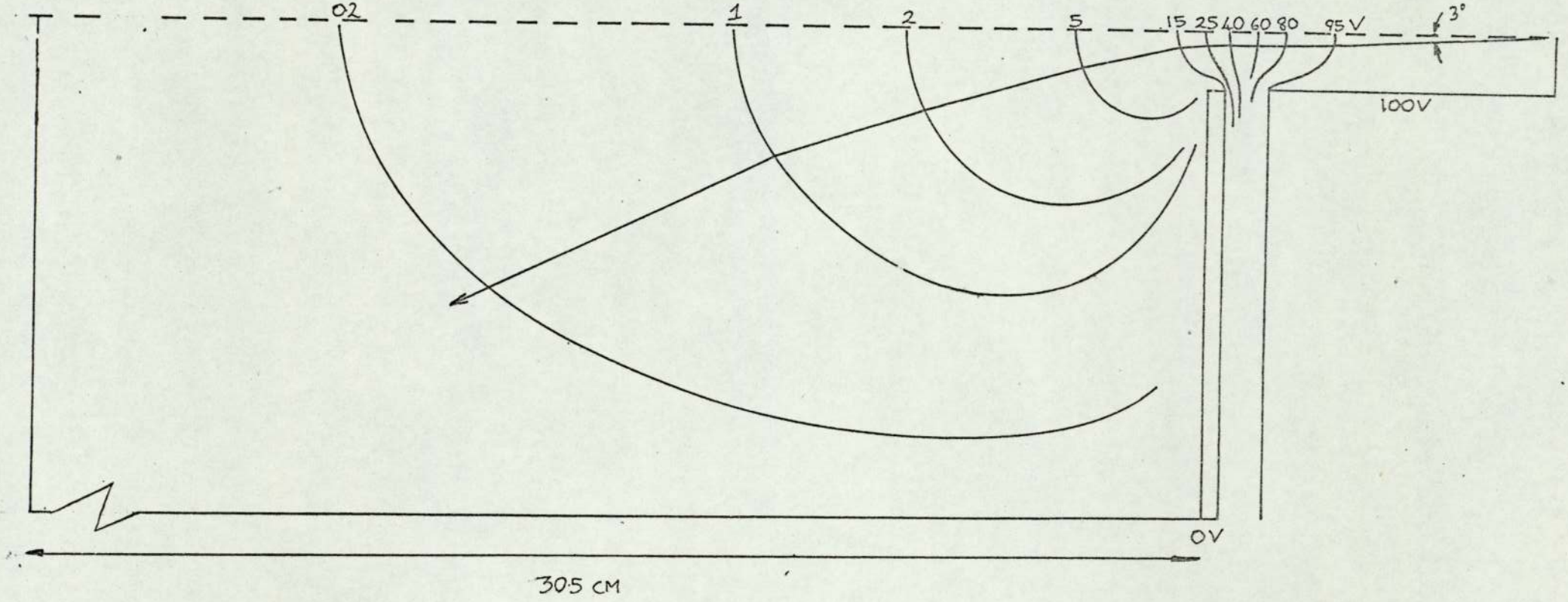

FIG. 5.11. EQUIPOTENTIALS IN THE FARADAY CAGE

5.3. Development of the field-emission electron gun

5.3.1. Introduction

An electrode system was required which would be placed in front of the basic thermionic emission analyser and would fulfil the following functions:

(a) to provide a potential to cause field-emission at the tip,

(b) to cause as large a part of the emitted beam as possible to enter the analyser, and

(c) to cause the beam entering the analyser to be as nearly parallel as possible.

The electrode system is here called a 'gun' because of its similar function to the electron gun of a thermionic emission analyser, i.e. to project a beam of electrons into the analyser.

5.3.2. First electron gun

Following the successful operation of the analyser for thermionically emitted electrons, the same electrode arrangement was tried for field-emission but with the first electrode at a positive potential with respect to the emitter. The emitter position and the anode voltages were varied and the total emission current and current at the second anode were measured. Sketch graphs of the measured anode current and total emission current for different emitter heights and anode potentials are shown in figures 5.12 to 5.16. The separation of the two anodes was 2mm. The total emission current increased rapidly as the potential of the first anode V_1 was increased, for a given value of the second anode potential of V_2. The lower the value of V_2 at a given value of V_1, the less the total current.

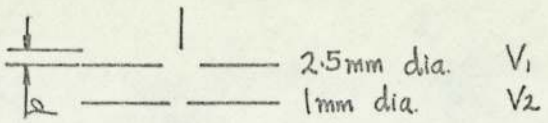

FIG. 5.12

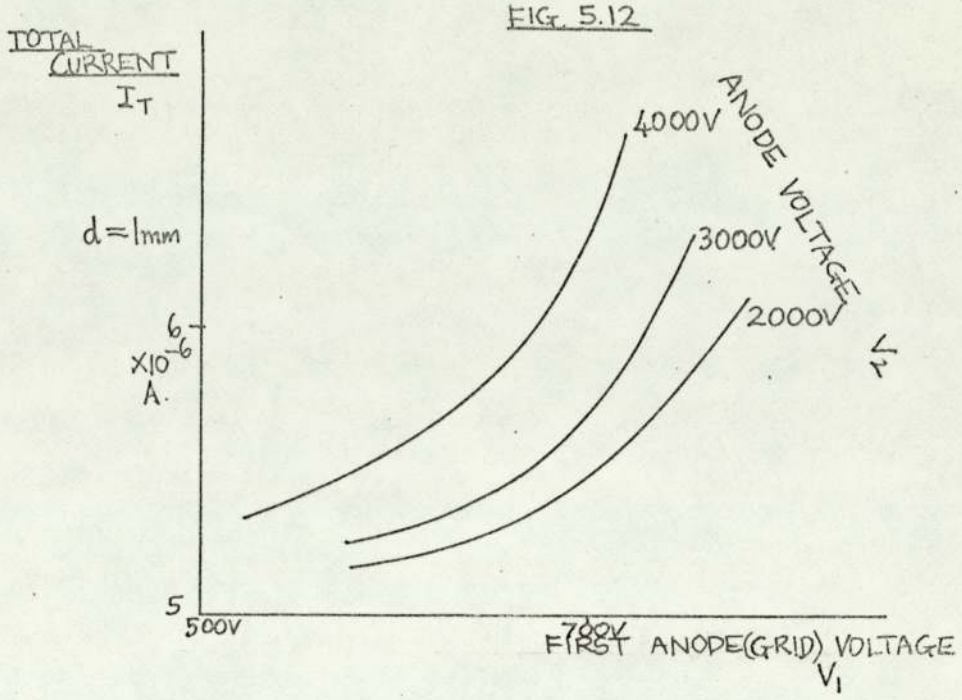

FIG 5.13

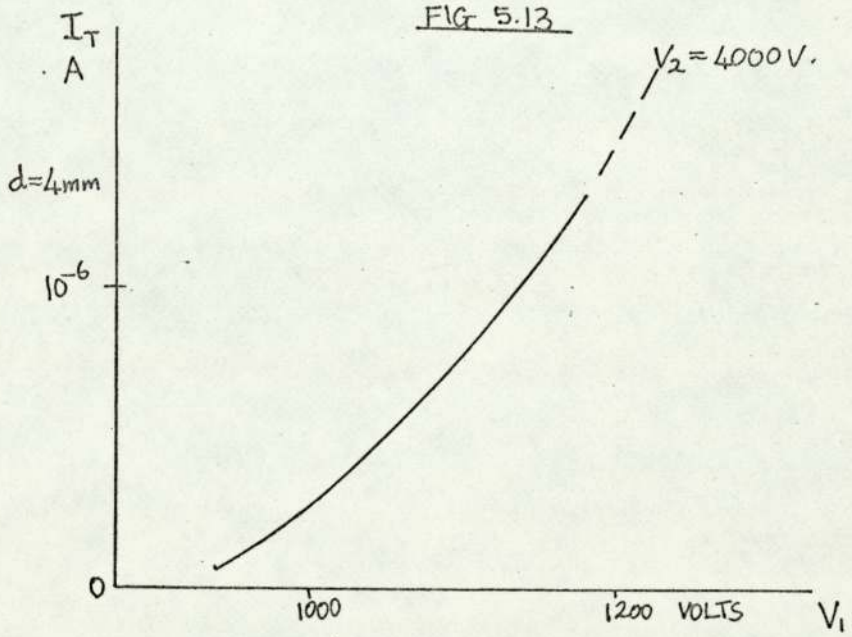

FIG. 5.14

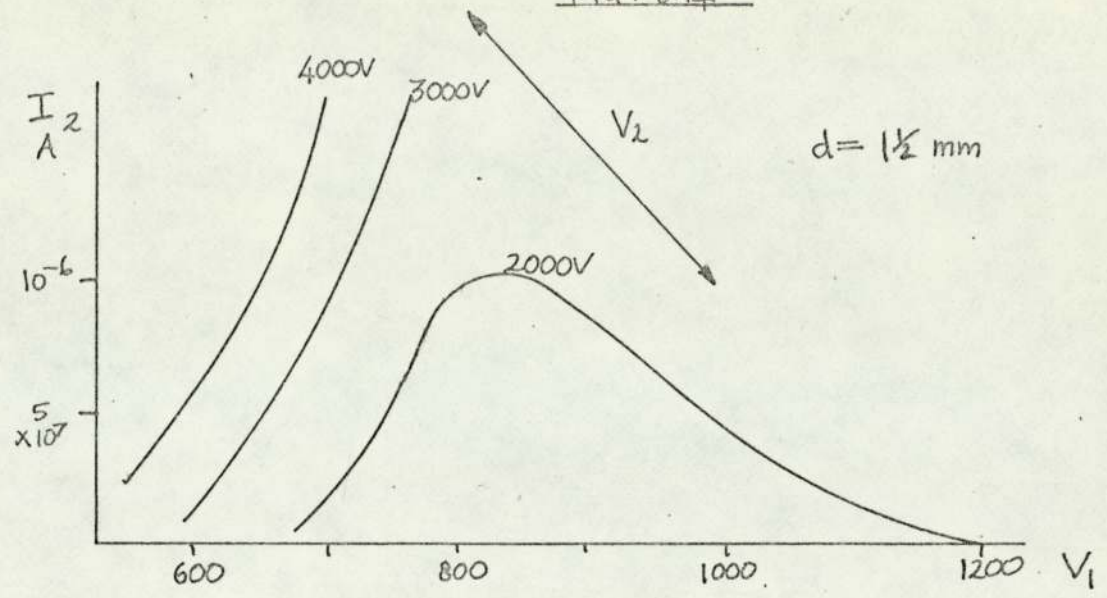

FIG. 5.15

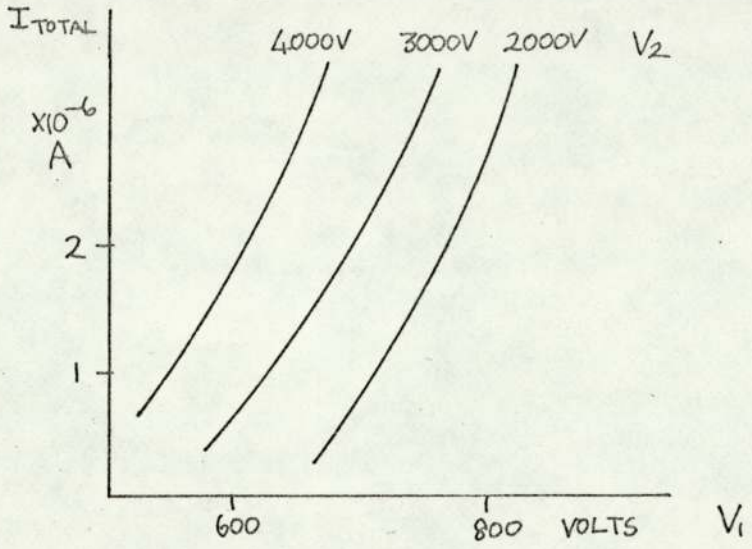

FIG. 5.16

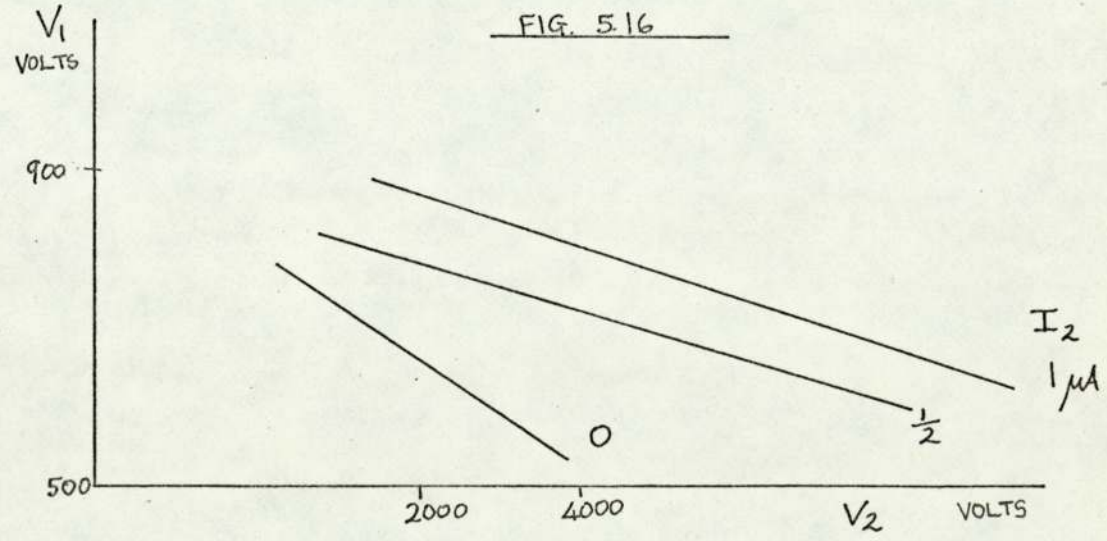

As the cathode-anode separation was increased, so the magnitudes of V_1 and V_2 had to be increased to give a particular emission current.

In the graph of the current at the second anode (I_2), against V_1 for a set of values of V_2, the curve for V_2 = 2000V (separation d = 1½mm) goes through a maximum rather than rising with increasing V_1. At V_2 = 1000V, there was no current detected at the second anode although it should be noted that the minimum current that could be measured was about 0.25μA. The graph of emission current against V_1 for a set of values V_2 shows that there was sufficient field penetration for V_2 to affect the emission current.

The peak in figure5.14 for V_2 = 2000V(V_1/V_2 = 0.4) indicates either that as V_1 increased, the subsequent increase in the field between the tip and the first anode, and the decrease in the field between the two anodes,meant that progressively less electrons reached the second anode, or that the emitter was off-axis and this became critical at these values of anode potential.

In this design no current was detected at the collector; probably the emitter was off-axis. For a system with many electrodes, a slight movement off-axis would result in the beam being unable to reach the collector. It was decided to deposit phosphor screens on the electrodes to determine the path of the electron beam under different conditions, and thereby find satisfactory working conditions for the gun.

5.3.3. Second electron gun

The experiments with the first gun system showed

that further information was needed on electrode configuration and potentials. In order to achieve this, a simple gun needed to be constructed in which the primary feature would be electrodes coated with phosphor which would clearly show the effect of anode potential on the electron beam.

The design tried was as shown in figure 5.17. The two electrodes were separated by a glass collar acting as an insulator and positioned in a beaker which had been coated with tin oxide. The coating was connected to the second electrode. The bottom of the beaker and the other two electrodes were coated with phosphor screens. Experiments with this simple system showed that the method would work and a slightly more sophisticated design was developed (figure 5.18).

5.3.4. Third electron gun (Figure 5.19).

The electrodes were supported using stainless steel beading and nuts, insulated with ceramic beads and glass tubes. The second electrode was again electrically connected to the lower section of a beaker which was coated with tin oxide, and phosphor screens were again used. The second electrode represented the first anode of the basic thermionic emission analyser. After construction, the beaker was placed on top of the analyser. The potential of the second and third electrodes was adjusted to give spots on each of them which appeared to be the same size and approximately the diameter of the second aperture. These conditions would give an approximately parallel beam with minimum loss in current. In addition it was required that the potential V_1 should be as low as possible, so as to increase the emitter lifetime, but the spot at the third electrode should be as bright as possible without electrical

FIG. 5.17

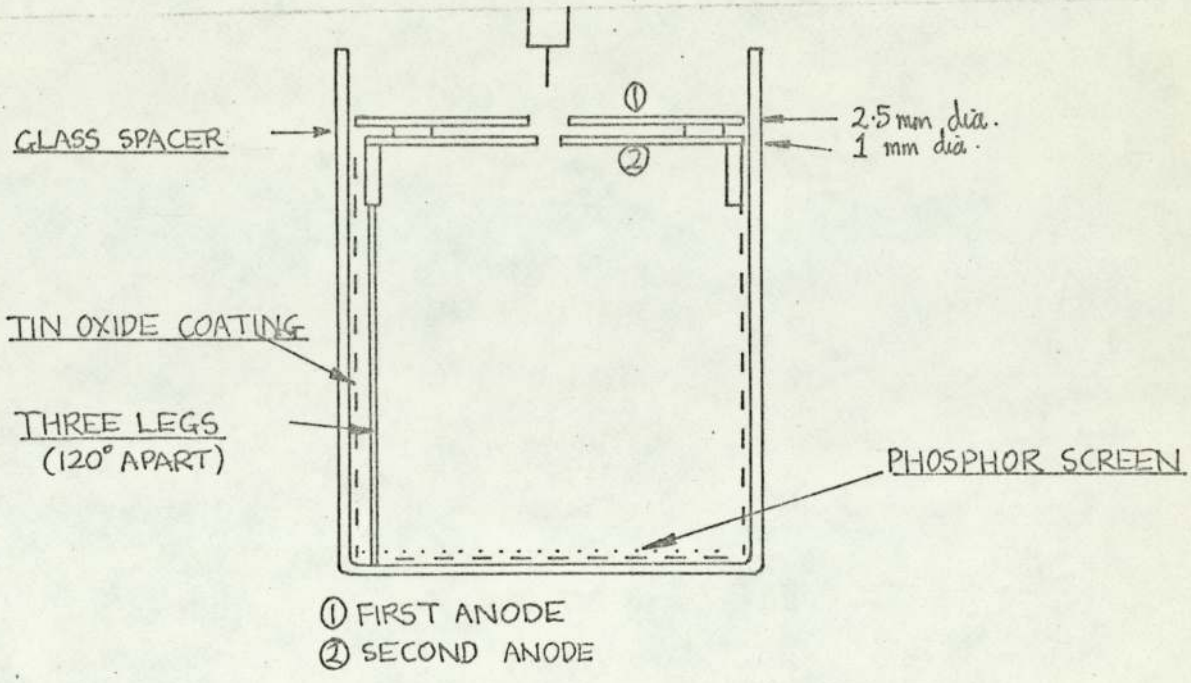

FIG. 5.18

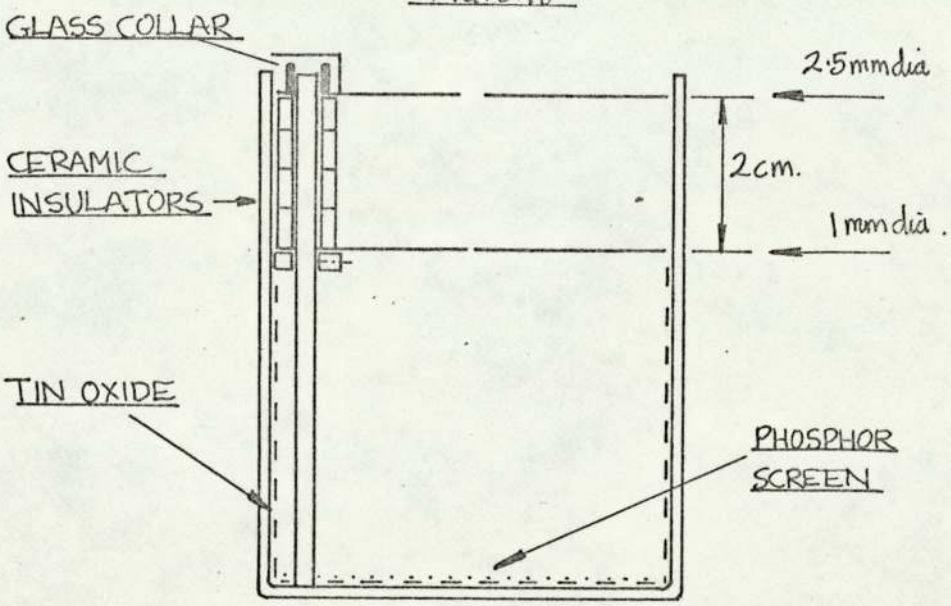

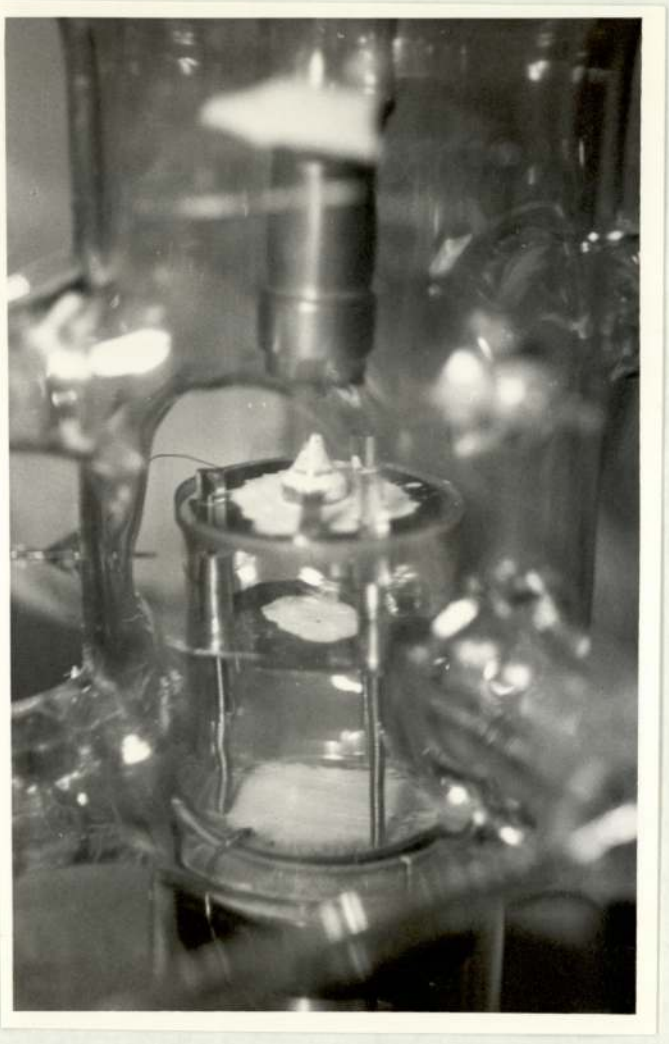

Third electron gun
Fig.5.19

breakdown occurring between the electrodes.

Typical results were as follows:

height of emitter above first anode: 1 cm;

with the emitter earthed, the total emission current was approximately 10^{-10}A.

$V_2:V_1$	Approximate image diameter mm		
	1st anode	2nd anode	3rd anode
6:1	4	1	1
$4\frac{1}{4}$:1	2	2	2
$3\frac{1}{2}$:1	2	4	1

The sizes of the spots were estimates because of the optical problem of measuring diameter through the curved surface of the glass chamber.

Attempts were made to increase the potential ratio but breakdown occurred across the insulators, presumably initiated by some sharp edges which were present in the device. Rough edges were removed and a cusp shaped electrode was fitted onto the first anode. It was thought that this shape might cause a concentration of the equipotential lines in the region around the emitter in such a way as to increase the density of the beam passing through the aperture in the electrode. With the emitter about 3 mm above the cusp, a spot less than 1 mm in diameter was formed at each of the three electrodes when a potential ratio of 7:1 was used. Although more experiments could have been carried out on the gun, it was decided that since it worked satisfactorily, it would be tried out with the energy analyser.

5.3.5. Use of the field emission gun with the energy analyser

Following the success of the field emission gun in

a beaker, another was constructed to fit onto the top of the analyser (figure 5.20). The top plate was a cusp-shaped electrode supported on three columns which were fixed in a stainless steel collar. When two separate H.T. supplies were used for V_1 and V_2, an apparent current was indicated on the electrometer, even when an emitter was not in the system. At first this was thought to be due to current leakage across the insulation of the gun. Running the system at about 1000V for twenty-four hours seemed to reduce the mean level of the electrometer reading. Although this "conditioning" reduced the spurious current, it was still of the order of 10^{-12}A. It was finally reduced to less than 10^{-14}A by obtaining the potentials of V_1 and V_2 from a potential divider consisting of fourteen 1MΩ resistors, instead of using two separate E.H.T. supplies. In this way the effect of fluctuations in the applied potentials was reduced since E.H.T. fluctuations from one supply were no longer superimposed on those of the other.

FIG. 5.20

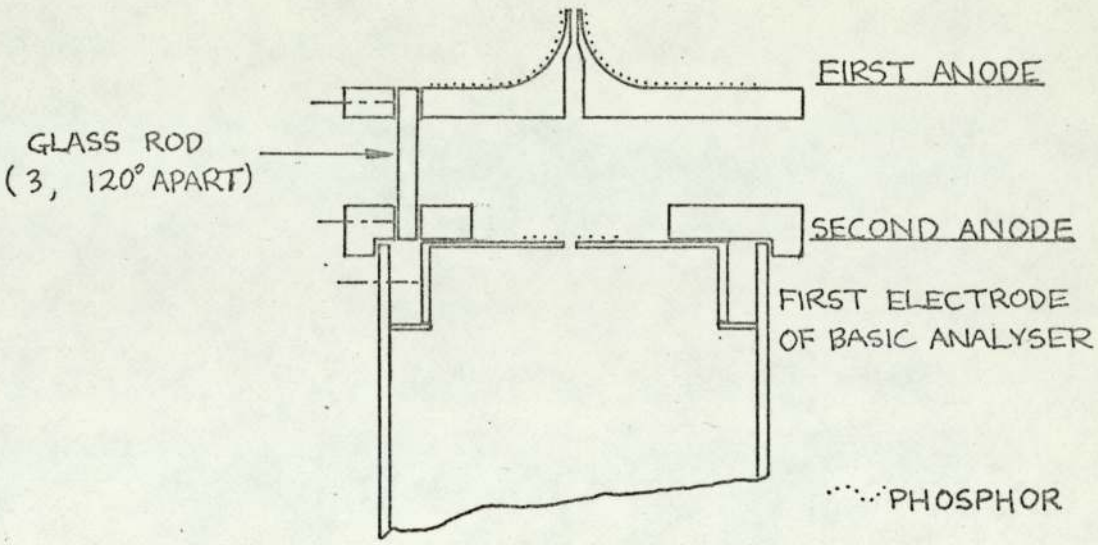

Electron gun used with energy analyser.

FIG. 5.21

FIG. 5.22

Electron gun in position on energy analyser

5.3.6. Electron gun lens properties

Carbon paper plots supplemented by computer equipotential calculations were used to see if the cusp shaped electrode would be more efficient in projecting the emitted lens into the analyser than a plane electrode.

Figure 5.23 shows the equipotential distributions in the region between an emitter and (a) a plane electrode and (b) a cusp shaped electrode; as determined from carbon paper plots. The emitter is represented as being at 0 V and the anode at 100 V. The emitter-electrode separation is the same in each case. It can be seen that equivalent equipotentials are nearer to the emitter for the plane electrode system than for the cusp. This trend is reversed near the anode.
For both geometries an electron beam would be expected to converge, and the convergence to be less for (a). This is confirmed by the electron trajectories shown for an electron emitted at 30° to the axis.

Computer calculations assumed that the system was bounded by an electrode at 0V. The inclusion of a boundary causes the 50 V equipotential to tend to bisect the angle between it and the anode; the other equipotentials follow the same trend. Fig.5.24.

Trajectories drawn for electrons emitted at 10° to the axis showed that a conical electrode (and therefore a cusp shaped one) would tend to converge the beam more than a plane one, thereby increasing the current density at the aperture. Fig.5.25.

FIG. 5.23

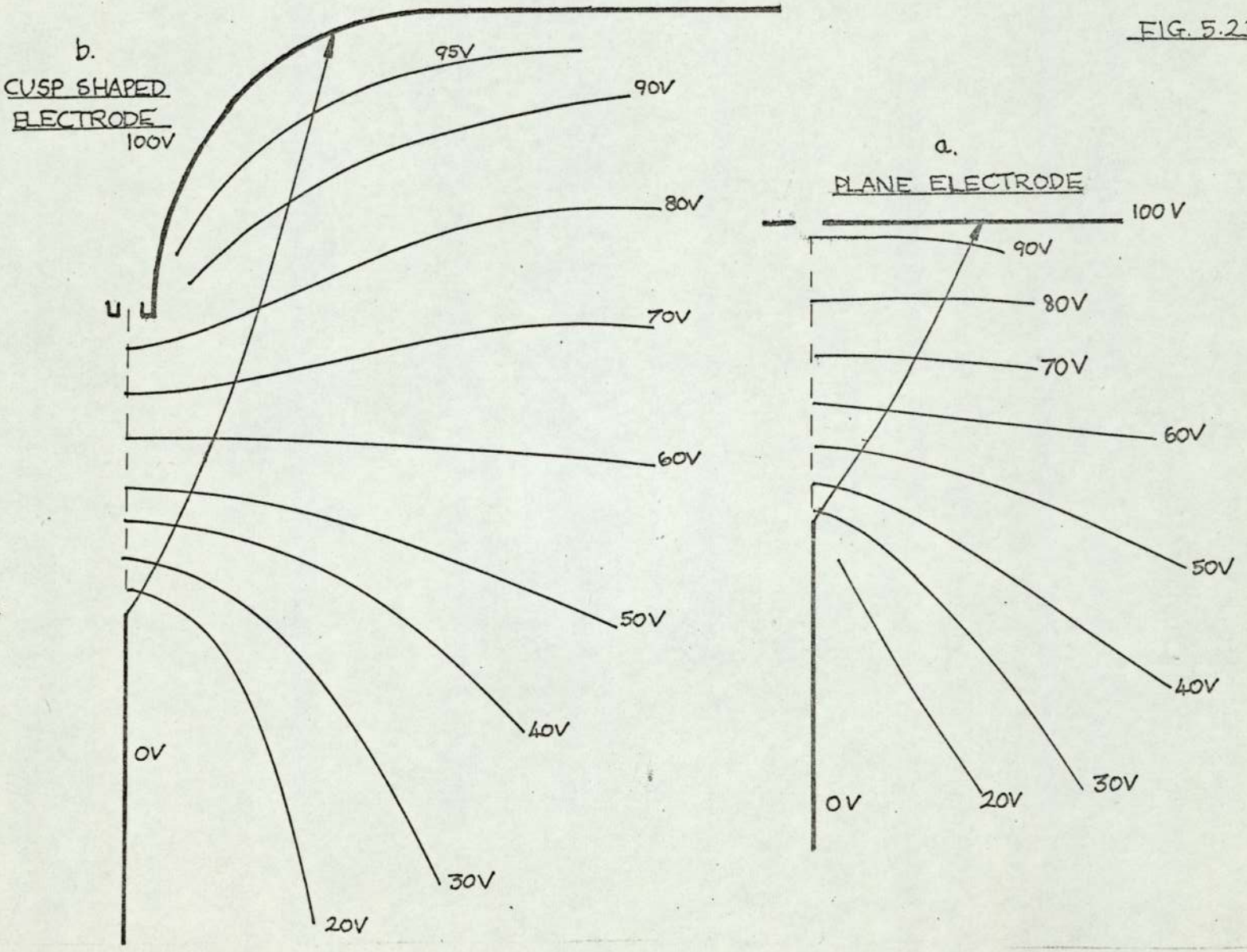
b.
CUSP SHAPED
ELECTRODE
100V
95V
90V
80V
70V
60V
50V
40V
30V
20V
0V
a.
PLANE ELECTRODE
100 V
90V
80V
70V
60V
50V
40V
30V
20V
0 V

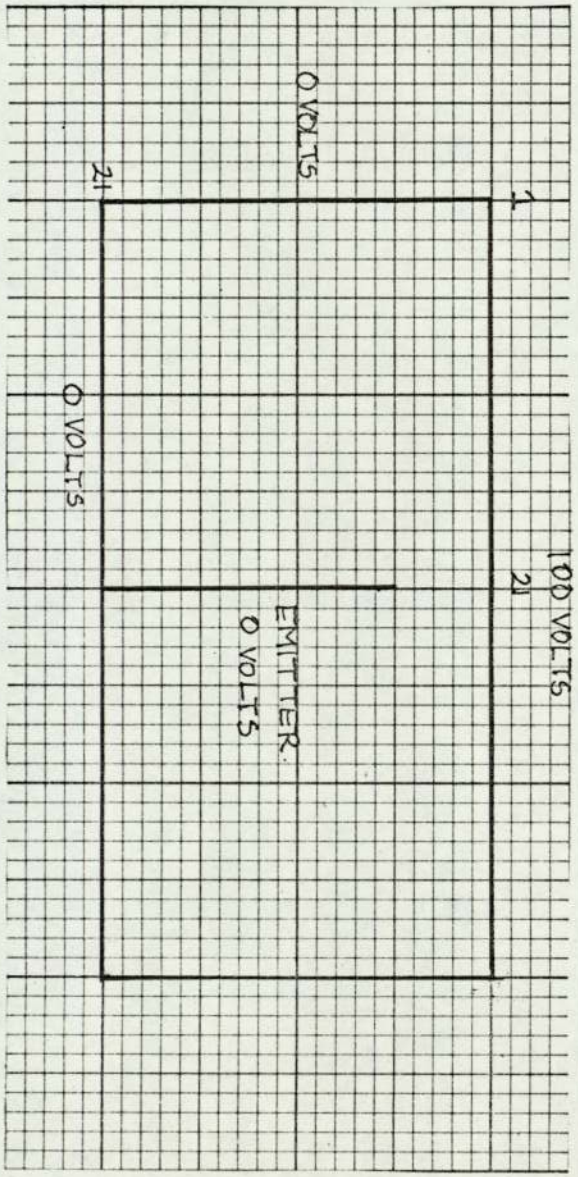

FIG. 5.24 a

ANODE										
1	3	5	7	9	11	13	15	17	19	21
100.0	100.0	100.0	100.0	100.0	100.0	100.0	100.0	100.0	100.0	100.0
0.0	69.3	83.1	87.8	89.7	90.5	90.5	89.8	88.4	86.6	85.6
0.0	49.0	68.2	76.2	79.8	81.2	81.1	79.7	76.9	73.1	70.5
0.0	36.2	55.9	65.6	70.3	72.2	72.0	70.0	65.8	55.8	53.8
0.0	27.8	46.0	56.2	61.6	63.7	63.4	60.8	55.2	45.6	32.9
0.0	22.0	38.1	48.1	53.6	55.8	55.4	53.3	45.7	33.0	0.0
0.0	17.8	31.7	41.0	46.4	48.6	48.1	44.7	37.5	24.4	0.0
0.0	14.6	26.6	35.0	40.0	42.1	41.5	37.9	30.8	18.7	0.0
0.0	12.1	22.3	29.8	34.3	36.2	35.6	32.1	25.4	14.6	0.0
0.0	10.1	18.8	25.3	29.4	31.0	30.3	27.1	21.0	11.8	0.0
0.0	8.4	15.8	21.4	25.0	26.4	25.7	22.8	17.4	9.6	0.0
0.0	7.0	13.2	18.0	21.1	22.3	21.7	19.0	14.4	11.3	0.0
0.0	5.8	11.0	15.1	17.7	18.7	18.1	15.8	11.9	6.4	0.0
0.0	4.8	9.1	12.5	14.7	15.5	15.0	13.0	9.7	5.2	0.0
0.0	3.9	7.4	10.2	12.0	12.7	12.2	10.6	7.9	4.2	0.0
0.0	3.1	5.9	8.1	9.6	10.2	9.8	8.4	6.2	3.3	0.0
0.0	2.4	4.6	6.3	7.4	7.9	7.6	6.5	4.8	2.5	0.0
0.0	1.8	3.3	4.6	5.4	5.7	5.5	4.7	3.5	1.9	0.0
0.0	1.2	2.2	3.0	3.5	3.8	3.6	3.1	2.3	1.2	0.0
0.0	0.6	1.1	1.5	1.8	1.9	1.8	1.5	1.1	0.6	0.0
0.0	0.0	0.0	0.0	0.0	0.0	0.0	0.0	0.0	0.0	0.0

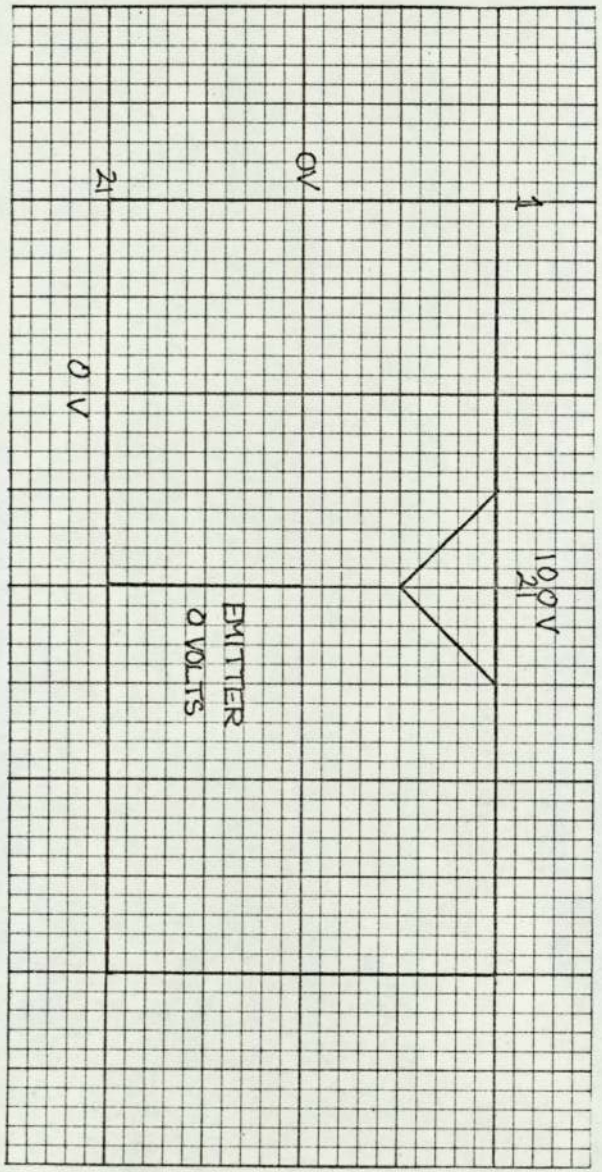

ANODE

1	3	5	7	9	11	13	15	17	19	21
100.0	100.0	100.0	100.0	100.0	100.0	100.0	100.0	100.0	100.0	100.0
0.0	69.5	83.5	88.5	90.9	92.4	93.6	95.3	100.0	100.0	100.0
0.0	49.4	69.0	77.6	82.1	84.8	87.1	89.9	95.5	100.0	100.0
0.0	36.7	57.1	67.7	73.6	77.4	80.4	83.9	89.7	100.0	100.0
0.0	28.5	47.5	58.8	65.7	70.2	73.7	77.4	82.9	92.5	100.0
0.0	22.8	51.1	58.4	63.2	66.8	70.4	75.0	82.9	89.3	100.0
0.0	18.7	33.7	44.4	51.6	56.5	60.1	63.1	66.5	71.3	77.3
0.0	15.6	28.7	38.5	45.4	50.2	53.4	55.7	57.5	59.1	60.5
0.0	13.1	24.5	33.4	39.8	44.2	47.0	48.5	48.6	47.0	44.6
0.0	11.1	20.9	28.8	34.6	38.6	40.9	41.6	40.1	35.3	26.7
0.0	9.4	17.9	24.8	30.0	33.5	35.3	35.2	32.5	24.8	0.0
0.0	8.0	15.2	21.2	25.7	28.7	30.0	29.4	26.0	17.7	0.0
0.0	6.7	12.9	18.0	21.9	24.4	25.3	24.3	20.7	13.1	0.0
0.0	5.6	10.8	15.1	18.4	20.4	21.0	19.9	16.4	9.8	0.0
0.0	4.6	8.9	12.5	15.2	16.8	17.2	16.0	12.9	7.5	0.0
0.0	3.7	7.2	10.1	12.2	13.5	13.7	12.7	10.0	5.7	0.0
0.0	2.9	5.6	7.8	9.5	10.5	10.6	9.7	7.6	4.2	0.0
0.0	2.1	4.1	5.8	7.0	7.7	7.7	7.0	5.4	3.0	0.0
0.0	1.4	2.7	3.8	4.6	5.0	5.1	4.6	3.5	1.9	0.0
0.0	0.7	1.3	1.9	2.3	2.5	2.5	2.3	1.7	0.9	0.0
0.0	0.0	0.0	0.0	0.0	0.0	0.0	0.0	0.0	0.0	0.0

EMITTER

FIG. 5.24 b.

FIG. 5.25.

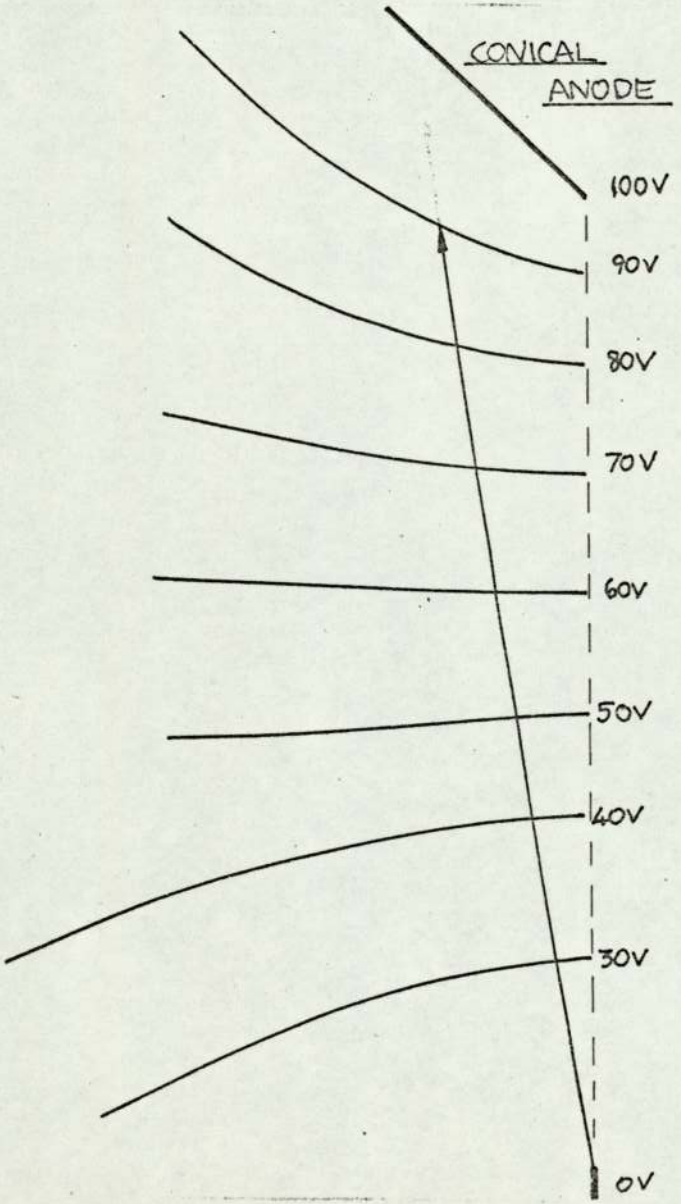
CONICAL ANODE
100V
90V
80V
70V
60V
50V
40V
30V
0V

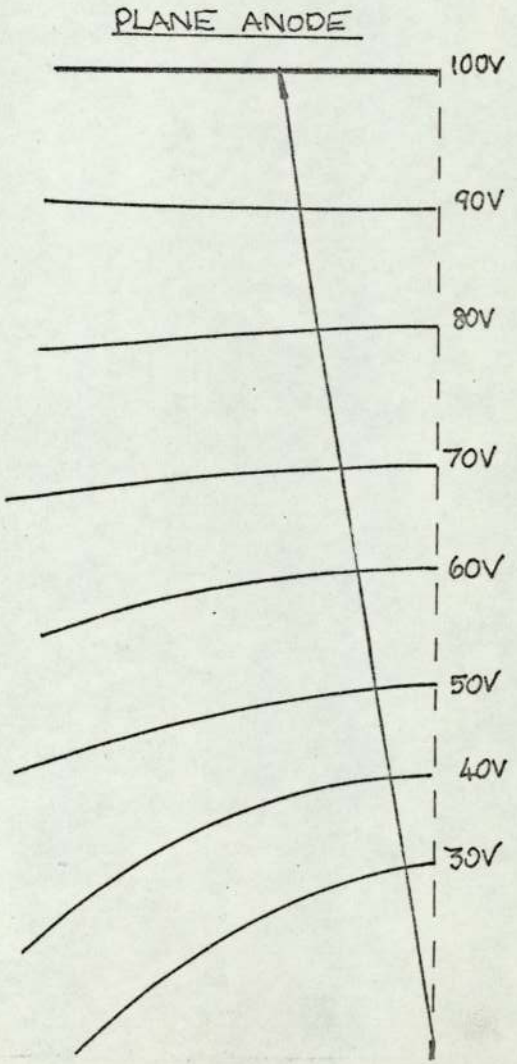
PLANE ANODE
100V
90V
80V
70V
60V
50V
40V
30V

In order to determine the effect of different anode potentials V_1 and V_2 and the separation of the emitter from the first anode, on the beam, some simple calculations were carried out using the Davisson-Calbick equation:

$$f = \frac{4V_1}{|E'| - |E|}$$

This gives the focal length of a thin lens of aperture R where $V/R >> E$ or E' , E and E^1 being the field strengths on either side of the plane electrode, the beam passing from the region with field strength E to that of strength E^1. If $E^1 < E$, $f < 0$ and the beam diverges.

The range of anode potential ratios used is normally between $V_1/V_2 = 1.0$ and 0.135. The separation of the two anodes is 2 cm.

Taking $V_1/V_2 = 1.0$ initially and $V_1 = 400$ V then $f = -4x$ cm where x is tip - first anode separation. Thus if the emitter is between 2 and 5 mm from the first anode, the beam will diverge, the focal length varying from 0.8 to 2 cm, i.e. becoming more parallel as the tip-anode separation increases.

If $V_1/V_2 = 0.135$ and $V_1 = 400$ V then $V_2 = 2960$.

$$f = \frac{1600x}{(1280x - 400)} \text{ cm if } x \text{ in cm.}$$

Again if x varies between 2 and 5 mm, the focal length will vary between -2.22 cm and + 3.34 cm, thus at an intermediate separation the beam will be parallel. Although these calculations will not exactly apply to either the cusp shaped anode or a flat one, it is clear that the smaller the anode potential ratio, the more parallel the beam, an ideal condition arising at a practical emitter-anode separation.

5.4. A simple field-emission analyser

Following the success of the simple guns which were built into beakers to facilitate use in the existing experimental chamber, a simple analyser was constructed as shown in photograph 5.26 . It was based on a combination of the Hartwig and Ulmer[1] analyser but with the first anode section incorporated. By leaving out one of the collimating apertures, it was hoped to obtain a larger collector current without a significant loss in resolution. The Faraday cage had a glass bottom (coated with tin oxide); this was to enable the electrodes to be aligned more easily. The analyser was in a glass beaker, coated with tin oxide. Each electrode was coated with phosphor so that the beam could be easily aligned onto the axis. Fig.5.27.

Thus there are three electrodes, the first being an anode at potential V_1, to control the emission current, the second at potential V_2 being to collimate and accelerate the beam. The third is a beam defining aperture and is followed by the glass Faraday cage which has a stainless steel top. The cage is guarded and the lead from it passes through a guarded metal tube in the wall of the chamber. It was necessary to terminate the experiments before this analyser could be evaluated. However, it was confirmed that the beam was very easy to align and the collector currents were of the order of 10^{-8}A. One of the integrated energy distributions is shown in figure 5.28. .

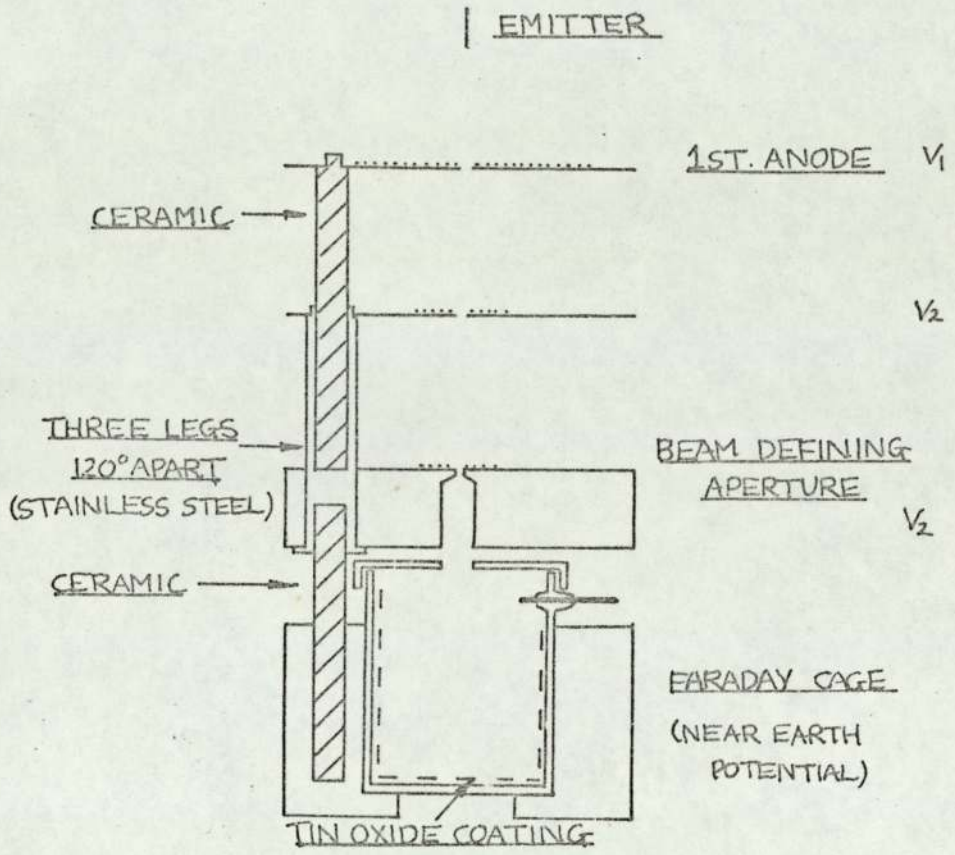

FIG. 5.27

Simple energy analyser

FIG. 5.26

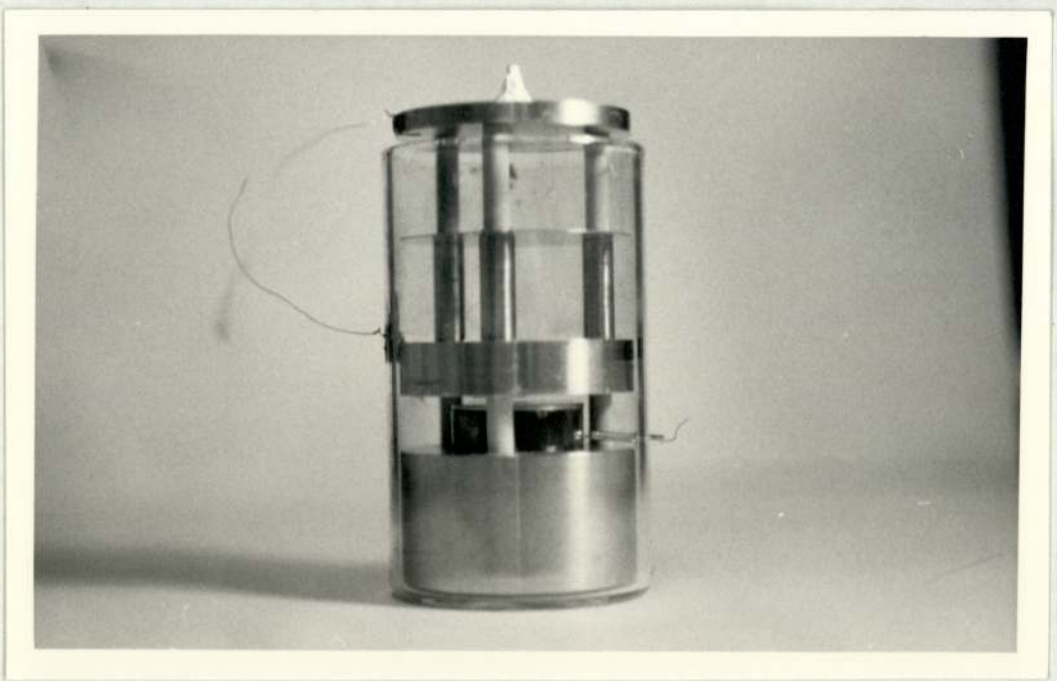

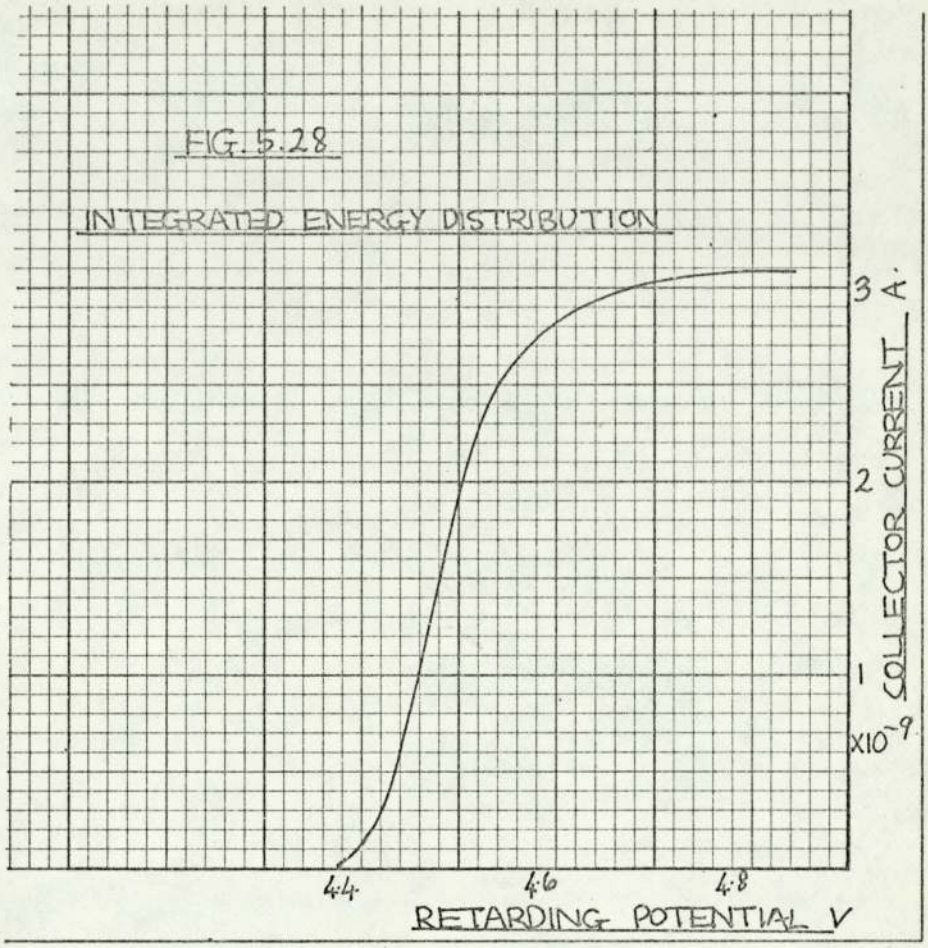
FIG. 5.28
INTEGRATED ENERGY DISTRIBUTION
3
2
1
X10⁻⁹
A.
COLLECTOR CURRENT
4·4
4·6
4·8
RETARDING POTENTIAL V

5.5. Fowler-Nordheim plots

A typical plot of log I/V^2 against $1/V$ (Fowler-Nordheim plot) is shown in figure 5.29. The linearity of this and other similar plots obtained indicated that the current density in all cases was less than that for space charge effects to occur. The plot shown was obtained for an emitter-electrode separation h = 1.5mm. The straight line has a slope m = 2.33×10^3. Assuming that the work function ϕ = 4.4eV, α = 1 and k = 5, the radius of the emitter is calculated to be 175 $\mathring{A} \pm 20\%$ (see section 2.1.4.2). The range of anode voltages corresponding to the emission current measured was 294 to 417 volts. Assuming ϕ = 4.4eV and s(y) = 1, the use of the equation

$$\frac{m}{V} = -2.97 \times 10^7 \times \frac{\phi^{3/2}}{F} s(y)$$

enables the range of electric field strengths corresponding to points on the graph to be calculated (see section 2.1.4.4). Thus the range is approximately 33 MV/cm to 46 MV/cm showing the typical magnitude of field strengths needed for field emission.

For a range of 294V to 417V, the current density changes from approximately 700 A/cm^2 to 2×10^5 A/cm^2 with an emission area of approximately 1300 $\mathring{A}^2$. The linearity of the curve throughout the voltage range indicates that space charge effects were not present. The calculated current density of 2×10^5 A/cm^2 confirms the absence of space charge, since its influence has never been noticed at current densities less than 10^7 A/cm^2.

The calculation of electric field strength is inaccurate because the work function of the emitter is not known accurately. In particular it might be wrong to assume

FIG. 5.29

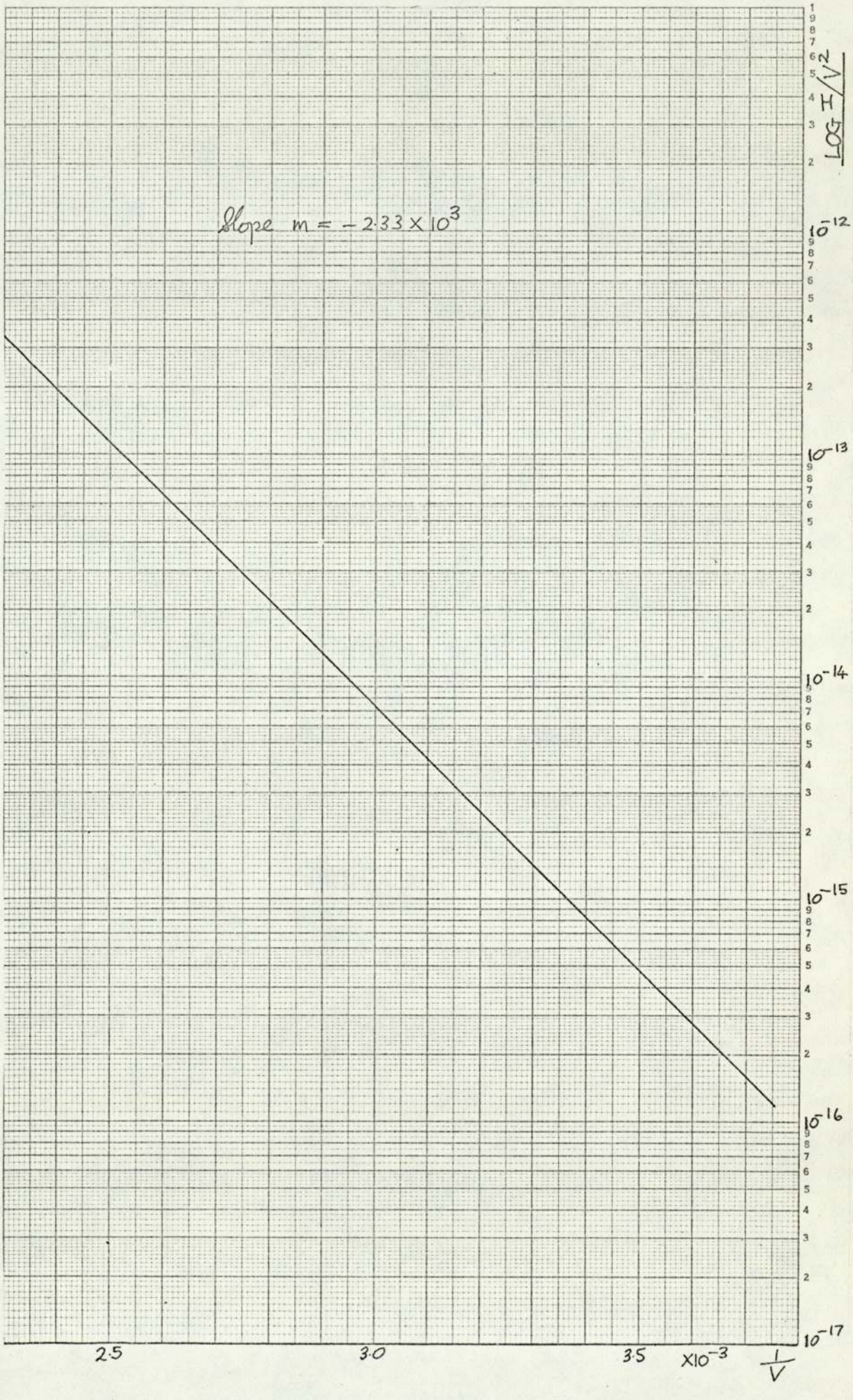
slope $m = -2.33 \times 10^3$
LOG I/V²
10^{-12}
10^{-13}
10^{-14}
10^{-15}
10^{-16}
10^{-17}
2.5
3.0
3.5
$\times 10^{-3}$
1/V

a value of 4.4eV at the lower anode voltage for which the emitting area is small, since for an emitter made from drawn tungsten wire, the central emission plane would be the (110) plane which has a higher work function. If the work function was higher, the emitter radius would be lower and the calculated field strength higher.

Experiments were done to investigate the effect of (1) emitter position, (2) electrode shape, (3) field desorption and (4) different ratios V_1/V_2 of the analyser electrode potentials, on the Fowler-Nordheim curve. All the measurements were made at a temperature of 22°C and a pressure of less than 2×10^{-9}Torr.

5.5.1. (1) Emitter position

An emitter was centred above the cusp-shaped electrode of the analyser and current and voltage measurements taken at two different heights. It appeared that the slope of the line became larger as the emitter to electrode separation increased (figure 5.30). In increasing the separation from 1.5 mm to 5.3 mm, the slope changed by 20 per cent.

When the emitter was rotated about 5°, the slope of the plot changed slightly although this was probably not significant.

The Fowler-Nordheim equation comprises both an exponential term and a pre-exponential term, each depends on the mean work function ϕ , the geometrical factor β , and the applied voltage; the pre-exponential term also depends on the emitting area. Increasing the anode-cathode separation apparently changes the slope of the Fowler-Nordheim plot, therefore either different crystal planes contribute to the emission or the geometrical factor β changes. β varies over the tip surface and depends both on

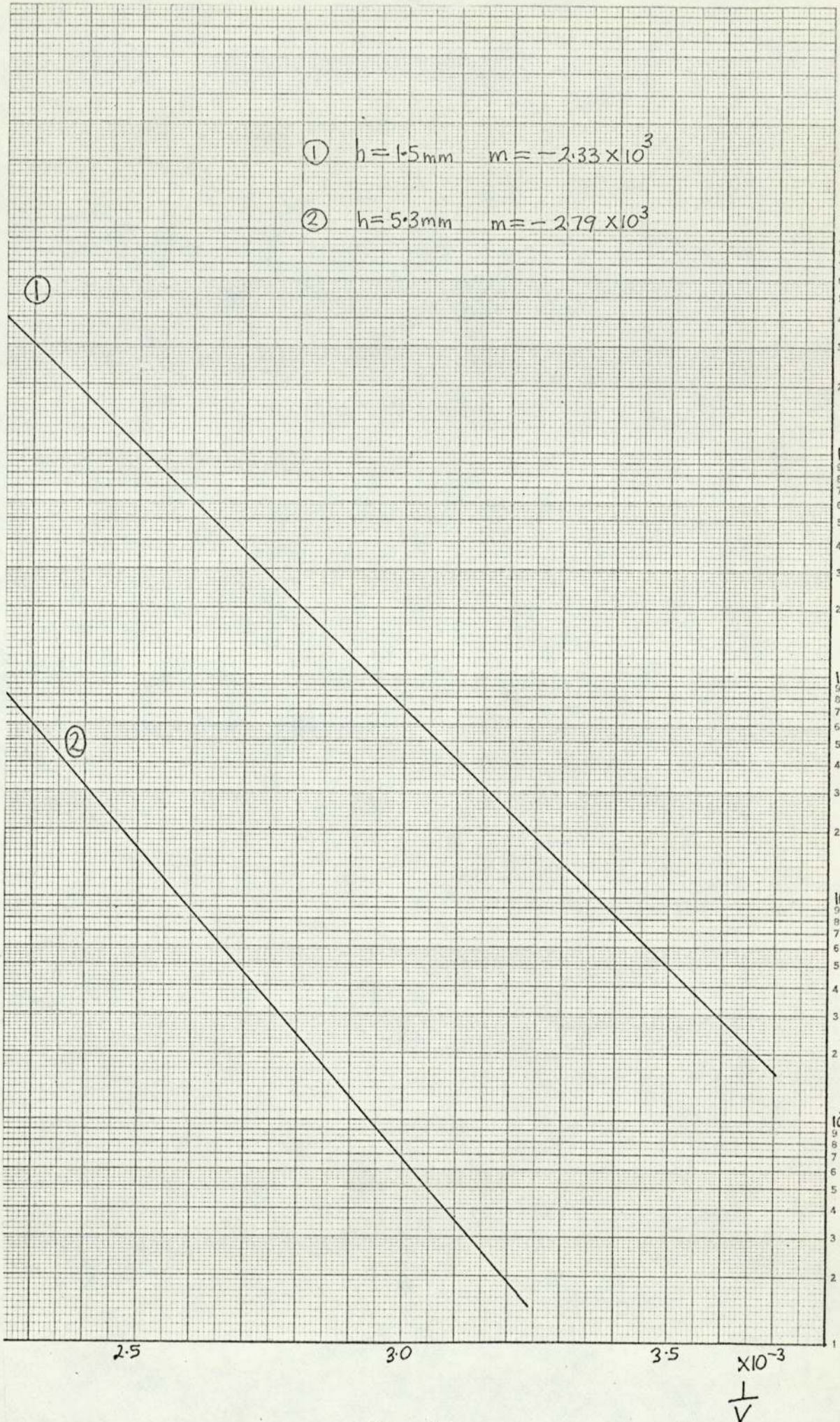
① h = 1·5mm m = −2·33 × 10³
② h = 5·3mm m = −2·79 × 10³
LOG I/V²
10⁻¹²
10⁻¹³
10⁻¹⁴
10⁻¹⁵
10⁻¹⁶
2·5
3·0
3·5
×10⁻³
1/V

FIG 5.30

tip geometry and adsorption on the emitter surface. It is possible that during the time taken to change the emitter position, significant adsorption occurred.

5.5.2. (2) Electrode shape

A Fowler-Nordheim plot was obtained with the emitter 4.8 mm above the cusp. It was then lowered to approximately 5 mm above the flat part of the anode, and an F-N plot obtained. There was no difference in the slopes of the plots, indicating that at this separation, electrode geometry did not effect the emission in such a way as to affect the slope. (Figure 5.31).

5.5.3. (3) Field desorption

Although an emitter can be cleaned by heating it up, the temperatures required are so high that surface migration occurs and the surface tension increases the radius of curvature of the tip. Since a small radius is required so that the cathode-anode potential can be kept as small as possible, field desorption is often used for emitter cleaning. The F-N plot enables the geometrical factor to be calculated if a value for the work function is assumed. Oxygen can be desorbed from a tungsten surface when a field of 400 MV/cm is applied. To ensure an emitter is perfectly clean, it is possible to evaporate tungsten from its own lattice. At room temperature this requires a field strength of approximately 500 MV/cm. Knowing the geometrical factor, the voltage needed can be calculated. At such a high field strength, the life of an emitter is quite short and often an emitter 'flashes' as the end is broken off by the high stress which is of the order of 0.1 N/m^2. It is preferable to monitor the field desorption process in order to clean the tip without applying a field great enough to damage it, there-

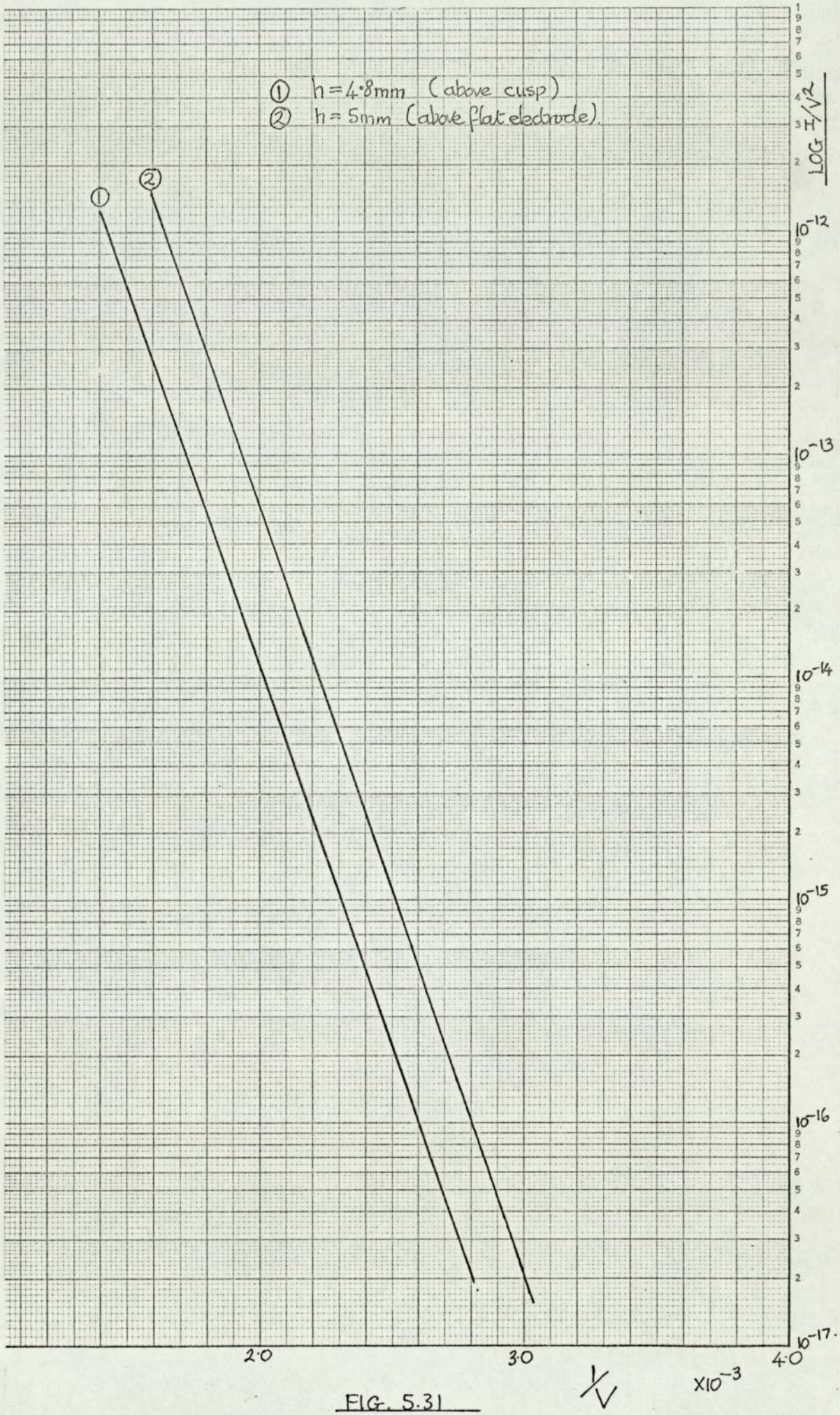
① h = 4·8mm (above cusp)
② h = 5mm (above flat electrode).
LOG I/V²
10⁻¹²
10⁻¹³
10⁻¹⁴
10⁻¹⁵
10⁻¹⁶
10⁻¹⁷
2·0
3·0
4·0
1/V
X10⁻³

FIG. 5.31

fore the a.c. desorption technique is sometimes used in which the field emission picture of the tip is formed whilst it is being cleaned. See section 4.9.

Figure 5.32 shows the effect of repeated desorption using an emitter of radius approximately 280 Å ± 20%, assuming a work function of 4.4eV. Since the emitter had not been cleaned at this stage, the work function was probably higher. If it was as high as 6eV, the calculated radius would have been 174 Å ± 20%. A field of 360 MV/cm was applied for nine minutes. (This value of the field strength was calculated assuming a radius of 280 Å, if the radius had been 174 Å the field strength would have been 574 MV/cm.)

After desorption the slope increased slightly and the calculated radius was 290 Å (ϕ = 4.4eV) or 182 Å (ϕ = 6eV). Assuming the original average work function of the tip surface had been as high as 6eV, then the calculated field of 574 MV/cm would have been large enough to cause field evaporation of tungsten, in which case it is unlikely that the emitter radius would have changed so little, thus the assumption of a work function as high as 6eV does not seem justified.

After further desorption for four minutes at 10 000 V, corresponding to a field strength of 690 MV/cm (if ϕ = 4.4eV), the slope increased significantly yielding a radius of approximately 465 Å. Further desorption for four minutes at 10 000V increased the slope further, corresponding to a tip radius of 650 Å.

Immediately following the first desorption at 10 000V, the emission current was monitored for twenty-one minutes (figure 5.33). The current rapidly fell from

FIG. 5.32

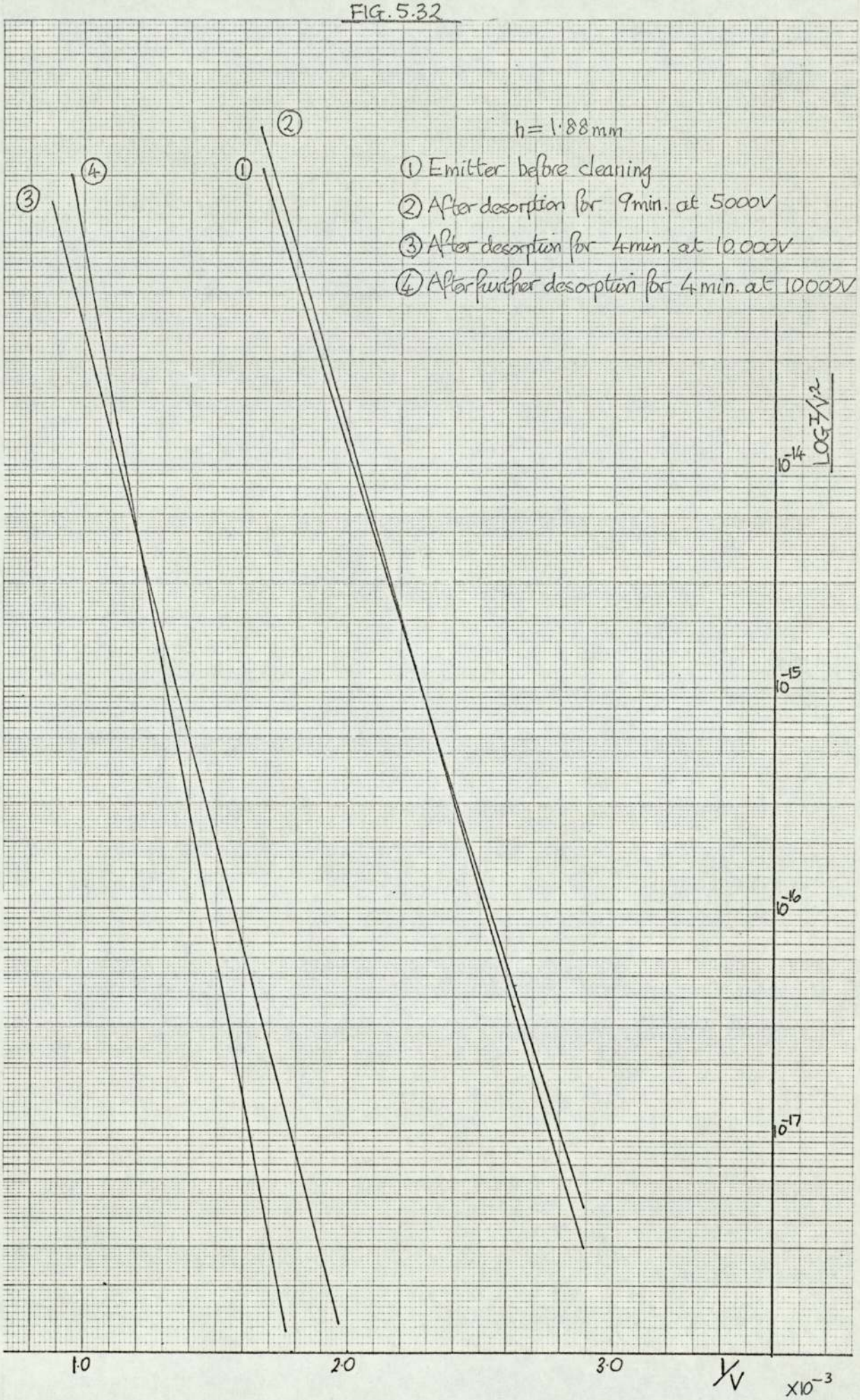
h = 1·88 mm
① Emitter before cleaning
② After desorption for 9 min. at 5000V
③ After desorption for 4 min. at 10,000V
④ After further desorption for 4 min. at 10000V
LOG I/V²
10⁻¹⁴
10⁻¹⁵
10⁻¹⁶
10⁻¹⁷
1·0
2·0
3·0
1/V
X10⁻³

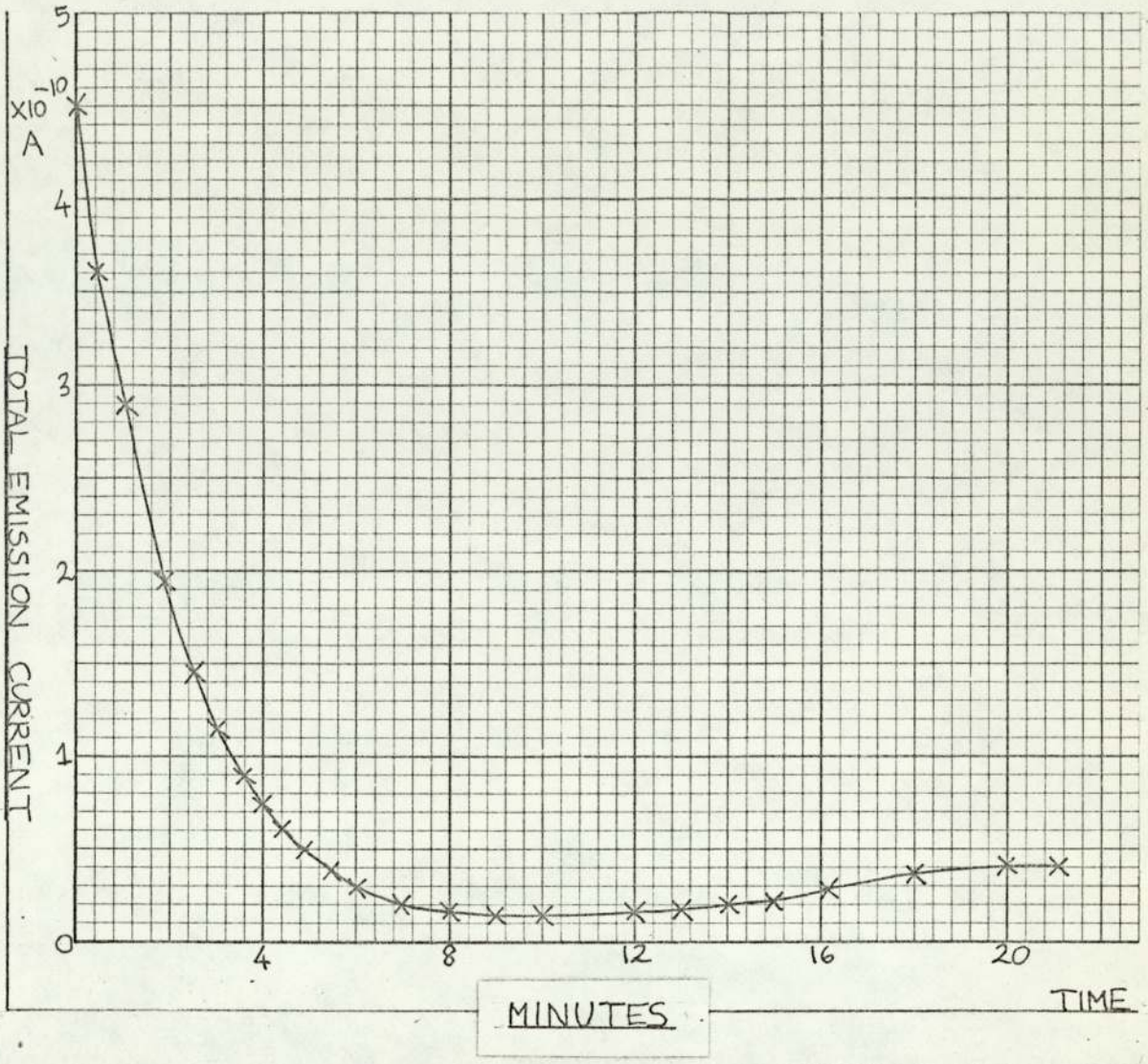

FIG. 5.33

Graph showing the effect of adsorption on emission current .

4.5×10^{-10}A and then started rising. Since the pressure was 7×10^{-9}Torr, this rapid drop in emitter current would presumably be due to the tip becoming contaminated and emphasises the need for operation under good vacuum conditions. In addition, it confirms that a field of about 690 MV/cm significantly cleans a tungsten emitter, since if the surface had not been cleaned, there would not be such a large change in emitter current, indicating a change in work function or in the nature of the potential barrier as caused by adsorption, see section 2.1.5 on the electronic energy levels of adsorbed atoms. In this reference an adsorbate is represented as a potential well as shown in figure 5.34, acted on by the applied field, in which the adsorbates have energy bands of various shapes and positions. Clearly this compound barrier affects the tunneling probability of an electron from the metal.

5.5.4.(4) Different ratios of the anode voltages V_1/V_2.

Fowler-Nordheim plots were taken for different ratios of the anode voltages V_1 and V_2, two of which have been plotted. Figure 535. The two slopes appear to be the same. For an approximately constant work function, log J varies linearly with m/V. If the slopes are the same, for a particular value of the potential difference V, the value of $K = \frac{m}{V}$ is the same. If the mean work function was constant, as would be the case for a clean system, and K is constant, then the electric field strength and current density would be constant. In this case, since the emission current has changed, the emitting area must have changed. (It should be noted that if the system is dirty then obtaining the same slope for each curve will not necessarily imply ϕ and β are constant.) Thus altering the ratio of the

FIG. 5.34

Energy diagram for an adsorbate on a metal surface.

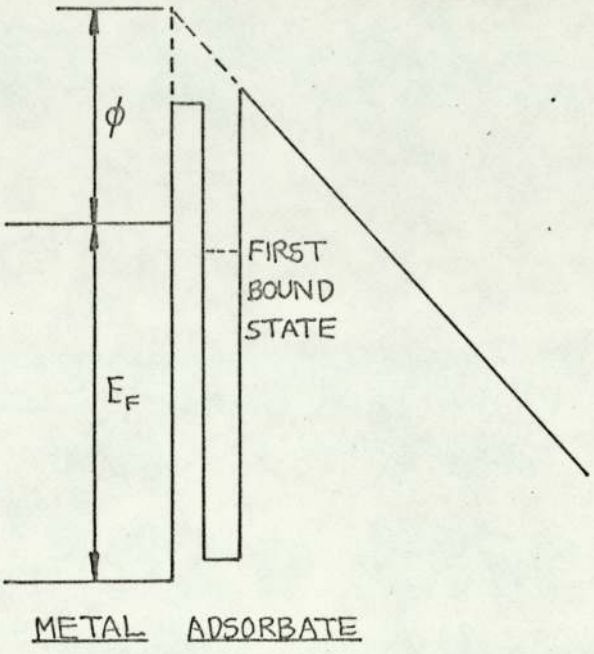

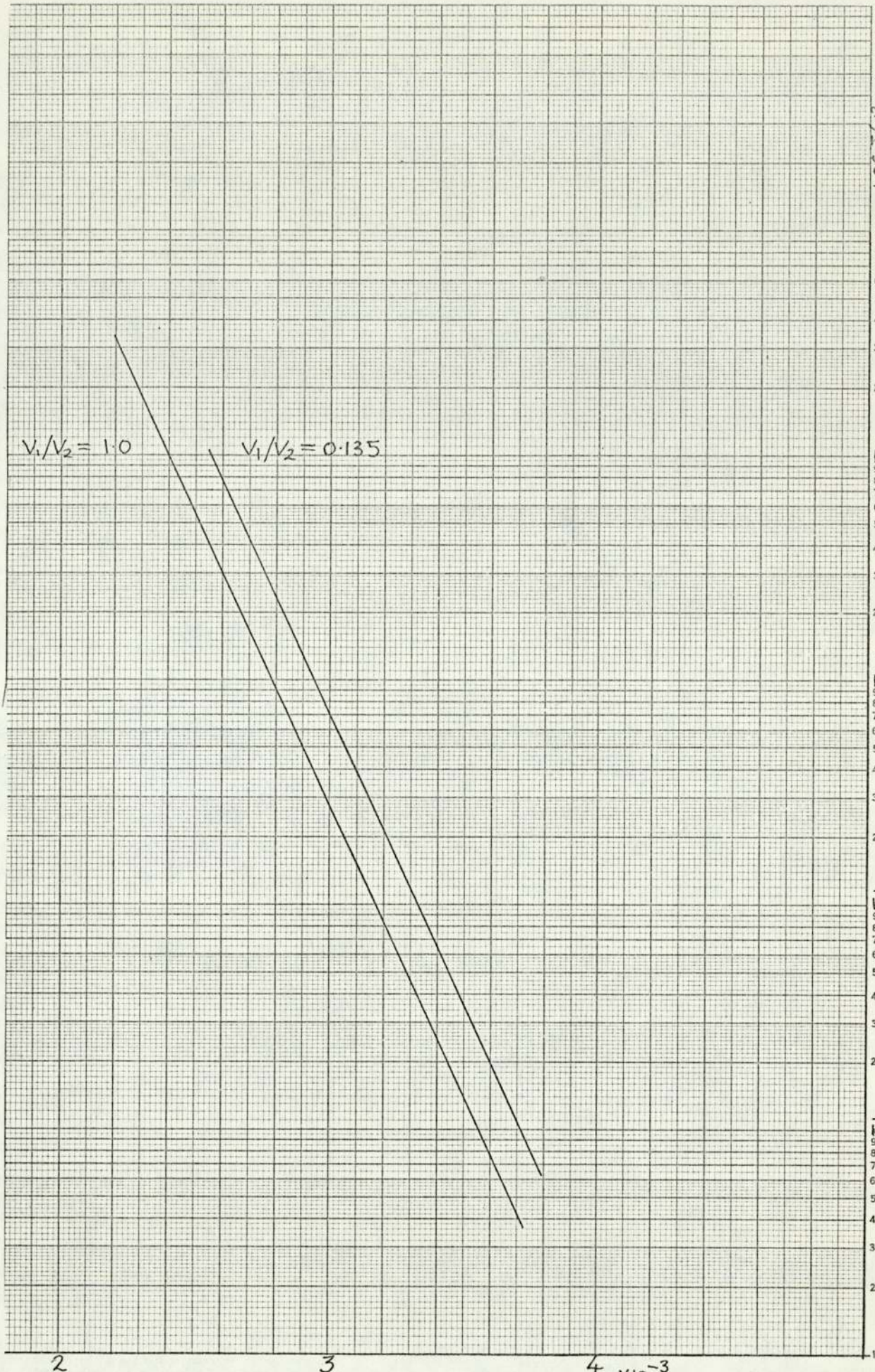
$V_1/V_2 = 1.0$
$V_1/V_2 = 0.135$
$\log I_2/A$
10^{-12}
10^{-13}
10^{-14}
10^{-15}
10^{-16}
2
3
4
$\times 10^{-3}$
$\frac{1}{V_1}$

FIG. 5.35

anode potentials V_1 and V_2 alters the emitting area of the tip. For the two plots shown, the gradient m = 2.6×10^3. The emitter - first anode separation was 1.9mm. At a voltage of 400 volts, m/v = 6.5. For values of work function between 4 and 6eV, the current density $J \approx 3.16 \times 10^4$ A/cm^2. At 400V, the emitting area for the plot of $V_1/V_2 = 0.135$ was approximately 7600 $\mathring{A}^2$ and for the plot $V_1/V_2 = 1.0$, the area was approximately 2500 $\mathring{A}^2$.

5.6. Field-emission measurements made with the energy analyser

Preliminary experiments carried out in testing the basic analyser and developing a suitable electron gun have been described elsewhere. In this part of the chapter, the results of an experiment to determine the effect of anode voltage ratio on collector current and total energy distribution measurements are described.

5.6.1. Effect of anode potential ratio on collector current

As the anode potential ratio was increased from 0.14 to 0.17, at constant V_2 (= 3000V), the collector current increased, see figure 5.36 . Log I_c $(V_1/V_2)^2$ increases with V_2/V_1. Figure 5.37 . As would be expected, the greater the voltage ratio, the greater the emission current. At a constant voltage ratio, an increase in V_2 would be accompanied by an increase in V_1. The Fowler-Nordheim equation shows that as the anode potential (V_1) increases, the current density increases, leading to a greater collector current (figure 5.36).

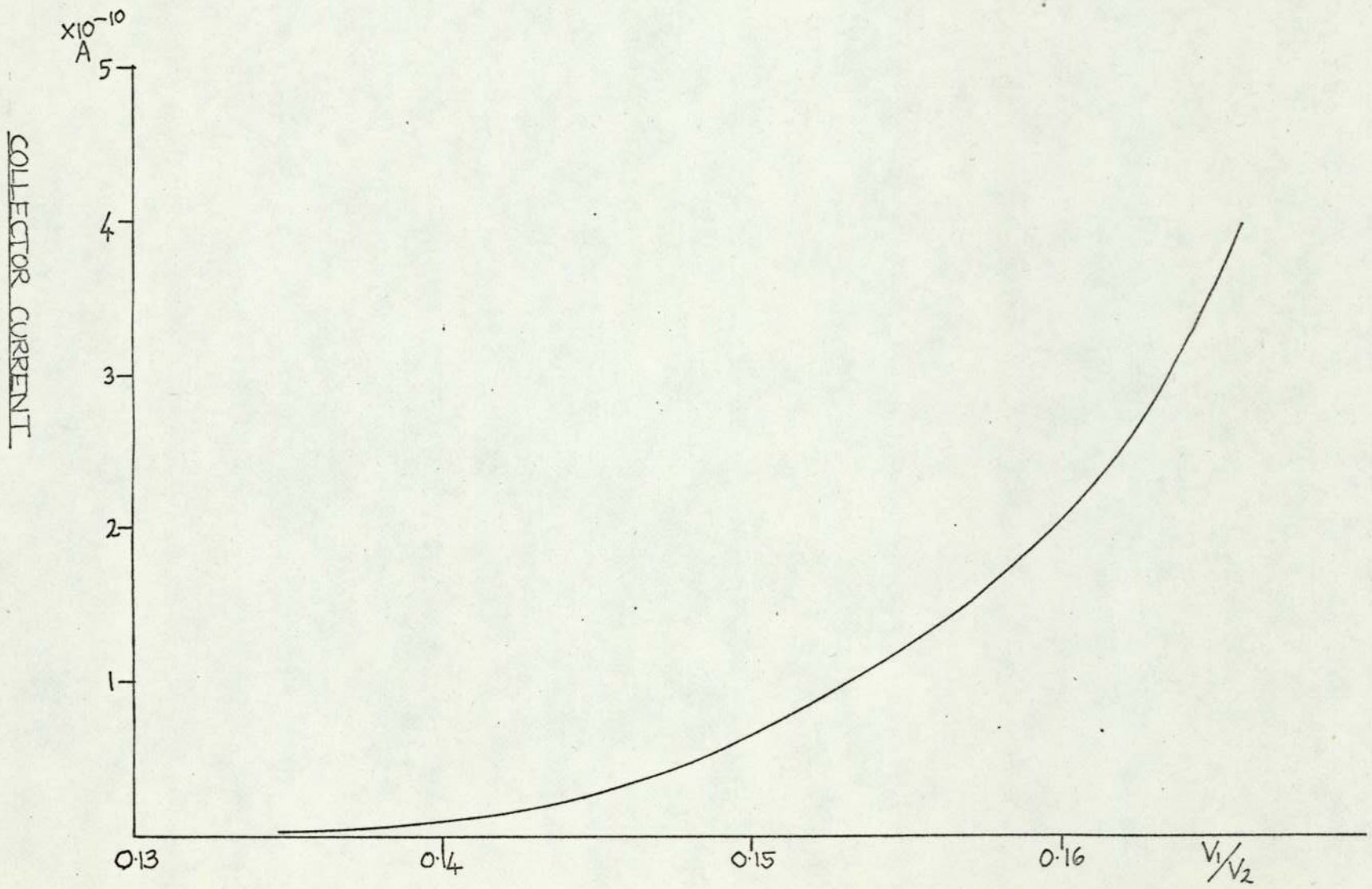

FIG. 5.36

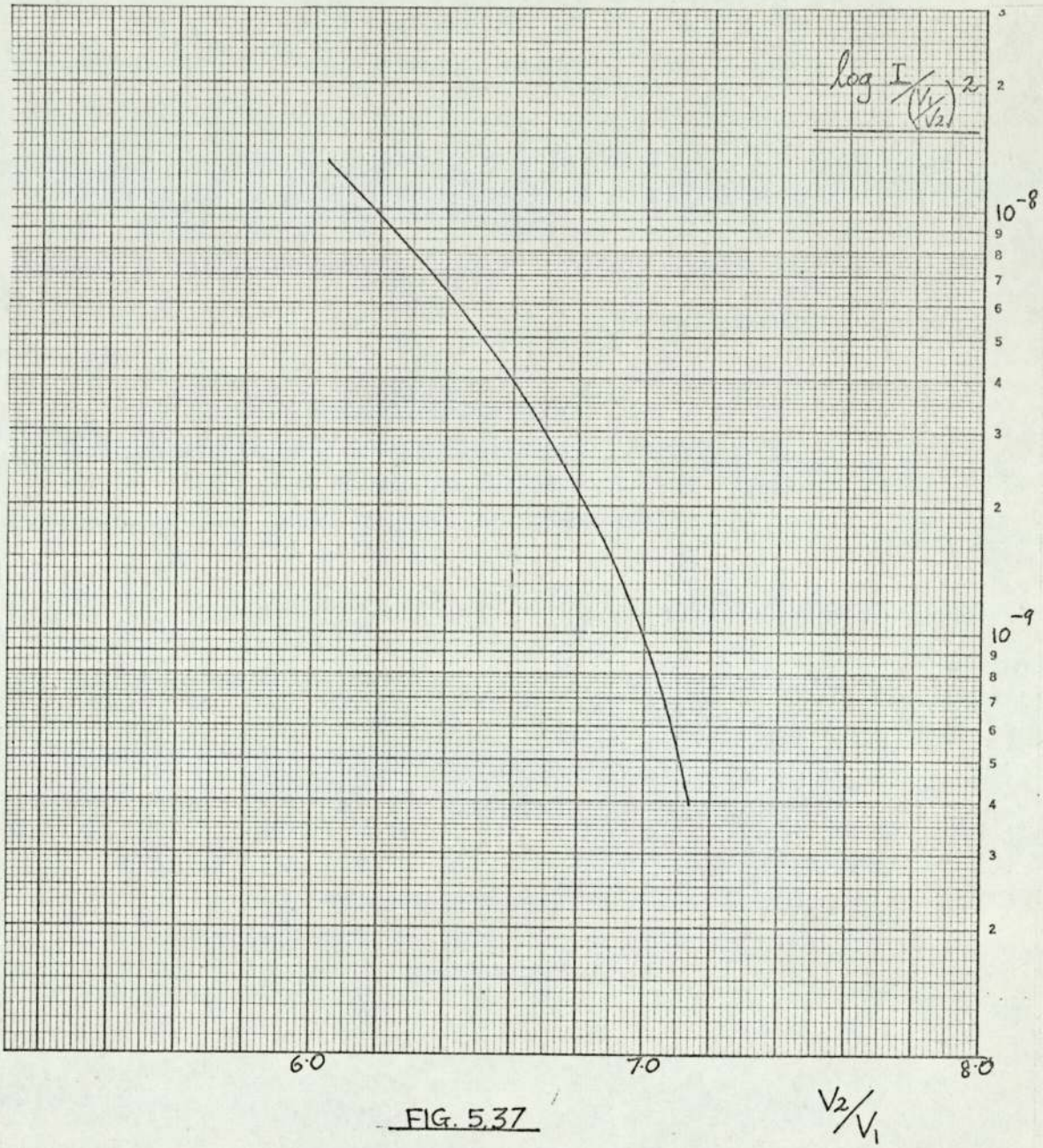

FIG. 5.37

5.6.2. Energy distribution measurements

At the beginning of an experiment, the emitter is centred over the first anode and adjusted until a spot is formed which falls over the aperture of the second anode. Its position is then changed slightly to give a form of field-emission pattern on the phosphor. The emitter is then cleaned by field desorption and adjusted to give maximum collector current.

After cleaning, a few measurements of the total emission current and anode potential V_1 are taken for a chosen ratio V_1/V_2. These enable the radius of the tip to be determined approximately. The retarding potential is then varied, typically between 4 and 10V and the electrometer reading is recorded either on the X-Y recorder or manually. The Fowler-Nordheim plot is then determined in more detail. This second measurement of I and V providing a check on whether the tip has changed (by adsorption) during the retarding potential measurements.

A typical graph of collector current against retarding potential is shown in figure 5.39 . It can be seen that the collector current is constant up to a point where it begins to become rapidly smaller, finally tailing off to the retarding potential axis. As explained elsewhere the width of the region in which the current decreases depends both on the temperature and any faults in the electron-optical system. At $0^{\circ}K$, the drop-off would ideally be a vertical line.

The results given are for emission at $22^{\circ}C$ and were not obtained for any one particular plane of the tungsten emitters used.

Example 1. The emitter was positioned approximately 1.8 mm above the first anode. After desorption at 3000V, the Fowler-Nordheim curve was plotted (figure 5.38) and the radius of the emitter was 210 Å ± 20%, making the assumptions described before when calculating approximate tip radius. The gradient of the Fowler-Nordheim plot was 2.86×10^3. V_1 = 436V and V_2 = 1525V, thus K = m/V = 6.56. Therefore log J = 4.30. The curve of collector current against retarding potential was normalised, and differentiated by taking the tangents to the curve every 0.02V. The differentiated curve is shown in figure 5.40 . The measured FWHM (full width at half maximum height) was 240 meV.

For a current density of approximately $10^4 A/cm^2$, the correction which needs to be applied to the FWHM of the total energy distribution is approximately 96 meV, if the work function is 4.4eV and the temperature 300° K. The correction at 295° K is also approximately 96 meV.

$$\phi = \frac{K\sigma_0\, t(y)}{2.01 \times 10^{-5}\, s(y)}$$

$$\approx \frac{6.56 \times (240 - 96) \times 1.05 \quad eV}{2.01 \times 10^{-5} \times 0.95}$$

$t(y) \approx 1.05, \quad s(y) \approx 0.95$

$$\approx \frac{6.56 \times 144 \times 1.05}{2.01 \times 10^{-5} \times 0.95} \, eV$$

$$\approx \underline{5.2eV}$$

FIRST EXAMPLE

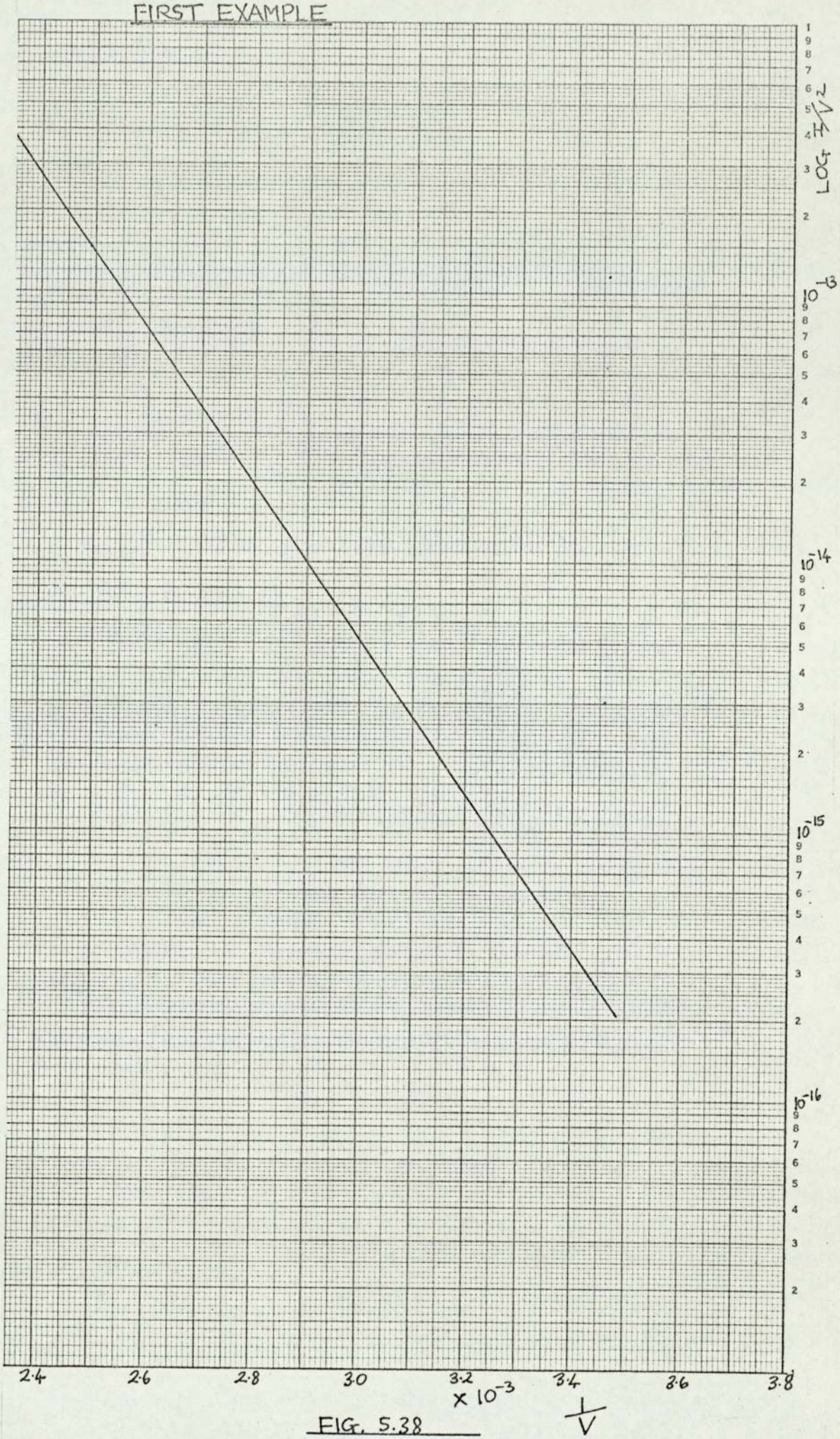

FIG. 5.38

Example 2. For the second example, figures 5.41 - 5.43 the separation of the emitter and first anode was 1.1 mm V_1 = 386V and V_2 = 2700V, the saturation current was 1.8×10^{-11}A. The slope of the Fowler-Nordheim plot was 2.86×10^3 giving a value of K = m/V = 7.41. This corresponds to current density of $2.5 \times 10^3 A/cm^2$. The broadening of the total energy distribution at 295°K is 93meV. The measured halfwidth was 205 ± 10 meV. Therefore, since the work function:

$$\phi = \frac{K \sigma_0 t(y)}{2.01 \times 10^{-5} s(y)} \quad , \quad \phi = 4.4 \pm 0.4 eV$$

where $t(y) \approx 1.04$ and $s(y) \approx 0.96$

The emitter radius r = 210Å ± 20% and assuming k = 5, the electric field strength F≈37 MV/cm. At V_1 = 386V, the emission current $I = 6.5 \times 10^{-9}$A.

If the current density was $2.5 \times 10^3 A/cm^2$, then the emitting area would have been $2.62 \times 10^4 Å^2$. A hemispherical tip of radius 210Å would have a surface area of $27.5 \times 10^4 Å^2$. The emission angle would have been about 50°.

Example 3. In the third example (figures 5.44-5.46) a flat first anode was used. The emitter-anode separation was 3 mm. V_1 = 493V, V_2 = 3450V. The slope of the Fowler-Nordheim plot was 3.22×10^3 and the current density $J = 2.09 \times 10^4 A/cm^2$. The FWHM of the total energy distribution was 220 meV. When a correction of 93 meV is applied, the corresponding halfwidth at 0°K becomes 127 meV. Assuming t(y) = 1.05 and s(y) = 0.95, ϕ = 4.5 ± 0.4 eV.

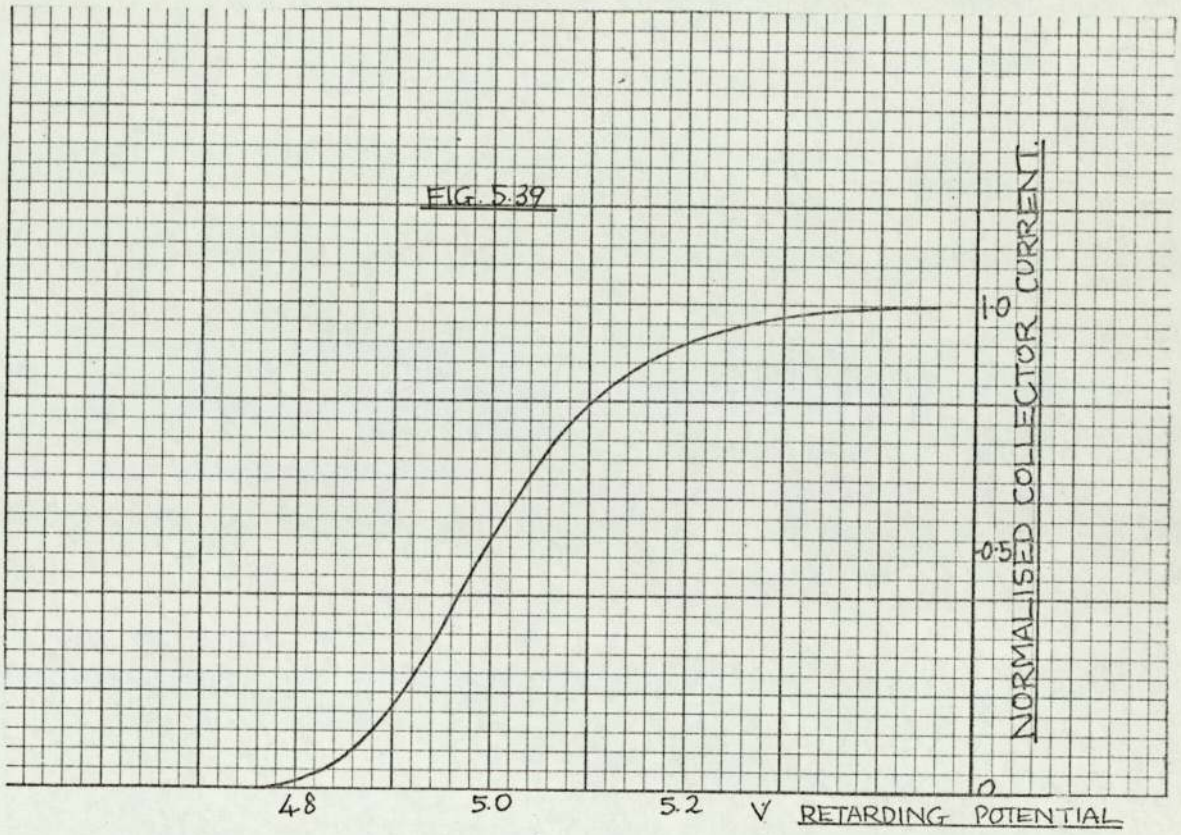
FIG. 5.39
NORMALISED COLLECTOR CURRENT.
1·0
0·5
0
4·8
5·0
5·2
V
RETARDING POTENTIAL

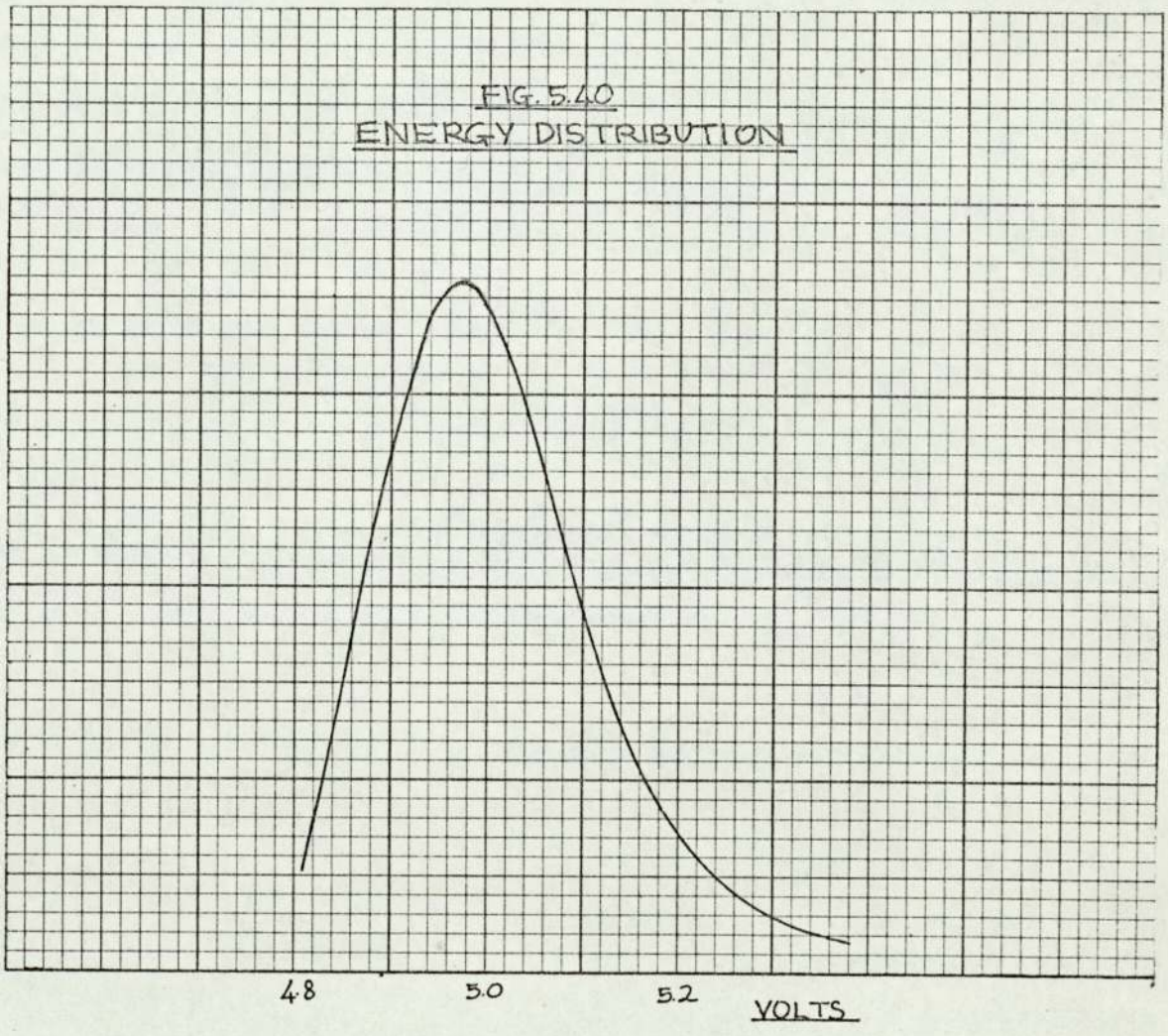
FIG. 5.40
ENERGY DISTRIBUTION
4·8
5·0
5·2
VOLTS

SECOND EXAMPLE

FIG. 5.41

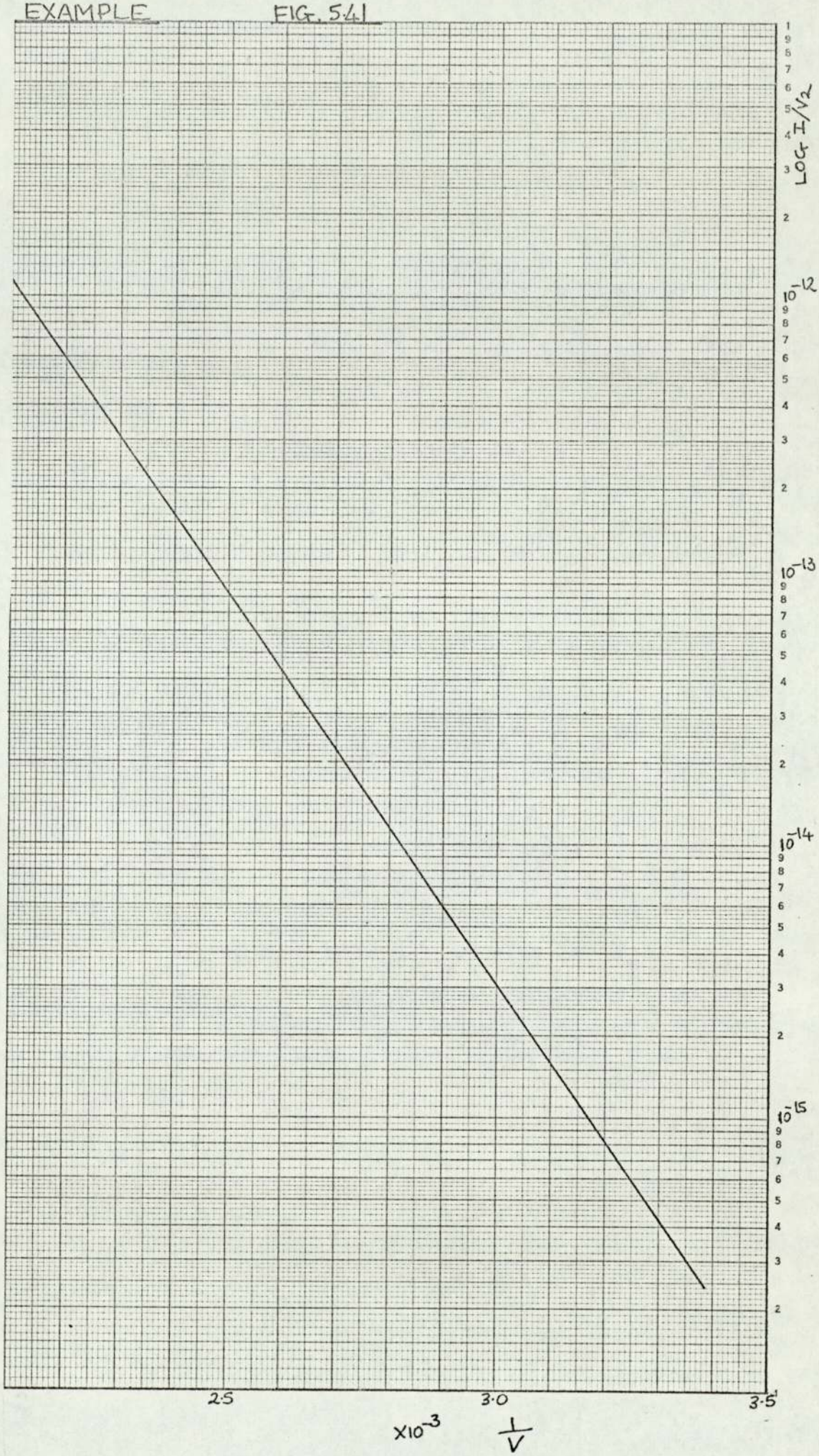

SECOND EXAMPLE

FIG. 5.4.2

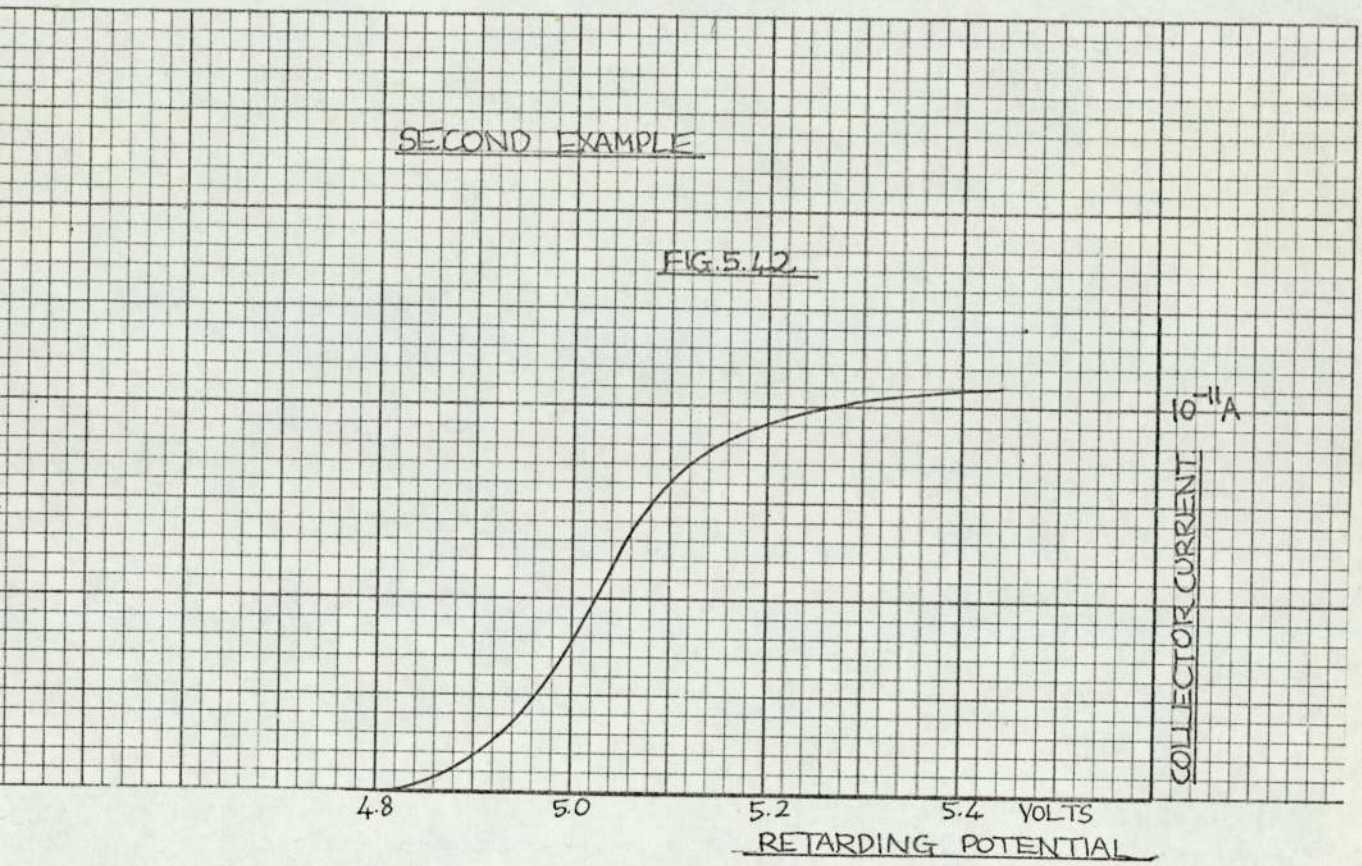

FIG 5.4.3
ENERGY DISTRIBUTION

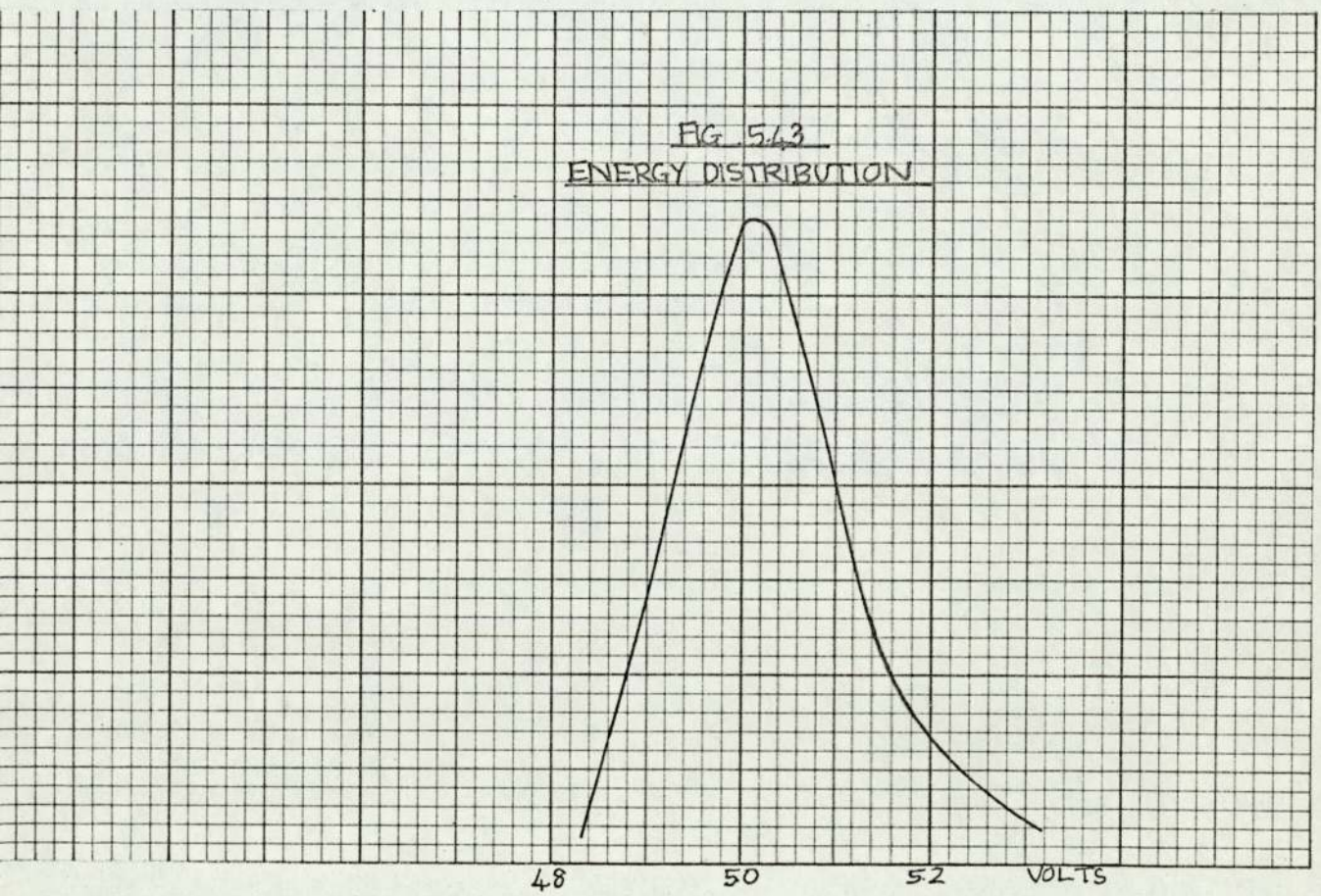

THIRD EXAMPLE

FIG. 5.44

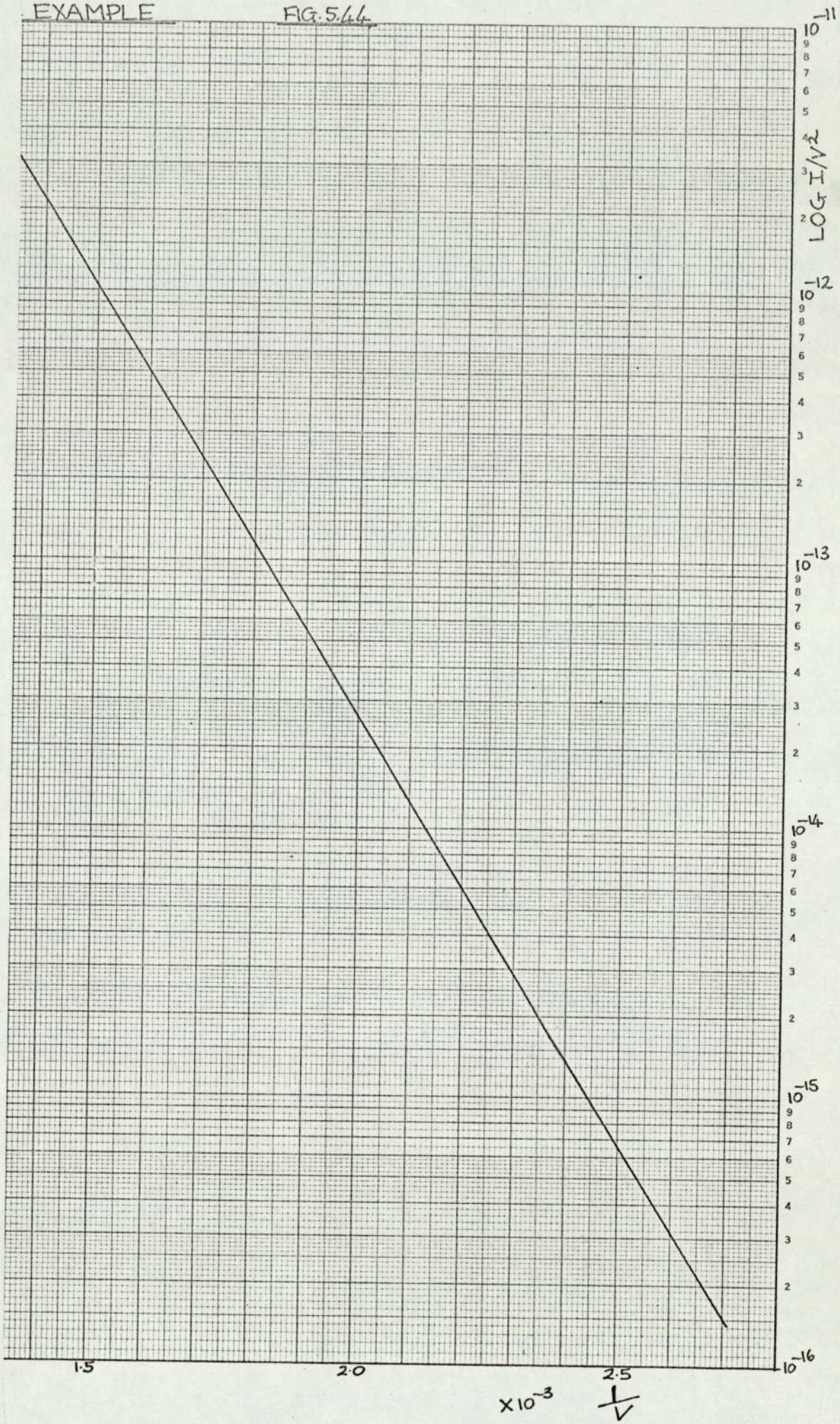

THIRD EXAMPLE FIG. 5.45.

ENERGY DISTRIBUTION

FIG. 5.46

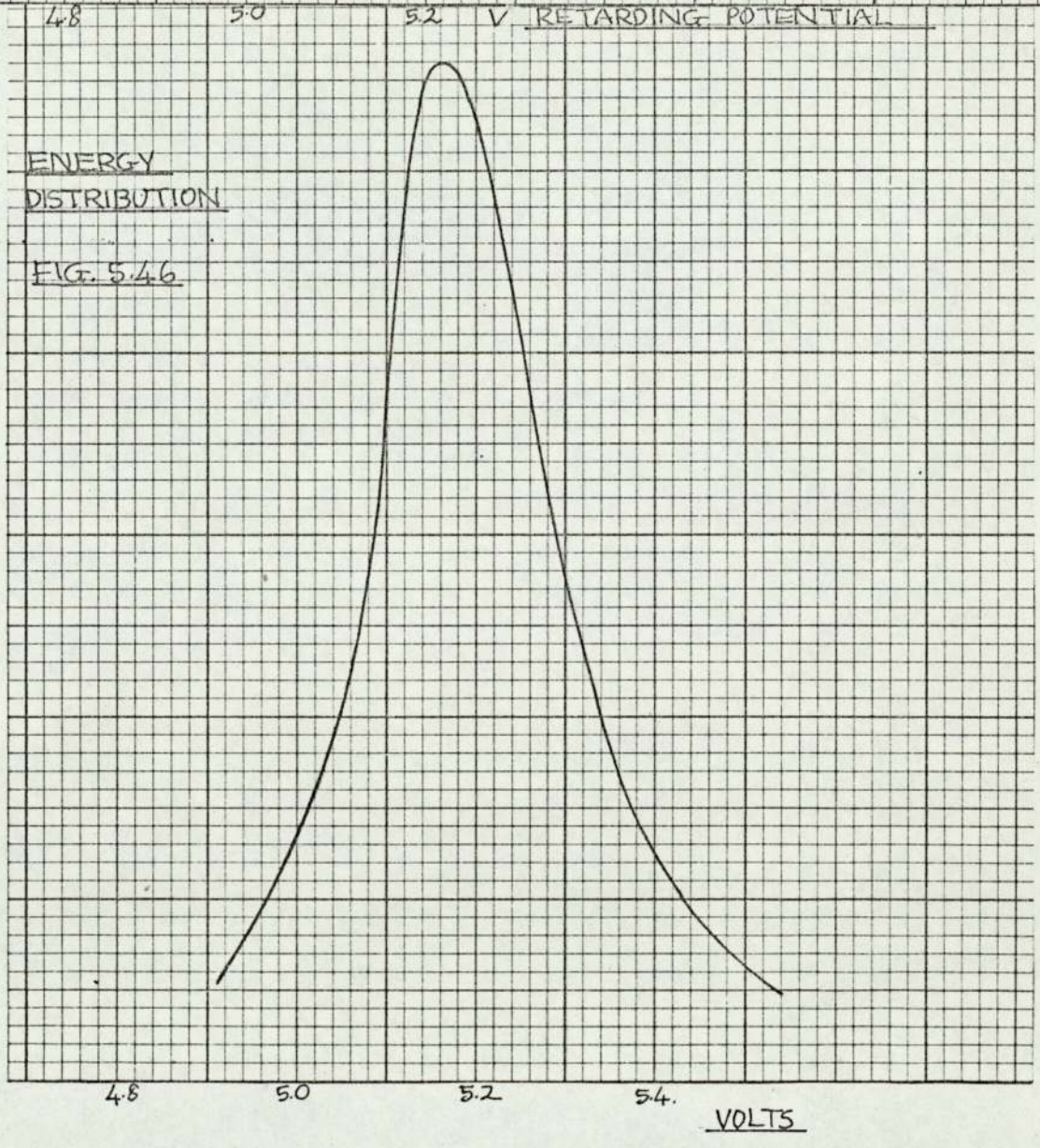

The emitter radius was 236 Å ± 20% and the electric field applied whilst the total energy distribution was being measured was 41.8MV/cm.

The intercept of the integrated curve with the retarding potential axis gives a measure of the work function of the collector (about 4.3eV for molybdenum). The analyser was cleaned by heating to 350°C and therefore the collector surface would not have been perfectly clean. This accounts for the intercept values being high.

In each of the examples given the integrated energy distribution tails off towards higher electron energies, as predicted for the distribution at temperatures above 0°K. Towards lower energies, the collector curve is constant, indicating that secondary emission was not a problem with the analyser.

The more steeply rising edge of the total energy distribution represents the energies of electrons around the Fermi level. At 0°K, this line would be vertical and correspond to the Fermi energy of the electrons. As the temperature is raised, this edge of the distribution becomes less steep as shown. At lower electron energies, the curve drops exponentially to zero, this drop being explained by the decrease in the barrier penetration probability.

Figure 5.47is an example of three phenomena encountered during earlier experiments. The integrated total energy distribution curve was obtained with the retarding potential applied to the emitter. A change in retarding potential from 4 to 8V led to an unexpected falling off of current with increasing retarding potential. This was never seen when the retarding potential was applied to the collector and therefore was probably not caused by secondary emission at the collector. The decrease

in current was probably the result of lens changes in the region between the emitter and the first anode. Thus, although V_1 = 150V and V_2 = 1160V, the small change in potential difference between the emitter and first anode had a significant effect on the integrated distribution curves.

The breadth of the rising part of the curve indicates that the emitter was not on the axis of the system and therefore changing the potential difference between the emitter and first anode probably deflected part of the emitted beam from the axis. This could cause a reduction in collector current as seen.

The two peaks in the curve were probably caused by enhanced emission through adsorbed material on the emitter. At the pressure of 10^{-8} mm, changes in the surface of the emitter were presumably occurring during the measurement of the collector current.

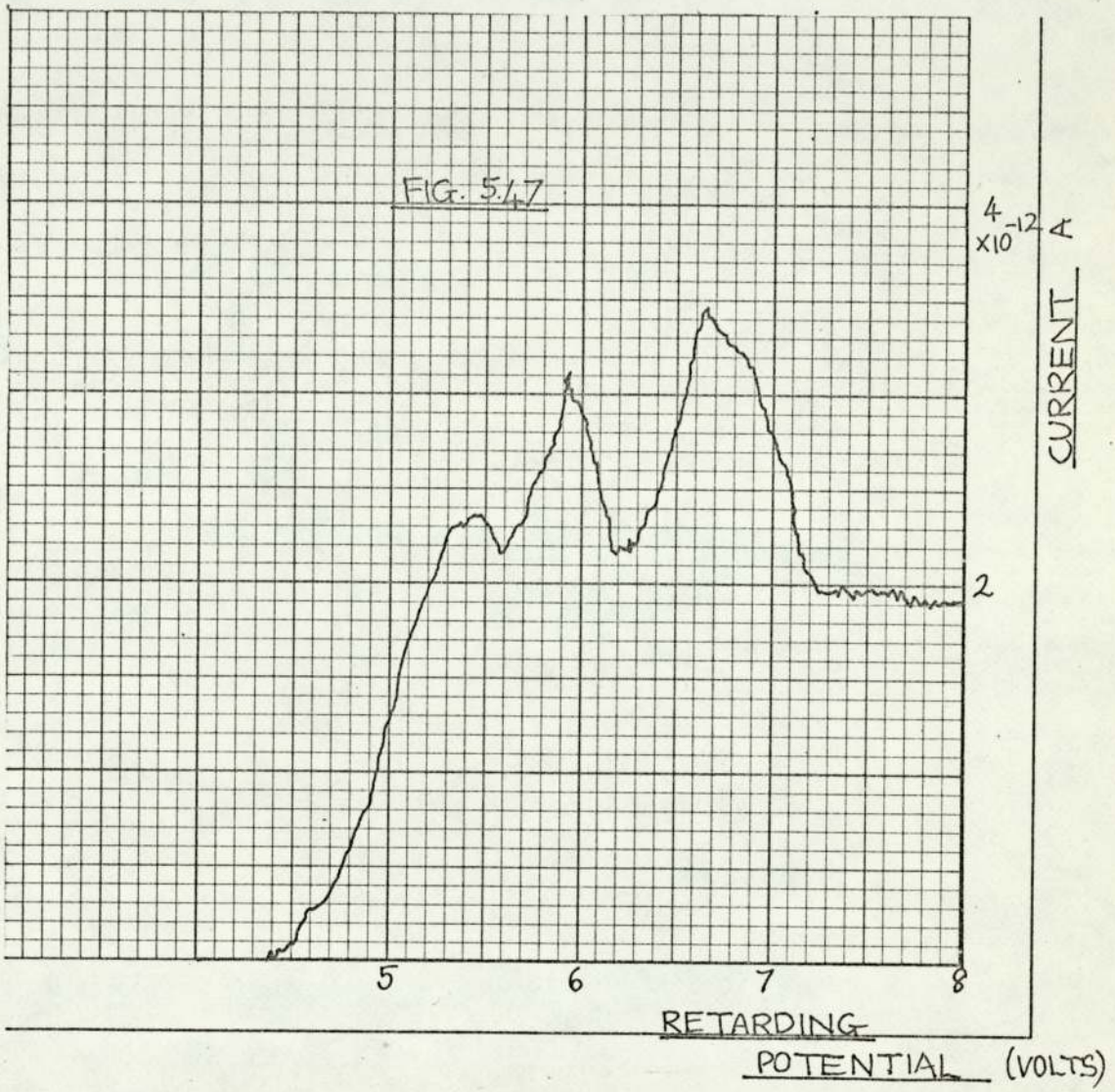
FIG. 5.17
4
×10⁻¹²
A
CURRENT
2
5
6
7
8
RETARDING
POTENTIAL
(VOLTS)

CHAPTER 6. Discussion

6.1. Introduction.

In this chapter, the work carried out will be reviewed, pointing out faults of the experimental system and possible improvements. Detailed discussion of the experimental results has been given in Chapter 5.

6.2. Thermionic emission analyser

The aim of the experiments was to construct an energy analyser suitable for measuring the total energy distribution of field-emitted electrons, and to use it to obtain the distribution for emission from tungsten. The analyser originally chosen was one successfully used by Hartwig and Ulmer[1] for thermionically emitted electrons because it had a claimed resolution of $\Delta E/E \approx 5\times10^{-6}$. Initially thermionic emission experiments were done to confirm that the analyser worked correctly, to gain experience in using an electrostatic lens system and in measuring small currents. These experiments included measurements of the variation of the thermionic energy distribution halfwidth with beam current density. It was seen that at a given temperature, the halfwidth increases with beam current.

The essential parts of an electrostatic retarding potential analyser for thermionic emission are described in section 3.2. They include:

(a) a system of electrodes to form an accelerated beam which arrives at the collector perpendicularly:

(b) a beam defining aperture which largely determines the resolution of the analyser:

(c) a retarding field region:

(d) an efficient collector:

(e) a gun to project as much as possible of the emitted

beam into the analyser.

The thermionic emission experiments not only confirmed that the analyser was working correctly but also verified Child's law and showed that an approximately linear relationship exists between the width of the thermionic energy distribution and different values of the saturation current obtained by varying the grid bias. On extrapolating the curve to zero saturation current, the width of the energy distribution was found to correspond reasonably well with the theoretical value at the temperature of the tungsten filament.

6.3. Field-emission analyser

In modifying the analyser for field-emission, improvements had to be made to the 'gun' and the collector. In principle, the basic thermionic emission analyser might be expected to work for field-emission without any intermediate electrode. This was tried in the first field-emission experiments but was unsuccessful, presumably because (a) the beam was very divergent and the fraction of emission current reaching the collector was too small to be measured, and (b) it was not possible to determine how well aligned the tip was.

The use of an intermediate electrode at a suitable potential offered the following advantages:

(a) by having anodes at two potentials, V_1 and V_2, the electron beam could be made less divergent and therefore caused a much greater fraction of the emitted current to arrive at the collector:

(b) the emission current could be controlled by V_1 which could be set to a low value to prolong emitter life whilst the ratio V_1/V_2 could be changed to optimise the collector

current (as in (a)).

In practice the final gun used developed from the thermionic emission system, i.e. with an electrode at a different potential to that of the tip or anode potential V_2. Although the grid of Wehnelt's cylinder which is used in thermionic emission to control the emitted current is usually biased negatively with respect to the emitting tungsten filament, a simple change from negative to positive potential for use in field emission was not sufficient to form a detectable beam at the Faraday cage. Experiments with this simple type of gun were described in section 5.3.2.

The principal practical difficulty with a system in which the two anodes are separated only by a few millimetres is that little information can be gained about beam alignment unless the beam reaches the collector; we would like to detect the beam at some intermediate point. In order to overcome this, the separation of the first anode from the second was increased, and each electrode was coated with phosphor. The further development of the gun was described in section 5.3.4. The final gun used with Hartwig and Ulmer's analyser incorporated a 'cusp' shaped electrode because it was thought that this shape might cause more of the emitted beam of electrons to pass to the second anode.

In principle the Faraday cage of Hartwig and Ulmer's analyser (which is approximately at earth potential) is kept electrically insulated from the body of the analyser which is at a potential of about 1000-2000V. In practice, the potential drop across the finite resistance of the insulator separating the two, causes a spurious current to appear

at the electrometer. This current was reduced by introducing a 'guard' (see section 4.3.3). Because of the difference between the coefficients of thermal expansion of the insulator and the metal components (stainless steel and molybdenum), the Faraday cage was designed so that the insulator would not crack during bake-out.

6.4. Field-emission microscope

A field-emission microscope was constructed and used in applying the a.c. field desorption technique to clean tungsten emitters. Unfortunately a high percentage of emitters break, presumably because the rapidly alternating stress causes fatigue. This was also noticed by Arthur[2] when cleaning germanium emitters.

Tips can be manufactured quickly and with a small radius of curvature, meaning that low anode voltages can be used to give relatively high emission currents thereby reducing the magnitude of any spurious currents or noise effects originating at the E.H.T. supply. In addition the risk of microdischarges or breakdown is reduced.

6.5. Field-emission experiments

Basic experiments on field-emission confirmed the Fowler-Nordheim relation and the effect of the following on the F-N plot:

(a) the emitter position;

(b) field desorption; and

(c) different ratios of the anode potential V_1/V_2.

Tip radii, electric field strengths and emission areas were calculated for typical emitters.

Experiments with the field-emission gun showed how the anode potential ratio affected collector current.

Measurements of the halfwidth of the total energy distribution have been combined with information from F-N plots to give a value of work function similar to the expected mean work function of tungsten. These experiments were done at room temperature.

6.6. Comparison of the Hartwig and Ulmer analyser (modified for field-emission) with an ideal analyser

The calculated resolution of the Hartwig and Ulmer analyser as used in these experiments is about 10^{-5} where it is assumed that $\Delta E/E \approx \theta^2$, θ being the deviation from the axis of the most inclined trajectory within the beam. Thus at an anode voltage V_2=1500V, the resolution determined solely by the aperture size would be 15meV. The resolution is usually determined at liquid helium temperature by comparison of the experimental and theoretical distributions, however this was impractical for this system and was not attempted.

The primary disadvantage of the Hartwig analyser is the small fraction of emitted current which is collected. The fraction of collected to emitted current is about 2×10^{-4} because the beam passes through several collimating apertures and the beam defining aperture.

A field-emission energy analyser needs a system to: (a) cause field emission, (b) accelerate the beam, and (c) retard it and cause the electrons to arrive normal to the collector. Usually the aim in designing an analyser is to obtain a large maximum collector current from the chosen region of the emitter for a low anode voltage, with a high

resolution. In these experiments, no attempt has been made to examine emission from particular planes and so the electrode system was required to direct as much of the emission as possible to form a parallel beam. Since most of the electrodes in the Hartwig analyser are used to collimate the beam, any system which makes a parallel beam without loss of current would be an improvement. Plummer and Young's[3] analyser (see section 3.2.1.1) is an example of this in which only one electrode aperture is used: (a) to provide a large potential for field-emission, (b) to accelerate the beam, and (c) as an aperture stop for the system, limiting the divergence of the beam. The lens effect at this aperture is reduced by having a cylinder under the electrode. The retarding field is provided by cylindrical lenses and a mesh. Although the current of electrons passing through the mesh is amplified by an electron multiplier, in principle a Faraday cage could be used. In which case, if the entrance of the cage is covered with a mesh, then the risk of losing electrons by secondary emission is reduced and the lens effect at the cage opening is decreased. Plummer and Young used an electron multiplier so that the effect of a single atom on the clean emitter surface could be detected. A useful total energy distribution could be obtained when the current passing through the probe hole was only 10^{-13}A. The claimed resolution was then 10 meV and the Plummer analyser probably represents the best design developed so far. Plummer considered improving the earlier analyser of Young and Muller[4] by constructing an analyser with a hemispherical mesh as collector. The beam would presumably be brought to a focus at the centre of the hemisphere; a shield would need to be provided to avoid loss of electrons by secondary

emission, as used in the Van Oostrom[5] design.

If it was required to use the Hartwig analyser to measure emission from particular planes, the cusp shaped electrode could be replaced by a flat one. This could be coated with phosphor and the separation of the emitter from the electrode increased so that the emission pattern would become clearer. Emission from a chosen plane could then be directed either by an electrostatic or magnetic field over the aperture.

6.7. Emitter cleaning

In order to obtain a high energy resolution, and have a long emitter lifetime, low anode voltages are required. Thus the emitter radius needs to be below 250Å. The present tip manufacturing technique is successful for making small diameter emitters but these tend to break easily when cleaned by the a.c. desorption method (see section 4.9.1.), probably by stress fatigue. Since stress increases with applied voltage, it was attempted to reduce the stress by increasing the desorption time, However, this was not effective because (a) an increase in desorption time of a hundredfold means that the required desorption field is only reduced by about 2 per cent, and (b) increasing the desorption time would be expected to increase the fatigue. If a d.c. field desorption is used, the emission pattern cannot be observed.

A better way of cleaning emitters which are required to keep a small radius of curvature (e.g. < 200Å), might be to remove most contaminants by thermal desorption, at a temperature in the range 1300-2000°K and complete the cleaning and shaping of the tip whilst examining the emission pattern using fairly long a.c. pulses e.g. $\frac{1}{2}$s. The

present tip wheel could be modified for thermal desorption by providing each emitter, mounted on a filament, with an extra lead; electrical connections could be made via four tungsten wires in the wall of the glass tube holding the tip wheel assembly.

6.8. Criticism of adjusting mechanism and vacuum pump

The adjusting mechanism was designed for the first experimental chamber. However, most of the facilities were not necessary for the simpler chamber, tips being positioned by adjusting the three vertical screws set 120° apart and rotating the tipwheel.

Even though the diffusion pump was a two stage one, the pumping speed was too slow. A better vacuum would have been obtained by using a faster pump placed closer to the experimental chamber.

CHAPTER 7. Conclusion

An analyser for the measurement of the energy distribution of field-emitted electrons has been used for emission from tungsten. This analyser was developed from one used by Hartwig and Ulmer[1] for thermionic emission.

In the course of the work several problems had to be overcome, e.g. methods of measuring the small currents at the collector of an analyser needed to be learnt, a guarded Faraday cage which would withstand baking at 300°C was designed, and a technique for efficiently manufacturing tips with a radius of less than 250 Å was developed.

The basic thermionic emission analyser was found unsuitable for field-emission without a special field-emission gun, and one was developed which allowed control of the emission and beam. Finally an analyser was constructed which combined the designs of the field-emission gun and energy analyser in a simplified form. This enabled the emitter beam to be easily detected and aligned along the analyser axis whilst giving a larger collector current. More time would be needed to evaluate the performance of this analyser.

Using the original analyser, both thermionic and field-emission were carried out; F-N plots were obtained under different conditions of anode potential ratio, tip condition and tip-anode separation. The effect of anode potential ratio on collector current was also examined. Typical field-emission total energy distributions were obtained and their widths combined with relevant information

for the corresponding emitter F-N plots to calculate a mean value for the work function of tungsten.

The faults in the experimental system, including the analyser, have been discussed. It is clear that recent developments in field-emission and vacuum technology are moving towards vacua better than 10^{-10} Torr with analysers capable of 10 meV resolution, obtaining useful emission from beam currents of only 10^{-13} A.

The design of such analysers requires the use of a computer program to determine the spherical and chromatic aberration of the lens systems for the optimisation of the analyser design.

A modern system needs to be capable of being operated from liquid helium temperature upwards. Emitters can now be made with radii less than 250 Å and until they can be inserted in the chamber as easily as specimens into an electron microscope, an interchangeable system like a tip wheel needs to be used.

References

Chapter 1

1 R.D. Young and E.W. Muller Phys.Rev. 113 115 (1959)

2 J. Arthur Surface Science (Netherlands) 2 389(1964)

3 A. Van Oostrom Philips Res.Rep. Suppl. 11 102(1966)

4 E.W.Plummer and R.D. Young Phys.Rev. B 1 5 (1970)

5 D.Hartwig and K.Ulmer Z.Physik 173 294 (1963)

Chapter 2

1 E.M.Charbonnier and E.E.Martin J.appl.Phys.33 1897 (1962)

2 R.D.Young Phys Rev. 113 1, 110 (1959)

3 as No.2.

4 A.Van Oostrom J.appl.Phys. 33 10 2917 (1962)

5 R.Gomer "Field Emission and Field Ionization" (1961)

6 L.W.Swanson and L.C. Crouser Phys.Rev.Lett.19 1179 (1967)

7 R.D.Young and H.E.Clark Phys.Rev.Lett. 17 7 351 (1966)

8 E.W.Plummer and T.N. Rhodin Appl.Phys.Lett. 11 6 194 (1967)

9 E.W.Plummer and R.D. Young Phys.Rev.B. 1 5 (1970)

10 E.C.Cooper and E.W. Muller Rev. Scient.Instrum. 29 309 (1958)

11 as No.5.

12 D.Hartwig and K.Ulmer Z.Physik 173 294 (1963)

13 O.Klemperer Reports on Progress in Physics 28 67 (1965)

14 H.Boersch Z.Physik 139 118 (1954)

15 J.A.Simpson and C.E. Kuyatt J. appl.Phys. 37 10 3805 (1966)

Chapter 3

1 R.D.Young Phys. Rev. 113 110 (1959)

2 H.Boersch Z. Physik 139 118 (1954)

3 G.Haberstroh Z. Physik 145 20 (1956)

4 A.A. Holscher Surface Science (Netherlands) 4 1 89 (1966)

5 R.D.Young and E.W. Muller Phys.Rev.113 115 (1959)

6 D.Hartwig and K.Ulmer Z.Physik 173 294 (1963)

7 E.W.Plummer and R.D.Young Phys.Rev. B 1 5 (1970)

8 as 5

9 J.Arthur Surface Science (Netherlands) 2 389 (1964)

10 as 5

11 A.Van Oostrom Philips Res.Rep.Suppl.11 102 (1966)

12 O.Klemperer Reports on Progress in Physics 28 77

13 G.Frost Z.Angew. Phys. 10 546 (1958)

14 J.A.Simpson and L.Marton Rev.Scient.Instrum 32 802 (1961)

15 A.H.Beck and C.E.Maloney Brit.J.Appl.Phys.18 845 (1967)

16 H.Boersch and S.Schweda Z.Physik 167 2 (1962)

17 as 8

18 R.Stratton Phys.Rev. 135 A.794 (1964)

19 A.M.Russell Phys.Rev.Lett.9 417 (1962)

20 A.M.Russell and E.Litov Appl.Phys.Lett.2 3 64 (1963)

21 I.L.Sokol'skaya and G.P.Shchbakov Sov.Phys.Solid State 3 167 (1961)

22 I.L. Sokol'skaya and G.P.Shcherbakov Sov.Phys. Solid State 4 2581 (1963)

23 J.Arthur Surface Science (Netherlands) 2 389 (1964)

24 R.Stratton Phys.Rev. 125 1 67 (1962)

25 L.W.Swanson and L.C.Crouser Phys.Rev.163 3 622 (1967)

Chapter 4

1 D.Hartwig and K.Ulmer Z.Physik 173 294 (1963)

2 A.B.Osborn R.A.E. Tech.Note CPM 69 (1964)

3 J.R.Bailey Supplemento al Nuovo Cimento 1 2 494 (1963)

4 R.H.Good and E.W.Muller Handbuch der Physik Springer Berlin 21 (1956)

5 F.Ashworth Advances in Electronics and Electron Physics 3 1 (1951)

6 R.Gomer "Field Emission and Field Ionisation"1961

Chapter 5

1 D.Hartwig and K.Ulmer Design of field-emission analyser Z.Physik, 173 294 (1963)

Chapter 6

1 D.Hartwig and K.Ulmer Z.Physik 173 294 (1963)

2 J.Arthur J.Phys.Chem. sol. 25 583 (1964)

3 E.W.Plummer and R.D.Young Phys.Rev.B 1 5 (1970)

4 R.D.Young and E.W.Muller Phys.Rev.113 115 (1959)

5 A.Van Oostrom Philips Res.Rep.Suppl.11 102 (1966)

Chapter 7

1 D.Hartwig and K.Ulmer. Z.Physik 173 294 (1963)